Biosynthetic Plasticity as a Means for the Discovery and Diversification of Natural Products

Zur Erlangung des akademischen Grades eines

Dr. rer. nat.

von der Fakultät Bio- und Chemieingenieurwesen
der Technischen Universität Dortmund
genehmigte Dissertation

vorgelegt von
Diplom-Pharmazeutin
Angela Sester
aus
Oberkirch

Tag der mündlichen Prüfung: 08.12.2021
1. Gutachter: Prof. Dr. Markus Nett
2. Gutachter: Prof. Dr. Jörg Pietruszka

Dortmund 2021

Zusammenfassung

Naturstoffe inspirieren fortwährend die Arzneistoffentwicklung, da sie zentrale Ausgangspunkte für die Strukturmodifikation und -optimierung darstellen. Daher ist die Entdeckung neuer Sekundärstoffe und ihrer biologischen Aktivität von zentraler Bedeutung, ebenso wie Studien zu entsprechenden Struktur-Wirkungsbeziehungen. Diese Arbeit zeigt, wie Präkursor-gesteuerte Biosynthese als universell einsetzbare Methode zur Untersuchung diverser Forschungsfragen eingesetzt werden kann. Die Derivatisierung der myxobakteriellen Naturstoffe Myxochelin B, Pseudochelin A, sowie Aurachin D gibt Einblicke in die natürliche Promiskuität der Biosynthesewege. Durch Zugabe von Benzoesäureanaloga in einem rekombinanten *Myxococcus xanthus* Stamm, wurde die Produktion von Myxochelin B und Pseudochelin A gesteigert, sowie auch 14 Derivate dieser Naturstoffe erzeugt. Es wurde gezeigt, dass diese Produkte eine ähnliche oder bessere Bioaktivität bezüglich der humanen 5-Lipoxygenasehemmung aufweisen als die zuvor getesteten Myxochelin A-Analoga. Auf diese Weise konnte das bisherige Wissen über ihre Struktur-Wirkungsbeziehungen erweitert werden. Zudem wurde *Stigmatella erecta* genutzt, um drei fluorierte Aurachin D Analoga zu generieren, welche eine vergleichbare antibiotische Potenz hatten wie die in der Natur gebildete Verbindung.

Ferner wurde in zwei Modellstämmen eine Methode zur Wirkstoffsuche entwickelt und getestet, die auf dem biosynthetischen Einbau von nicht natürlich vorkommenden, acetylenischen Präkursoren in Naturstoffe, der anschließenden Derivatisierung durch Click Chemie und UV/VIS Visualisierung beruht. Untersuchungen an *M. xanthus*, aber auch an *Ralstonia solanacearum* zeigten, dass sich Aminosäuren als biosynthetische Bausteine nur selten durch Analoga mit acetylenischen Funktionen ersetzen lassen. Die Zufuhr von Fettsäuren mit terminaler Alkinylgruppe war jedoch erfolgreicher und einige wurden in quantitativen Ausbeuten inkorporiert. Dies gelang u.a. in der Biosynthese des Antibiotikums Micacocidin, in welcher ein 5-Hexinsäure-haltiges Derivat generiert werden konnte. Dagegen war der Ralsolamycin-Biosyntheseweg weniger tolerant gegenüber den Fettsäureanaloga, lieferte aber dennoch messbare Mengen der alkinylhaltigen Produkte. Dieser Einsatz als chemische Sonden lieferte Erkenntnisse über die möglichen Inkorporationsmöglichkeiten, zeigte jedoch auch die Grenzen der Derivatisierung von Rohextraktproben auf.

Abstract

Natural products continuously inspire drug development as they represent key starting points for structural modification and optimization. Therefore, the discovery of new secondary metabolites and their biological activity is of vital importance, as are studies of corresponding structure-activity relationships. This work demonstrates how precursor-directed biosynthesis can be used as a universally applicable method to investigate diverse research questions.

Derivatization of the myxobacterial natural products myxochelin B, pseudochelin A, as well as aurachin D provides insight into the natural promiscuity of biosynthetic pathways. Addition of benzoic acid analogs in a recombinant *Myxococcus xanthus* strain, increased the production of myxochelin B and pseudochelin A, and also generated 14 derivatives of these natural products. These compounds were shown to have similar or improved bioactivity with respect to human 5 lipoxygenase inhibition than the previously tested myxochelin A analogs. In this way, previous knowledge of their structure-activity relationships was expanded. Furthermore, *Stigmatella erecta* was used to generate three fluorinated aurachin D analogs that had equivalent antibiotic potency to the compound formed in nature.

In addition, a drug discovery method based on the biosynthetic incorporation of non-naturally occurring acetylenic precursors into natural products, their subsequent derivatization by Click chemistry and UV/VIS visualization was developed and tested in two model strains. Studies on *M. xanthus* and *Ralstonia solanacearum* showed that amino acids as biosynthetic building blocks can rarely be replaced by analogs with acetylenic functions. However, the supply of fatty acids with terminal alkynyl groups was more successful and some were incorporated in quantitative yields. Among others, this was successful for the biosynthesis of the antibiotic micacocidin, in which case a 5-hexynoic acid-containing derivative could be generated. In contrast, the ralsolamycin biosynthetic pathway was less tolerant of the fatty acid analogs, but still yielded measurable amounts of the alkynyl-containing products. This application as chemical probes provided insights into the potential incorporation possibilities, but also demonstrated the limitations of derivatizing crude extract samples.

Eigenständigkeitserklärung

Hiermit erkläre ich, dass ich die vorliegende Arbeit selbst verfasst und keine anderen als die angegebenen Quellen und Hilfsmittel verwendet habe. Die geltende Promotionsordnung der Fakultät Bio- und Chemieingenieurwesen der Technischen Universität Dortmund ist mit bekannt. Die Hilfe eines Promotionsberaters wurde nicht in Anspruch genommen. Es haben Dritte weder mittelbar noch unmittelbar geldwerte Leistungen für Arbeiten erhalten, die im Zusammenhang mit der vorgelegten Dissertation stehen. Diese schriftliche Arbeit wurde in gleicher oder ähnlicher Form noch bei keiner anderen Hochschule als Dissertation eingereicht und auch nicht als Prüfungsarbeit für eine staatliche oder andere wissenschaftliche Prüfung verwendet.

Dortmund, 13.09.2021   Angela Sester

Danksagung

Declaration on the reproduction of previously published content

Parts of this work have been published by the author of this thesis and/or are based on data which were obtained in a MSc thesis performed at the Laboratory of Technical Biology under the supervision of the author. The following list gives a precise overview of the individual contributions.

Chapter 1.3.1 – 1.3.4 in parts modified from [C]

Chapter 3.1.2 – 3.1.5 in parts modified from [A] and [B]

Chapter 3.2 in parts modified from [A]

Chapter 3.3 in parts modified from [B]

Chapter 4.1 in parts modified from [A]

Chapter 4.2 in parts modified from [B]

Chapter 4.2 in parts based on data from [a]

Chapter 4.3.1 in parts modified from [C]

Chapter 5.2 in parts modified from [A] and [B]

Chapter 5.2.5 in parts based on data from [a]

Reprinted (adapted) with permission from [A] (J. Nat. Prod. 2019, 82 (9), 2544–2549.) Copyright (2019) American Chemical Society.

Reprinted (adapted) with permission from [B] (ChemBioChem, 2020, 21, 2268-2273). Copyright (2020) WILEY-VCH, Creative Commons CC BY 4.0 license.

Reprinted/adapted by permission from [C] Springer Nature Customer Service Centre GmbH: Springer Nature, "The Ecology of Predation at the Microscale" by Jurkevitch, E., Mitchell R. J., Eds.; Chapter "Secondary Metabolism of Predatory Bacteria" by Sester A., Korp J., Nett M., Copyright (2020).

Publications herein cited

A complete list of publications is presented in the appendix.

[A]   **Sester, A.; Winand, L.; Pace, S.; Hiller, W.; Werz, O.; Nett, M.** Myxochelin- and Pseudochelin-Derived Lipoxygenase Inhibitors from a Genetically Engineered *Myxococcus xanthus* Strain. *J. Nat. Prod.* **2019**, 82 (9), 2544–2549.

[B]   **Sester, A.; Stüer-Patowsky, K.; Hiller, W.; Kloss, F.; Lütz, S.; Nett, M.** Biosynthetic Plasticity Enables Production of Fluorinated Aurachins. *ChemBioChem* **2020**, 21 (16), 2268–2273.

[C]   **Sester, A.; Korp, J.; Nett, M.** Secondary Metabolism of Predatory Bacteria. In *The Ecology of Predation at the Microscale*; Jurkevitch, E., Mitchell, R. J., Eds.; Springer International Publishing, 2020.

Supervised student theses

[a]   **Stüer-Patowsky, K.** Präkursor gesteuerte Biosynthese von Aurachin Derivaten. Masters' Thesis, Laborary of Technical Biology, TU Dortmund University, **2019**.

Table of Contents

1   Introduction

1.1   From ancient medicine to modern drug discovery

Remedies from natural resources have a history of millennia. As humans tried to find cures in their environment, the earliest attempts to medicines were based on plant, fungal, animal and mineral products. Some of the oldest reports thereof are directly correlated with the founding of human civilization. As described in the Chinese culture, where the rather mythical figure Huang Ti, a founding father of the country, is associated with documentation of the "supposedly oldest medical book extant", *the Yellow Emperor's Classic of Internal Medicine*, dated circa 2600 B.C.[1] Deeply rooted therein are the principles of Traditional Chinese Medicine (TCM) which is still in use today and inspired also the Japanese Kampo medicine.[2] Likewise, the first cuneiform texts from Assur in ancient Mesopotamia, dating back to around 1300 B.C., include a collection of about 340 different plants, animal parts but also details on dosage forms to facilitate pharmaceutical application.[3] The *Ebers Papyrus*, which originates from ancient Egypt (ca 1500 B.C.), contains detailed recipes based e.g. on castor oil seeds or pomegranate roots. It inspired the greater medical development in the region, reaching to ancient Greece and the Arabic world where it laid the foundation for today's Western medical sciences.[4,5]

Different cultures established their own treatment options, but until the 19th century predominantly extracts, and compound mixtures were in use. The isolation and characterization of morphine from opium by Sertürner 1805 – 1817[6,7] eventually led to a dogma change, as it showed that isolated compounds carry the biological activity and can be used with improved dosing quality.[8] In the following years more and more compounds of biological origin were introduced to the field of medicine, from atropine[9] and ephedrine[10] to salicylic acid.[11] With the discovery of penicillin in 1928 by Alexander Fleming,[12] microorganisms were recognized as a new source of natural products. What had started with the discovery of the naturally produced antibiotic, did not only open the century of antibiotic discovery, but soon expanded into the much broader field of compound sourcing from microbes. The bacterial and fungal sources allowed targeted, relatively fast cultivation and preparation of crude material. Large scale screening by pharmaceutical companies and

research facilities enabled the discovery of a great variety of compounds with broad applicability.[13] With the emergence of DNA sequencing methods in 1977[14] another epoque in drug discovery was entered. Correlation of genetic information with the chemistry of natural product compounds allowed targeted analysis and mining of genome sequences with biotechnological means that continues to be the gold standard until today.

1.2   Natural products diversity in structures and activities

Natural products are nowadays found in almost every aspect of daily life, from cleaning compounds or pesticides to food supplements and medicines. They stand out through remarkable structural diversity and yet specific stereochemistry (Figure 1.1), with their size ranging from small molecules like salicylic acid to large peptides as polytheonamides,[15] but even more in their chemical constitution. While biomolecules like proteins, DNA, carbohydrates and lipids are mainly composed of carbon, oxygen, hydrogen, phosphor and sulfur, many natural products also include rare atoms like halogens[16–18] or boron.[19] Their chemical scaffolds may resemble those of abundant biomolecules but diverge frequently from their conserved patterns. In peptides, not only proteinogenic, but also a variety of non-proteinogenic amino acids can be incorporated[20,21] and peptide bonds may be found altered towards thioamides.[22] Occasionally, high degrees of unsaturation can be observed as a sequence of conjugated double bonds in myxochromides[23] or in the enediynes (e.g. calichemicin γ_1^I), where two triple bonds surround a double bond towards a highly reactive structural assemblage (Figure 1.1).[24] Reactivities and thus bioactivities are often introduced through different ring sizes from the smaller epoxide, cyclopropyl or beta-lactame moieties found respectively in toblerols[25] or penicillins,[26] with their characteristic ring strain and resulting reactivity, through 7- or 8-membered cycles represented in anthramycin[27] or paclitaxel,[28] up to macrolactones in macrolide antibiotics.[29] While some cyclic molecules feature planar aromatic structures, such as doxorubicin,[30] intramolecular crosslinks add spatial properties that extend the complexity to the third dimension, as exemplified by cittilin[31] or the glycopeptide vancomycin.[32] In some cases these bond formations lock the molecules in a particular manner, conferring rigid conformations for example to lassopeptides as microcin J25,[33] or di-naphthylisoquinoline mbandakamine A. In the latter, connection of the two subunits introduces additionally stereochemical hindrance, but also the antiprotozoal

activity.[34] Many compounds combine different structural elements, when e.g. fatty acids are merged with amino acids to form lipopeptides[35] or the macrolide antibiotics consisting of a
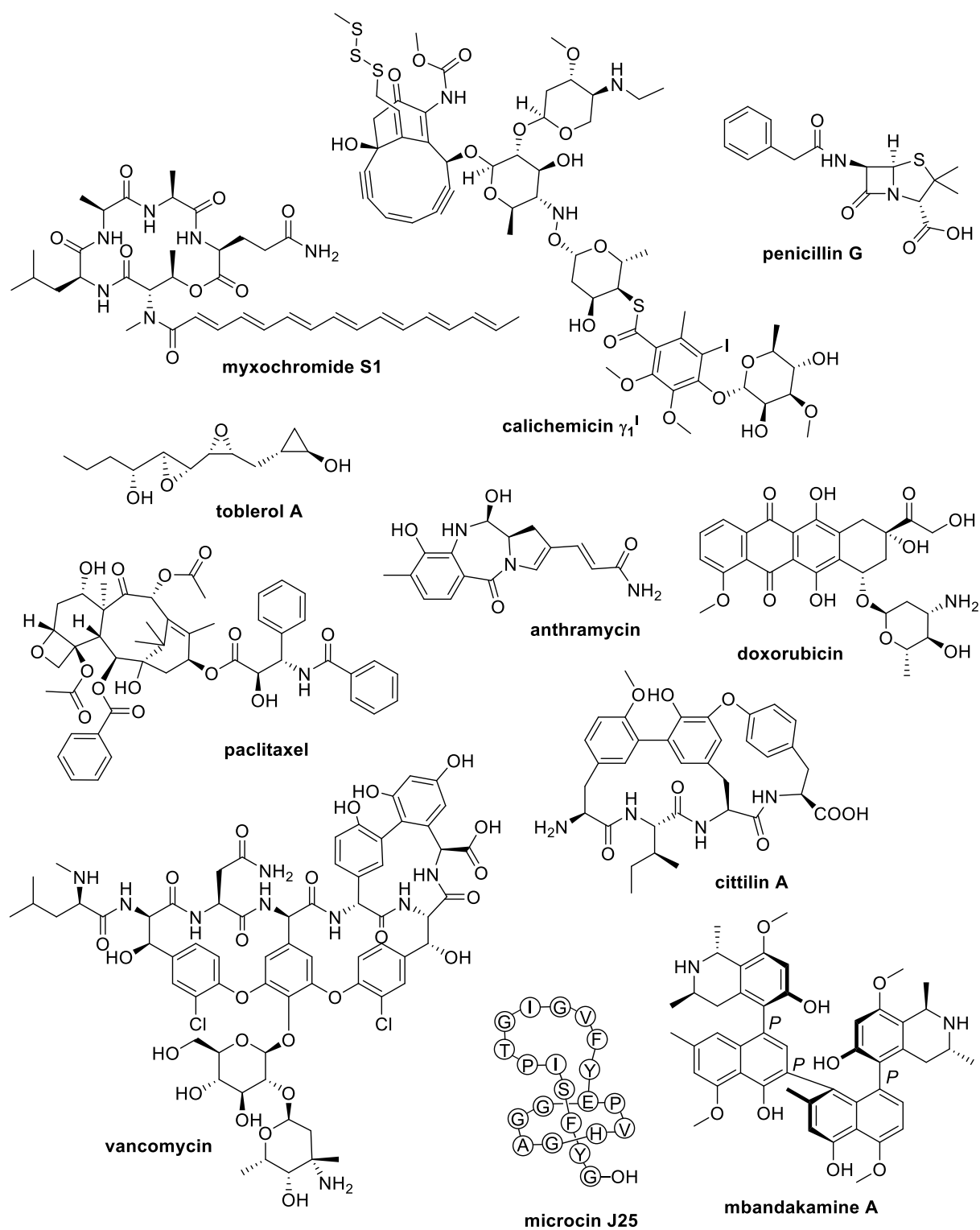
Figure 1.1 Natural products bearing diverse chemical features.

macrolactone backbone decorated with (amino-)sugar features.[36] In essence, all these chemical modifications contribute to the richness of structural diversity found in natural products.

These chemical features also come along with a wide range of biological activities that inspired drug innovation in the past century. Analysis of all small molecule drugs licensed since 1981 shows that one third of them are natural products, their derivatives, or mixtures thereof, while another third contains natural product-inspired pharmacophores or scaffolds. Only one third of all drugs can be ascribed to purely synthetic compounds.[37] Conversely, these findings also demonstrate that natural products are rarely used in their original form, but predominantly serve as templates in drug development. Modifications on natural products result in enhanced activity, adequate therapeutic windows or improved bioavailability.[38] Biological activities of natural products are manifold, ranging from antibacterial, antifungal, antiviral or antiparasitic properties that might be associated with their ecological function to antineoplastic, antidiabetic, or antiinflammatory effects and beyond. Nature-inspired structures are particularly eminent in antibacterial and antiparasitic drugs and play a major role as anti-cancer agents.[37] In this context it is noteworthy, that the ecological roles of these compounds are often not known[39] and thus not always coherent with their medical indications.

Traditionally, natural products are categorized into primary and secondary metabolites. The primary metabolites are deemed essential for an organism as they play key roles in growth, energy generation or reproduction. Their biosynthetic pathways are in general highly conserved, even across the three domains of life.[37,40] In contrast, secondary metabolites are considered nonvital. They give advantageous properties to the producer or its community,[39] e.g. the production of antibiotics to kill competing species,[41] quorum sensing molecules that allow intra-species communication and coordination,[42] or siderophores that facilitate iron uptake.[43] Their occurrence varies greatly among different species and not all products are produced at all times, but only as a reaction to certain events as limited nutrient supply, physical stress or as response to competitors.[44]

The term natural products is often used congruently with secondary metabolites although biosynthetic origin of various compounds demonstrates, that primary and secondary metabolism are both closely interconnected and cannot be strictly distinguished. Steroids or

carotenoids for example function as essential as well as optional compounds.[45] While it is often stated that natural products are evolutionary optimized towards improved biological functions,[46] this definition was challenged with a broader model including the Screening Hypothesis. Therein, the evolutionary advantage through single compounds was considered weak, but the fitness advantage of a certain organism was rather correlated with the unique chemical mix it presents in its portfolio. The diversity of produced compounds is facilitated by the promiscuity of the enzymes involved, accepting a variety of substrates, and generating an assorted palette of metabolites, among which some may possess advantageous properties.[45]

In this thesis, the term secondary metabolites will be used according to the traditional definition, though taking into consideration the limitations thereof as discussed above. The most objective categorization of natural products can be applied according to their biosynthetic origin and the most prominent classes will be introduced in the following.

1.3   Classes of natural products

Natural products can be classified according to their biosynthetic origin. The four most common biosynthetic classes are ribosomally synthesized and post-translationally modified peptides (RiPPs), non-ribosomal peptides (NRPs), polyketides (PKs), and terpenes. The three former are most relevant to this thesis and introduced in the following.

1.3.1 Ribosomally synthesized and post-translationally modified peptides

The text in this paragraph was taken with minor modifications from publication [C] of the author:

"RiPPs are made from proteinogenic amino acids, but due to extensive post-translational modifications these molecules exhibit unusual structural features that are not generally associated with ribosomal peptides. By definition, RiPPs are smaller than 10 kDa to distinguish them from post-translationally modified proteins.[21] The preliminary primary structure of RiPPs is encoded by a structural gene and the transcribed mRNA is initially translated into a precursor peptide. In most cases this precursor peptide consists of an N-terminal leader peptide, followed by the core region and occasionally a C-terminal recognition sequence,

which is relevant for dissection and cyclization. The processing of the precursor peptide is initiated upon recognition of the leader peptide by biosynthetic enzymes, which carry out various structural modifications in the core region. Such modifications can include the formation of α-β-unsaturated amino acids through dehydration of serine or threonine residues, intramolecular cyclizations to thiazol(in)es or oxazol(in)es, *S*-adenosylmethionine (SAM)-dependent methylations, as well as head-to-tail (N-to-C) macrocyclization. Finally, proteolysis cleaves off the leader peptide and, if applicable, the C-terminal recognition sequence and releases the matured RiPP for consecutive export.[21] An illustrative example for RiPP biosynthesis in a predatory bacterium is provided by cittilin A, which is produced by several *Myxococcus xanthus* strains.[47] For the biosynthesis of this tetrapeptide (Figure 1.2), a leader and core peptide (encoded by one gene), a cytochrome P450 monooxygenase (P450) and a methyltransferase are sufficient. The core peptide, with its sequence Tyr-Ile-Tyr-Tyr undergoes two P450 catalyzed phenol coupling reactions to form a C-C as well as a C-O-C bridge between the tyrosine residues. An *O*-methylation of a phenolic hydroxyl moiety
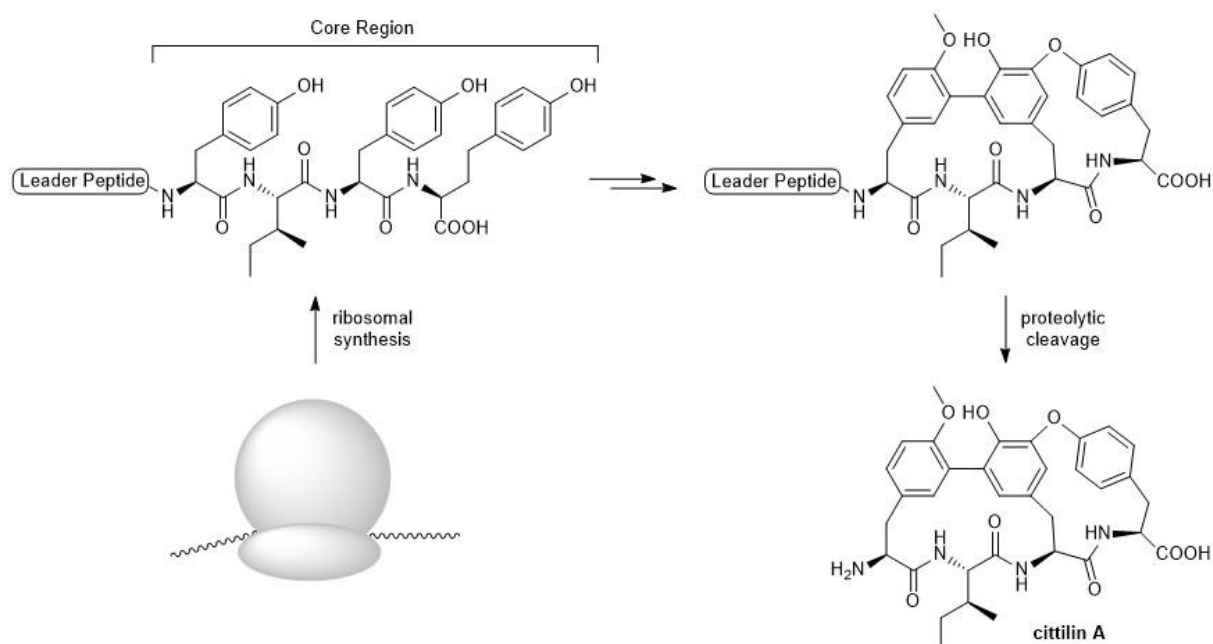
Figure 1.2 Biosynthetic route to cittilin A.
"The two phenol coupling reactions are catalyzed by the P450 enzyme MXAN_0683, while the O-methylation in the N-terminal tyrosine moiety is due to the SAM-dependent methyltransferase MXAN_0682."[49]

completes the post-translational modifications.[48] Cittilin biosynthesis exemplifies how a simple core structure of only four amino acids can be concisely transformed into a distinctive structural scaffold."[49]

1.3.2 Non-ribosomal peptides

The text in this paragraph was taken with minor modifications from publication [C] of the author:

"NRPs and also several PKs are produced by large enzyme complexes which operate in assembly line fashion.[50,51] For this, non-ribosomal peptide synthetases (NRPSs) and polyketide synthases (PKSs) are organized into modules, each of which is responsible for the incorporation of a defined building block into the final product. The modules are composed of several domains with specific catalytic activities that are relevant for the assembly.

In NRPs a peptide chain forms the structural backbone. It can feature proteinogenic as well as non-proteinogenic amino acids including D-isomers and β-amino acids. The minimum NRPS module consists of three domains. The adenylation (A) domain is responsible for the recognition and ATP-driven activation of the amino acid substrate, which is thereby acyl-adenylated. Next, the A domain transfers the activated substrate to the phosphopantetheinyl side chain of the consecutive peptidyl carrier protein (PCP) domain where it is covalently attached through a thioester bond. This activated ester is targeted by the condensation (C) domain, which links the amino acid monomer with the peptidyl intermediate from the preceding module through an amide bond. Optional domains in NRPS modules can further perform reduction or oxidation steps, intramolecular cyclization (Cy), epimerization (E), methylation (MT) or dehydration and, thereby, increase the structural variety within the peptide products.[20] In the terminal NRPS module, a thioesterase (TE) domain releases the product from the enzyme machinery, either by simple hydrolysis or by intramolecular macrocyclization. A noteworthy NRP, due to its potent antibacterial properties, is lysobactin which was discovered in *Lysobacter* sp. ATCC 53042.[52,53]

The biosynthesis of this antibiotic (Figure 1.3) follows the co-linearity paradigm by which an NRPS with 11 modules codes for 11 amino acids to form an undecapeptide.[54] In accordance with the module number and the predicted number of epimerizations, lysobactin is composed
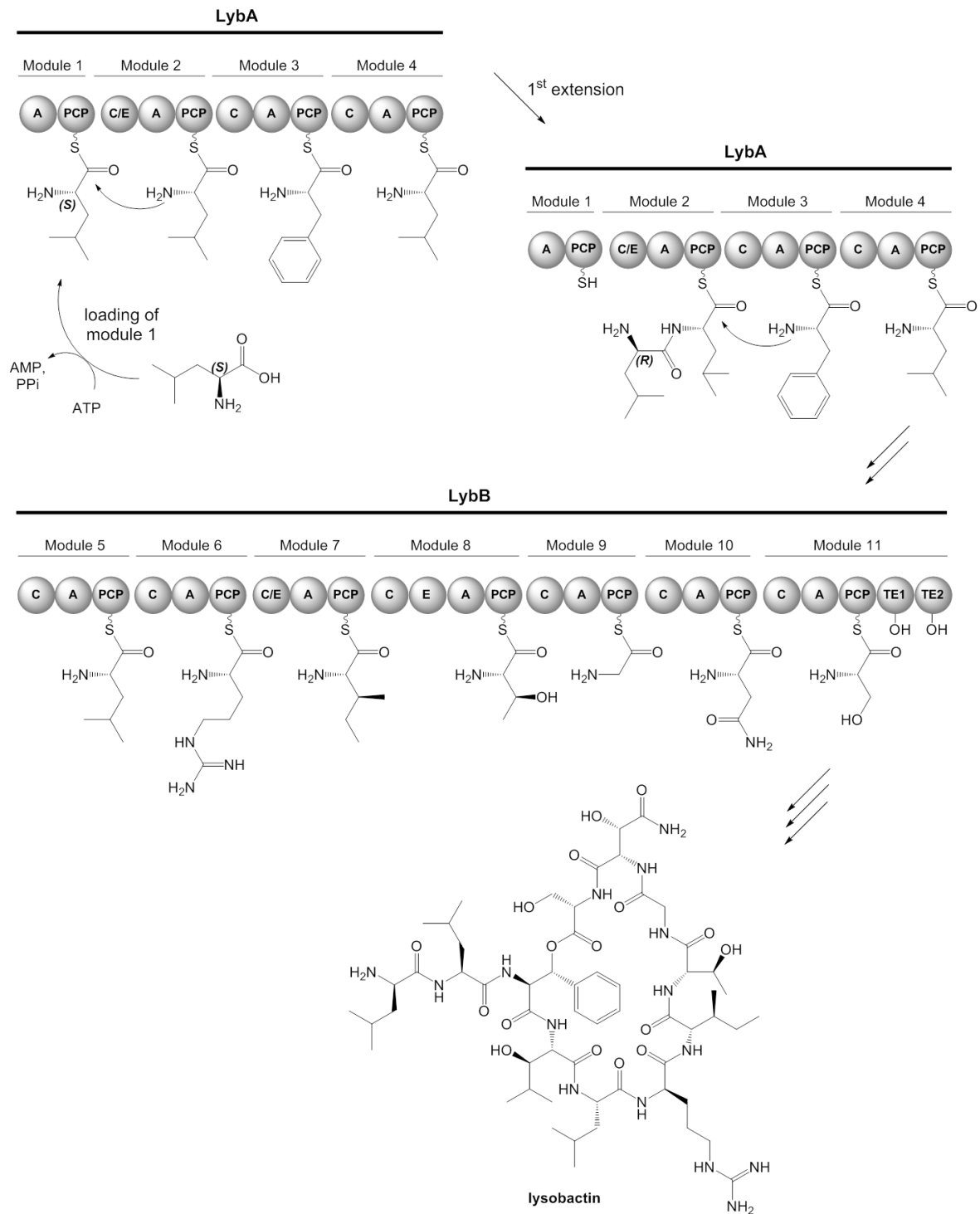
Figure 1.3 "NRPS assembly line of lysobaction with tethered amino acid monomers.
The loading of module 1 and the first extension reaction including the stereochemical inversion of the initially primed leucine moiety are shown in detail."[49]

of nine L- and two D-amino acids. Interestingly, the epimerizations that give rise to the D-leucine and D-arginine residues in lysobactin are not catalyzed by distinct E domains. Instead, these reactions are mediated by dual function C/E domains.[54,55] The only dedicated E

domain of the lysobactin assembly line, which is present in module 8, was proposed to be responsible for the side-chain epimerization from L-threonine to L-*allo*-threonine. A rather unusual feature in NRPS systems is the presence of a tandem TE domain. In the case of lysobactin, it was demonstrated that only the N-terminal TE domain is needed for macrocyclization and subsequent product release, whereas the C-terminal TE domain has a proofreading function through the deacylation of misprimed PCPs.[54″49]

1.3.3 Polyketides

The text in this paragraph was taken with minor modifications from publication [C] of the author:

"Similar to NRPSs, the majority of bacterial PKSs utilize thiotemplates for natural product biosynthesis, but their substrates are short-chain acyl-CoAs, such as malonyl-CoA or methylmalonyl-CoA.[56] These simple activated C2 or C3 units are selected by the acyltransferase domain (AT) of a PKS module and immediately tethered to an adjacent acyl carrier protein (ACP) domain, which previously underwent phosphopantetheinylation. A β-ketoacylsynthase (KS) domain then catalyzes the linkage of the monomer building block with the growing acyl chain via decarboxylative *thio*-Claisen condensation. The resulting β-keto group in the reaction product can be further processed by optional ketoreductase (KR), dehydratase (DH) and enoylreductase (ER) domains. At the end of the assembly-line biosynthesis, a TE domain cleaves off the acyl chain from the enzyme complex either by hydrolysis or by regioselective macrocyclization. The latter offloading mechanism was also observed in the biosynthesis of the gulmirecins, which are produced by the predatory myxobacterium *Pyxidicoccus fallax.*[36] Many PKs, including the gulmirecins, are further subjected to post-assembly line modifications, such as acylations and glycosylations. Overall, the assembly of gulmirecins represents almost a textbook example of modular PK biosynthesis, except that the AT domain for the activation of the starter unit is located in the first extension module and not in the loading module (Figure 1.4) Another peculiarity is the optional skipping of DH and ER domains, in the termination module, which was also described in the biosynthesis of the structurally related disciformycins.[57″49]
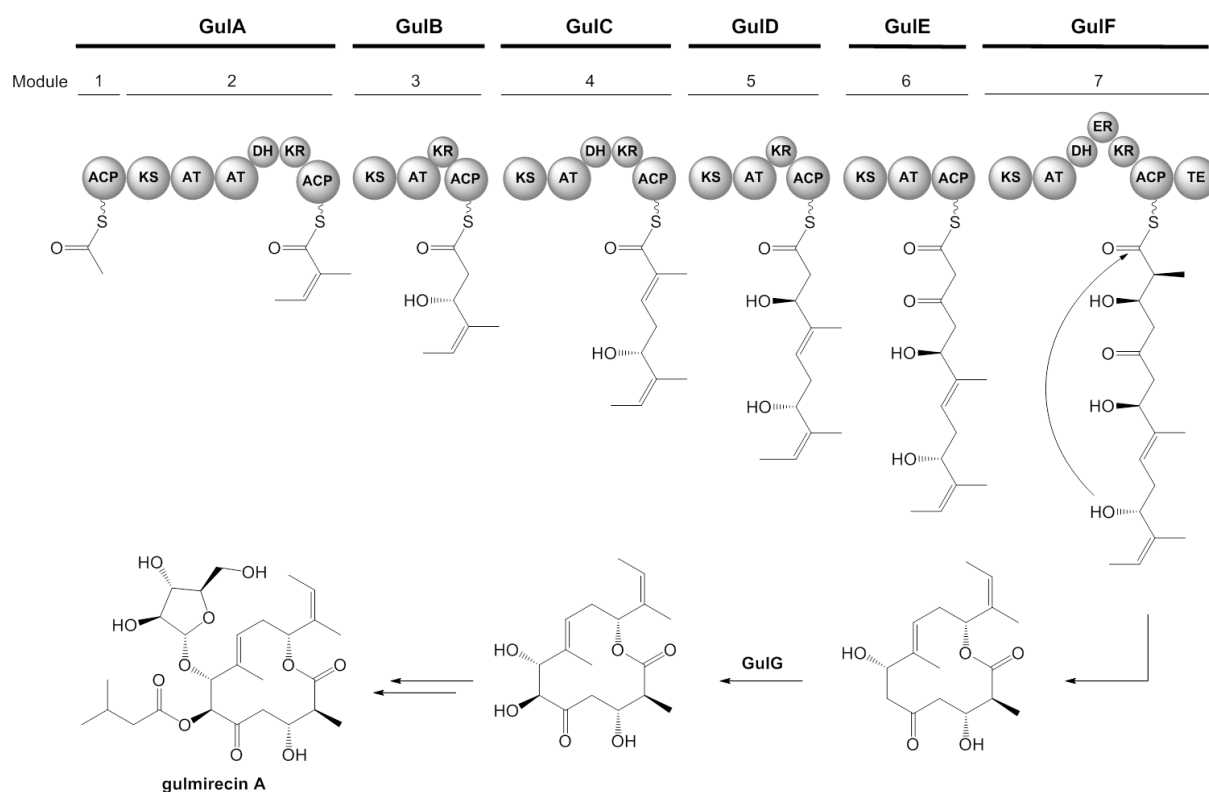
Figure 1.4 PKS assembly line and biosynthesis of gulmirecin A.
The ACP domains are depicted with the growing acyl chain.[49]

1.3.4 NRP-PK hybrid compounds

The text in this paragraph was taken with minor modifications from publication [C] of the author:

"In consideration of the similar construction mechanisms that are used by NRPSs and PKSs, it is no surprise that these two enzyme classes can also act in concert and, thereby, form mixed or hybrid assembly lines. All intermediates in NRP and modular PK biosynthesis are covalently bound to carrier proteins via thioester bonds, which guarantees a smooth transfer from a PKS to an NRPS module (or vice versa). Examples for secondary metabolites which derive from NRPS/PKS assembly lines are siphonazole and auriculamide (Figure 1.5), both of which were reported from predatory bacteria of the genus *Herpetosiphon*.[58,59] Soon after the discovery of siphonazole, feeding studies with isotopically labeled precursors indicated its mixed biosynthetic origin.[58] More recently, the biosynthetic gene cluster for the production of siphonazole was identified and the annotation of this locus revealed an assembly line consisting of 12 modules with a highly unusual domain architecture.[60] In the case of

auriculamide, a retrobiosynthetic analysis was conducted to trace candidate NRPS and PKS genes for its production in the genome of *H. aurantiacus.*[59] Subsequent biochemical analyses supported this assignment.[61"49]
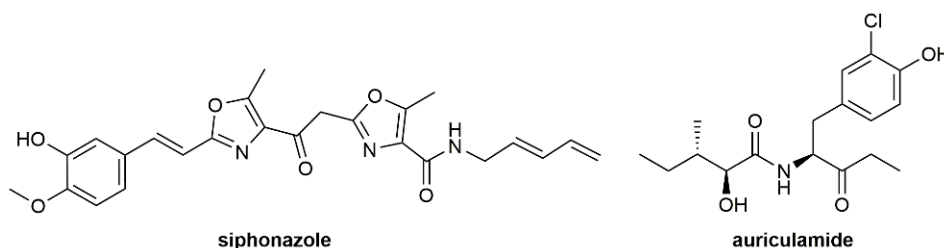
Figure 1.5 Structures of siphonazole and auriculamide.[49]

1.3.5 Natural products highlighted in this thesis

1.3.5.1 Myxochelin-type siderophores

Myxochelins are catecholate siderophores isolated e.g. from the myxobacteria *Myxococcus xanthus*,[47,62] *Stigmatella aurantiaca*[63,64] or *Pyxidicoccus fallax.*[65] They feature two catecholate units that are linked via amide bonds with L-lysine in its α and ε position. The structurally related pseudochelin A, produced by the marine γ-proteobacterium *Pseudoalteromonas piscicida* possesses a characteristic dihydroimidazole moiety.[66] Another variation of the
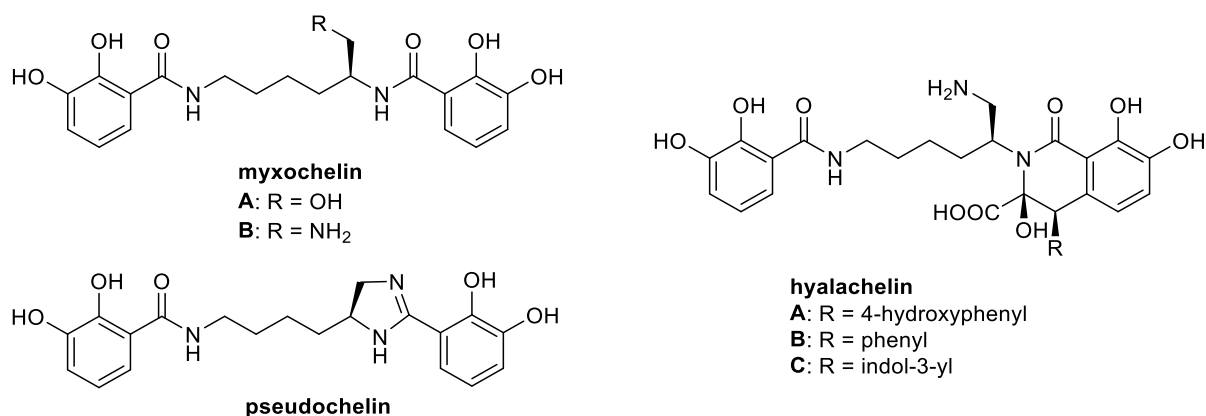
Figure 1.6 Compounds of the myxochelin family.

myxochelin scaffold is displayed by the hyalachelins, which originate from *Hyalangium minutum*. Here, one of the two catecholate unit is integrated into a substituted 1,2,3,4-tetrahydroisoquinoline ring (Figure 1.6).[67]

The assembly of myxochelin and pseudochelin building blocks starts with a compact NRPS system, composed of the three enzymes MxcE, MxcF, and MxcG. This system exhibits several deviations from the normal co-linearity model associated with NRPSs (Figure 1.7). While amino acids are typically channeled into NRPS systems, herein the aryl AMP ligase MxcE activates 2,3-dihydroxybenzoate and passes it onto the aryl carrier protein (ArCP) of MxcF. The enzyme MxcG tethers L-lysine in a similar manner to its PCP and presents the amino acid for two consecutive condensation reactions with MxcF-bound 2,3-diydroxybenzoate. MxcG lacks a thioesterase domain and applies a reductive mechanism for product release. The corresponding reaction is mediated by a C-terminal reductase domain (Red) and initially generates a myxochelin aldehyde intermediate. This reductase stands out through a double function, since it does not only release the assembled molecule from the NRPS enzyme complex, but also optionally catalyzes an additional reduction of the aldehyde, forming myxochelin A.[68] In myxochelin-producing bacteria, which possess the transaminase MxcL, the aforementioned aldehyde may also be converted into myxochelin B.[63,68]

Except for MxcE, MxcF and MscG, the myxochelin locus also encodes the enzymes for the biosynthesis of the aromatic precursor 2,3-dihydroxybenzoate. The 3-desoxy-D-arabino-hepulosonat-7-phosphate (DAHP) synthase AroA$_{A5}$ forms the homonymous early intermediate from phosphoenolpyruvate and erythrose-4-phosphate. DAHP is then further metabolized through shikimate to chorismate, which is converted by the isochorismate synthase MxcD into isochorismate. The latter is a substrate of the isochorismatase (IC) domain, which is exceptionally present in MxcF, cleaving off pyruvate, before MxcC finalizes 2,3-dihydroxybenoic acid synthesis by dehydrogenation. Early in this pathway chorismate may also branch off towards anthranilate biosynthesis, providing an essential building block for tryptophan or aurachin biosynthesis.[63] The aurachin biosynthesis is described in detail in chapter 1.3.5.2 of this thesis. AroA$_{A5}$ appears thus as a key enzyme that directs the biosynthesis of different secondary metabolite precursor molecules.
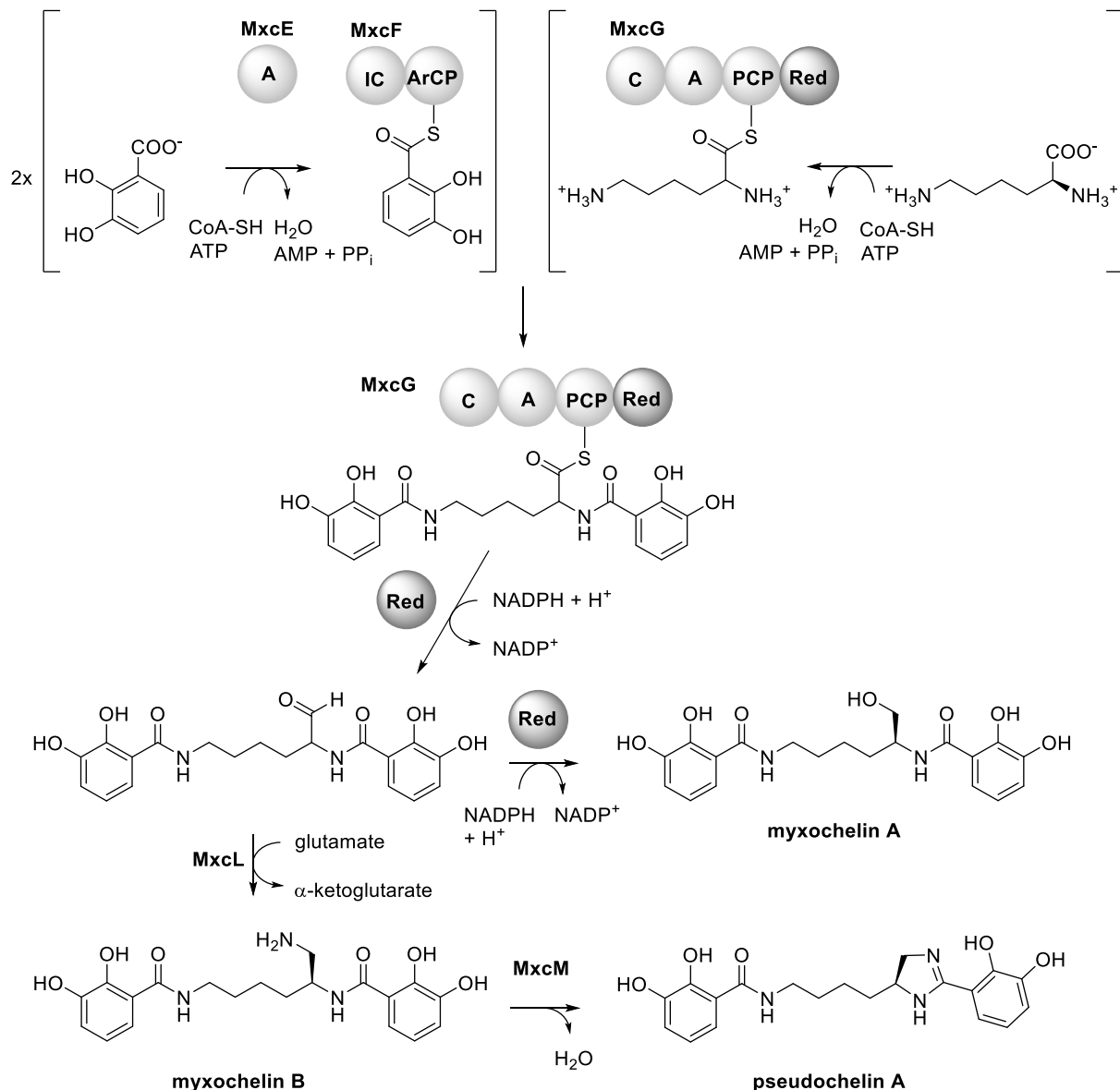
Figure 1.7 Biosynthetic pathway to myxochelin A, B and pseudochelin A.
The NRPS MxcG consists of a condensation (C), an adenylation (A), a peptidyl carrier protein (PCP), and a reductase (Red) domain. An intramolecular cyclization reaction of myxochelin B catalyzed by MxcM forms the dihydroimidazole moiety of pseudochelin A.[63,68]

While the biosynthesis of myxochelins was well understood at the time when this PhD project started, enzymatic conversion towards pseudochelin A was only recently unraveled.[62] Comparison of the *P. piscicida* S2040 genome with known myxochelin biosynthetic gene clusters (BGCs) disclosed an additional gene present in the former. Thereupon, the amidohydrolase MxcM was identified as the key enzyme that enables pathway extension from myxochelin B to pseudochelin A. *M. xanthus* produces myxochelin B as the main siderophore

but is devoid of *mxcM* and, therefore, not capable to synthesize pseudochelin A. This myxobacterium was thus selected for experimental "pathway combineering" with MxcM. Plasmid-based expression of *mxcM* in *M. xanthus* FB triggered the production of pseudochelin A, as expected.[62] The genetically engineered strain, *M. xanthus* pJK5, showed significant conversion of myxochelin B into pseudochelin A with an approximate rate of 50%. *In vitro* studies with the isolated His-tagged enzyme confirmed that MxcM is the responsible catalyst, which functions independent of co-factors and achieves similar turnover rates as observed *in vivo*.[62] The biosynthetic origin of hyalachelins remains still elusive, though myxochelin B was suggested as an intermediate, extended by a phenylalanine, tyrosine or tryptophan moiety.[67]

Myxochelins stand out through their anticancer and antiinflammatory properties. Myxochelin A inhibits colon-tumor cell invasion[69] and was thus identified as a promising lead structure for drug development. The myxochelins further exhibit antileukemic and antiinflammatory bioactivities correlated with their inhibition of the human 5-lipoxygenase (5-LO) as demonstrated first by Schieferdecker *et al.* for myxochelin A and C.[65] This key enzyme in the cascade from arachidonic acid to pro-inflammatory leukotriene A_4 carries a non-heme iron as the central element in its active center. Due to their nature as catecholate siderophores, it was initially hypothesized that iron complexation might cause 5-LO inhibition, as shown e.g. for the known inhibitor zileuton.[70] Testing a set of aryl-modified myxochelin A analogs for their iron chelating properties and likewise 5-LO inhibition indicated though that there is no correlation between these two features, but there must be another, yet to understand, mechanism.[71] Pseudochelin A was previously tested negative in an anti-inflammatory assay for inhibition of TNF-α production, as well as an anti-convulsive zebrafish model and antimicrobial bioactivity.[66] Investigation of its activities towards 5-LO inhibition are subject of this thesis. Except for their siderophore functions, no outstanding bioactivities were reported for hyalachelins to date.[67,72]

1.3.5.2 Aurachins

The aurachins are a group of quinoline-derived natural products initially isolated from the myxobacteria *Stigmatella aurantiaca* Sg a15[73] and *Stigmatella erecta* Pd e32,[74] but later also discovered in actinomycete bacteria, as *Rhodococcus* sp.[75] or *Streptomyces* sp.[76,77] From the

genus *Stigmatella* 12 derivatives were reported, namely aurachin A – I, K, L and P. These quinolines vary in the positioning of their farnesyl side chain, in their oxygenation pattern and in the occurrence of additional ring systems (Figure 1.8).[73,74]
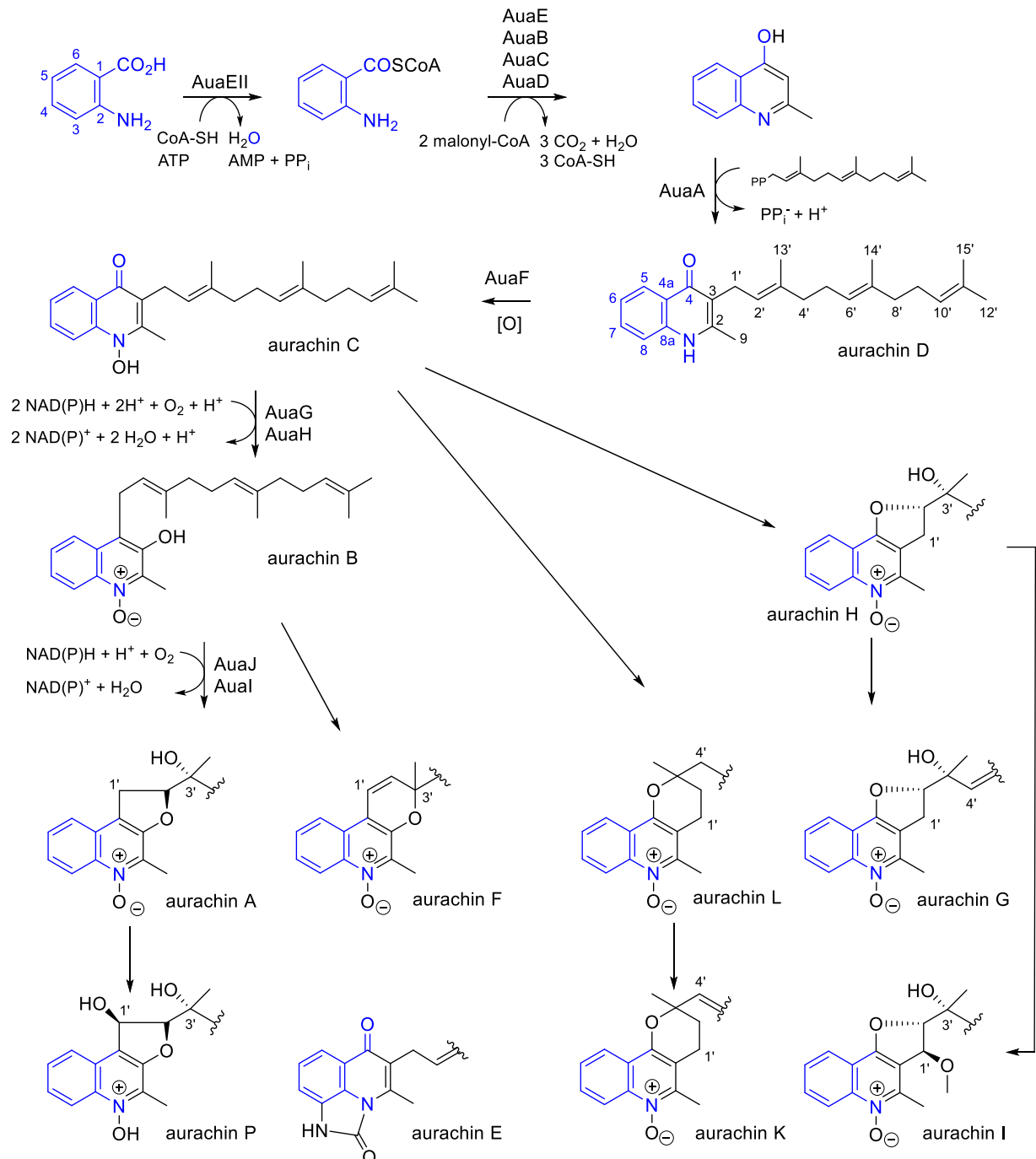
Figure 1.8 Biosynthetic pathway to aurachins.
The anthranilic acid building block is highlighted in blue.[73,74,78–83]

Biosynthetically, the aurachins originate from an unusual type II PKS system forming the core structure.[78,79] First, anthranilate is activated and loaded by the anthraniloyl-CoA ligase AuaEII and the anthraniloyl-CoA:ACP acyltransferase AuaE.[78] In comparison, both enzymes show a low sequence identity of 28% but their aryl binding sites exhibit high similarity and yet they catalyze two distinct reactions.[79] While AuaEII forms the anthraniloyl-CoA thioester, AuaE is responsible for substrate transfer onto the acyl carrier protein AuaB.[78,79] Afterwards AuaC and AuaD catalyze two successive decarboxylative Claisen condensations of the activated anthranilate with malonyl-CoA to produce 4-hydroxy-2-methylquinoline.[78,79] During these reactions AuaB holds the substrate in place, while AuaC (KSα) and AuaD (KSβ) act as ketosynthase and chain length factor, respectively.[78,79] The 4-hydroxy-2-methylquinoline intermediate is substrate of the prenyltransferase AuaA, which attaches a pyrophosphate-activated farnesyl residue in position 3 of the quinoline core. The product represents the first aurachin derivative in the biosynthetic cascade and is known as aurachin D.[82]

In the following, the oxidation by the Rieske [2Fe-2S] oxygenase AuaF introduces an *N*-hydroxy group forming aurachin C.[83] The relocation of the isoprenoid side chain to position 4 is carried out by AuaG and AuaH and leads to aurachin B. Briefly, a 2,3-epoxidation by the FAD-dependent oxidoreductase AuaG prepares for the following rearrangement, which was proposed to follow a semipinacol mechanism[84] or retro-Wittig/Claissen reaction sequence,[85] prior to a final reduction by AuaH.[84,85] Aurachin B can be further processed by the FAD-dependent monooxygenase AuaJ and the putative steroid delta-isomerase AuaI. While first a 2'-3'-epoxidation takes place, AuaI then facilitates epoxide opening through an intramolecular nucleophilic attack from OH-3, resulting in 3'-hydroxylation at the farnesyl, forming aurachin A.[83]

Genomic analysis of *S. aurantiaca* Sg a15 showed that the aurachin biosynthesis genes are distributed on three different loci in the chromosome and therein, additional genes are located with yet unknown functionalities. Up to now, no genes with a putative role in aurachin E-L and P biosynthesis were identified. It is therefore assumed that these aurachins result from unspecific derivatization by housekeeping enzymes or spontaneous reactions.[83] For aurachin E, a non-enzymatic synthesis was proposed, potentially resulting from artifact formation during isolation and purification.[80,81]

Promising bioactivities were reported early on for the aurachins, when these compounds were found to have antibacterial and antifungal effects. Unfortunately, however, these activities are accompanied by strong cytotoxicity, resulting from inhibition of the electron transport chain.[86] Subsequent investigations revealed that the aurachins inhibit complexes I and III of the respiratory chain, as well as photosystem II and the cytochrome b_6f complex.[73,87–91]

Systematic structure-activity relationship (SAR) studies of aurachins mainly focused on the variation of the farnesyl side chain in aurachin D.[92–94] While *in vitro* inhibition testing on respiratory complexes of *Escherichia coli* did not show any significant differences between aurachin D and analogs with truncated prenyl side chains,[92] the antimicrobial and cytotoxic activities of the derivatives were clearly reduced,[93,94] likely due to cellular uptake issues. Similar loss of bioactivity was reported for major expansion of the quinolone core by synthetic introduction of a 5,6-bound benzene or 6,7-methylenedioxy unit.[93] Further SAR studies on the aurachins are subject of this thesis.

1.4   Natural products from myxobacteria

1.4.1 Chemical diversity found in myxobacteria

Already since the discovery of the first myxobacteria by Thaxter at the end of the 19th century their peculiar lifestyle seized the attention of scientists.[95,96] These bacteria are typically found in soil, on decaying wood or animal dung[97] but occur also in marine environments[98] and thus live under frequently changing, partly harsh ecological conditions. They cope with these circumstances as they can generate resistant forms as myxospores or corresponding fruiting bodies as part of a dynamic developmental cycle that allows them to adapt in periods of limited nutrient supply and other unfavorable settings.[99] In addition, myxobacteria exhibit an exceptional collaborative behavior within a population, enabling coordinated swarming and gliding over surfaces that eventually facilitates a joint-effort predatory strategy observed in a range of myxobacterial families.[99] This tactic is often referred to as "wolf pack predation", since the members of a swarm collaborate to attack and kill other bacteria, similar to the coordinated and cooperative hunting observed in wolves.[42,100,101]

While behavioral observations dominated the early research questions on myxobacteria, it was soon hypothesized that the hunting and lysis of prey may be related to production of lytic enzymes as well as antibiotics[102] and an increased interest in the chemistry of bacterial predation emerged. In 1973 the first antibacterial compound, named antibiotic TA, was isolated from a *M. xanthus* strain and biologically characterized. However, the complete chemical structure remained elusive[102,103] until 10 years later it was proposed to be identical with myxovirescin A_1 from *Myxococcus virescens*.[104,105]

With growing knowledge about suitable cultivation conditions, an increasing number of compounds with diverse bioactivities were discovered in the following years.[102,106–108] Today, myxobacteria are among the most promising sources of natural products in the bacterial world. In 2010 Bérdy reported an estimated total of 17900 bacterial bioactive metabolites, of which 3.5% originate from the *Myxococcales*. While it is noteworthy that other groups as actinobacteria or cyanobacteria made up the largest fractions with 76.5% and 7.2%, respectively, it must be considered that all other identified producers together amount to as little as 12.7%. Thus, the 635 myxobacterial compounds counted in the respective study stand out as the third largest contribution to the bacterial chemical diversity.[109] While the precise number of derivatives varies in literature, there are certainly over 100 different core structures found exclusively in myxobacteria to date.[107,108,110] Therein, all major classes of compounds are represented, ranging from NRPs, PKs, NRP-PK hybrids and terpenes to RiPPs.[107,111] Further, they include unclassified types as the phenylpyrrole pyrrolnitrin,[16] the polyene ethers maracin and maracen,[18] or the acyloin-type soraphinols.[112] They display chemical features rarely found in other bacterial producers, as e.g. beta-methoxyacrylates found in cyrmenin[113] or myxothiazol,[114] as well as true steroid compounds.[115–117] Further, they employ unusual precursors in their biosynthetic machineries, including branched-chain acids like isovalerate, iso- or 2-methyl butyrate units derived from amino acids like leucine, valine or isoleucine, but also benzoate or cinnamate starter units, which are usually found in plants or cyanobacterial biosyntheses[116] (Figure 1.9).
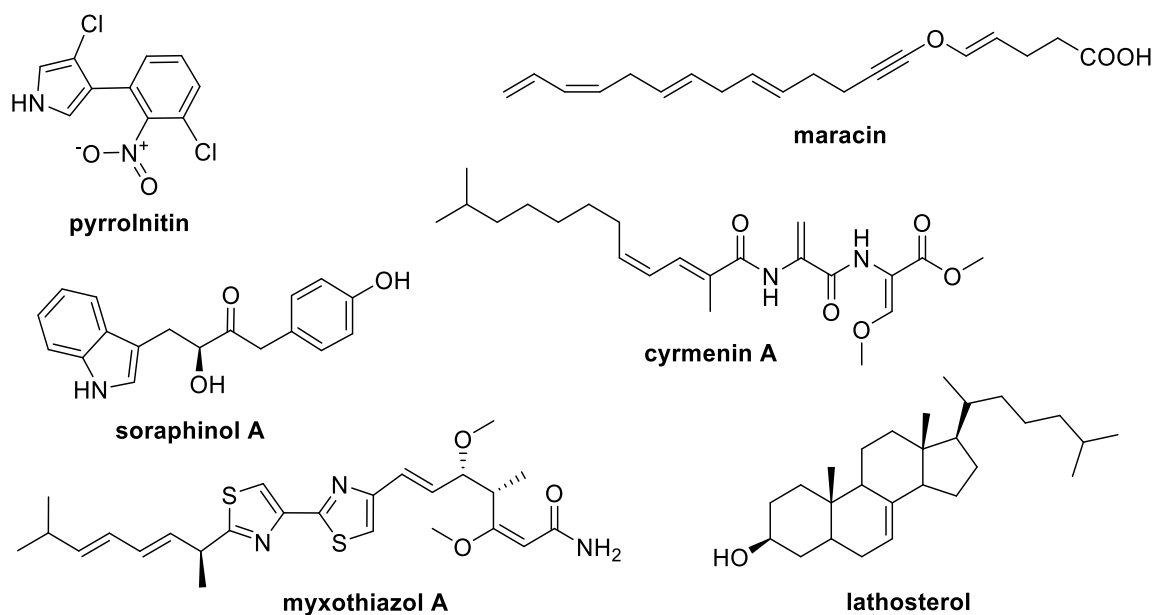
Figure 1.9 Natural products from myxobacteria.

1.4.2 Biosynthetic potential of myxobacteria and genome mining approaches

Success in identification of new secondary metabolites was greatly enhanced by the increasing availability and quality of genome sequencing data. Already in the 1970s and 80s the first biosynthetic genes were characterized in *Streptomyces* spp.*,* leading to a growing understanding of the functionality of biosynthetic processes and their genetic fundamentals.[118] The gene cluster coding for the polyketide soraphen A was the first one identified from a myxobacterium in 1995.[119] The corresponding locus was found by homology searches against *Streptomyces violaceruber.* This was until 1999 the only completed PKS cluster from myxobacteria. At the same time, in 1995, the NRPS cluster for saframycin Mx1 biosynthesis was discovered in *M. xanthus* Mx x48 and DM504 and characterized over the following decade.[120–122]

In 1995, another major breakthrough was reported with the publication of the first complete bacterial genome from *Haemophilus influenzae*.[123] Another 10 years later, sequencing of the first closed myxobacterial genome was accomplished, as the rather unusual *Anaeromyxobacter dehalogans* 2CP-C dataset was published by the U.S. Department of Energy Joint Genome Institute (DOE JGI) in 2006, with a size of 5 Mb.[124] In the same year The Institute for Genomic Research (TIGR) completed sequencing of the significantly larger 9 Mb

genome of the myxobacterial model strain *M. xanthus* DK1622.[123,125] With the rise of next generation sequencing techniques, increased affordability and thus accessibility, many more myxobacterial strains were sequenced and analyzed.

At the time of writing this thesis, the National Center for Biotechnology Information (NCBI) GenBank hosts 34 complete myxobacterial genome entries. The myxobacterial genomes vary significantly in size. While the chromsome of *A. dehalogans* is comparably small, with about the size of an *Escherichia coli* chromosome, the other myxobacterial chromosomes range from around 9 Mb in the *Cystobacterineae*[125,126] or 12 Mb in *Nannocystineae*,[127] to 16 Mb in representatives of the *Sorangineae.*[128]

The availability of fully sequenced genomes builds a valuable resource for various analyses addressing the evolution of genomes or the genes involved in signal transduction, fruiting body formation[123] or predation.[129] The field of natural products benefits particularly from the availability of this data, since it allows to uncover the hidden biosynthetic potential of the strains, which was previously not accessible through purely chemical approaches. They enable innovative methods for "genome mining", aiming at correlation of molecules with their biosynthetic origins by assigning gene clusters to the respective compounds and genes and respective enzymes to distinct chemical moieties in the final metabolite. Conversely, analysis of DNA sequences allows prediction of the metabolic products, even if the encoded compounds are unknown. These applications range from pure bioinformatics *in silico* tools towards automated analyses for identification of genetic elements as well as their functional annotation, to applications combining genome data with chemical or analytical elements.[51] Their success is driven by the growing knowledge about the architecture of the enzyme machineries and the respective genetic elements involved, as the experimentally proven datasets enable and support predictions.

Classical genome analyses rely on homology searches against core enzymes involved in the assembly of secondary metabolites as PKs, NRPs, RiPPs or terpenes. These biosynthesis enzymes show a high degree of conservation in their amino acid sequences, which is harnessed to screen genetic libraries for homologues and thus identify further candidate enzymes and gene clusters surrounding the detected anchor element.[118] In PKSs, the AT or KS and in NRPSs the C or A domains make suitable probes.[51] Additionally, in the AT domains of

PKSs, the conserved GHSxGE motif allows prediction of the substrate specificity[130] and for A domains in bacterial NPRSs the Stachelhaus code describes the patterns that determine amino acid specificity.[131] For terpene clusters known terpene synthases and cyclases can serve as genetic probes. In RiPP mining, class-specific enzymes are used, as for example LanM dehydratases or ATP-dependent cysteine proteases for lanthipeptides or lasso peptides, respectively.[132] Besides conserved regions there are though many exceptions found that limit pure homology-based computational predictions and impose the necessity of complementary experimental data. For examples some domains exhibit loose substrate specificity, allowing the introduction of different building blocks and thus creation of derivatives. Specific modules may also deviate from the co-linearity observed in "classical" type I PKSs or NRPSs and rather function in an iterative fashion which hampers predictions, a phenomenon often observed in myxobacteria,[133] e.g. in the biosyntheses of alkylpyrones[134] or flaviolin.[135] Recent review articles even concluded that only a minority of pathways follows the simple, predictive logic and the majority require experimental analysis.[136–139] Moreover, the sequences of some enzymatic sites catalyzing additional tailoring reactions on the core molecule as macrolactonization, glycosylation and hydroxylations do not suffice for reliable predictions yet.[137]

By now a representative collection of myxobacterial gene clusters were identified and characterized.[133] As earlier exemplified for saframycin Mx1, soraphen A and others,[133] initial research efforts focused on the identification of clusters corresponding to known compounds, laying a solid foundation for the more challenging task to identify unknown compounds based on genetic information, facilitated by the biochemical precedencies and examples studied. Thereby, the combination of sequencing and chemical data led to success in the identification of a range of compounds.

Among the most prominent examples for a combined effort of bioinformatics and chemistry is the discovery of the polyene salinilactam A from the marine streptomycete *Salinispora tropica* CNB-440.[140] A primary genome screening revealed the plurality and diversity of natural products gene clusters encoded, although the draft genome could initially not be fully assembled. The uncharacterized *slm* biosynthetic gene cluster got into focus of detailed investigation and revealed a 10-module PKS system that was predicted to code for a polyene

macrolactam compound. Chemical analysis of the UV chromatogram identified peaks with characteristic absorption spectra associated with such conjugated double bond systems, guiding the isolation of salinilactam A. The structure elucidation was hindered by fast compound degradation and interpretation of NMR analyses constrained by signal overlay resulting from the repetitive polyene part of the molecule. Therefore, the exact composition of the molecule remained initially unclear. By the logic of the co-linearity rule, the domain analysis of the PKS system focused on the reductase functionalities, guided an *in silico* prediction of a hypothetical structure that was eventually verified by complementary NMR experiments. In course of this endeavor the biosynthetic gene cluster (BGC) was also assembled and the difficulties around repetitiveness were circumvented by the information provided by the chemical structure. In this particular case, closure of the BGC also facilitated completion of the genome assembly based on the interdependent trinity of bioinformatic analysis of the cluster, theoretical product prediction and chemical analyses.[140]

Limitations to such predictions were for example described in course of discovering the myxochromide derivatives S_{1-3} from *Stigmatella aurantiaca* DW4/3-1. Analysis of their NRPS/PKS hybrid gene cluster disclosed the presence of only one PKS module. Its targeted knock-out readily abolished three peaks in the UV chromatogram with global maxima at 420, 406 and 424 nm. Their similar UV absorption profiles indicated that these three belong to the same group of compounds and the presence of a larger conjugated system therein, appearing as a polyunsaturated side chain. Detailed analysis disclosed the iterative type I PKS nature of the module, including a complete reductive loop composed of a KR, DH and an ER domain, though the latter appears to be inactive. The repetitive chain elongation alternates between 8 or 9 cycles and it can accept likewise acetate as well as propionate starter units, leading to the three derivatives S_{1-3}. These findings are further complicated by an additional module skipping in the NRPS part of the biosynthesis, yet the compounds show the same peptide core and variations appear only in the polyene tail. Overall, the structure of these myxochromides would not have been reliably predictable solely from the genetic information, but chemical analysis proved to be indispensable to identify iterations and flexibility in precursor selection.[141]

This example also applied deuterium-labelled precursor feeding to verify the origin of biosynthetic building blocks. In modified version, this method can also help to identify compounds in a mixture or crude extract. In case the genetic information allows prediction of the substrate specificity, targeted feeding and comparative analysis may be key to connect genetic information to the chemical counterpart. This can be conclusive in GC-/LC-MS set-ups where a specific mass shift is expected, and likewise in NMR experiments where NMR-active cores may be introduced and enriched (e.g. $^{13}C/^{15}N$) or abolished through an exchange of ^1H with ^2D. In the discovery of 2-hydroxysorangiadenosine from *Vitiosangium cumulatum*, likewise combined chemical and genetic efforts were exerted. Upon compound isolation and structure elucidation of the sesquiterpene-nucleoside, the biosynthetic origin from adenosine and leucine was unraveled through feeding of labelled building blocks. Sequencing confirmed genes coding for the underlying precursor-supply pathway and the respective gene cluster found through homology search for terpene and diterpene cyclases.[142]

A number of myxobacterial compounds were discovered by an approach combining mutagenesis and metabolic profiling, in which postulated biosynthetic pathways were disrupted by targeted gene knockout. A comparison of the metabolic profiles from mutant and wildtype strain through HPLC-UV/VIS or -MS detection then led to the identification of peaks associated with the targeted pathway. This approach is still a gold standard for straight-forward correlation of a postulated genetic origin to a corresponding compound, resulting e.g. in the discovery of the PKS-NRPS clusters of rhizopodin in *S. aurantica,*[143] macyranones in *Cystobacter fuscus,*[144] or the RiPP genes of crocagins in *Chondromyces crocatus*.[145] In all these cases, the genetic and chemical methods go hand-in-hand with each other. The NRP myxoprincomide is even named after the principal component analysis (PCA) used to identify this compound, by a combination of targeted mutagenesis with LC-HRMS screening of extracts and statistical analysis thereof.[146]

Another approach is used in mining based on resistance genes. BGCs may often not only include or neighbor the genes relevant for production of the encoded compounds, but also regulatory elements, transporters or resistance mechanisms as degrading enzymes or modified target proteins.[118] This logic was applied e.g. in a self-resistance guided search for topoisomerase inhibitors in *Pyxidicoccus fallax*. Knowing that the gene product may function

as an antibiotic itself, the producing strain must carry an inherent detoxifying mechanism as self-protection. Targeted search for the resistance-conferring pentapeptide repeat protein (PRP) genes in the genome of *P. fallax* led to the discovery of a BGC. Its heterologous expression yielded pyxidicyclines that had indeed the predicted antibiotic activity.[147] Similarly, a group of alkylpyrones was identified from *M. xanthus*.[134] Alternatively, the search may also follow a target-based strategy, where additional copies of housekeeping genes in close proximity of BGCs may identify these as a potential target of the encoded secondary metabolite. The encoded homologous protein may represent a variation that prevents self-inhibition, while the essential function is maintained. The discovery of the thiotetronic acid BGC guided by a fatty acid synthase analog may serve as an example for a target-based strategy.[148] Regulatory elements are often associated with BGCs, connecting them with primary metabolism or external stimuli, such as the availability of trace metals. Variation of such related specific parameters were harnessed for example to access siderophores that were silent under laboratory cultivation conditions or to increase production yields in the native producer. Metabolic profiling of a *Massilia* sp. under iron-limited as well as iron-saturated conditions yielded massiliachelin as a new siderophore.[149] Since the genetic background of iron or zinc regulation is well understood,[150] targeted search for such controlling elements on the genetic level facilitates screening for correspondingly regulated BGSs. The search for similar regulator binding sites in a genome may also identify co-regulated genes that belong to a coherent cluster. This is for example exploited in the application CASSIS,[151] that is specialized towards fungal systems where genes of the same BGC are highly co-regulated.[152]

1.4.3 *In silico* screening for overall genetic potential

As exemplified in the previous section, a multitude of methods are available to analyze genetic information and to predict secondary metabolite gene clusters in bacterial genomes. This cannot only be applied to specific case studies, but more generally allows a targeted and efficient decision which organisms or gene clusters might be of particular interest. A widely applied tool is the "antibiotics and secondary metabolite analysis shell" (antiSMASH), which predicts not only the location and size of the genes, but also reports BLAST analyses and proposes compounds correlating with the clusters.[153]

An overall analysis of a set of myxobacterial genomes revealed that an average of 13.0% of their full genome is dedicated to secondary metabolism.[126] Among the analyzed myxobacteria, a remarkable difference is observed between the four predatory Myxococcaceae, that allot about 14.7% of their genetic capacity for these functions and the two cellulolytic Sorangiineae strains with 9.5%, which allows to hypothesize that predatory representatives display a higher density of BGCs within their genomes, which supposedly may account to their complex lifestyle and predatory activity.[126] Comparable potential percentage is otherwise only found in actinobacteria and fungi.[154]

More extensive studies ascertained the untapped biosynthetic potential encoded in the myxobacteria[155–157] and showed that greater taxonomic distances also come along with the likeliness to find chemically distinct compounds.[158] These insights allow prioritization of strains based solely on their genetic information, tackling the constraint of rediscovering known compounds, as it allows to focus on the features with unknown properties. It may also help to find strains that produce similar compounds or enzymes in targeted search for derivatives with potentially improved (bio)activities. This was exemplified in the search for myxochromides, yielding four new lipopeptides of this natural product family.[159] Thorough analyses of the BGC architecture provide also information about their evolutionary origin. In case of the aurafuron BGC it was suggested that its ketosynthase domains are more closely related to those from myxobacteria, than to KS domains from *Streptomyces* spp. that produce similar compounds.[160]

As outlined above, many natural products have been discovered through methods based on an increasing understanding of their genetic origin and biosynthesis. Despite these many successes, several drawbacks remain. For example, many of these predictions rely on data of known genetic elements and compounds. This potentially hinders the discovery of truly new features and chemistry, since unprecedented structures are difficult to predict. Heterologous expression of genes and clusters with unknown functions could provide access to new compounds, but although expression systems have advanced in recent decades, this theoretically simple approach is often hampered by, for example, incompatibility of regulatory sequences, differences in GC content or codon usage, and lack of modifying enzymes encoded outside the chosen cluster.[83,161]

1.5   Diversification and labelling of natural products

Natural products can be derivatized by a range of methods, from total synthesis to production of hybrid compounds in genetically engineered microorganisms. In comparison to many synthetic methods, biotechnological means allow derivatization in a regio- and stereocontrolled manner.

1.5.1 Precursor-directed biosynthesis and mutasynthesis

A rather simple method to generate natural product derivatives is the supplementation of microbial producers with analogs of biosynthetic building blocks. Suitable precursors include e.g. halogenated amino acids, aryl carboxylic acids or fatty acid analogs. Given that these molecules are taken up by the cells and they do not exhibit relevant toxicity to the chosen strain, they may replace the natural substrate in the biosynthesis.[162] This effort, known as precursor-directed biosynthesis is particularly promising in the field of natural products, since enzymes involved in secondary metabolism are known to exhibit a broader substrate tolerance as those from primary metabolism.[163] This straight-forward approach does not allow targeted incorporation towards a selected derivative. Instead, it generally leads to precursor flow into multiple derivatives along with the natural compound. This complicates subsequent purification efforts.[162,164] Yet, this *in vivo* method allows to use long biosynthetic pathways and circumvents protein purification or cofactor regeneration. Its applicability may though be hindered by the limited substrate tolerance of the biosynthetic units downstream of the promiscuous module.[165] An advancement of this technique was introduced as "mutasynthesis". Targeted inactivation of a gene involved in precursor or intermediate biosynthesis eliminates the competition between the natural and an artificial building block, as the production of the former is abolished. Mutasynthesis increases the yield of the desired natural product analog, because the native form is not produced.[164,166,167] This method is though limited when molecules from primary metabolism are involved, like proteinogenic amino acids or malonyl-CoA, because their production is vital for the cell. Both techniques, precursor-directed biosynthesis and mutasynthesis, harness enzymatic substrate tolerance which likewise limits the possible conversions. By means of genetic engineering, substrate specificity and thus product yield may though be improved.[168–171]

Precursor-directed biosynthesis is of particular relevance for this thesis, to explore the plasticity of biosynthetic pathways, to generate derivatives for SAR studies and as chemical probes for natural products discovery. Not only modular biosynthesis assembly lines, like NPRS, PKS and their hybrids, but also ribosomal peptide synthesis[172] or non-modular biosyntheses[173–175] are accessible for external precursor supply.

Most polyketides use malonyl-CoA and methylmalonyl-CoA as building blocks. Due to their inherent substrate specificity, only a modest variety of chemical functionality is found, including extender units modified at the C2 position with various alkyl chains, amines, hydroxyls, and halogens.[176–178] In addition, specialized starter units can prime not only the classical acetyl or propionyl-CoA, but also benzoic or fatty acid derivatives.[79,134,179]

This enzyme flexibility was used e.g. in derivatization of the myxobacterial epothilone C. Heterologous expression of the respective biosynthetic machinery in *E. coli* provided a suitable platform to feed a synthetic SNAC-derivatized intermediate. The final three enzymes of the pathway facilitated production with the same titer as observed in the native producer, but with the advantages of fast growth and stable production in the heterologous host.[165]

In soraphen biosynthesis, a set of halogenated aromatic starter blocks was channeled into the PKS pathway of *Sorangium cellulosum*, replacing the native benzoyl-CoA. This revealed not only the enzymatic discrimination between phenylalanine, cinnamate and benzoate starters, but also the preferred acceptance of fluoro precursors over the chloro and bromo analogs. This provided an insight into the biosynthetic details and allowed SAR studies of their antifungal activities against the plant pathogen *Botrytis cinerea*.[180] In another study, an engineered *E. coli* strain, harboring biosynthetic prerequisites for heterologous production of erythromycin was harnessed to introduce alkyne and alkene functionalities into the pathway. This led to the identification of an alkyne derivative equipotent to the natural antibiotic and yet functionalized with a handle for subsequent modifications by so-called "Click chemistry" (see chapter 1.5.2).[181]

Moreover, A domains of NRPS may be used even more efficiently to shuttle new features into natural products through modified amino acids. Supplementation of a *Chrondromyces crocatus* culture with fluorotryptophan yielded the respective chondramide derivatives[182] and

similarly vermittilin was derivatized in its fungal producer.[183] Equally, halogenated tyrosines and phenylalanines were successfully used to generate modified peptide cores of uridyl- or lipopeptides.[184,185] Alkyne and azide amino acids are also tested as precursors for these assembly lines. There is no standard protocol established, yet a growing number of studies exemplify the potential of NRPS promiscuity. The feeding of *Microcystis* strains with diverse amino acids featuring terminal alkyne and azide moieties yielded over 40 different microcystins. Through the newly introduced functionalities, a fluorogenic dye could be coupled and the effects on its cytotoxicity investigated. Both modifications had no effect on the bioactivity giving insight into the SAR of this compound class.[186] Targeted engineering of NRPS adenylation domains can be applied to even further use these assembly lines for incorporation of functionalized amino acids.[187] In PKS/NRPS assembly lines that incorporate fatty acids, analogs of those provide another gateway to introduce new chemistry, as shown for antimycins[188,189] or micacocidins.[190]

1.5.2 Bioorthogonality and Click chemistry

The aforementioned "Click chemistry" is a powerful tool widely applied in modern chemistry. Its principle and potential lies in the desirable advantages, as Click reactions can be performed in aqueous environments at modest temperatures. Furthermore, these reactions are stereospecific, they give high yields and only unproblematic byproducts. Of particular interest for biochemical applications is, that these reactions are defined as bioorthogonal, since the two specified reaction partners exclusively undergo the targeted reaction, without interference with common biomolecules. This allows *in situ* reactions in mixtures before complicated purification steps are undertaken.[191,192] A great variety of such reactions were developed in recent years, including reaction pairs as *trans*-cyclooctene or alkenes with tetrazine, thiols with alkenes or alkynes under light activation, dienes and dienophiles as Diels-Alder reactants as well as dibenzocyclooctyne or terminal alkynes with azides and more.[193]

A catalyzed version of the thermal Huisgen reaction, the copper(I)-alkyne/azide cycloaddition (CuAAC), is among the most commonly applied reactions in Click chemistry.[194] Through the Cu+ catalyst, alkynes or cyanides and azides react in a directed fashion, forming a 1,2,3-triazole or tetrazole ring, respectively, that connects both reactants (Figure 1.10). It is considered the

only universal Click reaction, since many others are not truly biorthogonal, limiting their applicability.[194]
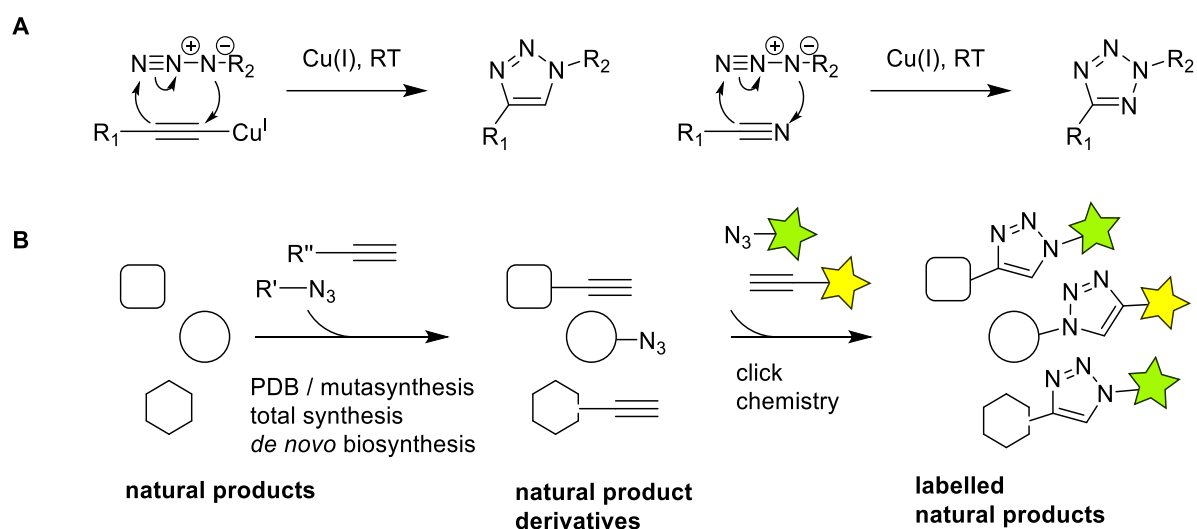
Figure 1.10 CuAAC reaction in natural products research.
A. Reaction scheme of an alkyne-azide and nitrile-azide reaction under Cu(I) catalysis[194] **B.** Applications of natural products derivatization coupled with Click chemistry. (Modified after Zhu and Zhang, 2015)[195]

In natural products research, Click chemistry was previously applied in total synthesis of biomolecule analogs,[196–198] and in a combined chemoenzymatic approach. Therein, synthetic peptide backbone analogs of the glycopeptide antibiotic tyrocidine were prepared, containing propargylglycine units instead of the natural amino acids. These were macrocyclized via the natural Tyc TE domain, and this scaffold derivatized through CuAAC with diverse sugar moieties. The resulting compounds gave SAR insights and yielded congeners with an improved therapeutic index over the natural product.[199] Such handles can likewise be used to link two molecules of different functionalities towards dual drugs, (e.g. with anti-proliferative and anti-inflammatory activity)[200] or to couple them for drug delivery with nanocarriers[201] or hydrogels.[202] It also became a valuable tool to study modes of action in target identification of natural products[203–205] or, similarly, to examine the catalytic A domain activities of NRPS. For the latter, alkyne-modified probes were added *in vitro* to A and holo-PCP domains, either purified or in cell lysates. After activation of the probe and binding to the PCP, these were subjected to a CuAAC Click reaction with biotin azide, covalently linking biotin to the domain. Streptavidin-coated solid phase was subsequently applied to pull down only activated proteins

from the mixture, and correlate activating vs. non activating A domains with the alkyne substrates.[206]

Also in *de novo* drug discovery, Click reactions can be applied to detect compounds with natural alkyne functionality, as described for the prymnesin toxins,[207] or to trap unstable polyynes from crude mixtures to circumvent their degradation and enable structure elucidation.[208] One method developed is based on derivatization of raw extracts that are expected to contain alkyne-bearing metabolites. The azide counterpart is coupled to a fluorophore which is bound to solid support beads. Separation of the solid phase was used to pull out the desired compounds that were released through linker cleavage and subsequently subjected to HPLC-UV and -MS analysis. Similarly, this method serves as a tool to guide purification through chemodosimetric identification of relevant fractions.[209]

2 Scope of this Thesis

Natural products make important lead structures in drug development. Additionally, many microbes were identified by genome sequencing as resources for the discovery of yet unknown compounds. This thesis is comprised of three parts, aiming at the diversification of the bioactive myxochelins and aurachins in order to conduct SAR studies as well as *de-novo* compound discovery through chemical labelling of suitable target molecules.

2.1 Myxochelin- and pseudochelin-derived lipoxygenase inhibitors

Myxococcus xanthus is a natural producer of myxochelins A and B. Recently, its biosynthetic pathway was complemented with MxcM, an enzyme necessary for pseudochelin A biosynthesis.[62] Herein, both, the wild type and genetically engineered *M. xanthus* strains were probed through precursor-directed biosynthesis for incorporation of non-natural building blocks. Supplementation with 2,3-dihydroxybenzoic acid analogs featuring different hydroxy or fluoro substitution patterns are subject of this experiment, towards subsequent SAR studies. Since myxochelin A is known as an inhibitor of the pro-inflammatory enzyme human 5-lipoxygenase,[65] the inhibitory effects of myxochelin B, pseudochelin A and the newly generated derivatives are studied in chapter 4.1.

2.2 Precursor-directed biosynthesis of unnatural aurachins

The aurachins were early on recognized to exhibit potent bioactivities as antifungal, antibacterial and antiplasmodial compounds. Yet, previous SAR studies only focused on the farnesyl residue in aurachin C and D.[75–77,92–94] To expand the existing SAR knowledge, creation and testing of aurachin D variants with different substituents on the quinolone core was desired. Anthranilic acid condensed with two malonyl-CoA units are the natural precursors of the quinoline core according to isotopic labelling studies[80] as well as biochemical experiments (Figure 1.8).[78,83,210] To challenge the biocatalytic promiscuity of the aurachin biosynthesis enzymes, fluoro and chloro derivatives of anthranilic acid were fed to *Stigmatella erecta*, a wild-type producer of aurachins.[74] Inspired by the similarities to the known antibiotic ciprofloxacin, subsequent antibiotic activity tests conclude this experiment (chapter 4.2).

2.3   Click chemistry-facilitated labelling of natural products

The advantages of precursor-directed biosynthesis can also be used to endow natural products *in vivo* with structural residues that may serve as handles for subsequent derivatization. Supplementation of cultures with alkyne- or azide-modified amino acids or fatty acids can yield natural product derivatives harboring entities that are less common in nature and that make likewise suitable educts for Click chemistry reactions. The bioorthogonal characteristics thereof can be harnessed to link these defined chemical entities with suitable counterparts in a selective and straightforward manner.[211] Feeding and incorporation of unnatural alkyne precursors represents a promising method to furnish secondary metabolites with such a reaction handle. Azide functionalities are suitable counterparts for a copper catalyzed [3+2] azide-alkyne (CuAAC) reaction that allows flagging of alkyne moieties with azide-modified chromophore molecules[191] with the aim to visualize and detect new molecules. To develop a respective method, two natural product-producing bacteria are investigated: (*i*) *Myxococcus xanthus* is a known producer of various amino acid-derived compounds.[47] It is analyzed bioinformatically and by LC-MS in order to identify candidate NRPS, PKS-NRPS or RiPP pathways with sufficient substrate tolerance towards alkyne amino acid precursors. (*ii*) The plant pathogenic bacterium *Ralstonia solanacearum* possesses pathways for the production of the NRP ralsolamycin and the PK-NRP micacocidin.[212,213] In the biosynthesis of both compounds fatty acids are utilized as building blocks and, in case of micacocidin, previous studies revealed a relaxed substrate tolerance of the biosynthetic enzymes for olefinic and halogenated fatty acid derivatives.[190] In these two target organisms, precursor feeding studies are conducted to establish a suitable protocol for the subsequent Click derivatization in crude extracts, as detailed in chapter 4.3.

3 Experimental Section

3.1 General experimental procedures

3.1.1 Chemicals

Unless elsewhere stated, all compounds were purchased from abcr (Germany), Acros Organics (Germany), Alfa Aesar (Germany), Carl Roth (Germany), Deutero (Germany), jena bioscience (Germany), Sigma-Aldrich (Germany), VWR (Germany). Deionized water (dH$_2$O) was used if not elsewhere stated. Water purified with Milli-Q® Reference Water Purification system is named ddH$_2$O.

3.1.2 (Semi-)Preparative HPLC

HPLC separations were conducted on a Shimadzu HPLC system (LC-20AD) equipped with a SPD-M20A PDA detector.

3.1.3 Liquid chromatography-coupled mass spectrometry analyses

The text in this paragraph was taken with minor modifications from publication [B] of the author:

"Liquid chromatography-mass spectrometry (LC/MS) analyses were carried out with an Agilent 1260 Infinity LC system connected to a UV detector and Compact Q-TOF mass spectrometer (Bruker Daltonics, Bremen, Germany). The Q-TOF was interfaced with an electrospray ionization source. Analyses were routinely performed in positive ion mode using a capillary potential of 4.5 kV"[214], "desolvation gas (N$_2$) temperature of 220°C and a dry gas (N$_2$) flow rate of 12 L min^{-1}. HPLC flow rate was 0.4 ml min^{-1} on a Nucleodur RP 18 ec column (100 x 2 mm, 2.7 µm; Macherey-Nagel) and a gradient from 5 to 98% acetonitrile in water supplemented with 0.1% formic acid over 10 min, followed by 5 min at 98% acetonitrile."[162]

3.1.4 NMR analyses

NMR measurements were carried out at ambient temperature, using 500, 600 and 700 MHz Avance III HD spectrometers (Bruker Biospin GmbH). The 500 MHz system featured a Prodigy

probe, while the 600 and 700 MHz systems were equipped with 5 mm helium cooled cryoprobes. Methanol-d_4 served as solvent and internal standard for all samples. The solvent signals were referenced to δ_H 3.31 ppm and δ_C 49.0 ppm.[214] Residual trifluoroacetic acid was referenced to δ_F -76.5 ppm.

3.1.5 UV absorption and optical rotation analyses

UV absorptions were determined with a UV-1800 photometer (Shimadzu, Kyoto, Japan). A polarimeter 341 (PerkinElmer, Waltham, MA, USA) was used to measure the optical rotation. These measurements were conducted with a 1 dm cuvette at 20°C and 589 nm.[214]

3.1.6 Software

Software used in this thesis is listed in Table 3.1.

Table 3.1 Software

Software	Supplier
ChemDraw Pro 14	*CambridgeSoft* (Waltham, USA)
TopSpin 4.0.7	*Bruker* (Bremen, Germany)
Compass HyStar 3.2 SR 4	*Bruker* (Bremen, Germany)
Data Analysis	*Bruker* (Bremen, Germany)
LabSolutions	*Shimadzu* (Duisburg, Germany)

3.2 Myxochelin- and pseudochelin-derived lipoxygenase inhibitors

3.2.1 Strains and cultivation conditions

The strains and medium used in this study are listed in Table 3.2 and Table 3.3.

Table 3.2 Microorganisms for myxochelin and pseudochelin production

Strain	Genotype	Reference
Myxococcus xanthus FB (DSM 16526)	wild type	*DSMZ* (Braunschweig, Germany)
Myxococcus xanthus FB (DSM 16526)	pJK5	Korp *et al.*, 2018[62]

Table 3.3 Cultivation medium for *Myxococcus xanthus* FB

Medium	Compound	Amount
CTPM	Bacto Casitone	10 g
pH 7.5	KH_2PO_4	0.14 g
	Tris	1.21 g
	$MgSO_4$	0.69 g
	vitamin B_{12}	0.5 mg
	ddH_2O	1000 mL

M. xanthus wild type and pJK5 were cultured in CTPM liquid medium (30°C, 130 rpm). For the *M. xanthus* pJK5 strain the medium was supplemented with kanamycin (50 mg L^{-1}).

3.2.2 Production and purification of myxochelin B and pseudochelin A derivatives

Myxochelin B_1 and B_2 were produced and purified in collaboration with M.Sc. L. Winand (Laboratory of Technical Biology, TU Dortmund University). The following text was taken with minor modifications from publication [A] of the author:

Both *M. xanthus* strains "were grown in 5 L Erlenmeyer flasks containing 1.5 L of modified CTPM medium supplemented with 2% (w/v) Amberlite XAD7HP (Sigma Aldrich). The precursors benzoic acid (100 mg/L), salicylic acid (35 mg/L) and 6-fluorosalicylic acid (100 mg/L) were each added as filter-sterilized solutions to the CTPM medium prior to the inoculation of the bacterium. After six days of cultivation, the XAD7HP resin was recovered by filtration, rinsed with water, and eluted with methanol. The purification of the myxochelin and pseudochelin-derived compounds from the respective methanol extracts was achieved by two-step reverse-phase HPLC on a Nucleodur 100-5 C_{18} ec VarioPrep column (125 x 21 mm, 5 µm; Macherey-Nagel). The first separation was performed using a linear gradient of methanol in water supplemented with 0.1% trifluoroacetic acid: 37% to 53% methanol within 63 min, 63% to 100% over 2 min, and 100% methanol for an additional 7 min with a flow rate of 4 mL/min. Final purification was accomplished with the same eluents, albeit under isocratic conditions. The methanol concentration varied from 32% for the separation of myxochelin up to 55% for the isolation of compounds myxochelin B_6 and pseudochelin A_9. Only in case of analog pseudochelin A_6, another gradient elution (37% to 48% methanol over 63 min) was necessary."[214]

3.2.3 Activity assay of human recombinant 5-lipoxygenase

This assay was performed by Dr. Simona Pace (Chair of Pharmaceutical and Medicinal Chemistry, Friedrich Schiller University Jena, Germany). The following text was taken with minor modifications from publication [A] of the author:

"Human recombinant 5-LO was prepared as previously described.[215] The purified enzyme was incubated with the test compounds in PBS (pH 7.4) containing EDTA (1 mM) and ATP (1 mM) for 10 min at 4°C. After a short pre-warming phase at 37°C for 30 s, 5-LO product formation was initiated by addition of $CaCl_2$ (2 mM) and arachidonic acid (20 μM). Following 10 min of incubation at 37°C, the reaction was terminated by addition of 1 mL ice-cold methanol, and the formation of 5-LO products (all-*trans* derivatives of leukotriene B_4 and 5-hydro(pero)xyeicosatetraenoic acid) was analysed by reverse-phase HPLC."[214]

3.3 Precursor-directed biosynthesis towards aurachin congeners

3.3.1 Strains and cultivation conditions

The strain and medium used in this chapter are listed in Table 3.4 and Table 3.5. The *S. erecta* wild type strain was cultured in modified Zein liquid medium (30°C, 130 rpm).

Table 3.4 Microorganism for aurachin production

Strain	Genotype	Reference
Stigmatella erecta Pd e32 (DSM 53688)	wild type	DSMZ (Braunschweig, Germany)

Table 3.5 Cultivation medium for *Stigmatella erecta*

Medium	Compound	Amount
Modified Zein pH 7.3	corn starch (Maizena, Unilever)	10 g
	Bacto Peptone (Thermo Fisher Scientific)	1 g
	$MgSO_4$ x 7 H_2O	1 g
	vitamin B_{12}	0.5 mg
	ddH_2O	1000 mL

3.3.2 Incorporation studies

Aurachin D and 8-Fluoroaurachin D were produced and purified by M. Sc. Katrin Stüer-Patowsky as part of her Master Thesis (Laboratory of Technical Biology, TU Dortmund University). The following text was taken with minor modifications from publication [B] of the author:

S. erecta was grown in modified Zein medium. "To facilitate the recovery of secreted aurachins, adsorber resin XAD7HP (2% w/v) was added prior to sterilization. The medium was inoculated with seed culture (10% v/v inoculum) and the fermentation was conducted in an incubator shaker at 30 °C and 130 rpm for 7 days. Anthranilic acid or its halogenated derivatives were supplemented as filter-sterilized aqueous solutions (33 mg L^{-1}) after inoculation of the medium. For extraction the adsorber resin was separated from the culture broth by filtration, washed with water and retained compounds eluted three times with acetone and methanol. The extract was dried and used for quantitative evaluation or compound purification."[162]

3.3.3 Quantitative analysis of aurachin production

Culture extracts were obtained from 1.5 L cultures by XAD7HP-aided recovery (3.3.2). After removal of the solvent on a rotary evaporator, the dried extracts were redissolved in 1.5 mL methanol, filtered and subjected to LC-ESI-MS analysis.[162] The area under the curve (AUC) of each extracted ion chromatograms was normalized to the AUC of myxothiazol.

3.3.4 Compound purification

The text in this paragraph was taken with minor modifications from publication [B] of the author:

"Dried raw extracts were resuspended in 60% aqueous methanol (100 mL) and extracted three times with dichloromethane (60 mL). Aurachins were exclusively present in the dichloromethane fraction. The purification continued with an initial on a VarioPrep C18 gravity column (125 x 20 mm, 5 μm; Macherey-Nagel) by two consecutive isocratic elutions with pure methanol and 90% aqueous methanol, respectively. The aqueous eluent was supplemented with 0.1% (v/v) trifluoroacetic acid and the flow rates were set to 4 mL min^{-1}.

For 6-fluoro aurachin D, an additional purification on a Nucleodur Gravity column (250 x 10 mm, 3 μm; Macherey-Nagel) was performed (60% to 100% acetonitrile in water supplemented with 0.1% (v/v) trifluoroacetic acid within 10 min, followed by 100% acetonitrile for an additional 10 min), at a flow rate of 2 mL min^{-1}."[162]

3.3.5 Antibacterial activity screening

Antimicrobial activity testing was performed by an agar diffusion assay. *Escherichia coli* SG458, *Pseudomonas aeruginosa* SG137, *Staphylococcus aureus* (MRSA) 134/94 and *Mycobacterium vaccae* IMET 10670 were used as test organisms. In the test, 50 μL compound test solution (500 μg mL^{-1} in DMSO) was supplied into 9 mm holes on agar plates suitable for test organism cultivation. Ciprofloxacin (5 μg mL^{-1}) was used as positive control.[162]

3.4   Click chemistry-facilitated labelling of natural products

3.4.1 Strains and cultivation conditions

The strains and media used in this chapter are listed in Table 3.6 to Table 3.8. *R. solanacearum* was incubated at 28°C, 150 rpm. *M. xanthus* strains were cultured at 28°C, 130 rpm.

Table 3.6 Microorganism for alkyne precursor feeding experiments

Strain	Genotype	Reference
Ralstonia solanacearum GMI1000	wild type	Boucher *et al.*, 1987[216]
Myxococcus xanthus GJV1	wild type	Krug *et al.* 2008[47]

Table 3.7 Cultivation medium for *Myxococcus xanthus* GJV1

Medium	Compound	Amount
CTT	Bacto Casitone	10 g
pH 7.6	Tris-HCl	1.21 g
	K_2HPO_4	0.35 g
	$MgSO_4$ x 7 H_2O	2.0 g
	ddH_2O	1000 mL

Table 3.8 Cultivation medium for *Ralstonia solanacearum*

Medium	Compound	Amount
Iron-limited ¼ M63	NH_4SO_4	0.5 g
pH 7.0	KH_2PO_4	3.4 g
	$MgSO_4$ x 7 H_2O	61.5 mg
	glucose	2.0 g
	sodium acetate	0.2 g
	ddH_2O	1000 mL
FB-1	KH_2PO_4	0.55 g
pH 7.0	K_2HPO_4	0.73 g
	Casamino acids	1.0 g
	yeast extract	1.0 g
	fructose	10 g
	trace element solution	1 mL
Trace element solution	$MgSO_4$ x 7 H_2O	6 mg
	$ZnSO_4$ x H_2O	0.06 mg
	$Ca(NO_3)_2$ x 4 H_2O	0.10 mg
	$MnSO_4$ x 4 H_2O	0.04 mg
	$FeCl_3$	0.06 mg
	ddH_2O	100 mL

3.4.2 Metabolic profiling of *M. xanthus* GJV1 and feeding of alkyne amino acids

220 mL of *M. xanthus* GJV1 were grown in CTT medium for 7 days (28°C, 180 rpm). Two cultures were additionally supplemented with 10 mg filter-sterilized D/L-propargylglycine and L-homopropargylglycine each. All cultures were extracted threefold with 200 ml ethyl acetate. Dried extracts were resuspended in 1 mL of methanol and insoluble residues filtered before supply to mass spectrometry analysis (chapter 3.1.3). Compound identification was based on extracted ion chromatograms of monoisotopic masses (m/z [M+H]$^+$ and [M+Na]$^+$).

3.4.3 Production of alkyne micacocidins

100 mL of *R. solanacearum* in ¼ M63 minimal medium were fermented for 5 days (28°C, 150 rpm). Cultures were grown with the addition of 10 mg of 4-pentynoic acid, 5-hexynoic acid or 6-heptynoic acid, as well as a combination of 5-hexynoic acid and 6-heptynoic acid.

Three successive extractions with 100 mL ethyl acetate and solvent removal resulted in a dry extract. It was resuspended in 1 mL methanol and centrifuged for 2 min at 17,000 rpm. 100 µL of the clear supernatant were transferred to a vial and supplied to mass spectrometry analysis (chapter 3.1.3). The remaining 900 µL of extract were again dried and used in the subsequent reaction (chapter 3.4.6).

3.4.4 Preparation of 5-hexynoic micacocidin

For the production of 5-hexynoic micacocidin, *R. solanacearum* was grown in 5 L Erlenmeyer flasks (3x 3 L cultures) using ¼ M63 medium supplemented with 100 mg L^{-1} 6-heptynoic acid. The fermentation was conducted at 30°C, 130 rpm for 5 days. Cultures were combined and extracted three times with equal amounts of ethyl acetate. The solvent was evaporated and the residual extract was resuspended in 3 mL methanol. After filtration through a 0.22 µm filter and addition of 1 g Ga(NO$_3$)$_3$ the mixture was incubated at room temperature over night. The sample was purified by a two-step HPLC run (see chapter 3.1.2) on a Nucleodur Gravity column (250 x 10 mm, 3 µm; Macherey-Nagel) starting with a gradient from 5% to 100% methanol in 0.1% trifluoroacetic acid-supplemented water over 20 minutes followed by 5 minutes at 100% at a flow rate of 3 mL min^{-1}. As a second step with the same column, eluent and flow rates gradient from 80% to 100% methanol over 20 min was applied. The dried extract was analyzed by LC-UV/VIS, LC-MS as well as 1D and 2D NMR experiments (see chapter 3.1.3 and 3.1.4).

3.4.5 Probing of fermentation toward alkyne ralsolamycins

200 mL of *R. solanacearum* in FB-1 full medium were initially fermented for 2 days at 30°C and then for 3 days at 25°C, 150 rpm. The cultures were grown with the addition of 15 mg of myristic, palmitic, 13-tetradecynoic, 15-hexadecynoic acid, as well as D/L-propargylglycine or L-homopropargylglycine. For compound recovery 8 g of XAD7HP adsorber resin was supplied to each sample and stirred for 1 h. Afterwards, the resin was separated from the broth by filtration. The resin was washed with water and adsorbed compounds were then eluted three times with 100 mL methanol. The dried extracts were resuspended in 1 mL methanol, filtered and supplied to mass spectrometry analysis (see chapter 3.1.3).

3.4.6 Click reaction protocol

The dried extracts (chapter 3.4.3) were resuspended in 500 µL reaction premix (Table 3.9) and incubated for 11 h at 25°C, 500 rpm in a ThermoMixer (Eppendorf). The reaction mix was centrifuged for 2 min at 10000 g and 200 µL supernatant was transferred to a HPLC vial. The sample was spiked with 5 µL 14.5 mM salicylic acid as internal standard.

Table 3.9 Reaction premix for the Click reaction

Compound	Stock concentration	Amount per reaction	Final concentration
KH_2PO_4 buffer pH 7	100 mM	460 µL	-
$CuSO_4$ x 5 H_2O	20 mM	5 µL	0.2 mM
sodium ascorbate [a]	200 mM	25 µL	10 mM
6-carboxyfluorescein azide	5.2 mM	10 µL	0.1 mM

[a] freshly prepared

Thereof, 50 µL were supplied to a HPLC system with an Nucledur Sphinx RP column (150 x 4.6 mm, 5 µm; Macherey-Nagel) and a gradient system of methanol in 25 mM ammonium carbonate buffer at pH 8. The samples were run at a flow rate of 1.5 mL min^{-1} (5% isocratic methanol for 5 min continued by a gradient to 100% methanol over 15 min and following 10 minutes 100% methanol). Eluting compounds were monitored at wavelengths of 230, 359 and 496 nm. 5 µL were supplied to mass spectrometry analysis (chapter 3.1.3) for compound identification.

4   Results and Discussion

4.1   Myxochelin- and pseudochelin-derived lipoxygenase inhibitors

To increase the structural diversity of the naturally made myxochelins, *Myxococcus xanthus* was employed. "This bacterium is a native producer of both myxochelin A and B,[47,126,217] and its myxochelin pathway can be even further expanded by heterologous expression of the imidazoline synthase gene *mxcM*, leading to the additional formation of pseudochelin.[62] Feeding of such a recombinant *M. xanthus* strain with different aryl carboxylic acids hence appeared as a promising approach to gain access to myxochelin B- and pseudochelin-derived myxochelins."(Modified after Sester *et al.*, 2019, publication A)[214]

4.1.1 Precursor-directed biosynthesis

Parts of the following text were taken with minor modifications from publication [A] of the author:

"In consideration of the substrate incorporation previously observed in *P. fallax*,[71] three compounds, *i.e.*, benzoic acid, salicylic acid and 6-fluorosalicylic acid, were selected for the feeding studies in *M. xanthus*. Since myxochelin B is the direct biosynthetic precursor of pseudochelin,[62] the generation of the latter inevitably affects the yield of the former and its derivatives. In order to secure sufficient material for biological testing, the myxochelin B-derived myxochelins were thus produced in the wild-type strain of *M. xanthus*, which lacks the necessary *mxcM* gene for the formation of pseudochelin. Moreover, every *M. xanthus* culture (wild-type and recombinant) was supplemented with the adsorber resin XAD7HP to improve the myxochelin and pseudochelin yield, respectively.[71] After six days of incubation, the resin was recovered from the culture broth by filtration and then extracted with methanol. The presence of myxochelins and pseudochelins was probed by LC-MS analysis. Due to the random incorporation of the 2,3-dihydroxybenzoate surrogates at two possible positions in myxochelins and pseudochelin, up to nine non-natural derivatives could be detected in the extracts of the recombinant strain, three for each natural compound, albeit at varying concentrations, after the feeding of a single precursor molecule."[214] (Figure 4.1, Table 4.1, Table 4.2).
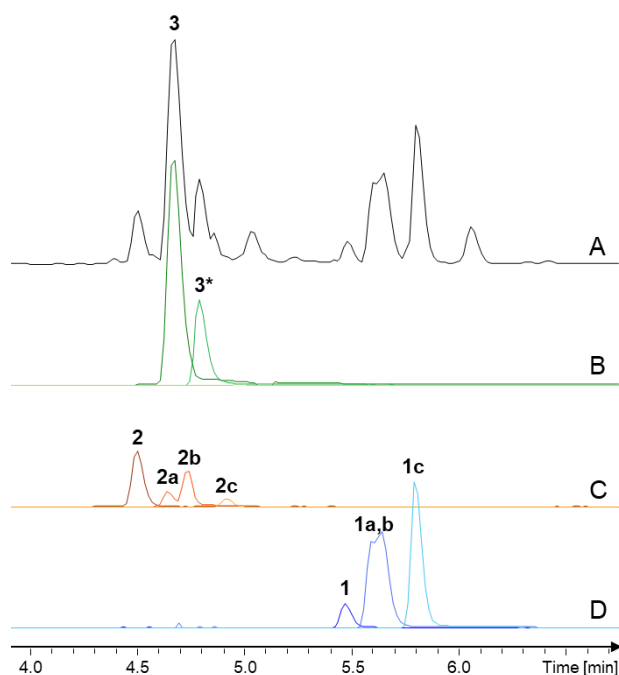
Figure 4.1 „Base peak chromatogram from a crude culture extract of a recombinant *mxcM*-expressing *M. xanthus* strain, which had been fed with benzoic acid.
A. Merged extracted ion chromatograms (EIC) **B.** EIC of pseudochelin A (**3**) and its derivatives.
C. EIC of myxochelin B (**2**) and its derivatives B_1-B_3 (**2a**-**2c**) **D.** EIC of myxochelin A (**1**) and its derivatives A_1-A_3 (**1a**-**1c**). The peak labeled with **3*** could not be unequivocally assigned to pseudochelin A_1 and/or A_2."(Modified after Sester *et al.*, 2019)[214]

In comparison to the production of the naturally occurring myxochelin B, all derivatives were found in diminished quantity. Precursor feeding with benzoic acid gave the lowest yields after purification, compared with salicylic acid or 6-fluorosalicylic acid. This indicates that a 2-hydroxy functional group in the benzoic acid surrogate is important for enzymatic conversion (MxcE to MxcG and MxcL, Figure 1.7). This applies equally to incorporation in both, the western and eastern region of the final molecule. Salicylic acid or 6-fluorosalicylic acid yielded greater quantities if the non-natural building block was ε-connected to the lysinamine backbone, rather than α-bound, suggesting that incorporation at this position follows a more promiscuous fashion (Table 4.1). Production of pseudochelins is primarily dependent on yields attained for their direct precursor analogs of myxochelin B. Accordingly, benzoic acid-fed cultures only yielded pseudochelin A_1 to A_3 at trace levels (Table 4.2). For salicylic acid feeding the pseudochelins A_4 to A_6 were found in approximately the same ratio as the corresponding myxochelin B analogs, suggesting that the key enzyme MxcM readily accepts these three precursors for the 4,5-dihydroimidazole formation. For 6-fluorosalicylic acid feeding, positioning of this xenobiotic precursor in the eastern part of myxochelin B_8 does not hinder

44

Table 4.1 Production yield and inhibitory effects (IC$_{50}$ values) of myxochelin B and its derivatives B$_1$-B$_9$ on 5-lipoxygenase (5-LO) in comparison to myxochelin A. (Modified after Sester *et al.*, 2019)[214]
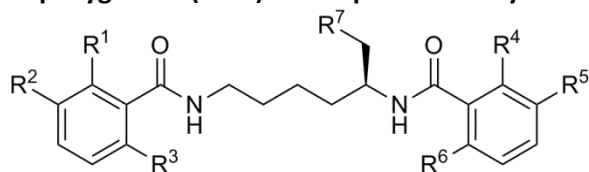
Derivative	R^1	R^2	R^3	R^4	R^5	R^6	R^7	5-LO IC$_{50}$ [μM]^a	Yield [mg/L]^b
A	OH	OH	H	OH	OH	H	OH	1.9 ± 0.6	n.d.
B	OH	OH	H	OH	OH	H	NH$_2$	1.4 ± 0.5	6.1
B$_1$	H	H	H	OH	OH	H	NH$_2$	n.d.	0.9
B$_2$	OH	OH	H	H	H	H	NH$_2$	n.d.	0.9
B$_3$	H	H	H	H	H	H	NH$_2$	n.d.	< 0.1
B$_4$	OH	H	H	OH	OH	H	NH$_2$	10 ± 6.2	3.7
B$_5$	OH	OH	H	OH	H	H	NH$_2$	5.6 ± 2.6	1.4
B$_6$	OH	H	H	OH	H	H	NH$_2$	> 10	2.3
B$_7$	OH	H	F	OH	OH	H	NH$_2$	> 10	3.7
B$_8$	OH	OH	H	OH	H	F	NH$_2$	9.3 ± 4.5	2.2
B$_9$	OH	H	F	OH	H	F	NH$_2$	n.d.	0.1

^{a}data are the mean ± SE of single determinations obtained in three independent experiments;
^{b}yield after HPLC purification; Abbreviations: n.d., not determined

Table 4.2 Production yield and inhibitory effects (IC$_{50}$ values) of pseudochelin A and its derivatives (A$_1$-A$_9$) on 5-lipoxygenase (5-LO). (Modified after Sester *et al.*, 2019)[214]
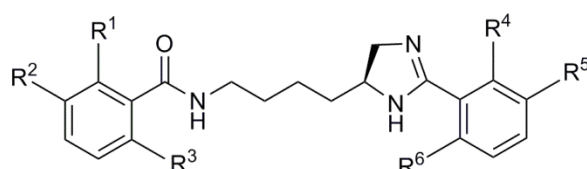
Derivative	R^1	R^2	R^3	R^4	R^5	R^6	5-LO IC$_{50}$ [μM]^a	Yield [mg/L]^b
A	OH	OH	H	OH	OH	H	0.9 ± 0.3	15.9
A$_1$	H	H	H	OH	OH	H	n.d.	< 0.1
A$_2$	OH	OH	H	H	H	H	n.d.	< 0.1
A$_3$	H	H	H	H	H	H	n.d.	< 0.1
A$_4$	OH	H	H	OH	OH	H	2.2 ± 0.9	2.4
A$_5$	OH	OH	H	OH	H	H	1.5 ± 0.7	0.7
A$_6$	OH	H	H	OH	H	H	> 10	1.7
A$_7$	OH	H	F	OH	OH	H	1.1 ± 0.5	0.5
A$_8$	OH	OH	H	OH	H	F	2.2 ± 0.6	2.3
A$_9$	OH	H	F	OH	H	F	n.d.	0.1

^{a}data are the mean ± SE of single determinations obtained in three independent experiments;
^{b}yield after HPLC purification; Abbreviations: n.d., not determined

transformation by MxcM, whereas placement in the western part clearly impairs the reaction, potentially caused by the fluorine atom.

"Those myxochelins that derived from myxochelin A and that had previously been described[71] or that seemed to be only present at trace levels were not considered in the following purification efforts. Owing to the complexity of the extracts, a satisfactory separation was usually only accomplished by two consecutive HPLC runs. The yields after purification ranged from 0.1 to 3.7 mg L^{-1} (Table 4.1 and Table 4.2). In total, 14 derivatives (myxochelin B$_1$, B$_2$, B$_4$-B$_9$, pseudochelin A$_4$-A$_9$) could be fully structurally characterized by MS and NMR analyses." (Modified after Sester et al., 2019, publication [A])[214]

4.1.2 Structure elucidation of myxochelin B analogs

Myxochelin B$_1$ to B$_3$ were identified in the culture extract fed with benzoic acid. Myxochelin B$_1$ exhibits a *m/z* of 372.1919 [M+H]$^+$ which indicates the chemical formula C$_{20}$H$_{25}$N$_3$O$_4$ and accounts for 10 degrees of unsaturation. The UV maxima observed at 313, 248 and 223 nm (Figure S2) are similar to those of natural myxochelin B as reported before.[218] Concordant with the proposed chemical formula, the ^{13}C NMR spectrum exhibits 20 signals in total, which can be categorized according to their chemical shifts. Two signals are due to carbonyl functionalities that are assigned to amide moieties (C-7, C-7''). Twelve additional signals correspond to sp^2-hybridized, aromatic carbon atoms (C-1' to C-6' and C-1'' to C-6''), whereas the remaining 6 represent aliphatic carbon atoms (C-1 to C-6) (Table 4.3, Figure S4). The aromatic carbons were assigned to two benzene moieties. The ^{1}H NMR data shows 8 signals with shifts typical for aromatic protons (H-4' - H-6' and H-2'' - H-6''), and 11 with aliphatic nature (H-1 to H-6). ^{1}H-^{13}C heteronuclear single-quantum coherence (HSQC) was applied to correlate the protons with the directly-bound carbons. Analysis of the ^{1}H-^{1}H correlation spectroscopy (COSY) spectrum identified three independent spin systems which could be connected through ^{1}H-^{13}C heteronuclear multiple bond correlation (HMBC) data (Figure 4.2, Table 4.3, Figure S3 – Figure S7).

The aliphatic backbone was identified as one continuous spin system from CH$_2$-6 through CH$_2$-1. The low field shift of signals CH$_2$-1, CH-2 and CH$_2$-6 indicated a neighboring heteroatom for each position, assigned as amino group and two *N*-linked amide functionalities, respectively. The observed COSY correlations established CH$_2$-1 and CH$_2$-6 to be the terminal

46

units in the spin system. Therein, H-1a and H-1b appear as diastereotopic protons at two distinct chemical shifts with a characteristically large geminal ^2J coupling constant of 13.0 Hz. The neighboring stereocenter (CH-2) connects to the linear CH_2-3 through CH_2-6 alkane chain. The second spin system ranges from H-2'' to H-6'' and represents five protons, whereas the pairs H-2'' and H-6'' as well as H-3'' and H-5'' appear chemically equivalent and thus only three signals are observed that stand for an unsubstituted phenyl moiety. The third spin system is composed of the three aromatic protons H-4' to H-6'. ^{13}C chemical shifts of C-2' and C-3' indicated hydroxylations in these positions and HMBC connection between H-6' and carbonyl C-7' confirmed that the three unsubstituted positions are located directly next to C-1'. Correlations observed between H-6' and C-2' as well as H-4' and C-3' further support the structure of a 2,3-dihydroxybenzoic acid moiety. Finally, evaluation of the ^1H-^{13}C HMBC data clarified, that the phenyl amide moiety is connected to the ε-end of the aliphatic backbone, as seen from correlation and the chemically equivalent H-2'' and H-6'' to 7'' plus likewise of H-6 to C-7'' over the linking amide nitrogen. Accordingly, the catechol amide unit is attached in position 2 completing the molecule (Figure 4.2). Comparison with the native myxochelin B NMR data reported earlier[219] validated the signals observed in the homologous part of the molecule. Optical rotation was determined as $[\alpha]^{20}_D$ −9.26° (c 0.45, MeOH) and comparison with literature values of the natural analog[69] revealed the single chiral center to be *S*-configured.

For myxochelin B_2 a very similar dataset was recorded. The molecular formula and thus the degrees of unsaturation as well as the UV properties were identical with the values observed for myxochelin B_1. The ^{13}C and ^1H NMR spectra also show the same number of signals and similar coupling pattern (Figure 4.2, Table 4.3, Figure S9 – Figure S10). Correspondingly, three individual ^1H spin systems were observed by COSY, specifically an aliphatic backbone (CH_2-1 to CH_2-6), a benzamide (C-1' to C-7') and a catechol amide (C-1''to C-7''). The key difference lays in the assembly of the three parts. As deduced from the HMBC data, H-6' as well as H_2-6 correlate with C-7, thus the catechol amide moiety is connected at the ε-nitrogen of the lysine-derived aliphatic part and the benzamide at the opposite end. With an optical rotation of $[\alpha]^{20}_D$ −8.95° (c 0.42, MeOH) myxochelin B_2 also represents the *S*-configured enantiomer.

Myxochelin B_3 was identified by HR-MS and comparison with the unfed culture extract since it was produced at trace level quantity.
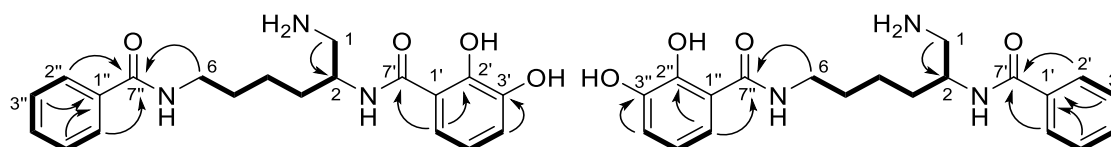
Figure 4.2 Correlations observed for myxochelin B₁ and B₂.
COSY (bold lines) and selected HMBC (arrows) interactions, relevant for structure elucidation.

Table 4.3 NMR data recorded for myxochelin B₁ and B₂ (methanol-d_4)

	Myxochelin B₁				Myxochelin B₂			
pos.	δ_C (ppm), type	δ_H, M (*J* in Hz)	COSY	HMBC	δ_C (ppm), type	δ_H, M (*J* in Hz)	COSY	HMBC
1	45.2, CH₂	a: 3.18, dd (13.0, 3.8)	1b	2	45.1, CH₂	a: 3.17, dd (13.0, 3.8)	1b	2
				2				
		b: 3.03, dd (13.0, 10.1)	1a, 2			b: 3.02, dd (13.0, 9.9)	1a	2, 3
2	49.1, CH	4.38, ddt (10.1, 7.0, 3.8)	1b, 3	-	49.6, CH	4.33, ddt (9.9, 7.2, 3.8)	1, 3	1, 3
3	32.5, CH₂	1.73, m	2, 4	1, 2, 4, 5	32.7, CH₂	1.73, m	1, 2	1, 2, 4, 5
4	24.2, CH₂	a: 1.55, m	3, 4b	2, 3, 5, 6	24.3, CH₂	a: 1.56, m	3, 4b	2, 3, 5, 6
		b: 1.48, m	3, 4a			b: 1.48, m	3, 4a	
5	30.1, CH₂	1.69, m	3, 6	3, 4, 6	30.0, CH₂	1.67, m	3, 6	3, 4, 6
6	40.4, CH₂	3.40, t (6.9)	5	4, 5, 7''	40.0, CH₂	3.40, t (6.9)	5	4, 5, 7''
1'	116.7, C	-	-	-	135.1, C	-	-	-
2'	150.2, C	-	-	-	128.5, CH	7.83, d (7.8)	3'	4', 6', 7'
3'	147.4, C	-	-	-	129.6, CH	7.43, t (7.8)	2', 4'	1', 5'
4'	119.9, CH	6.95, dd (8.0, 1.5)	5'	2', 3', 6'	133.0, CH	7.53, t (7.8)	3', 5'	2', 6'
5'	119.7, CH	6.70, t (8.0)	4', 6'	1', 2', 3', 6'	129.6, CH	7.43, t (7.8)	4', 6'	1', 3'
6'	119.0, CH	7.27, dd (8.0, 1.5)	5'	2', 3', 4', 7'	128.5, CH	7.83, d (7.8)	5'	2', 4', 7'
7'	172.5, C	-	-	-	171.4, C	-	-	-
1''	135.8, C	-	-	-	116.8, C	-	-	-
2''	128.2, CH	7.74, dd (7.0, 1.5)	3''	4'', 6'', 7''	150.2, C	-	-	-
3''	129.5, CH	7.41, t (7.5, 7.0)	2'', 4''	1'', 5''	147.4, C	-	-	-
4''	132.6, CH	7.50, dt (7.5, 1.5)	3'', 5''	2'', 6''	119.6, CH	6.92, d (8.0)	5''	2'', 6''
5''	129.5, CH	7.41, t (7.5, 7.0)	4'', 6''	1'', 3''	119.6, CH	6.68, t (8.0)	4'', 6''	1'', 3''
6''	128.2, CH	7.74, dd (7.0, 1.5)	5''	2'', 4'', 7''	118.6, CH	7.16, d (8.0)	5''	2'', 4'', 7''
7''	170.4, C	-	-	-	171.5, C	-	-	-

Myxochelin B_4 to B_6 were found in the culture extract fed with salicylic acid. Derivatives B_4 and B_5 exhibit similar pseudomolecular ions with *m/z* of 388.1877 and 388.1862 [M+H]$^+$, which indicate the identical chemical formula $C_{20}H_{25}N_3O_5$. The molecular formula accounts for 10 degrees of unsaturation. Both, myxochelin B_4 and B_5 exhibit an identical UV spectrum with local maxima at 242 nm and 303 nm. Analysis of their ^{1}H and ^{13}C NMR data (Table 4.4, Figure S11 - Figure S16) and the respective COSY as well as HSQC data revealed the presence of an aliphatic backbone (CH_2-1 to CH_2-6) and two additional partial structures, comprising of a catechol as well as a 2-hydroxyphenyl moiety. HMBC spectroscopy clarified the amide-connected backbone structure and one major difference between these two molecules: Myxochelin B_4 carries the salicylamide in positions C-1'' to C-7'' and the catechol amide represents C-1' to C-7'. For myxochelin B_5 the two moieties are interchanged.

Myxochelin B_6 exhibits a *m/z* of 372.1936 [M+H]$^+$ indicating the chemical formula $C_{20}H_{26}N_3O_4$ with 10 double bond equivalents. It shows a UV spectrum with local maxima at 237 nm and 301 nm. Subsequent analysis of the corresponding set of NMR data (Table 4.4, Figure S17 – Figure S19) showed that this derivative carries two identical salicylamide moieties bound to the central aliphatic chain and thus represents the double-substituted derivative of natural myxochelin B. The optical rotation analysis of myxochelin B_4 to B_6 identified them as the *S*-enantiomers.

Myxochelin B_7 to B_9 were isolated from the culture fed with 6-fluorosalicylic acid. The B_7 and B_8 compounds show pseudomolecular masses of *m/z* 406.1770 and 406.1752, respectively, both matching with a chemical formula of $C_{20}H_{24}FN_3O_5$. As for the previously described myxochelins, this formula corresponds to 10 double bond equivalents. Their UV spectra appear with local maxima at 242 nm and 307 nm. Their ^{13}C NMR spectra show identical signals in the aliphatic region as the previous myxochelins (C-1 to C-6), but significant differences were observed for the sp^2-hybridized signals in the low field. Therein, for myxochelin B_7 seven and for myxochelin B_8 six signals were split into doublets resulting from heteronuclear coupling with fluorine. Corresponding to literature values[220], the direct $^1J_{C,F}$ coupling exhibits a characteristic large coupling constant of 248 Hz, for the $^2J_{C,F}$ values in the range of 25 to 14 Hz are found, and for ^3J to ^4J they further decrease (Table 4.4). Accordingly, for myxochelin B_7 the ^3J values that stand for the correlation between F-6'' and C-7'' have a coupling constant of 1.8 Hz. In myxochelin B_8, the equivalent F-6' to C-7' correlation is not detectable, probably due to

Table 4.4 ^{1}H and ^{13}C NMR data recorded for myxochelin B$_4$ to B$_9$ (methanol-d_4)

	Myxochelin B$_4$		Myxochelin B$_5$		Myxochelin B$_6$	
pos.	δ_C, type	δ_H, M (*J* in Hz)	δ_C, type	δ_H, M (*J* in Hz)	δ_C, type	δ_H, M (*J* in Hz)
1	45.1, CH$_2$	a: 3.18, dd (13.1, 2.5) b: 3.04, dd (13.0, 10.0)	45.2, CH$_2$	a: 3.18, dd (13.1, 3.4) b: 3.04, dd (13.1, 10.0)	45.1, CH$_2$	a: 3.18, dd (13.2, 3.5) b: 3.04, dd (13.4, 9.8)
2	49.0, CH	4.38, m	49.1, CH	4.37, m	49.2, CH	4.40, m
3	32.5, CH$_2$	1.73, m	32.6, CH$_2$	1.74, m	32.6, CH$_2$	1.74, m
4	24.3, CH$_2$	a: 1.55, m b: 1.48, m	24.3, CH$_2$	a: 1.55, m b: 1.49, m	24.3, CH$_2$	a: 1.55, m b: 1.49, m
5	30.0, CH$_2$	1.68, m	30.0, CH$_2$	1.69, m	30.0, CH$_2$	1.69, m
6	40.0, CH$_2$	3.40, m	40.0, CH$_2$	3.39, t (6.5)	40.1, CH$_2$	3.40, m
1'	116.6, C	-	116.9, C	-	116.8, C	-
2'	150.2, C	-	161.1, C	-	161.1, C	-
3'	147.3, C	-	118.4, CH	6.90, dd (8.3, 1.2)	118.5, CH	6.90, dd (8.3, 1.1)
4'	119.9, CH	6.94, dd (7.9, 1.6)	135.1, CH	7.38, ddd (8.4, 7.1, 1.7)	135.1, CH	7.38, ddd (8.3, 7.2, 1.8)
5'	119.7, CH	6.70, t (8.0)	120.2, CH	6.88, ddd (8.0, 7.2, 1.2)	120.2, CH	6.87, ddd (8.0, 7.2, 1.2)
6'	119.0, CH	7.27, dd (8.1, 1.6)	129.2, CH	7.79, dd (8.0, 1.7)	129.2, CH	7.80, dd (8.0, 1.8)
7'	172.5, C	-	172.0, C	-	172.0, C	-
1''	117.0, C	-	116.8, C	-	117.0, C	-
2''	161.1, C	-	150.1, C	-	161.1, C	-
3''	118.4, CH	6.87, dd (8.3, 1.2)	147.3, C	-	118.5, CH	6.87, dd (8.3, 1.0)
4''	134.7, CH	7.35, ddd (8.3, 7.2, 1.8)	119.6, CH	6.91, dd (8.3, 1.2)	134.7, CH	7.35, ddd (8.3, 7.2, 1.8)
5''	120.1, CH	6.84, ddd (8.0, 7.2, 1.2)	119.6, CH	6.68, t (8.0)	120.1, CH	6.84, ddd (8.0, 7.2, 1.2)
6''	128.7, CH	7.69, dd (8.0, 1.8)	118.6, CH	7.16, dd (8.1, 1.3)	128.7, CH	7.69, dd (8.0, 1.8)
7''	171.0, C	-	171.5, C	-	171.0, C	-

Table 4.4 continued.

	Myxochelin B₇		Myxochelin B₈		Myxochelin B₉	
pos.	δ_C, ($J_{C,F}$ in Hz), type	δ_H, M ($J_{H,H}$ / $J_{H,F}$ in Hz)[a]	δ_C, ($J_{C,F}$ in Hz), type	δ_H, M ($J_{H,H}$/$J_{H,F}$ in Hz)[a]	δ_C, ($J_{C,F}$ in Hz), type	δ_H, M ($J_{H,H}$/$J_{H,F}$ in Hz)[a]
1	45.1, CH₂	a: 3.19, dd (13.3, 2.9) b: 3.04, dd (13.3, 10.0)	44.8, CH₂	a: 3.17, dd (13.1, 3.8) b: 3.07, dd (13.2, 9.8)	44.9, CH₂	a: 3.17, dd (12.9, 3.8) b: 3.08, dd (13.2, 9.8)
2	49.1, CH	4.38, m	49.3, CH	4.40, m	49.0, CH	4.40, m
3	32.5, CH₂	1.73, m	32.4, CH₂	1.72, m	32.3, CH₂	1.73, m
4	24.1, CH₂	a: 1.55, m b: 1.49, m	24.1, CH₂	a: 1.58, m b: 1.50, m	24.0, CH₂	a: 1.60, m b: 1.52, m
5	29.8, CH₂	1.68, m	29.9, CH₂	1.69, m	29.8, CH₂	1.67, m
6	40.1, CH₂	3.41, t (6.6)	40.0, CH₂	3.40, m	40.1, CH₂	3.43, m
1'	116.6, C	-	107.7, d (14.8), C	-	n.d., C	-
2'	150.2, C	-	162.3, d (5.0), C	-	n.d., C	-
3'	147.3, C	-	114.4, d (1.9), CH	6.74, dd (8.4, 1.2)	114.4, CH	6.74, dd (8.4, 1.0)
4'	119.9, CH	6.93, dd (8.0, 1.3)	134.6, d (12.4), CH	7.33, dt (8.4, *6.7*)	134.6, d (12.3), CH	7.34, dt (8.3, *6.8*)
5'	119.7, CH	6.70, t (8.0)	107.0, d (24.8), CH	6.62, ddd (*11.5,* 8.3, 1.2)	107.0, d (24.8), CH	6.63, ddd (*11.6,* 8.2, 1.0)
6'	119.0, CH	7.28, dd (8.0. 1.3)	162.3, d (248.0), C	-	162.3, d (248.0), C	-
7'	172.6, C	-	169.4, C	-	169.5, C	-
1''	107.4, d (14.8), C	-	116.7, C	-	n.d., C	-
2''	162.6, d (4.9), C	-	150.2, C	-	n.d., C	-
3''	114.4, d (2.8), CH	6.70, dd (8.4, 1.2)	147.3, C	-	114.4, CH	6.71, dd (8.4, 1.0)
4''	134.2, d (12.5), CH	7.29, dt (8.4, *6.8*)	119.5, CH	6.91, dd (7.9, 1.4)	134.2, d (12.6), CH	7.31, dt (8.4, *6.7*)
5''	106.8, d (24.5), CH	6.59, ddd (*11.5,* 8.2, 1.2)	119.5, CH	6.68, t (8.0)	106.8, d (24.7), CH	6.59, ddd (*11.7,* 8.3, 1.0)
6''	162.3, d (247.0), C	-	118.6, CH	7.17, dd (8.1, 1.4)	162.3, d (247.0), C	-
7''	168.4, d (1.8), C	-	171.6, C	-	168.4, C	-

[a] $J_{H,F}$ values are displayed in italics, n.d. = not detected

limited signal resolution and indiscernible signal splitting. This explains the difference in the two spectra.

Analysis of the ^{1}H NMR and the corresponding COSY data confirmed the aliphatic backbone analogously to the other myxochelins and identified again two aromatic spin systems. One could again be attributed to a catechol unit and the other one to the 6-fluorosalicylic acid moiety. The coupling between fluorine and protons resulted in additional splitting of the aromatic proton signals in the fluorine neighboring, leading to characteristic $^3J_{H,F}$ couplings of about 13.2 Hz and $^4J_{H,F}$ couplings of about 6.7 Hz (Table 4.4). HSQC and HMBC evaluation assigned myxochelin B$_7$ to carry the 6-fluorosalicyl part in positions C-1'' to C-7'' as seen from long-range coupling from CH$_2$-6 of the aliphatic central part to carbonyl C-7'' as well as the aromatic CH-3'' and CH-5'' to C-7''. Likewise, the catechol amide is located in positions C-1' to C-7', deducted from correlation of aliphatic CH-2 as well as aromatic CH-5' and CH-6' to the second carbonyl C-7'. For myxochelin B$_8$, the arrangement of the two aromatic building blocks is reversed.

Myxochelin B$_9$ was found to have a *m/z* of 408.1747 [M+H]$^+$, corresponding to a chemical formula of C$_{20}$H$_{23}$F$_2$N$_3$O$_4$ accounting again for 10 degrees of unsaturation. The UV spectrum shows maxima at 234 nm and 303 nm. ^{1}H as well as ^{13}C NMR spectra present the previously described signals of the aliphatic backbone (CH$_2$-1 to CH$_2$-6). Two additional spin systems were deduced from COSY data and were identified as 6-fluorosalicylic acid units exhibiting similar fluorine to carbon, as well as fluorine to proton couplings (C-1' to C-7' and C-1'' to C-7''). The signals could be assigned by evaluation of the chemical shifts and the collected correlation data of myxochelin B$_7$ and B$_8$. Accordingly, the 6-fluorosalicylic acid was assigned as partial structure in the western and eastern part of myxochelin B$_9$. The optical rotation values of myxochelin B$_7$ to B$_9$ all show negative signs as found for the other myxochelins, illustrating the *S*-configuration of these molecules.

A data summary of all discussed myxochelin B derivatives is presented in Table 4.4.

4.1.3 Structure elucidation of pseudochelins

Pseudochelin A_4 to A_6 were isolated from cultures fed with salicylic acid. Derivatives A_4 and A_5 were found by their pseudomolecular ions m/z 370.1759 and 370.1741 [M+H]$^+$, respectively, representing the chemical formula $C_{20}H_{24}N_3O_4$. The latter corresponds to 11 calculated degrees of unsaturation and indicates one additional double bond or ring structure within the molecule compared to myxochelin B congeners. UV data exhibits maxima at 249 nm and 302 nm (myxochelin B_4) as well as 245 nm and 312 nm (myxochelin B_5). In both molecules, the ^{13}C spectrum shows 20 signals, of which six can be attributed to aliphatic carbons (C-1 to C-6). Fourteen carbons are sp^2-hybridized according to their chemical shifts. Two of these carbons must form double bonds with heteroatoms. While C-7'' is part of an amide moiety, C-7' forms a ketimine partial structure (Table 4.5). The remaining 12 aromatic carbons belong to two substituted phenyl partial structures, which were further confirmed by the ^1H NMR data together with their correlations deduced from a COSY spectrum. These show two distinct aromatic spin systems, one composed of three and the other of four protons creating a catechol as well as a 2-hydroxyphenyl substructure. The aliphatic protons constitute a third spin system spanning from CH$_2$-1 to CH$_2$-6. The chemical shifts of H$_2$-1, H-2 and H$_2$-6 are indicative of adjacent nitrogen atoms. The protons H-1a and H-1b show distinct chemical shifts and stand out with their large geminal coupling constant of about 11.5 Hz. After assignment of directly-bound carbons through HSQC, long range coupling observed in HMBC spectra was used to assemble the three spin system and to distinguish the two derivatives. For pseudochelin A_4, relevant couplings were found from CH$_2$-6 to C-7'' and further connection from CH-6'' to C-7'', identifying the western part of the molecule as a salicylamide unit (C-1'' to C-7''). On the opposite end of the aliphatic carbohydrate chain the diastereotopic protons H-1a and H-1b both correlate with CH-2 and CH$_2$-3 along the linear chain, but equally with C-7'. The catechol spin system analogously connects CH-6' with C-7' as the linking atom between the two parts and confirms its location in the eastern part of the molecule (C-1' to C-7'). Combination of the shielded chemical shift of C-7', HMBC evaluation and the remaining double bound equivalent suggested that the dihydroimidazole connects CH$_2$-1, CH-2 and C-7' over two bridging nitrogens (Figure 4.3).

For pseudochelin A_5, the left and right aromatic partial structures were found to be interchanged. The HMBC analysis shows that the catechol moiety (C-1'' to C-7'') correlates

from CH-3'' and CH-6'' to C-7'' which also connects to CH$_2$-6. The 2-hydroxyphenyl unit though links from CH-6' to C-7' as part of the dihydroimidazole ring. As observed for pseudochelin A$_4$, long range correlations from CH$_2$-1 to C-7' form the upper bridge and herein an additional correlation between CH-2 and C-7' is observed, giving the 5-membered ring structure.
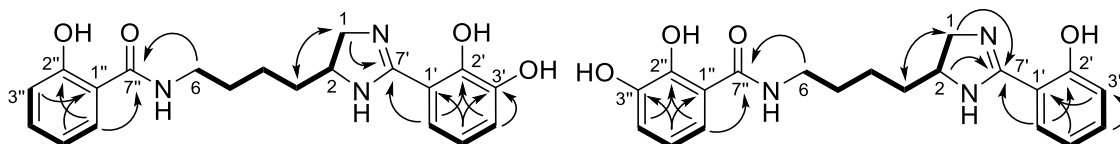

Figure 4.3 Correlations observed for pseudochelin A$_4$ and A$_5$
COSY (bold lines) and selected HMBC (arrows) interactions, relevant for structure elucidation

The absolute configuration of pseudochelin A was previously determined by comparison of its experimental circular dichroism spectrum with corresponding theoretical calculations and found to be 2*S* configured.[66] Pseudochelin A exhibits a negative optical rotation $[\alpha]^{20}_D$.[66] The values found for pseudochelin A$_4$ and A$_5$ show the same negative sign and accordingly their stereochemistry represents similarly the *S*-enantiomer.

Pseudochelin A$_6$ exhibits a pseudomolecular mass with *m/z* 354.1830 [M+H]$^+$ and a chemical formula of C$_{20}$H$_{23}$N$_3$O$_3$ was calculated from this value. Consistent with pseudochelin A$_4$ and pseudochelin A$_5$, the molecule features 11 double bound equivalents. Its UV spectrum shows maxima at 243 nm and 303 nm. The ^{13}C NMR data shows again 20 signals, including six aliphatic carbon atoms, 12 aromatic and two carbonyl type carbon atoms. Together with the ^{1}H NMR data, a substructure was deduced that is equivalent to the aliphatic region of the two pseudochelins described before, with a butyl chain that connects to a dihydroimidazole moiety (CH$_2$-1 to CH$_2$-6). Furthermore, two aromatic spin systems are obvious from the COSY spectrum, featuring four protons each. These two spin systems were identified as 2-hydroxyphenyl units (C-1' to C-6' and C-1'' to C-6''). HSQC and HMBC analysis confirmed the linkage of the three parts through coupling through C-7' and C-7'' similar as described for the previous two derivatives, forming a pseudochelin with two modified aromatic residues. Optical rotation analysis indicated the *S*-configuration for this derivative.

Pseudochelin A_7 to A_9 were identified in the culture extract fed with 6-fluorosalicylic acid. The A_7 and A_8 derivatives exhibit pseudomolecular masses of m/z 388.1650 and 388.1682 [M+H]$^+$, respectively, both in accordance with the chemical formula $C_{20}H_{22}FN_3O_4$, accounting for 11 degrees of unsaturation. Their UV spectra appear with local maxima at 244 nm and 310 nm. The highfield region of their ^{13}C NMR spectra is consistent with the previously described pseudochelins (C-1 to C-6), but in the downfield region, seven putative additional signals for pseudochelin A_7 and six putative additional signals for A_8 were found. As described before for fluorinated myxochelin B derivatives, these additional "signals" are due to signal splitting induced by fluorine to carbon heteronuclear coupling (Table 4.5). Accordingly, the ^{1}H NMR and COSY data show three spin systems, the aliphatic backbone (CH$_2$-6 to CH$_2$-3) connected with the 4,5-dihydroimidazole (CH-2 and CH$_2$-1), and two aromatic units. The splitting of the proton signals in one aromatic spin system is indicative of heteronuclear coupling with fluorine. Interpretation of HSQC and HMBC data gave the final structures of these two derivatives. Pseudochelin A_7 bears a 6-fluorosalicylamide moiety in positions C-1'' to C-7'' and a catechol unit in C-1' to C-6'. Conversely, in pseudochelin A_8 these two partial structures are interchanged with C-1' to C-6' representing the 2-hydroxy-6-fluorophenyl moiety and C-1'' to C-7'' as the 2,3-dihydroxybenzamide part. The optical rotation values $[\alpha]^{20}_D$ exhibited negative metrics and confirmed both derivatives as 2S-enantiomers.

Pseudochelin A_9 with its m/z of 408.1747 [M+H]$^+$, corresponds to the calculated chemical formula of $C_{20}H_{23}F_2N_3O_4$ accounting again for 11 degrees of unsaturation. The UV spectrum shows maxima at 234 nm and 303 nm. The NMR dataset was evaluated as described before. Due to limited yield and thus concentration not all carbons could be assigned from the ^{13}C, HSCQ and HMBC data. Additional signals were assigned based on similarities with chemical shifts and correlation data from pseudochelin A_7, A_8 as well as myxochelin B_7, B_8 and B_9. This provided concluding information that pseudochelin A_9 is indeed the derivative bearing two 2-hydroxy-6-fluorophenyl aromatic parts. The stereochemistry of this derivative could not be determined.

Pseudochelins A_1 to A_3 were only produced at trace levels and could only be detected by MS, but not characterized by NMR. A summary of all discussed pseudochelin A derivatives is shown in Table 4.5.

Table 4.5 ^{1}H and ^{13}C NMR data recorded for pseudochelin B$_4$ to B$_9$ (methanol-d_4)

pos.	Pseudochelin A$_4$		Pseudochelin A$_5$		Pseudochelin A$_6$	
	δ_C, type	δ_H, M (*J* in Hz)	δ_C, type	δ_H, M (*J* in Hz)	δ_C, type	δ_H, M (*J* in Hz)
1	50.6, CH$_2$	a: 4.13, m b: 3.73, dd (11.8, 7.7)	50.5, CH$_2$	a: 4.13, t (11.3) b: 3.73, dd (11.4, 7.6)	50.5, CH$_2$	a: 4.13, t (11.4) b: 3.73, dd (11.5, 7.6)
2	58.1, CH	4.38, m	58.1, CH	4.38, m	58.1, CH	4.38, m
3	35.6, CH$_2$	a: 1.88, m b: 1.79, m	35.6, CH$_2$	a: 1.88, m b: 1.80, m	35.6, CH$_2$	a: 1.89, m b: 1.80, m
4	23.0, CH$_2$	1.52, m	22.9, CH$_2$	1.52, m	23.0, CH$_2$	1.52, m
5	30.2, CH$_2$	1.72, m	30.2, CH$_2$	1.72, m	30.3, CH$_2$	1.72, m
6	40.0, CH$_2$	3.44, t (6.8)	40.0, CH$_2$	3.44, t (7.0)	40.0, CH$_2$	3.44, t (7.0)
1'	109.3, C	-	109.3, C	-	109.3, C	-
2'	149.0, C	-	159.7, C	-	159.7, C	-
3'	147.6, C	-	118.2, CH	7.07, d (8.4)	118.5, CH	7.07, dd (8.4, 0.9)
4'	121.3, CH	7.10, d (7.9)	137.6, CH	7.57, ddd (8.4, 7.3, 1.8)	137.5, CH	7.57, ddd (8.4, 7.3, 1.7)
5'	121.3, CH	6.87, m	121.4, CH	7.04, dd (8.0, 7.3)	121.4, CH	7.04, ddd (7.9, 7.3, 1.0)
6'	120.1, CH	7.16, d (8.0)	130.7, CH	7.70, dd (8.0, 1.8)	130.7, CH	7.71, dd (8.0, 1.7)
7'	164.5, C	-	164.3, C	-	164.3, C	-
1''	117.0, C	-	116.8, C	-	117.0, C	-
2''	161.1, C	-	150.2, C	-	161.1, C	-
3''	118.5, CH	6.87, m	147.4, C	-	118.2, CH	6.89, dd (8.2, 1.2)
4''	134.7, CH	7.37, t (7.9)	119.6, CH	6.92, dd (7.9, 1.7)	134.7, CH	7.37, ddd, (8.3, 7.2, 1.7)
5''	120.1, CH	6.87, m	119.6, CH	6.71, t (8.0)	120.1, CH	6.87, ddd (7.8, 7.3, 1.2)
6''	128.8, CH	7.73, d (7.9)	118.6, CH	7.20, dd (8.1, 1.7)	128.8, CH	7.73, dd (7.9, 1.7)
7''	171.0, C	-	171.5, C	-	171.0, C	-

Table 4.5, continued

	Pseudochelin A$_7$		Pseudochelin A$_8$		Pseudochelin A$_9$	
pos.	δ_C, ($J_{C,F}$ in Hz), type	δ_H, M ($J_{H,H}$/$J_{H,F}$ in Hz)^a	δ_C, ($J_{C,F}$ in Hz), type	δ_H, M ($J_{H,H}$/$J_{H,F}$ in Hz)^a	δ_C, ($J_{C,F}$ in Hz), type	δ_H, M ($J_{H,H}$/$J_{H,F}$ in Hz)^a
1	50.5, CH$_2$	a: 4.14, t (11.3) b: 3.74, dd (11.3, 7.4)	50.3, CH$_2$	a: 4.14, t (11.5) b: 3.74, dd (11.5, 7.4)	50.3, CH$_2$	a: 4.15, t (11.5) b: 3.76, dd (11.6, 7.4)
2	58.1, CH	4.39, m	58.3, CH	4.42, m	58.4, CH	4.42, m
3	35.6, CH$_2$	a: 1.88, m b: 1.80, m	35.5, CH$_2$	a: 1.87, m b: 1.80, m	35.5, CH$_2$	a: 1.88, m b: 1.80, m
4	22.9, CH$_2$	1.53, m	22.8, CH$_2$	1.51, m	22.7, CH$_2$	1.53, m
5	30.1, CH$_2$	1.72, m	30.2, CH$_2$	1.71, q (7.2)	30.1, CH$_2$	1.72, q (7.2)
6	40.1, CH$_2$	3.46, t (6.9)	40.0, CH$_2$	3.43, t (6.9)	40.1, CH$_2$	3.46, t (6.9)
1'	109.2, C	-	100.3, d (13.4), C	-	n.d., C	-
2'	149.2, C	-	160.3, d (5.0), C	-	160.2, d (5.0), C	-
3'	147.7, C	-	113.7, d (2.9), CH	6.87, d (8.5)	113.7, d (3.4), CH	6.87, d (8.4)
4'	121.3, CH	7.09, d (7.8)	137.4, d (12.2), CH	7.53, dt (8.5, *6.6*)	137.4, d (12.5), CH	7.53, dt (8.5, *6.6*)
5'	121.1, CH	6.85, t (7.8)	107.9, d (22.2), CH	6.81, dd (*11.2*, 8.4)	107.9, d (22.1), CH	6.82, dd (*11.2*, 8.4)
6'	120.1, CH	7.16, d (7.8)	162.9, d (254.0), C	-	162.9, d (254.0), C	-
7'	164.6, C	-	160.5, C	-	160.5, C	-
1''	107.5, d (15.0), C	-	116.8, C	-	n.d., C	-
2''	162.7, d (4.7), C	-	150.2, C	-	162.3, d (4.7), C	-
3''	114.5, d (2.5), CH	6.72, d (8.3)	147.3, C	-	114.5, d (4.3), CH	6.72, d (8.4)
4''	134.2, d (12.3), CH	7.32, dt (8.3, *6.8*)	119.6, CH	6.92, dd (7.9, 1.5)	134.2, d (13.2), CH	7.32, dt (8.4, *6.8*)
5''	106.8, d (24.3), CH	6.63, dd (*11.6*, 8.3)	119.6, CH	6.71, t (8.0)	106.8, d (24.6), CH	6.63, dd (*11.7*, 8.3)
6''	162.4, d (247.0), C	-	118.6, CH	7.20, dd (8.1, 1.6)	n.d., C	-
7''	168.5, d (2.0), C	-	171.5, C	-	n.d., C	-

^{a} $J_{H,F}$ values are displayed in italics

4.1.4 Structure-activity relationship on 5-lipoxygenase inhibition

Parts of the following text were taken with minor modifications from publication [A] of the author:

"The ten analogs (myxochelin B_4-B_8 and pseudochelin A_4-A_8) were obtained in sufficient quantities to allow biological testing. After individual exposure of isolated human recombinant 5-LO to the test compounds including myxochelin A, B and pseudochelin A, the enzymatic conversion of arachidonic acid into all-*trans* derivatives of leukotriene B_4 and 5-hydro(pero)xyeicosatetraenoic acid was quantified by HPLC. Consistent with previous investigations,[65,71] a potent bioactivity for myxochelin A against 5-LO (IC_{50} = 1.9 µM) was observed. For comparison, the FDA-approved 5-LO inhibitor zileuton possessed only slightly better efficiency in this cell-free assay, with an IC_{50} value of 0.5 µM.[215] The two other natural products, myxochelin B and pseudochelin, which were tested for the first time for their 5-LO inhibitory properties in this study, were found to be even more active than myxochelin A with IC_{50} values of 1.4 and 0.9 µM, respectively. It is interesting that the observed increase in 5-LO inhibition of the bacterial metabolites is paralleling the biosynthetic reaction sequence, in which the formation of myxochelin B and pseudochelin A requires additional enzymatic processing in comparison to myxochelin A.[62,217] Whether this gradual improvement in bioactivity occurred by chance or by evolutionary constraints cannot be answered right now, though further analyses in this direction would be certainly warranted considering the recent discovery of lipoxygenases in myxobacteria.[221–223]

Of the tested myxochelin B derivatives, B_6 and B_7 failed to inhibit 5-LO product formation at concentrations lower than 10 µM. The analogs B_4 and B_8 showed considerably higher IC_{50} values than their parental molecule, whereas the replacement of the 2,3-dihydroxybenzoate moieties in pseudochelin A was surprisingly well tolerated. Except for pseudochelin A_6, which lacks both catechol moieties, the pseudochelin A derivatives retained most of their bioactivity (Table 4.1 and Table 4.2)."[214] In comparison to the previously reported IC_{50} values from myxochelin A derivatives,[71] all tested myxochelin B derivatives show lower inhibitory potency, indicating that the amino group effects the inhibition negatively. In contrast, the corresponding pseudochelin congeners exhibit similar or only slightly weaker inhibitory properties.

4.1.5 Discussion

"Based upon these results, the previous structure-activity relationship (SAR) data could now be further refined.[71] The molecular mode of action of 5-LO inhibition by the myxochelins and pseudochelins is still unclear. In general, 5-LO inhibitors are classified as redox-active compounds, active site iron chelators, substrate mimetics (competitive inhibitors) or non-competitive inhibitors.[224]" (Modified after Sester *et al.*, 2019)[214]

Recent crystal structure analysis of 5-LO with the redox-type inhibitor nordihydroguaiaretic acid (NDGA) gave detailed insights into its mechanism of action. When NDGA is placed in the active site cavity, it provokes disordering of relevant alpha-helical structures in the enzyme. Additionally, the slender structure of the inhibitor makes it reach deep into the active site pocket, where it is tethered by only one interaction between one catechol unit and arginine-596. This position causes the opposite catechol to shield the central iron and thus to inhibit the catalytic activity (Figure 4.4).[225] Due to structural similarities with myxochelins or pseudochelins, a similar mechanism may be hypothesized. However, for detailed insight into the influence of the various substitution patterns, and moreover, the lysinol- or dihydroimidazole-derived backbone, experimental data or a computational model is needed.
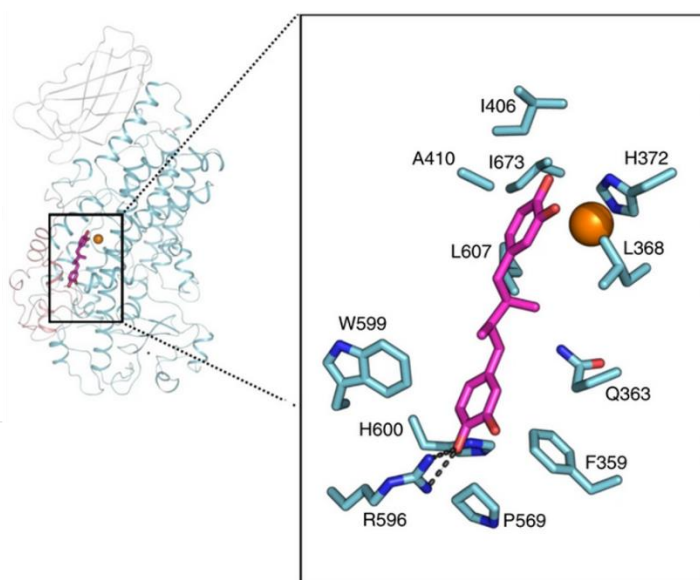
Figure 4.4 Modelled protein structure of Stable 5-lipoxygenase with NDGA as inhibitor
Left side shows Stable-5-LO modelled with amino-terminal domain in gray and catalytic domain in gray. On the right side, zoom into the active site cavity. The relevant amino acids are highlighted and NDGA (pink) positioned deep in the ravine, tethered by R596. The catalytic iron is depicted as orange sphere. (Modified after Gilbert et al., 2020)[225]

Additionally, it is still possible that these compounds partially inhibit 5-LO due to the complexation of the active site iron.

"In summary, it has become evident that the presence of an imidazoline ring next to a catechol or phenolic moiety is beneficial for 5-LO inhibition. In contrast, the replacement of both catechol units by salicyl moieties will negatively affect the inhibitory properties. Furthermore, it turned out that the bioactivity of myxochelin B and pseudochelin A cannot be further improved by introducing a single salicyl or 6-fluorosalicyl moiety into the biosynthesis. Since these two aryl carboxylic acids were considered to represent the most promising candidates for obtaining more active compounds on the basis of our a previous investigation,[71] one may conclude that the natural product pseudochelin A is already perfectly adapted to the inhibition of 5-LO and further optimization will likely require the evaluation of additional structural variations in the region linking the two catechol units."(Modified after Sester *et al.*, 2019, publication A)[214]

This might include shortening of the chain length, e.g. by introduction of the homologous ornithine instead of lysine. Modifications are conceivable for example by site-directed mutagenesis or domain exchange to adapt the Stachelhaus code, or active site mutation by directed evolution[226] of the MxcG A domain. This might facilitate production of myxochelin A, B as well as pseudochelin derivatives with a CH_2-shortened central part. Highly desirable would also be the generation of an MxcM analog that accepts myxochelin A as a substrate and consequently forms modified pseudochelins bearing an oxazoline instead of dihydroimidazole ring. This could be achieved through directed evolution and might not only allow diversification of natural myxochelin A, but also facilitate a semisynthetic approach to convert artificial analogs that were described before.[215,227,228] Alternatively, MxcM homologs as the *Streptomyces* amidohydrolases CbxE[229] or NatAM[230] could be tested to see if they enable such transformation.

The proposed enzyme engineering could be realized in the heterologously *mxcM*-expressing *E. coli* strain that was harnessed to generate MxcM for characterization studies,[231] taking advantage of more established genetic modification tools. Its robust nature and catalytic activity even in organic solvents[231] are valuable properties with regard to its potential future applications as a biocatalyst.

Finally, the limited biosynthetic production yield of artificial myxochelins could be improved by a mutasynthetic approach, in which 2,3-dihydroxybenzoic acid (DHBA) synthesis could be interrupted. This would eliminate the availability of the natural precursor DHBA and the incorporation of non-natural surrogates could preferentially occur, even beyond those already tested.

4.2 Precursor-directed biosynthesis towards aurachin congeners

Work presented in this chapter was performed in collaboration with B.Sc. Katrin Stüer-Patowsky in the course of her Masters' thesis (Laboratory of Technical Biology, TU Dortmund University).

The known producer of aurachins, *Stigmatella erecta,*[74] was employed to explore the promiscuity of the aurachin biosynthesis pathway concerning the incorporation of fluoro- and chloroanthranilic acids. These precursors do not naturally occur in this bacterium, and their feeding was expected to result in the production of aurachin derivatives. The corresponding feeding experiments were conducted in shaken Erlenmeyer flasks. The cultures were supplemented with adsorber resins to bind the secreted aurachins. At the end of cultivation, these resins were collected by filtration and then eluted with acetone and methanol. The resulting crude extracts were used for LC-MS analysis.[162]

4.2.1 Metabolic profiling and anthranilic acids probing

Metabolic profiling of the extracts indicated the production of known compounds from *S. erecta*, including myxochelin B, myxalamides or myxothiazol A and a variety of aurachins. In accordance with previous reports,[80] supplementation of anthranilic acid boosted the production of natural aurachins. An example of the diversity of produced compounds is displayed in Figure 4.5. The aurachins appear as the main components. Aurachins A and H, B and C, or F, K and L could not be assigned unambiguously, as they have the same molecular mass and do not significantly differ in their UV spectra.

The added anthranilic acid precursors had different effects on the aurachin titers and the growth of the producing strain. While the supplementation of anthranilic acid boosted the production of natural aurachins, as previously reported,[80] halogenated anthranilic acids had a deleterious effect on both, aurachin titers and the growth of *S. erecta*. The growth defects were observed with all unnatural precursors, irrespective of their fluorine or chlorine substitution pattern. According to previous reports from mycobacteria,[232] halogenated anthranilic acids interfere with tryptophan metabolism, which might also explain the observations in this study.
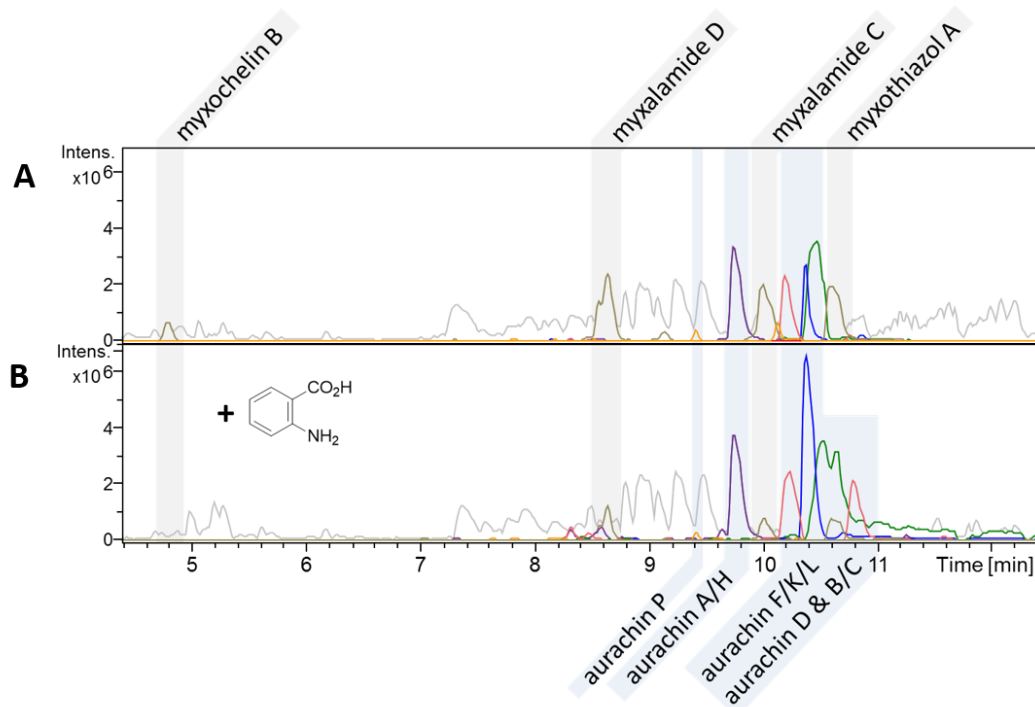
Figure 4.5 Metabolic profiling of *S. erecta* extracts by HPLC-MS.
A. Without and **B.** with supplementation of anthranilic acid. Aurachin D (blue) and aurachin B/C (green) dominate the spectrum, in particular in setting **B**. Aurachin P (orange), aurachin A/H (purple), aurachin F/K/L (red). Other compounds: Myxochelin B, myxalamide D, C, myxothiazol A (gold).

4.2.2 Quantification of halogenated aurachins

The text in this section was taken with minor modifications from publication [B] of the author:

"In the presence of halogenated anthranilic acids, attenuated growth of *S. erecta* was observed, irrespective of the fluorine or chlorine substitution pattern. This may hint at interferences with tryptophan metabolism, as recently reported for mycobacteria.[232] Previous studies had already indicated that the biosynthesis of individual aurachins is linked to the growth phase of the producing bacterium.[73] *S. erecta*, like many other myxobacteria, does not grow homogeneously in liquid media, but is known to form cellular aggregates.[106] As this feature makes it very difficult to precisely determine the growth stage of *S. erecta*, the amounts of biosynthesized aurachins were normalized to the production of myxothiazol A. This known secondary metabolite from *S. erecta*[74] does not recruit anthranilic acid for its biosynthesis and its production profile is similar to the aurachins.[114,233] The results of this quantification are illustrated in Figure 4.6."[162]
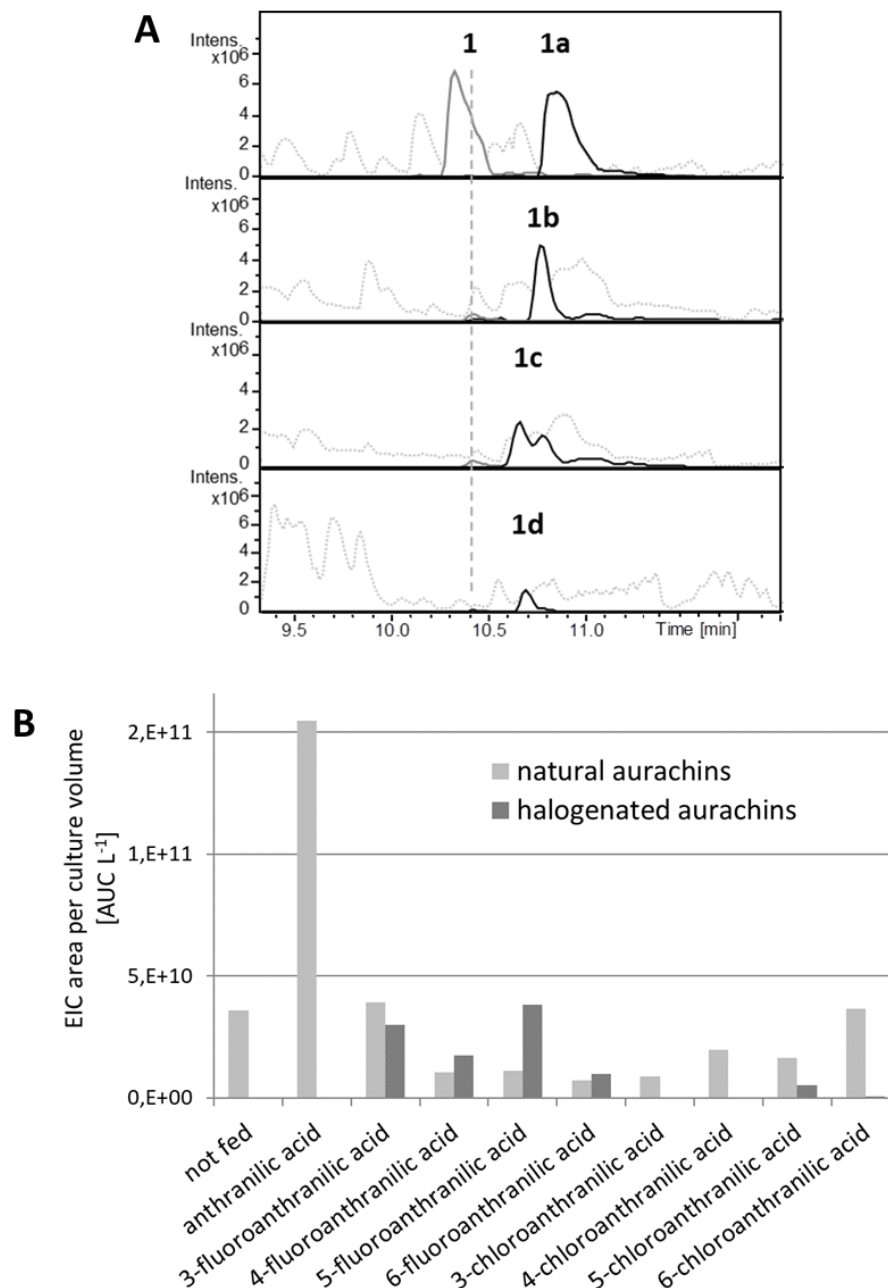
Figure 4.6 Quantification of aurachins in *S. erecta* crude extracts after feeding with halogenated anthranilic acids.
A. HPLC-MS chromatograms after feeding fluoroanthranilic acids. Base peak chromatogram with extracted ion chromatograms of aurachin D (**1**, grey) and the derivatives 8-fluoroaurachin D (**1a**), 7-fluoroaurachin D (**1b**), 6-fluoroaurachin D (**1c**) and 5-fluoroaurachin D (**1d**) (black). **B.** Normalized quantification of aurachins after feeding with fluoro- and chloroanthranilic acids. EIC = extracted ion chromatogram. (Modified after Sester *et al.*, 2020)[162]

"The total amount of aurachins increased by a factor of four when compared to unsupplemented cultures, which suggests that the availability of the natural aromatic precursor is a limiting factor in the biosynthesis. In contrast, the cultivation in the presence of

halogenated anthranilic acids had a lower impact or even decreased the production level. Moreover, significant differences in the utilization of the unnatural precursors became obvious. While all fluoroanthranilic acids could be converted into novel aurachins, albeit to different extent, the biosynthesis enzymes were obviously much less tolerant with regard to chlorinated starter units. Except for the incorporation of 5-chloroanthranilic acid, only trace amounts of chloroaurachins were detected by LC-MS. Among the fluorinated precursor analogs, 5-fluoroanthranilic acid showed the highest conversion, followed by the aromatic acids bearing the halogen substituent in positions 3 and 4, respectively. In comparison, the 6-fluoroanthranilic acid-derived aurachins were produced in much lower quantities. These results indicate that the introduction of halogen atoms in aurachin biosynthesis depends both on the nature of the halogen (F > Cl) and on the substitution pattern of the precursor molecule (pos. 5 > 3 > 4 > 6). In none of the feeding settings, the anticipated acyl-CoA derivatives of halogenated anthranilic acids were found, whereas correspondingly substituted 4-hydroxy-2-methylquinolines were detected at trace levels in cultures supplemented with fluoro- as well as 4- and 5-chloroanthranilic acids. Since no accumulation of any intermediate was observed, it is likely that substrate discrimination already occurs in the early steps of aurachin biosynthesis."[162]

4.2.3 Purification and structure elucidation of aurachin derivatives

Parts of the following text were taken with minor modifications from publication [B] of the author:

"In order to enable full NMR-based structural characterization, feeding studies were repeated on multiliter scale to produce sufficient quantities of some aurachin analogs. Owing to the very low production titers that were achieved (Figure 4.6 and Table 4.6) and a laborious chromatographic separation process (Figure 4.7), only the most abundant derivatives could be isolated in appreciable amounts. In case of novel fluoroaurachins the purification procedure was significantly facilitated by ^{19}F NMR guided fractionation (Figure S47). The recovery of 6-chloro-aurachin remained unsuccessful despite repeated attempts."[162]

"8-fluoroaurachin D (0.5 mg) originated from a 10-L culture of *S. erecta* grown in the presence of 3-fluoroanthranilic acid. The [M+H]$^+$ ion peak of 8-fluoroaurachin D possesses a *m/z* value of 382.2546, corresponding to a molecular formula of $C_{25}H_{32}FNO$ and 10 double bond

Table 4.6 Production yield of aurachin D and corresponding derivatives after feeding of halogenated anthranilic acids (Modified after Sester *et al.*, 2020)[162]

Supplement	Halogenated derivative	Yield of aurachin D [µg L⁻¹]	Yield of halogenated derivative [µg L⁻¹]
-		8.3	-
anthranilic acid		83.3	-
3-fluoroanthranilic acid	8-fluoroaurachin D	40.5	53.3
4-fluoroanthranilic acid	7-fluoroaurachin D	1.0	18.4
5-fluoroanthranilic acid	6-fluoroaurachin D	1.3	43.8
6-fluoroanthranilic acid	5-fluoroaurachin D	0.7	16.2
3-chloroanthranilic acid	8-chloroaurachin D	1.7	< 0.1
4-chloroanthranilic acid	7-chloroaurachin D	2.8	< 0.1
5-chloroanthranilic acid	6-chloroaurachin D	3.2	10.4
6-chloroanthranilic acid	5-chloroaurachin D	8.1	< 0.1

Figure 4.7 "LC-MS analysis of an extract from a *S. erecta* culture fed with 3-fluoroanthranilic acid A. Base peak chromatogram. **B.-E.** Extracted ion chromatograms for **B.** aurachin D (**1**), **C.** aurachin B/C, **D.** 8-fluoroaurachin D (**1a**), **E.** 8-fluoroaurachin B/C." (Modified after Sester *et al.*, 2020)[162]

equivalents. UV maxima at 241, 321 and 333 nm as well as NMR data (Figure S48 - Figure S52) of the purified compound are almost consistent with those of aurachin D,[73,80] which suggested a closely related molecular architecture."[162]

The ^{13}C NMR spectra exhibits 29 putative signals in total, showing four more than predicted by the chemical formula. By their chemical shifts they can be grouped into 10 aliphatic carbon atoms in the high field, 18 in the low field representing aromatic or other sp^2-hybridized atoms, and one in the far low field (δ_C 177.8 ppm), hinting at a carbonyl functionality. Analysis of the ^1H NMR and COSY data revealed three aromatic protons constituting one spin system (CH-5 to CH-7). In H-6 and H-7, their heteronuclear correlation with F-8 prompts signal splitting with additional coupling constants of $^4J_{H,F}$ = 4.9 Hz and $^3J_{H,F}$ = 11.1 Hz, respectively. H 2', H-6' and H-10' represent three protons which are directly bound to a double bond each, and are thus part of three olefinic units, which themselves are connected by methylene bridges. In this partial structure, the COSY spectrum shows long-range correlations in addition to the expected vicinal couplings. An example is H-2', which features cross peaks in the COSY spectrum not only with the neighboring H_2-1' but also with H_3-13' and H_2-4'. A correct assignment in this and related cases was possible by analysis of the J values and HMBC data, respectively. After the ^1H-bound carbons were assigned through HSQC analysis, a farnesyl unit was deduced in conjunction with HMBC data. In particular, the assignment of C-3', C-7' and C-11' was only achieved through $^1H,^{13}C$ long-range interactions, as the corresponding carbons are not directly attached to protons. The HMBC spectrum also confirmed the atom assignment in the aromatic moiety. Both, H-5 and H-7, couple with C-8a, while H-5 additionally correlates with the carbonyl C-4 part of the vinylogous amide. The correlation of H-6 with C-4a establishes the trisubstituted benzene ring with the carbons C-4a to C-8a. In accordance with the observed heteronuclear coupling constants, the fluorine proposed by the chemical formula calculation is located at position 8. The fluorine-carbon couplings also explain the four excess "signals" in the ^{13}C NMR spectrum. The methyl protons of CH_3-9 exhibit HMBC correlations with C-2 and C-3. The two latter are also coupling partners to H_2-1' which additionally correlates with C-4, forming an α-β-unsaturated (C-2, C-3) carbonyl (C-4) partial structure. Additionally, comparison with the reported UV maxima of aurachins A – D[73] reinforced the presence of a larger conjugated system that also harbors the proposed nitrogen atom, completing the quinolone building block. The aforementioned HMBC correlations from

CH₂-1' to C4 of the quinolone moiety and to CH-2' as well as C-3' of the farnesyl side chain allow a linkage of the two partial structures (Figure 4.8, Table 4.7). Comparison with NMR data of aurachin A – L[80] and RE[75] confirmed the assignment of the signals and verified the structure as 8-fluoroaurachin D.
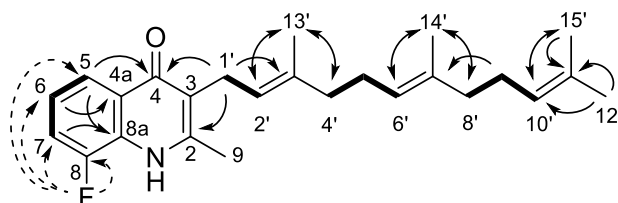
Figure 4.8 Correlations observed for 8-fluoroaurachin D
Selected COSY (bold lines), HMBC (arrows) and heteronuclear ¹⁹F-¹³C/¹H (dashed arrows) interactions, relevant for structure elucidation.

Table 4.7 NMR data recorded for 8-fluoroaurachin D

pos.	δ_C, ($J_{C,F}$ in Hz) type	δ_H, M ($J_{H,H}$ / $J_{H,F}$ in Hz)[a]	COSY	HMBC	pos.	δ_C, ($J_{C,F}$ in Hz) type	δ_H, M ($J_{H,H}$ / $J_{H,F}$ in Hz)[a]	COSY	HMBC
1	-	-	-		1'	24.8, CH₂	3.40, d (6.9)	2', 13'	2, 3, 4, 2', 3'
2	150.4, C	-	-	-	2'	123.5, CH	5.09, dt (6.9, 1.2)	1', 13'	4', 13'
3	121.7, C	-	-	-	3'	136.1, C	-	-	-
4	177.8, C	-	-	-	4'	40.7, CH₂	2.03, m	5'	2', 3', 5', 6', 13'
4a	127.1, C	-	-	-	5'	27.2, CH₂	2.10, m	4', 6'	2', 3', 4'
5	122.0, d (4.0), CH	8.02, dd (7.9, 1.3)	6, 7	4, 7, 8a	6'	125.3, CH	5.04, dt (6.9, 1.4)	5', 14'	8', 14'
6	123.9, d (6.9), CH	7.30, dt (7.9, *4.9*)	5, 7	4a	7'	135.9, C	-	-	-
7	116.7, d (16.9), CH	7.43, ddd (7.9, 1.3, *11.1*)	6	5, 8a	8'	40.8, CH₂	1.87, m	9'	6', 7', 9'
8	153.3, d (247.1), C	-	-	-	9'	27.8, CH₂	1.92, m	8', 10'	8'
8a	130.1, C	-	-	-	10'	125.3, CH	4.98, ddt (7.0, 1.5, 1.4)	9', 12', 15'	15'
9	18.0, CH₃	2.51, s	-	2, 3	11'	132.0, C	-	-	-
					12'	25.8, CH₃	1.60, d (1.4)	9', 10'	10', 11'
					13'	16.3, CH₃	1.81, d (1.2)	1', 2'	2', 4'
					14'	16.2, CH₃	1.55, d (1.4)	5', 6'	6', 7', 8'
					15'	17.6, CH₃	1.49, d (1.5)	9', 10'	9', 10', 11'
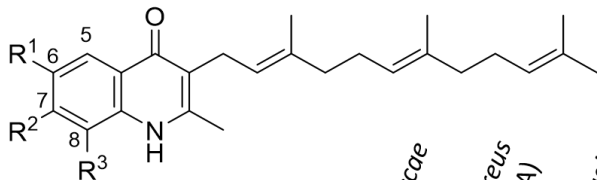
Purification of the extract from the 4-fluoroanthranilic acid culture via multi-step HPLC yielded 0.3 mg of 7-fluoroaurachin D. MS and UV data of this metabolite(Figure S53) were consistent with the previously isolated 8-fluoroaurachin D. The structural relatedness of the two compounds was also obvious from an inspection of their ^{1}H NMR spectra, even though the splitting pattern and coupling constants of the aromatic signals showed some deviations. In the case of 7-fluoroaurachin D, the data indicated the presence of a 1,2,4-trisubstituted benzene ring, and not a 1,2,3-trisubstitution as in 8-fluoroaurachin D. In conjunction with ^{13}C and 2D NMR data (Figure S54 -Figure S57) the full structure of 7-fluoroaurachin D was deduced.

Likewise, 0.3 mg of 6-fluoroaurachin D were obtained from a culture supplemented with 5-fluoroanthranilic acid. The structure elucidation followed the same procedure as described before and was integrated into the interpretation of high-resolution ESI-MS and UV spectra (Figure S58) as well as NMR data (Figure S59 - Figure S62).

4.2.4 Structure-activity relationship studies

The text in this section was taken with minor modifications from publication [B] of the author:

"Having these novel non-natural derivatives at hand, structure-activity relationship studies appeared feasible. The isolated compounds were tested in an agar diffusion assay to assess their antibiotic activities against a panel of four bacterial test strains. This analysis revealed that the generated derivatives 8-, 7- and 6-fluoroaurachin D are equipotent to aurachin D (Figure 4.9). Thus, fluorine introduction does not significantly alter the observed bioactivity profile. In comparison to the reference ciprofloxacin, however, the antibacterial activities of aurachin D and its analogs turned out to be comparatively weak. Furthermore, we noted that the aurachins only show partial inhibition against the test bacteria. This observation might indicate spontaneous resistance."[162]

	R¹	R²	R³	*E. coli*	*M. vaccae*	*S. aureus (MRSA)*	*P. aeruginosa*
aurachin D	H	H	H	15 p	16 p	12 p	15 p
8-fluoroaurachin D	H	H	F	14 p	15 p	0	17 p
7-fluoroaurachin D	H	F	H	15 p	19 p	13 p	15 p
6-fluoroaurachin D	F	H	H	15 p	18 p	12 p	17 p
ciprofloxacin	-	-	-	23	22 p	0	26

Figure 4.9 Aurachins isolated in this study and their antibacterial activities
Results of the agar diffusion assay with ciprofloxacin as positive control. Values indicate the diameter of the respective inhibition zone in mm. p, partial inhibition (= few colonies within the inhibition zone). The aurachins were tested at a concentration of 0.5 mg mL^{-1}, whereas ciprofloxacin was tested at a concentration of 0.005 mg mL^{-1}. (Modified after Sester *et al.*, 2020)[162]

4.2.5 Discussion

Parts of the following text were taken with minor modifications from publication [B] of the author:

"This study shows for the first time that the aurachin pathway exhibits sufficient plasticity to enable precursor-directed biosynthesis. The biosynthetic enzymes generally accepted fluorine substitution at the anthranilic acid precursor but were less permissive with regard to the more bulky chlorine atom. Furthermore, it was demonstrated that the C-5 position of the anthranilic acid precursor is particularly suited for the introduction of functional groups. Therefore it can be assumed that the pursued strategy is generally applicable for systematic SAR investigations. Although three fluoroaurachins were successfully generated and structurally and biologically characterized in this study, it is evident from their titers that the production conditions were not favorable. This is in part due to the replacement of the originally described production medium,[74] which is no longer commercially available. Moreover it can be reasoned with the biosynthetic dispersion into several products including a number of minor aurachins in addition to aurachins A - D and their halogenated variants.[80]

To improve the aurachin yields different approaches are conceivable. The genetic inactivation of late-stage pathway enzymes in *S. erecta* could lead to an accumulation of early biosynthetic

intermediates, thereby reducing the chemical complexity of the respective extracts. Heterologous expression of the entire or partial aurachin gene cluster provides the means to bypass natural regulation and, hence, to increase the yield. In particular the focus on only one or two derivatives that appear early in the biosynthetic pathway as aurachin D or C, would cumulate production yields and simplify purification. "To overcome growth inhibition by anthranilic acid analogs, a strain could be chosen that is more resistant to these building blocks. Alternatively, the enzymatic conversion of anthranilic acid into tryptophan could be disrupted. In this way, unnatural anthranilic acids could not be recruited for tryptophan generation and, therefore, not interfere with primary metabolism.[234] The inactivation of *S. erecta* anthranilate synthase could further eliminate the competition with the natural precursor and hence enable mutasynthesis. The feasibility of such an approach is, however, hardly predictable. Previous studies in the field targeted only non-essential pathways to dedicated building blocks of secondary metabolism, such as 3-hydroxy-, 3-hydroxy-4-methyl-, or 3-amino-5-hydroxy-anthranilic acid.[235–238]"[162] Directed evolution toward fluoro- or chloro-tolerant mutant strains could ultimately increase tolerance of *S. erecta* towards fluorinated precursors that interact with primary metabolism. In this way, an *E. coli* strain was adapted to convert fluoroindole precursors into tryptophane derivatives.[239] Total synthesis approaches with halogenated aniline reactants as starting material might also provide access to halogenated congeners, potentially also 5-substituted aurachins.[93]

As an alternative route to chlorinated or brominated aurachins, the regioselective 7-, 6- or 5-tryptophan halogenases PruA/RebH, ThaI or PyrH, respectively,[240] could be tested on natural aurachin D. Similarly, treatment with the promiscuous iodinase VirX1 could increase halogen-derivatization options, as it accepts e.g. anthranilamide as substrate.[241] Knowing that fluorination of aurachin D does not diminish bioactivity, alternative halogenation is also desirable in perspective of increased lipophilicity and thus bioavailability as a prospective drug.[241]

With larger quantities in hand additional biological testing of such derivatives could be further extended. As mentioned, the aurachin structure does show similarities to the widely-used synthetic class of quinolone antibiotics including ciprofloxacin, active mainly against Gram-negative bacteria and clinically used to treat infectious diseases of e.g. the respiratory and urinary tract.[242] The equipotent activity of fluorine congeners marks a starting point for further

investigation of other halogenated derivatives. Its structure also resembles various biomolecules, suggesting further potential applications. Endochin and alike compounds were found to be active against toxoplasmosis, malaria and other protozoa-caused diseases.[243,244] Natural aurachin C and E indeed possess potent antiplasmodial properties against *Plasmodium falciparum*, comparable to licensed anti-malarial drugs as chloroquine or artemisinin. In this context aurachin E stands out due to its comparable low cytotoxicity within this compound class,[81] which makes it another interesting candidate for SAR optimization.

While the respiratory toxins 2-heptyl-4-hydroxyquinoline-*N*-oxide (HQNO)[73] or 2-alkyl-4(1*H*)-quinolone *N*-oxides (AQNOs) from the pathogen *Pseudomonas aeruginosa* and its derivatives show antibacterial activities,[245] they are also structurally related to Pseudomonas Quinolone Signal (PQS) molecules, essential for quorum sensing (Figure 4.10).[246] Investigation of related bioactivities may shed further light onto the therapeutic potential but also the ecological roles of this natural product family.
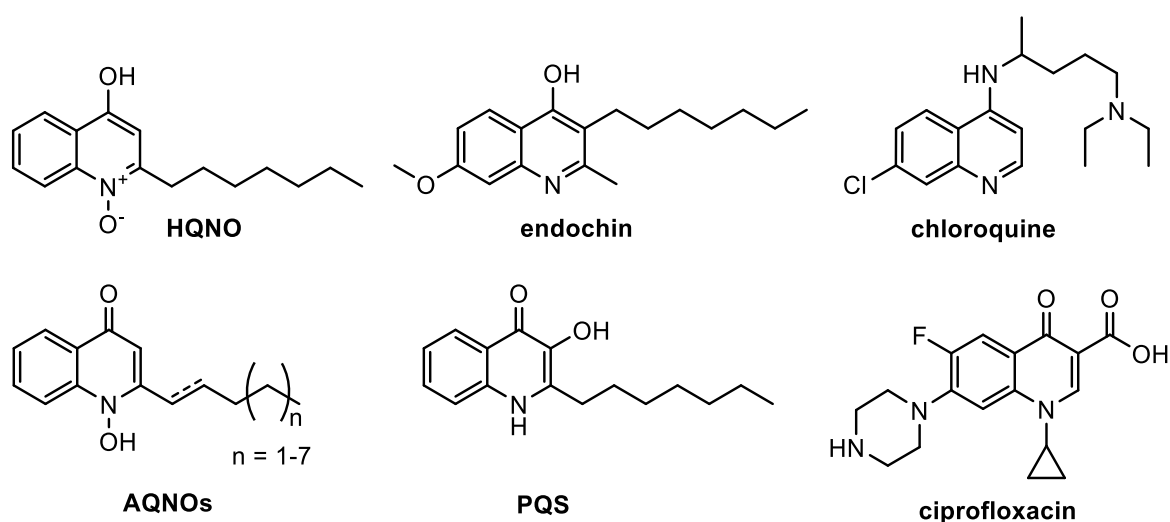
Figure 4.10 Quinoline- or quinolone-derived natural products and synthetic antibiotics.

4.3 Click chemistry-facilitated labelling of natural product derivatives

Gene cluster analysis in *M. xanthus* was performed in cooperation with Dr. J. Korp (Laboratory of Technical Biology, TU Dortmund University).

To test the universal concept of natural product discovery by alkyne feeding, a proof of concept study was first conducted with *M. xanthus* and *R. solanacearum* as model organisms. Their natural products were investigated as potential candidates and later probed for their tolerance towards alkyne precursor compounds.

4.3.1 Metabolic profiling and alkyne feeding in *M. xanthus*

Bioinformatic analysis of the *M. xanthus* DK1622 genome revealed the presence of 27 biosynthetic gene clusters, identified by antiSMASH 3.0, manual annotations of the myxochelin BGC and based on literature data for cittilin and alkylpyrones.[126,247] Of these, 66% are involved in the biosynthesis of NRPs, PKs or hybrids thereof, which thus represent the most prominent group of secondary metabolites in the genome. Six clusters (22%) are predicted to code for RiPPs and only 2 for terpenes. For 11 of the 27 BGCs biosynthetic products were previously reported and characterized (Table 4.8).

Since NRP, PK-NRP hybrid and RiPPs clusters can be considered as potential targets for alkyne amino acid incorporation, *M. xanthus* GJV1, a strain highly similar to DK1622,[47] was screened by LC-MS for the production of the respective compounds. In this analysis, various secondary metabolites could be detected, namely cittilin A (*m/z* 631.2762 [M+H]$^+$), myxochelin A (*m/z* 405.1656 [M+H]$^+$), myxochelin B (*m/z* 404.1816 [M+H]$^+$), myxovirescin (*m/z* 624.4470 [M+H]$^+$), DKxanthenes -534 , -518 and -560 (*m/z* 535.2551, 519.2602, and 561.2708, resp. [M+H]$^+$), as well as myxalamids A, B and C (*m/z* 416.3159, 402.3003, and 388.2846, resp. [M+H]$^+$) (Figure 4.11).

Table 4.8 Biosynthetic gene clusters in the genome of *M. xanthus* DK1622, their predicted or known products and the metabolites found in *M. xanthus* GJV1 as part of this thesis.

	Location of BGC on chromosome[a]	NP class	Predicted product[b]	Biological function or activity / Mode of action	Derivative found in GJV1
1	MXAN_0682-0689	RiPP	**cittilin**	neurotensin receptor antagonist[31,47,248]	A
2	MXAN_0894–0904	Terpene	**carotenoids**	photoprotection[249]	n.d.
3	MXAN_1289–1292	NRP	dipeptide		
4	MXAN_1527–1531	other	**E signal**	sporulation, fruiting body formation[250,251]	n.d.
5	MXAN_1588–1608	NRP	hexapeptide		
6	MXAN_2796–2798	NRP/PK	unknown		
7	MXAN_2852–2857	RiPP	type II lantibiotic		
8	MXAN_3459–3463	PK	unknown		
9	MXAN_3554–3556	RiPP	bacteriocin		
10	MXAN_3617–3625	NRP/PK	unknown		
11	MXAN_3626–3638	NRP/PK	lipopeptide		
12	MXAN_3639–3647	NRP	**myxochelin**	siderophore, inhibition of lipoxygenase[65,252]	A, B
13	MXAN_3779	NRP/PK	**myxoprincomide**	predation[146,253]	n.d
14	MXAN_3928–3950	NRP/PK	**antibiotic TA (myxovirescin)**	predation antibiotic/inhibition of type II signal peptidase[41,254–256]	A1
15	MXAN_4000–4003	NRP/PK	lipopeptide		
16	MXAN_4077–4080	NRP/PK	**myxochromide**	unknown[23,159,257]	n.d
17	MXAN_4290–4305	NRP/PK	**DKxanthene**	sporulation, fruiting body formation[258,259]	-534, -518, -560
18	MXAN_4402–4407	NRP/PK	lipopeptide		
19	MXAN_4409–4415	NRP/PK	lipopeptide		
20	MXAN_4525–4530	NRP/PK	**myxalamid**	antifungal/inhibition of NADH: ubiquinone oxidoreductase[260–262]	A, B, C
21	MXAN_4589–4601	NRP	lipopeptide		
22	MXAN_4602–4605	RiPP	unknown		
23	MXAN_5829	RiPP	bacteriocin		
24	MXAN_6247	Terpene	**geosmin**	warning signal[111,263–265]	n.d.
25	MXAN_6388–6389	RiPP	type II lantibiotic		
26	MXAN_6392–6405	PK	unknown		
27	MXAN_6635–6639	PK	**alkylpyrones**	inhibition of topoisomerase[134,266]	n.d

[a] The assignments were made on the basis of literature data or manual annotations. They differ from previously reported data, which had been obtained using automated genome mining tools.[126] [b] products which were actually observed are highlighted in bold. n.d. not detected. (Modified after Sester *et al.*, 2020, publication [C])[49]
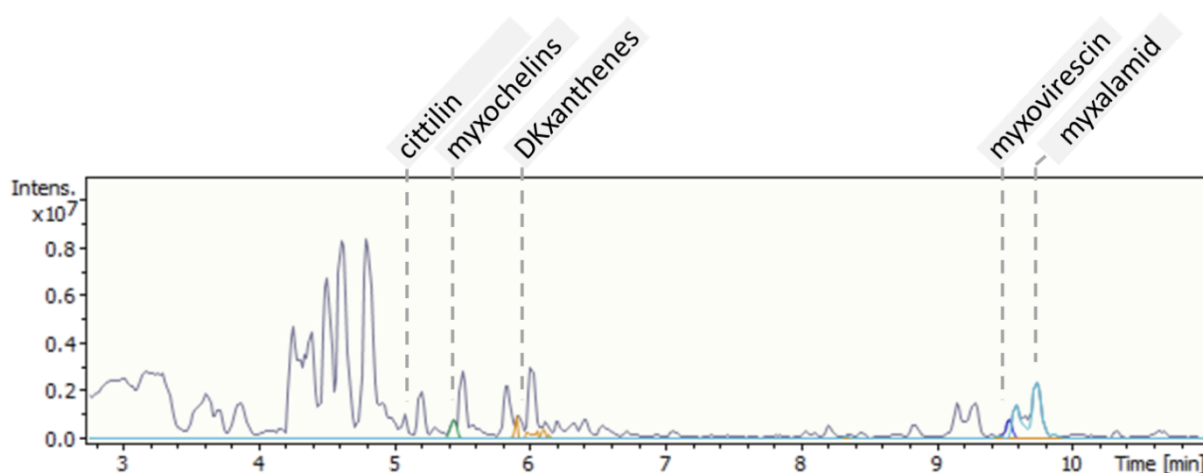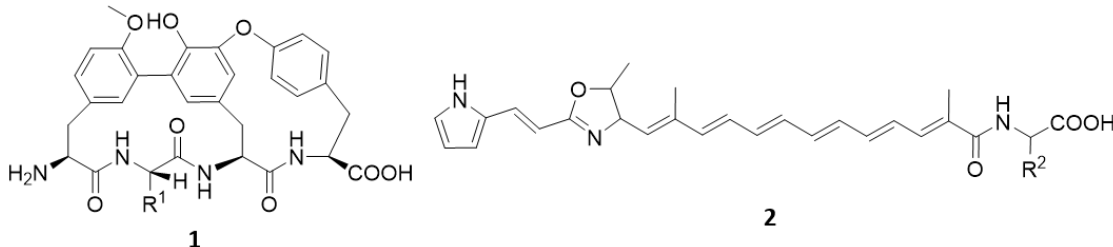
Figure 4.11 Metabolic profiling of *M. xanthus* GJV1 extract by HPLC-MS.
BPC with respective EICs highlighted in colour. Derivatives detected are specified in Table 4.8.

Afterwards, feeding studies targeting cittilins, DKxanthenes and myxalamids were performed with D/L-propargylglycine and L-homopropargylglycine. These artificial amino acids are relatively small in size and were thus considered promising candidate surrogates to mimic proteinogenic amino acids. The selected natural products are known to incorporate the L-configured amino acids. Thus, L-configured homopropargylglycine was chosen for feeding experiments. Propargylglycine was only available as a mixture of both enantiomers, yet it was expected that the biosynthetic machineries would select the correct configuration.

The alkyne-fed cultures were then screened for derivatives of the previously identified compounds. For this purpose, structures of possible analogues were predicted, and the extracts screened via LC-MS for the respective mass traces. For example, the broad, space-consuming isoleucine side chain of cittilin or the glutamine building block of DKxanthenes represent promising targets for replacement with an alkyne amino acid (Figure 4.12). For myxalamids A – C the alanine was replaced in an analogous way. For myxovirescin and the myxochelins such building block exchange was not considered suitable due to significant steric differences in molecular architecture. Despite the variety of molecules considered, the calculated values did not match with the observed masses in the LC-MS chromatograms of the culture extracts from the feeding experiments with D/L-propargylglycine or L-homopropargylglycine. Thus, either cellular precursor uptake is impaired or the known biosynthetic pathways of *M. xanthus* appear not to tolerate alkyne amino acids as substrates.

This finding leads to the conclusion, that *M. xanthus* DK1622 with its known secondary metabolites is not a suitable strain to test the feasibility of Click chemistry-facilitated labelling.

Compound	1	1a	1b	2	2a	2b
R =	R¹	R¹	R¹	R²	R²	R²
m/z [M+H]⁺	631.2762	613.2293	627.2449	535.2551	500.2544	514.2700
found	+	-	-	++	-	-

Figure 4.12 Examples of theoretical, predicted derivatives of cittilin A (1) or DKxanthene-534 (2). The bulky amino acid segments were exchanged with alkyne residues at R_1 or R_2, respectively.

4.3.2 Probing micacocidin biosynthesis with alkyne fatty acids

Due to these limitations, *Ralstonia solanacearum* GMI 1000 was considered as an alternative test strain for alkyne precursor incorporation. Feeding studies were carried out to probe its micacocidin biosynthetic pathway for acceptance of alkyne fatty acids as building blocks. This was considered more promising, as previous studies had already indicated a tolerance for unsaturated (olefinic) as well as halogenated fatty acid alternatives.[190] To mimic the natural precursor hexanoic acid, a set of ω-alkyne homologues with chain lengths from C5 to C7 were supplemented during cultivation. Expected products are depicted in Figure 4.13.

The extracts were first analyzed by LC-MS to identify micacocidin as well as its derivatives and to determine relative yields (Figure 4.14). In the unfed negative control (Figure 4.14A), three dominant peaks correspond to metal complexes of micacocidin. These include the Cu^{2+} and Fe^{3+} complexes that had been described previously as micacocidin B and C, respectively,[267] as well as an Al^{3+} chelate, as reported earlier for the similar compound yersiniabactin.[268] Their identities were confirmed by HR-MS, where the Cu^{2+} and Fe^{3+} complexes appear with their characteristic isotope patterns, and the Al^{3+} complex matches calculated values (Figure S1).

Supplementation of 4-pentynoic acid and 6-heptynoic acid (Figure 4.14 B and D, E) gave rise to the alkyne micacocidin derivatives 3-butynoic micacocidin and 5-hexynoic micacocidin, respectively. The former was produced in minor quantity, whereas the latter stands out with distinct peaks due to different metal chelates formed during cultivation and extraction.
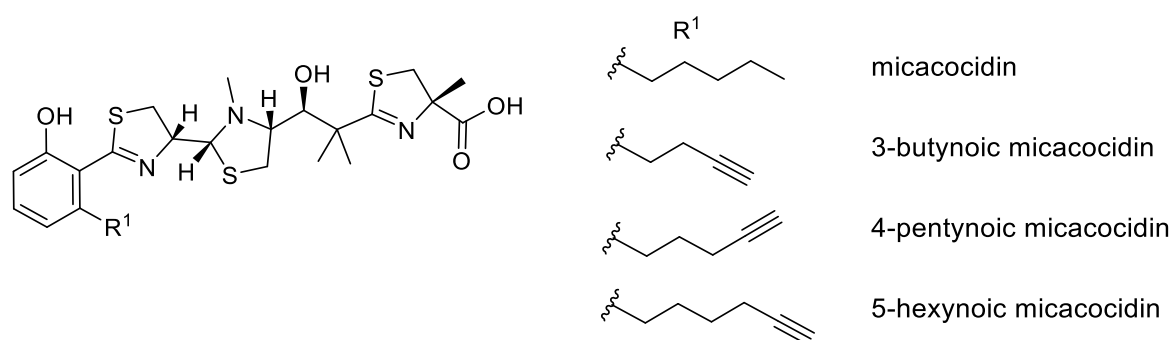
Figure 4.13 Structure of micacocidin and the potential alkyne congeners, resulting from feeding experiments with C5 to C7 ω-alkyne fatty acids.
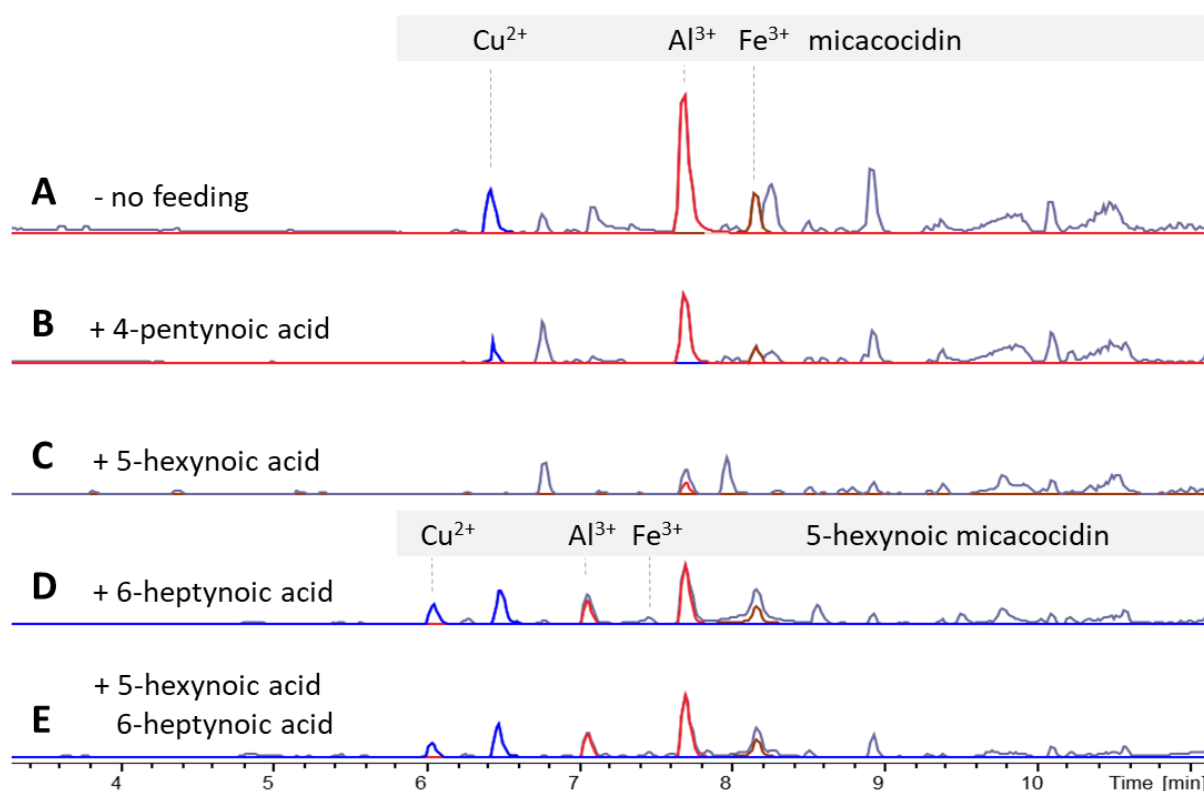
Figure 4.14 Metabolic profiling of *R. solanacearum* extracts after feeding C5 - C7 ω-alkyne fatty acids. LC-MS chromatogram of crude extracts, EICs of micacocidins highlighted in color.

Similar to the natural micacocidins, the alkyne congeners appear as metal complexes, mainly bound with Cu^{2+} and Al^{3+}. Addition of 5-hexynoic acid to the culture seems to impair micacocidin production and alkyne congeners are not found in the extract. Combined feeding of 5-hexynoic acid and 6-heptynoic acid gave a chromatogram similar to Figure 4.14D, supporting initial findings that the biosynthetic machinery readily accepts 6-heptynoic acid, but not 5-hexynoic acid.

Overall, in LC-MS analyses, the Al^{3+} complexes gave the most dominant peaks, which might though originate from superior ionization properties by the mass spectrometer and may not reflect actual complex distribution. This limited comparability constrained absolute quantification of micacocidin derivatization. However, a relative quantification was carried out with AUCs from extracted ion chromatograms (EICs). Each of the natural micacocidin complexes in the unfed culture were set to 100% and AUCs derived from the feeding settings calculated as proportional values within the same metal complex class. Specifically, alkyne congener complexes were related to the respective natural micacocidin metal complex. Quantification shown in Table S1 details the qualitative findings and shows that 4-pentynoic acid feeding yields an average of 1% alkyne micacocidin compared to the unfed culture, whereas 6-heptynoic acid supplementation results in 14% alkyne micacocidin product.

4.3.3 Isolation and structure elucidation of 5-hexynoic micacocidin as Ga^{3+} complex

To verify incorporation of alkyne fatty acids, 5-hexynoic micacocidin was chosen as an exemplary compound. After preparation of extract from 6-heptynoic acid-fed *R. solanacearum* culture, the different metal complexes discovered in the initial screening were challenged with excess amount of gallium(III)-nitrate for re-complexation. Analysis of the treated extract showed, that only minor amounts of Cu^{2+}, Al^{3+} and Fe^{3+} chelates remain and two main Ga^{3+} complexes, representing the natural as well as alkyne micacocidin, were generated. The 5-hexynoic micacocidin was purified via HPLC and characterized spectroscopically (chapter 5.2.6, Figure S64 - Figure S69). The observed mass of 5-hexynoic micacocidin Ga^{3+} matches with the calculated monoisotopic mass ($C_{28}H_{36}N_3O_4S_3Ga$, theoretical *m/z* 642.1040 $[M+H]^+$, $\Delta - 1.4$ ppm), and the HPLC-UV/VIS spectrum shows local maxima at 239, 275 and 359 nm. 1D and 2D NMR data is consistent with literature values of natural micacocidin Ga^{3+} complex reported earlier,[190] in particular for the thiazol(idine)

backbone. Yet, relevant differences occur in the fatty acid residue where the alkyne moiety is expected for this new molecule (Figure 4.15, Table 4.9). Therein, the COSY interactions show subsequential correlations within the aliphatic part from H_2-7 to H_2-10. The analysis of the HSQC data indicates a chemical shift of 18.8 ppm for C-10. The presence of the alkyne
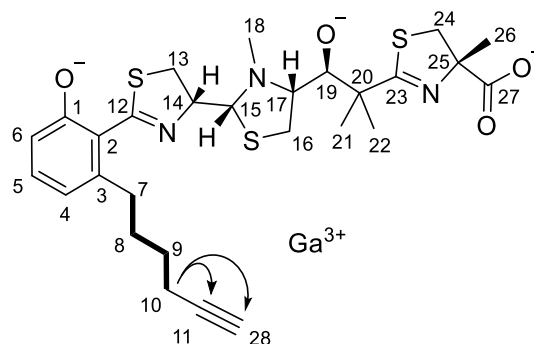
Figure 4.15 5-Hexynoic micacocidin Ga^{3+}: Numbering and correlations observed in the fatty acid-derived region.
Selected COSY (bold lines) and HMBC (arrows) interactions, relevant for structure elucidation.

Table 4.9 NMR data recorded for 5-hexynoic micacocidin Ga^{3+}

pos.	δ_C, type	δ_H, M	pos.	δ_C, type	δ_H, M
1	168.2, C	-	15	82.0, CH	4.54, d (10.6)
2	117.2, C	-	16	40.6, CH_2	a: 3.65, dd (9.2, 7.7)
					b: 3.22, dd (11.8, 9.2)
3	146.6, C	-	17	75.8, CH	3.65, dd (10.0, 7.7)
4	121.6, CH	6.64, dd (7.4, 1.4)	18	48.6, CH_3	2.55, s
5	135.9, CH	7.22, dd (8.4, 7.3)	19	81.3, CH	3.69, s
6	122.0, CH	6.75, dd (8.4, 1.3)	20	46.6, C	-
7	36.8, CH_2	a: 3.19, ddd (14.3, 11.0, 5.4)	21	29.2, CH_3	1.58, s
		b: 2.95, ddd (14.3, 10.9, 5.4)			
8	32.8, CH_2	a: 1.81 m	22	24.2, CH_3	1.37, s
		b: 1.73, m			
9	29.8, CH_2	1.63, m	23	194.8, C	-
10	18.8, CH_2	2.24, m	24	39.6, CH_2	a: 3.73, d (12.3)
					b: 3.45, d (12.3)
11	85.0, C	-	25	83.7, C	
12	179.6, C	-	26	24.2, CH_3	1.67, s
13	34.7, CH_2	a: 3.63, dd (10.9, 8.1)	27	178.7, C	-
		b: 3.29, dd (13.6, 11.0)			
14	73.3, CH	4.78, ddd (13.6, 10.6, 8.0)	28	69.7, CH	2.23, m

functionality was confirmed by correlations observed in the HMBC, where H_2-10 (δ_H 2.24 ppm) couples with C-11 (δ_c 85.0 ppm) and C-28 (δ_c 69.7 ppm). It is noteworthy to mention, that the HSQC shows correlations between H_2-10 and C-10, but not between the postulated H-28 and C-28. However, a reference spectrum recorded for commercial 6-heptynoic acid exhibits the same phenomenon with identical coupling patterns in these positions equivalent to CH_2-8 through CH-28 in 5-hexynoic micacocidin. δ_c values are also consistent with the SDBS database entry for 6-heptynoic acid.[269]

4.3.4 Additional feeding experiments with *R. solanacearum*

Besides micacocidin, *R. solanacearum* is also a known producer of ralsolamycin A and B.[212] Similar to micacocidin biosynthesis, a fatty acid is used as a starter unit for the production of ralsolamycin (R^1 in Figure 4.16). In this case palmitic acid (C16) is loaded onto the NRPS assembly line after activation by a fatty acid AMP ligase (FAAL). Additionally, the eighth building block of ralsolamycin represents a position with potential to introduce alkyne amino acids (R^2 in Figure 4.16). Due to the relaxed substrate specificity of the corresponding NRPS A domain, naturally either valine or isoleucine are incorporated, forming ralsolamycin A or ralsolamycin B, respectively.[212] To investigate promiscuity of the FAAL and the gatekeeping A-domain, and to create a range of alkyne ralsolamycin congeners, a series of feeding studies with fatty acids and amino acids were carried out as detailed in Figure 4.16 and Table 4.10.

LC-MS analysis of the extract from a control culture confirmed the production of the previously reported ralsolamycins A and B. Furthermore, two mass traces were detected which corresponded to ralsolamycin derivatives incorporating myristic instead of palmitic acid residues. Exogenous supply of these two fatty acids during cultivation (Table 4.10 **A**, **B**) did not improve ralsolamycin production, but in contrast, decreased the observed amounts of ralsolamycin A and B to trace levels. In contrast, supplementing the cultures with the alkyne equivalents 13-tetradecynoic and 15-hexadecynoic acid (Table 4.10 **C**, **D**) did not affect ralsolamycin production and gave rise to two new peaks in each feeding setting, matching with calculated mass values of alkyne myristic and palmitic acid-derived ralsolamycins. On the other hand, feeding of D/L-propargylglycine and L-homopropargylglycine (Table 4.10 **E**, **F**) had no detectable effect on ralsolamycin biosynthesis. A targeted search by MS did not provide
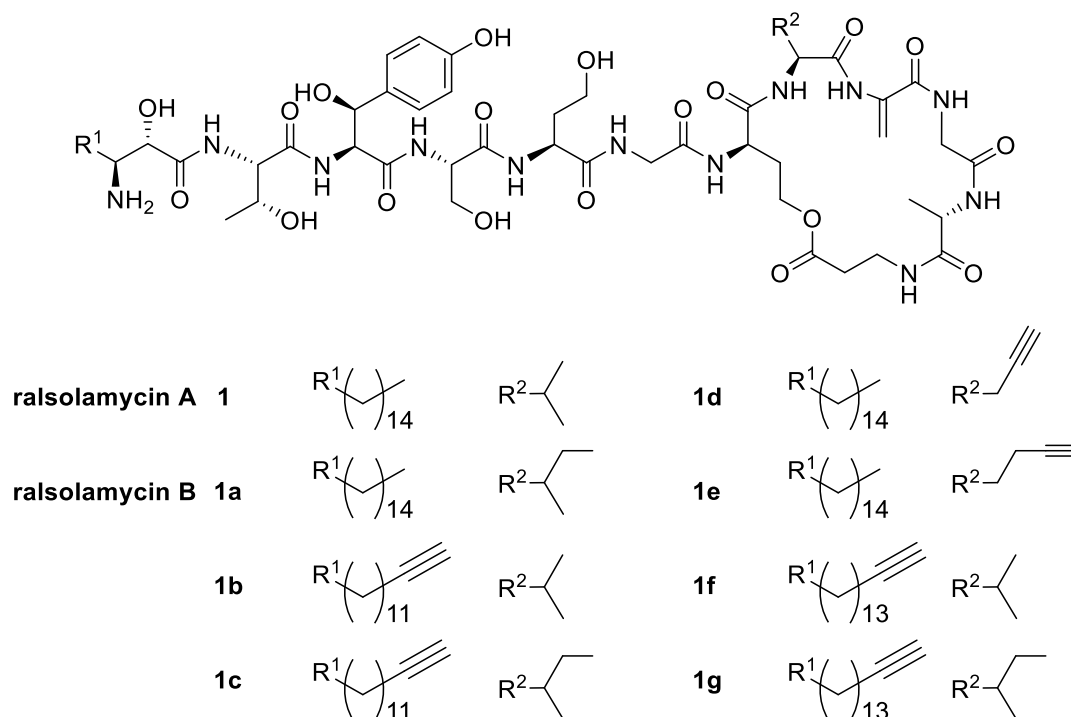
Figure 4.16 Ralsolamycins and derivatives anticipated in alkyne feeding experiments
Ralsolamycin A (**1**) and B (**1a**) and conceivable analogs derived from 13-tetradecynoic acid (**1b**, **c**), propargylglycine (**1d**) and homopropargylglycine (**1e**), and 15-hexadecynoic acid (**1f**, **g**).

Table 4.10 Feeding studies targeting ralsolamycins

#	Precursor	Incorporation	Derivative produced (Figure 4.16)	Ralsolamycin A, B titer
control	-	O	**1, 1a**	control
A	myristic acid	+	n.d.	decreased
B	palmitic acid	+	**1, 1a**	decreased
C	13-tetradecynoic acid	+	**1b, c**	unchanged
D	15-hexadecynoic acid	+	**1f, g**	unchanged
E	D/L-propargylglycine	-	-	unchanged
F	L-homopropargylglycine	-	-	unchanged

[a] **+** incorporation observed, **-** no incorporation, n.d. not detected.

any evidence for the predicted derivatives, resulting from the exchange of the valine/isoleucine residue with the alkyne amino acids. In summary, incorporation of 13-tetradecynoic and 15-hexadecynoic acid resulted in the desired compounds (Figure 4.16 **1b**, **1c**, **1f** and **1g**), though at low production yield. Incorporation of the alkyne amino acids was not observed.

In summary, the *R. solanacearum* feeding experiments revealed, that alkyne fatty acids with a similar chain length to the natural precursors are suitable candidates to introduce alkyne functionalities into micacocidin and ralsolamycins, respectively. Since the former was found to be significantly more abundant, it was considered the most suitable model compound for the following method development towards a robust Click reaction for chromophore labelling. At first, the precursors alone were subjected to a variety of reaction conditions and subsequently *R. solanacearum* crude extracts tested in the optimized setting.

4.3.5 Prototype Click reactions with precursors

Various parameters like temperature, copper concentration and reactant ratio were tested in prototype reactions, of the respective precursors D/L-propargylglycine (DL-PG) or 6-heptynoic acid (6HepA) with the fluorophore 6-carboxyfluorescein azide (6-FAM-N$_3$). The results were monitored by HPLC-DAD analysis at 496 nm and area under the curve (AUC) ratios applied to quantify the conversion.

As detailed in Table 4.11, the reactions for DL-PG did not give the desired product, but a high degree of unspecific degradation of the fluorophore could be observed, rather than a targeted reaction towards the merged product. All chromatograms show a variety of peaks with a global maximum of 496 nm, yet, this impedes assignment of the desired product by HPLC-DAD only. Subsequent analysis of the test reactions by LC-MS revealed product formation only with minor yield and the observed side products cannot be correlated with other potentially expected derivatives of 6-carboxyfluorescein or DL-PG. Overall, DL-PG appears to interfere with the performed reaction, resulting in a degradation of the fluorophore.

In contrast, for 6HepA, preferred reaction conditions could be concluded from these prototype reactions. Alone the alternation of the azide to alkyne ratio from 2:1 up to 1:20 strongly improves the reaction yield towards better turnover and doubles the yield at conditions of 25°C and 250 µM Cu$^+$. Further, an increase of either the copper concentration from 100 µM to 250 µM or the temperature from 25°C to 40°C gives significantly improved product formation. Overall, reactions number **7**, **8**, **10** and **11** (Table 4.11) yield 80% of desired product. Hence, these reaction conditions were identified as the most robust for further derivatization of raw extract material.

Table 4.11. Results from test reactions of D/L-propargylglycine and 6-heptynoic acid with 6-carboxyfluorescein azide (6-FAM-N$_3$) under various reaction conditions, all over night

	Reaction #	Azide : Alkyne ratio	D/L-propargylglycine		6-heptynoic acid	
			6-FAM-N$_3$ [%]	Yield [%]	6-FAM-N$_3$ [%]	Yield [%]
25°C, 100 µM Cu$^+$	1	2:1	99.1	0	99.5	0
	2	1:1	96.7	0	99.6	0
	3	1:2	99.5	0	98.9	0.4
	4	1:10	99.4	0	89.2	6.7
	5	1:20	99.4	0	73.7	17.7
25°C, 250 µM Cu$^+$	6	2:1	44.4	0	51.2	41.4
	7	1:2	0	0	0	79.5
	8	1:20	0	0	0	80.1
40°C, 100 µM Cu$^+$	9	2:1	35.5	0	-	-
	10	1:2	-	-	8.7	78.4
	11	1:20	0	0	0	81.9
40°C, 250 µM Cu$^+$	12	2:1	49.4	0	70.1	27.3
	13	1:2	0	0	13.4	73.2
	14	1:20	0	0	0	75.4

4.3.6 Click derivatization of *R. solanacearum* extracts

The five extracts of *R. solanacearum* fed with alkyne fatty acids (chapter 4.3.2) were subjected to a Click reaction derivatization with 6-FAM-N$_3$ (Figure 4.17).

Subsequently two analytical evaluation strategies were applied, firstly by HPLC-UV/VIS and secondly via HPLC-MS (Figure 4.18). The alkaline conditions of the HPLC-UV/VIS eluents (buffered to pH 8) are ideal for detection of the fluorescein-derived marker (Figure 4.18 **1**) at high specificity and sensitivity, since it exhibits an absorption maximum at 496 nm with a higher absorption coefficient than under acidic conditions. As expected, the extract without alkyne supplementation is dominated by 6-FAM-N$_3$, but it is also found as residual traces in the alkyne-fed cultures. In the latter, the most abundant peaks were identified as the triazole products of 6-FAM-N$_3$ merged with the supplied precursor alkyne fatty acids.
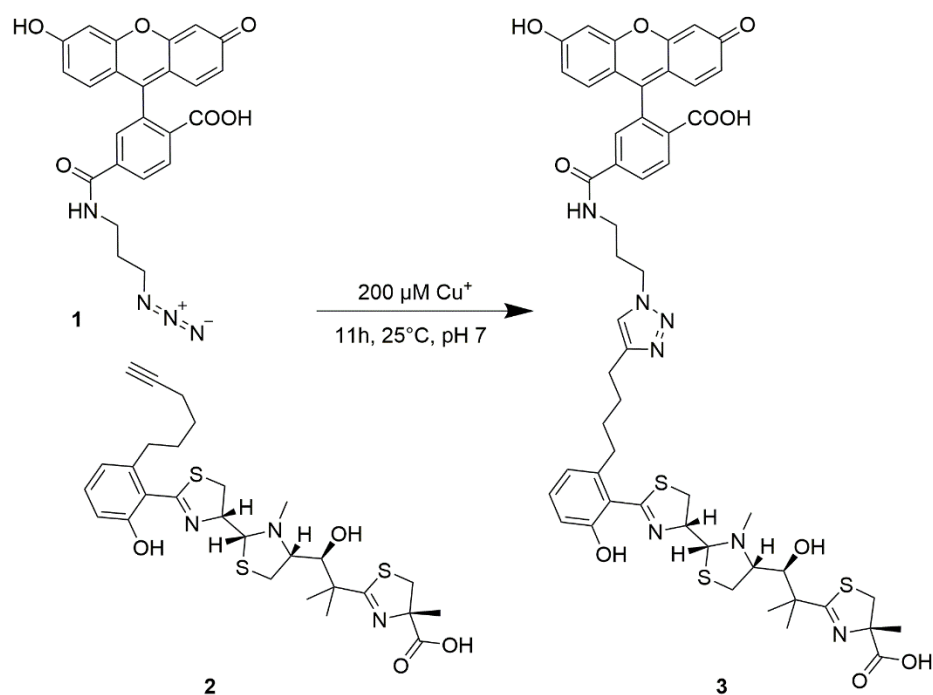
Figure 4.17 Labelling of alkyne micacocidins with a fluorophore marker
Exemplified CuAAC Click reaction of 6-carboxyfluorescein azide (6-FAM-N$_3$) (**1**) and 5-hexynoic micacocidin (**2**), resulting in the triazole (3+2) product thereof (**3**).
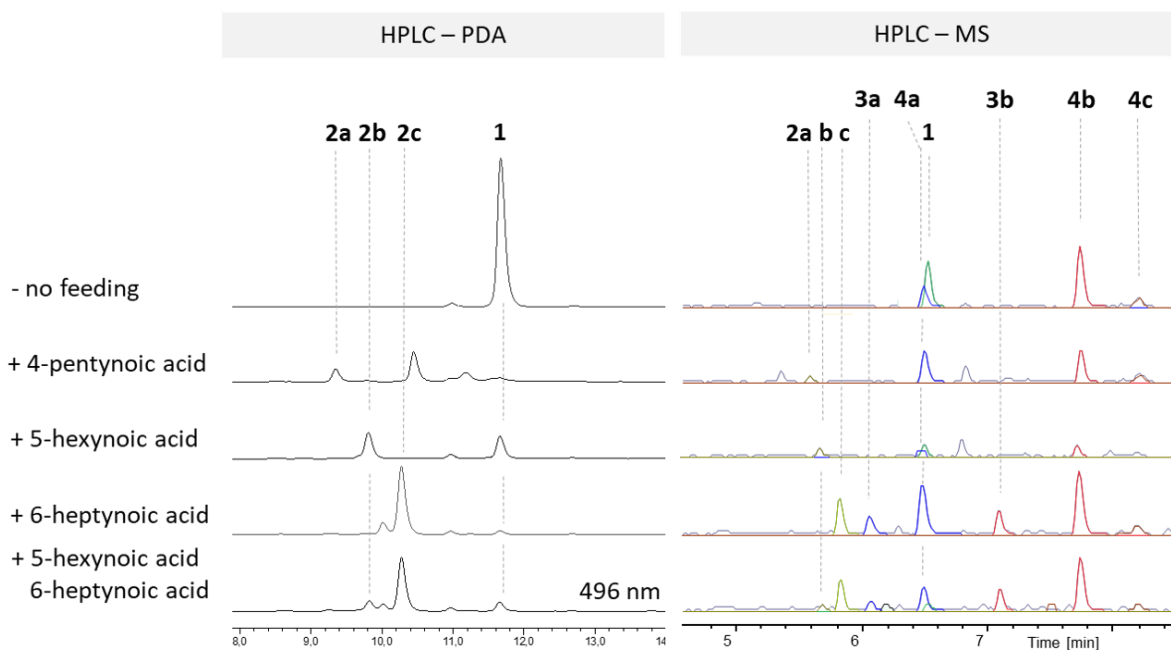
Figure 4.18 HPLC-UV/VIS and HPLC-MS analysis of *R. solanacearum* extracts fed with alkyne fatty acid precursors, after Click reaction with 6-FAM-N$_3$
Identified major compounds include: 6-FAM-N$_3$ (**1**); Triazole (3+2) product of 6-FAM-N$_3$ with 4-pentynoic acid (**2a**), 5-hexynoic acid (**2b**), 6-heptynoic acid (**2c**); 5-hexynoic micacocidin complexes with Cu^{2+} (**3a**) or Al^{3+} (**3b**); Natural micacocidin complexes with Cu^{2+} (**4a**), Al^{3+} (**4b**) or Fe^{3+}(**4c**).

Corresponding HPLC-MS analyses confirmed the prevalent presence of 6-FAM-N_3-derivatized precursors, together with residual alkyne micacocidins, indicating incomplete reaction turnover. Natural micacocidin complexes are also still present in all the extracts as observed before the derivatization. Their chemistry was not influenced by the reaction, which confirms stability of micacocidin chelates under reaction conditions and selectivity of the Click reaction towards alkyne reaction handles. A targeted search for masses corresponding to the alkyne micacocidin complex merged with 6-FAM-N_3 revealed that only minor quantities of the desired product were formed. For the most abundant derivative, 6-heptynoic acid-derived micacocidin, the corresponding UV/VIS chromatogram recorded in parallel at the HPLC-MS set-up did not exhibit the respective peaks, but only one strong peak corresponding to the derivatized precursor (Figure 4.18 **2c**).

Since 6-heptynoic acid was identified to have the highest alkyne incorporation rate, the corresponding 5-hexynoic micacocidin-Al^{3+} chelate was chosen as the model compound. Its 6-FAM-N_3 derivative is expected to display a combined UV/VIS spectrum of both chromophore regions within the molecule. 6-FAM-N_3 has its distinct maximum at 496 nm and 5-hexynoic micacocidin-Al^{3+} is assumed to differ only marginally from its natural micacocidin-Al^{3+} analog with its distinct maxima at 276 and 359 nm. Therefore, the unsupplemented culture extract as negative control was compared to the 6-heptynoic acid-fed example and both evaluated in detail at 359 and 496 nm (Figure 4.19). Minor peaks that occurred at both wavelengths but exclusively in the supplemented culture were selected and their UV/VIS spectra were examined. 6-FAM-N_3, 6-heptynoic acid-derivatized 6-FAM-N_3 and micacocidin-Al^{3+} showed spectra as expected and discussed above. However, all newly observed peaks only resembled the spectrum of the educt 6-FAM-N_3 without additional maxima (exemplary shown for Figure 4.19, **4** and **5**). Although the interpretation is limited by signal strength, it can be concluded, that under the tested conditions and at 496 nm, the desired alkyne-micacocidin-6-FAM-N_3 product is not detectable.
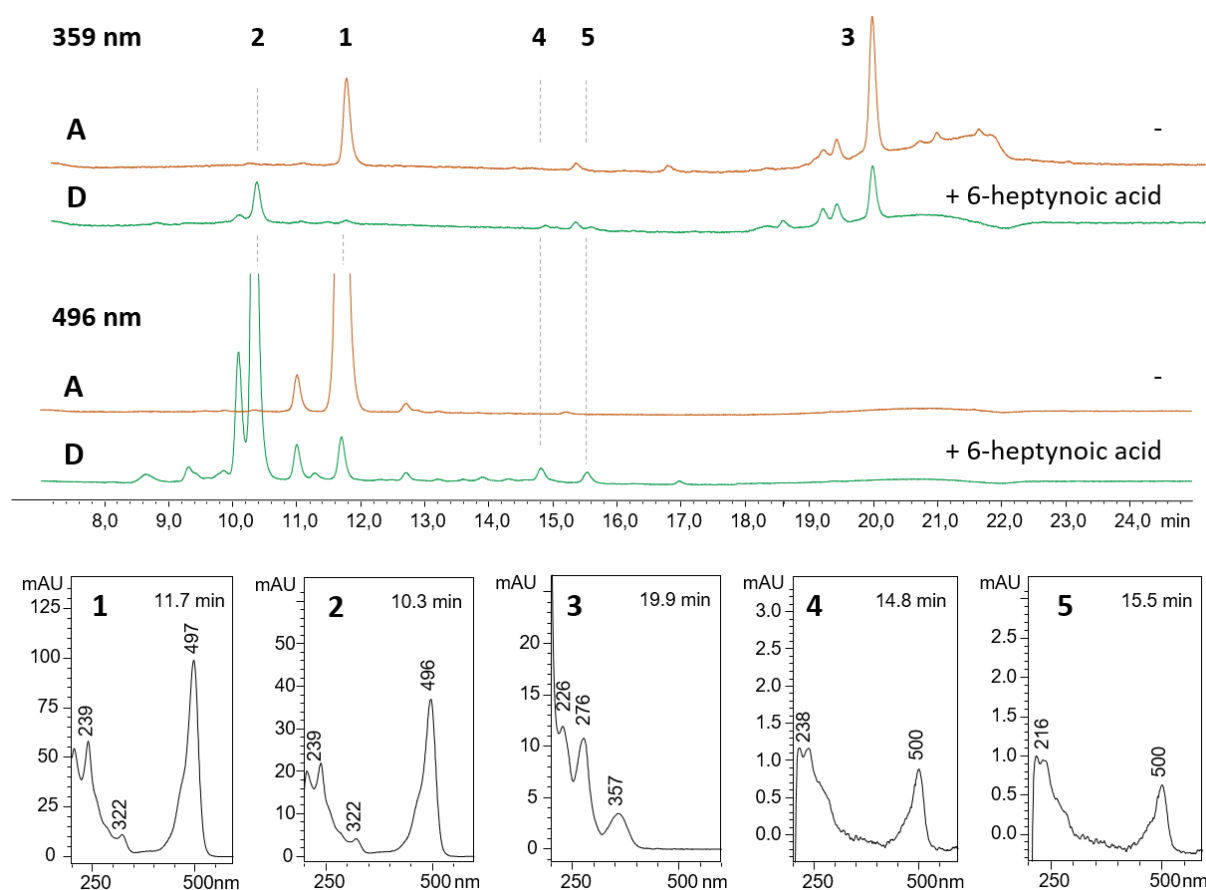
Figure 4.19 Comparison of UV/VIS absorption at 361 and 496 nm after Click reaction in 6-heptynoic acid-fed cultures.
6-FAM-N$_3$ (**1**), 6-FAM-N$_3$-heptynoic acid (**2**), micacocidin-Al^{3+} complex (**3**), unknown compounds (**4**, **5**). In chromatograms at λ = 496 nm new peaks arise after Click reaction. These were compared to the chromatograms at 359 nm, the local maximum observed for micacocidin-Al^{3+}, for both settings, without feeding (**A**) and after feeding 6-heptynoic acid (**D**). UV/VIS spectra from **D** at the relevant time points. **4** and **5** relate to new peaks at 496 nm but show no pattern that combines the features of **1** and **3**.

To understand restrictions in these Click reaction processes, relative reaction yields were calculated from the HPLC-UV/VIS chromatogram at 496 nm (Table 4.12). For this purpose, the chromatograms from 4 – 16 min were integrated to determine the overall AUC and the areas of the single compounds rated proportionally. Considering that the precursors were all supplied in equal quantities, their reaction yields towards the expected precursor-chromophore yields vary by factor 10, ranging from 8.3% to 85.7% for 4-pentynoic acid and 6-heptynoic acid, respectively (Table 4.12 **B**, **D**). Conversely, unspecific side reactions take up to 74.9% of the marker chromophore 6-FAM-N$_3$ (Table 4.12 **B**).

Table 4.12 Results from raw extract derivatization with 6-carboxyfluorescein azide

#	Precursor(s)	HPLC-UV/VIS at 496 nm			
		6-FAM-N$_3$ (%)	Alkyne-micacocidin-6-FAM-N$_3$ product yield (%)	Precursor-6-FAM-N$_3$ product yield (%)	Other (%)
blank	-	99.5	-	-	0.5
A	-	99.5	-	-	0.5
B	4-pentynoic acid	16.8	0.0	8.3	74.9
C	5-hexynoic acid	37.8	-[a]	44.9	17.3
D	6-heptynoic acid	4.2	0.0	85.7	10.1
E	5-hexynoic acid + 6-heptynoic acid	11.2	0.0	60.0	28.8

[a] 5-hexynoic acid-derived micacocidin was not produced

A possible explanation for the observed yield variance might be that reaction conditions were initially optimized for 6-heptynoic acid, which eventually gave the highest percentage of predicted product. In contrast to a desired robust and widely applicable reaction set-up, the chosen conditions seem to allow a variety of side reactions that diverge chromophore reactant away from the alkyne target moieties. This experiment did not allow UV/VIS-guided detection of the alkyne micacocidin chelates even though they are present in major amounts. Accordingly, the derivatization of alkyne ralsolamycins, which had only been produced in trace amounts, was omitted.

4.3.7 Discussion

This project depicts, that in particular alkyne fatty acids are suitable building blocks to introduce acetylenic residues into secondary metabolites. This concept was proven by generating alkyne micacocidin congeners in quantitative and ralsolamycin derivatives in minor amounts in *R. solanacearum*. Feeding experiments with alkyne amino acids were unsuccessful for ralsolamycin, as they were for *M. xanthus* as a producer of numerous and diverse natural products. Regardless, the success for incorporation of an alkyne fatty acids also requires prerequisite knowledge about potentially accepted substrates. The example of micacocidin showed that extension or shortening the chain length by only one CH$_2$ unit drastically reduces the incorporation success. Therefore, the length of the artificial fatty acid should not deviate too much from the length of the natural one to allow incorporation.

A suitable Click reaction protocol was established with 6-carboxyfluorescein azide as chromophore marker and 6-heptynoic acid as target compound, resulting in 80% product yield. The molar reactant ratio azide to alkyne was initially set to 1:20, which leads to underrepresentation of the azide marker molecule. This is advantageous with regards to assay pricing, since a 1:1 ratio (equaling 10 mg 6-heptynoic acid) would generate marker costs of around 300 € per reaction. The tested 1:20 ratio however impairs a complete turnover of all alkyne functional groups present, which is limiting success in the setting of untargeted raw extract derivatization for two major reasons. Firstly, the extraction process should target recovery of a maximum number of compounds, assuring that all potential candidate compounds are analyzed. This waives the option to exclude the alkyne precursor molecule from the extract and creates an internal competition between supplemented compound and derivatized molecules. Additionally, secondary metabolites are often produced in low quantities and their alkyne-derived mimicry result in even lower yields. The potential strategy to increase precursor concentration towards higher production though aggravates such rivalry circumstances in azide marker consumption.

The micacocidin example also disclosed that chelating natural products may further complicate the identification process, because instead of one defined natural product multiple coordinated variants may be formed. In an untargeted experiment the desired products are unknown and such a multitude of complexes, resulting from the same compound, may disperse the peak intensity, hinder detection, or even deplete it below detection limit.

In summary, one of the most limiting factors was the detection limit in combination with high pricing of labelling chromophore. Therefore, alternative analytical methods should be employed to overcome these issues. Metabolomics analysis based on mass spectrometry data was recently developed, that allows creation of metabolic networks, clustering similar compounds based on their MS-MS fragmentation pattern. This tool, called "Global Natural Products Social Molecular Networking",[270] could be applied to identify the targeted alkyne-derivatives of micacocidins, ralsolamycins or unknown compounds. A specialized application targeting different ion species of the same molecule could help circumvent the observed complications when a compound chelates different metal ions, resulting in multiple peaks caused by one natural product.[271] Nevertheless, this requires high resolution MS equipment to achieve the data quality needed.

4.4 Final remarks

The studies presented in this thesis exemplify how precursor-directed biosynthesis as a universally applicable method can be employed to tackle various research questions. The derivatization of myxochelin B, pseudochelin A and aurachin D gave insights into the natural promiscuity of the biosynthetic assembly lines. Inspired by earlier feeding experiments in *P. fallax*,[71] 14 novel derivatives of myxochelin B and pseudochelin A were generated by artificial precursor feeding in an engineered *M. xanthus* strain in this PhD project. These products were found to have a similar or better bioactivity concerning 5-LO inhibition than the previously tested myxochelin A analogs and allowed to extend previous knowledge of structure-activity relationships of this compound class. Precursor-directed biosynthesis proved to be a rapid and effective method as no genetic manipulation is required. In particular, the dual incorporation of the 2,3-dihydroxybenzoic acid-like building blocks allowed generation of up to six derivatives with one feeding in the *M. xanthus* strain expressing MxcM. On the other hand, the limited acceptance of e.g. benzoic acid as precursor points out limits of the natural enzyme promiscuity and demands manipulation of the biosynthetic pathway for such poorly incorporated precursors. The bioactivities of pseudochelin A, but also its derivatives A_5 and A_7, stand out with 5-LO IC_{50} values that outcompete their myxochelin B equivalents, highlighting the relevance and potential of the dihydroimidazole moiety. They also suggest prospective experiments to optimize the molecules' inhibitory properties and moreover encourage testing of more myxochelins for their antileukemic potential.

It also shows that even 30 years after the discovery of this compound group new questions and ideas can arise. The insight into the biosynthetic pathway to pseudochelin A, for example, revealed the flexibility and versatility of the MxcM enzyme. This is particularly interesting with regard to its potential application as a biocatalyst, e.g. for semisynthesis, and moreover makes it a promising starting point for enzyme evolution towards alternative heterocycle-forming biochemistry.

Similarly, aurachin derivatization was achieved through feeding of halogenated anthranilic acid derivatives. Culture supplementation with 6-fluoroanthranilic acid and chlorinated precursor molecules though did not suffice for quantitative production, due to limited

incorporation. Herein precursor toxicity, presumably through crosstalk with primary metabolism, and limited substrate tolerance of the biosynthetic pathway exemplify once more limitations of the direct feeding approach. Inspired by the clinically used fluoroquinolone antibiotic ciprofloxacin, the three generated fluorinated aurachin D analogs, were found to have equipotent antibiotic bioactivities as the natural compound. Previously reported antiparasitic and anticancer bioactivities[93] of aurachins suggest further testing of these derivatives as potential future drug candidates in those fields.

The last study explored the possibility of alkyne precursor feeding coupled with Click chemistry derivatization towards untargeted compound discovery in two model strains. A range of amino acid-incorporating biosynthetic pathways of *M. xanthus* failed to accept the artificial surrogates D/L-propargylglycine and L-homopropargylglycine toward the corresponding peptide natural products, and the same was observed for ralsolamycin biosynthesis in *R. solanacearum*. In contrast, the feeding of fatty acids with a terminal alkyne group was more successful. Some of these fatty acid analogues were incorporated into the micacocidin scaffold in quantitative yields, whereas the ralsolamycin biosynthetic pathway was less tolerant regarding the utilization of these precursors. Still, measurable amounts of derivatives were produced.

Despite these limitations in yields, precursor-directed biosynthesis with fatty acids featuring a terminal alkyne group was found appropriate to investigate the experimental design. *R. solanacearum* was a suitable model organism because both assayed example compounds, micacocidin and ralsolamycin, are produced in different amounts. This reflects a realistic setup, as natural products in general may be abundant or barely detectable, testing the limits of applicability.

The optimized Click derivatization with 6-carboxyfluorescein azide showed fast turnover and satisfactory yields in aqueous conditions and thus followed the Click principle to be selective and bioorthogonal, even when the microbial raw extract was chosen as starting material. Regrettably, the project was halted because the free alkyne precursors outcompeted the natural products analogs in the Click reaction, since the latter were produced with limited yields. Yet, the initial strategy could be tested with alternative, MS-based detection set-ups. For future experiments, combination of *in silico* substrate prediction to determine suitable

alkyne fatty acid analogs, and chemical wet-lab experiments is advisable. Genetic manipulation of production strains could enable generation of enhanced substrate tolerance or improve metabolic flux of the building blocks involved.

Overall, these three projects show the inherent potential of precursor-directed biosynthesis, but also showcase limitations of this approach, as it is e.g. dependent on cellular uptake or natural promiscuity of the biosynthetic assembly lines. To find matching surrogates, prerequisite knowledge is needed, e.g. by bioinformatic analyses.

In summary, it has been shown how the biosynthetic flexibility of enzymes can be exploited to generate natural product analogs and likewise to use precursors as chemical probes that allow specific labeling of the compounds. Furthermore, the found and characterized natural product derivatives could extend the SAR knowledge in these substance groups and demonstrate once more the importance of natural products as lead structures in drug development.

5   Appendix

5.1   General Appendix
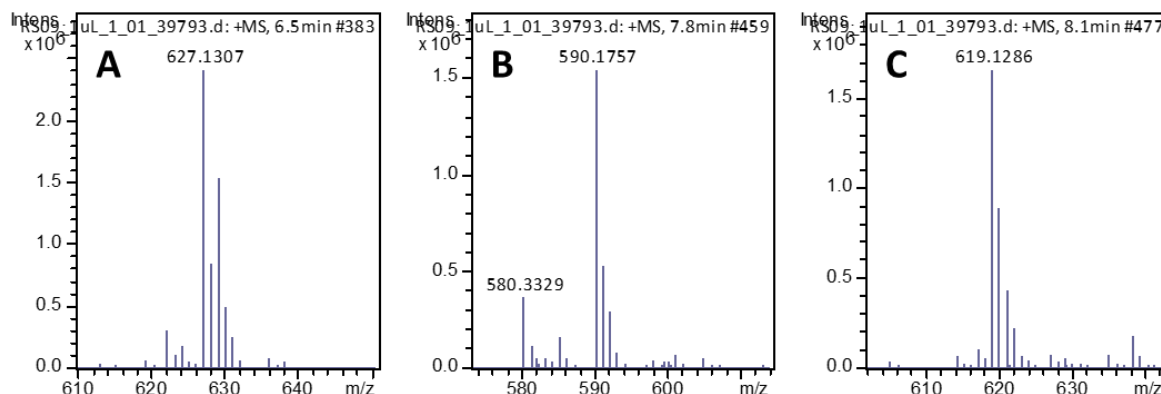
Figure S1 HR-MS spectra of micacocidin complexes. A. micacocidin-Cu^{2+}, $C_{27}H_{37}N_3O_4S_3Cu$, Theoretical *m/z* [M+H]$^+$ 627.1315, Δ -1.27 ppm; **B.** micacocidin Al^{3+}, $C_{27}H_{36}N_3O_4S_3Al$, Theoretical *m/z* [M+H]$^+$ 590.1756, Δ +0.17 ppm, **C.** micacocidin Fe^{3+}, $C_{27}H_{36}N_3O_4S_3Fe$, Theoretical *m/z* [M+H]$^+$ 619.1290, Δ -0.65 ppm.

Table S1 Relative production titers of micacocidin complexes and their alkyne derivatives before Click reaction. Natural micacocidin complexes in the negative control (**A**) set to 100%. Analogs of respective metal complex as relative percentage to negative control (%).

d#	Precursor(s)	Natural micacocidin (%)				Alkyne micacocidin (%)			
		Cu^{2+}	Al^{3+}	Fe^{3+}	Av.[a]	Cu^{2+}	Al^{3+}	Fe^{3+}	Av.[a]
A	-	100.0	100.0	100.0	100.0	-	-	-	-
B	4-pentynoic acid	30.9	45.9	36.5	37.8	1.7	1.3	0.0	1.0
C	5-hexynoic acid	0.2	3.9	0.0	1.4	0.0	0.0	0.0	0.0
D	6-heptynoic acid	53.2	22.9	50.5	42.2	27.8	8.3	6.1	14.1
E	5-hexynoic acid + 6-heptynoic acid	50.0	25.0	36.9	37.3	20.5	8.5	5.8	11.6

[a] Av = average percentage of Cu^{2+}, Al^{3+} and Fe^{3+} complex portions.

Table S2 Relative production titers of micacocidin complexes and their alkyne derivatives <u>after</u> Click reaction. Natural micacocidin complexes in the negative control (**A**) set to 100%. Analogs of respective metal complex as relative percentage to negative control (%).

#	Precursor(s)	Natural micacocidin (%)			Alkyne micacocidin (%)		
		Cu^{2+}	Al^{3+}	Fe^{3+}	Cu^{2+}	Al^{3+}	Fe^{3+}
A	-	100.0	100.0	100.0	-	-	-
B	4-pentynoic acid	119.8	37.0	65.0	1.7	0.6	0.0
C	5-hexynoic acid	13.5	15.4	22.5	0.0	0.1	0.0
D	6-heptynoic acid	223.0	84.6	115.1	80.9	29.2	24.2
E	5-hexynoic acid + 6-heptynoic acid	89.5	67.8	61.1	33.8	24.2	15.4

5.2   Spectroscopic Data

5.2.1 Myxochelin B

$[\alpha]^{20}_D$ –8.63 (c 0.87, MeOH);

UV/VIS (MeOH) λ_{max} (log ε): 249 (sh) (3.97), 314 (3.56) nm; NMR data as previously reported.[219]

5.2.2 Pseudochelin A

$[\alpha]^{20}_D$ –24.12 (c 0.28, MeOH);

UV/VIS (MeOH) λ_{max} (log ε): 253 (3.96), 319 (3.42) nm; NMR data as previously reported.[62,66]

5.2.3 Myxochelin B derivatives

5.2.3.1 Myxochelin B$_1$

Figure S2 HPLC-UV spectrum and ESI-MS spectrum of myxochelin B$_1$.
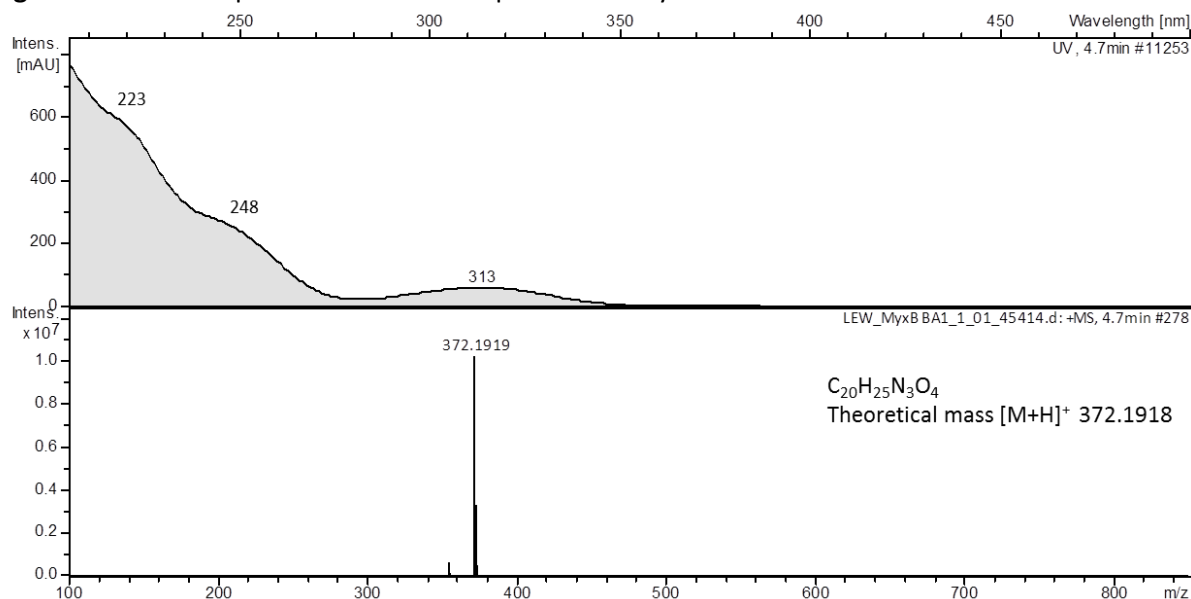
^{1}H NMR (600 MHz, methanol-d_4, 300 K) δ 7.74 (1H, dd, J = 7.0, 1.5 Hz, H-2''), 7.74 (1H, dd, J = 7.0, 1.5 Hz, H-6''), 7.50 (1H, dt, J = 7.5, 1.5 Hz, H-4''), 7.41 (1H, t, J = 7.5, 7.0 Hz, H-3''), 7.41 (1H, t, J = 7.5, 7.0 Hz, H-5''), 7.27 (1H, dd, J = 8.0, 1.5 Hz, H-6'), 6.95 (1H, dd, J = 8.0, 1.5 Hz, H-4'), 6.70 (1H, t, J = 8.0 Hz, H-5'), 4.38 (1H, ddt, J = 10.1, 7.0, 3.8 Hz, H-2), 3.40 (2H, t, J = 6.9 Hz, H-6), 3.18 (1H, dd, J = 13.0, 3.8 Hz, H-1a), 3.03 (1H, dd, J = 13.0, 10.1 Hz, H-1b), 1.73 (2H, m, H-3), 1.69 (2H, m, H-5), 1.55 (1H, m, H-4a), 1.48 (1H, m, H-4b);

^{13}C NMR (150 MHz, methanol-d_4, 300 K) δ 172.5 (C, C-7'), 170.4 (C, C-7''), 150.2 (C, C-2'), 147.4 (C, C-3'), 135.8 (C, C-1''), 132.6 (CH, C-4''), 129.5 (CH, C-3''), 129.5 (CH, C-5''), 128.2 (CH, C-2''), 128.2 (CH, C-6''), 119.9 (CH, C-4'), 119.7 (CH, C-5'), 119.0 (CH, C-6'), 116.7 (C, C-1'), 49.1 (CH, C-2), 45.2 (CH$_2$, C-1), 40.4 (CH$_2$, C-6), 32.5 (CH$_2$, C-3), 30.1 (CH$_2$, C-5), 24.2 (CH$_2$, C-4);

[α]$^{20}_D$ –9.26 (c 0.45, MeOH);

UV/VIS λ$_{max}$ (MeOH) nm (log ε): 248 (sh) (3.84), 316 (3.23) nm;

HRMS (ESI): *m/z* 372.1919 (calcd for C$_{20}$H$_{26}$N$_3$O$_4$, 372.1918).

Figure S3 ^{1}H NMR spectrum (600 MHz, CD$_3$OD) of myxochelin B$_1$.
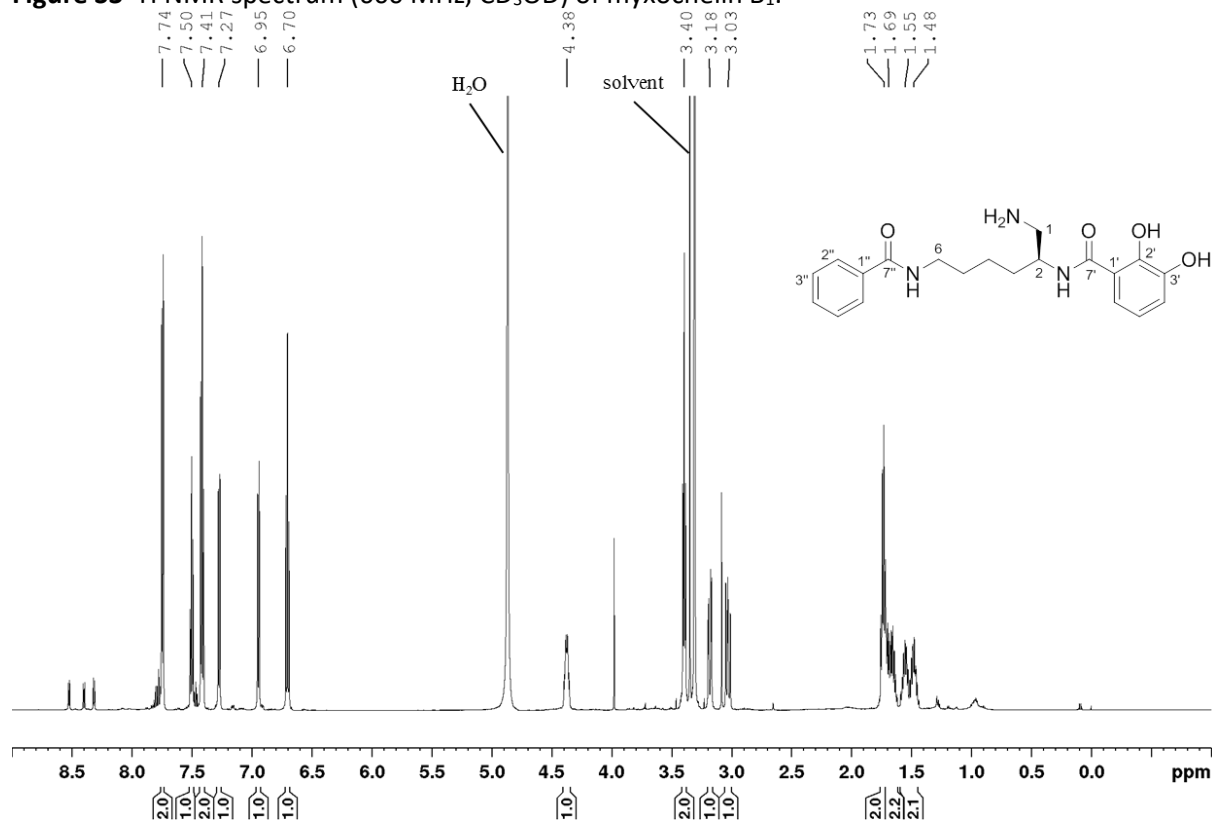
Figure S4. ^{1}H-decoupled ^{13}C NMR spectrum (150 MHz, CD$_3$OD) of myxochelin B$_1$.
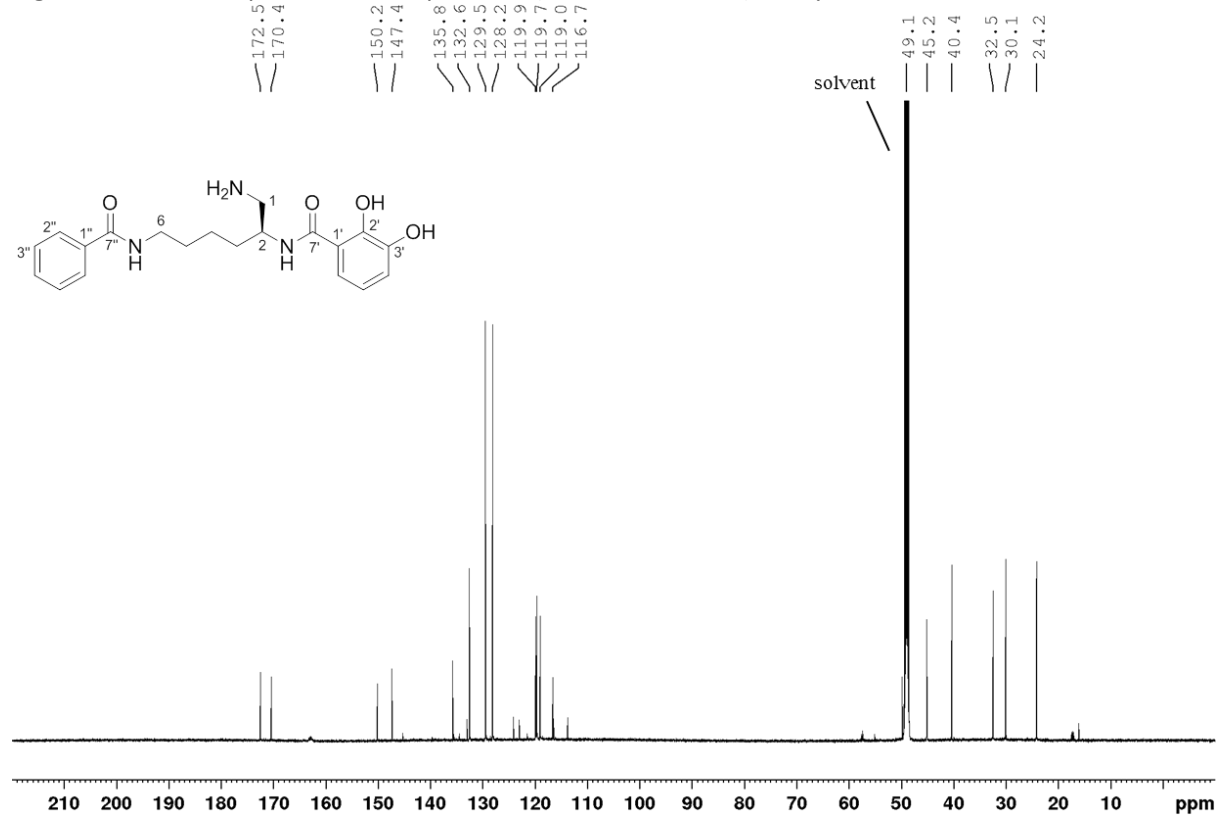
Figure S5. ^{1}H, ^{1}H COSY spectrum of myxochelin B$_1$ (CD$_3$OD).
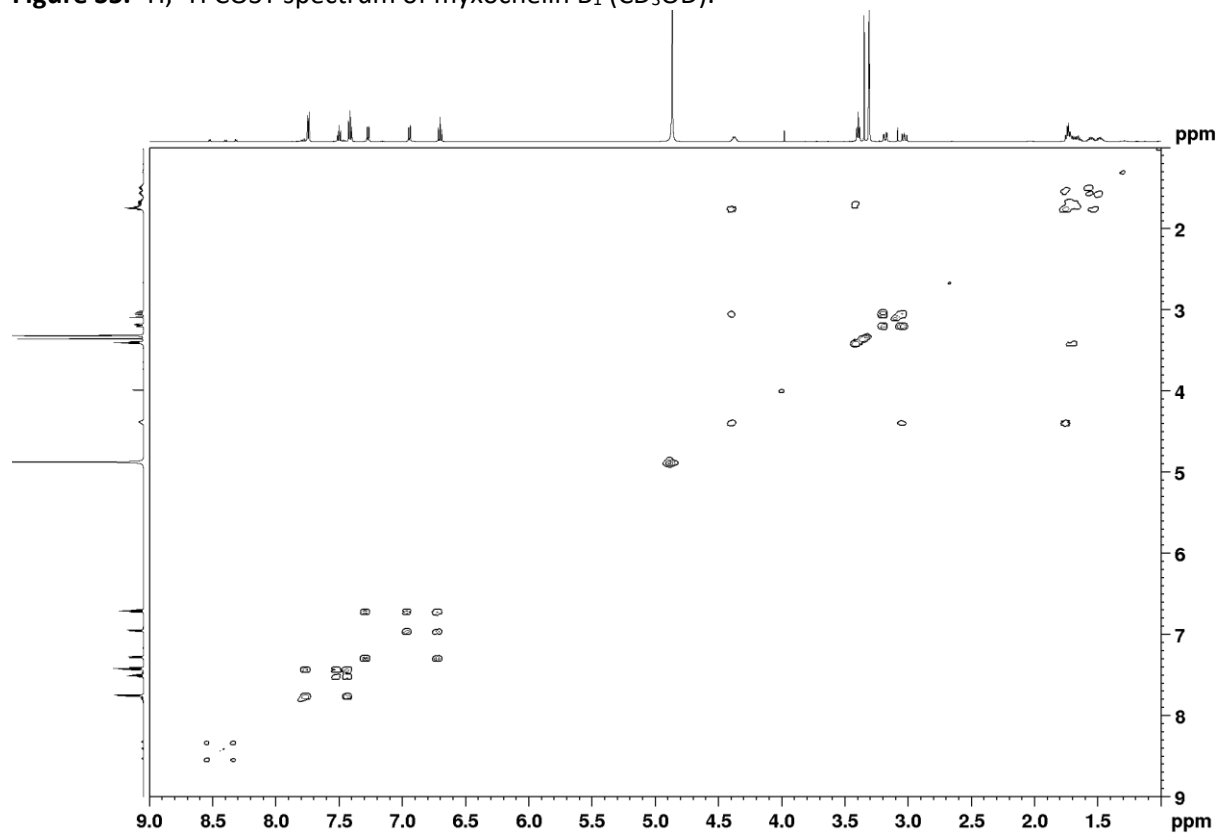
Figure S6. ^{1}H, ^{13}C HSQC spectrum of myxochelin B$_1$ (CD$_3$OD).
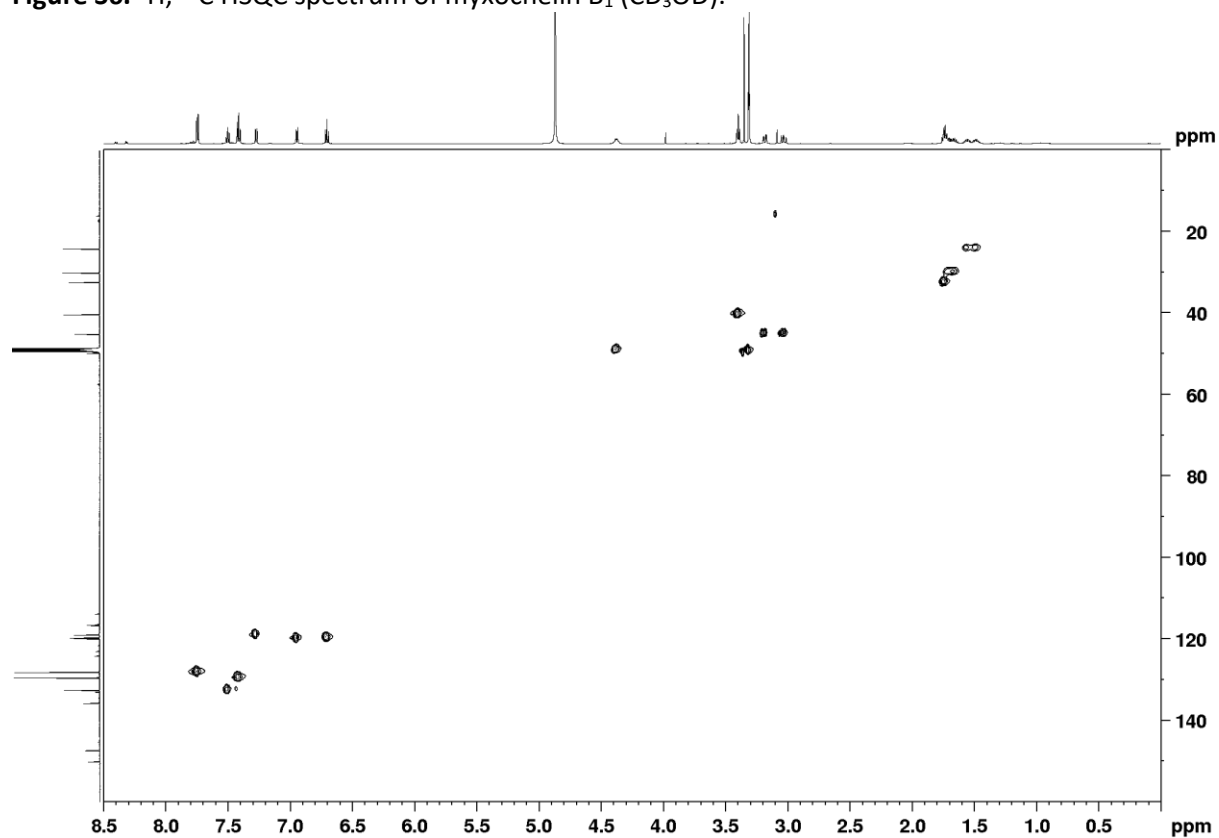
Figure S7 ^{1}H, ^{13}C HMBC spectrum of myxochelin B$_1$ (CD$_3$OD).
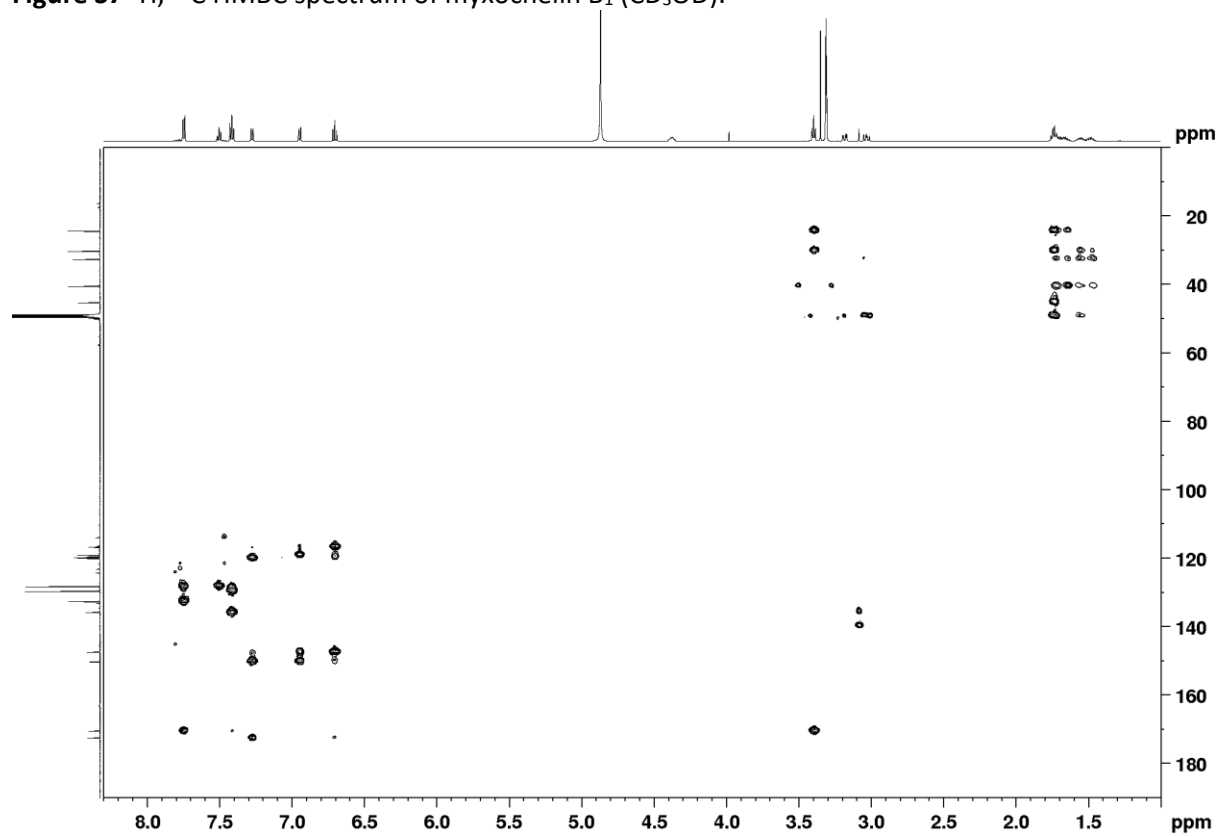
5.2.3.2 Myxochelin B$_2$

Figure S8. HPLC-UV spectrum and ESI-MS spectrum of myxochelin B$_2$.
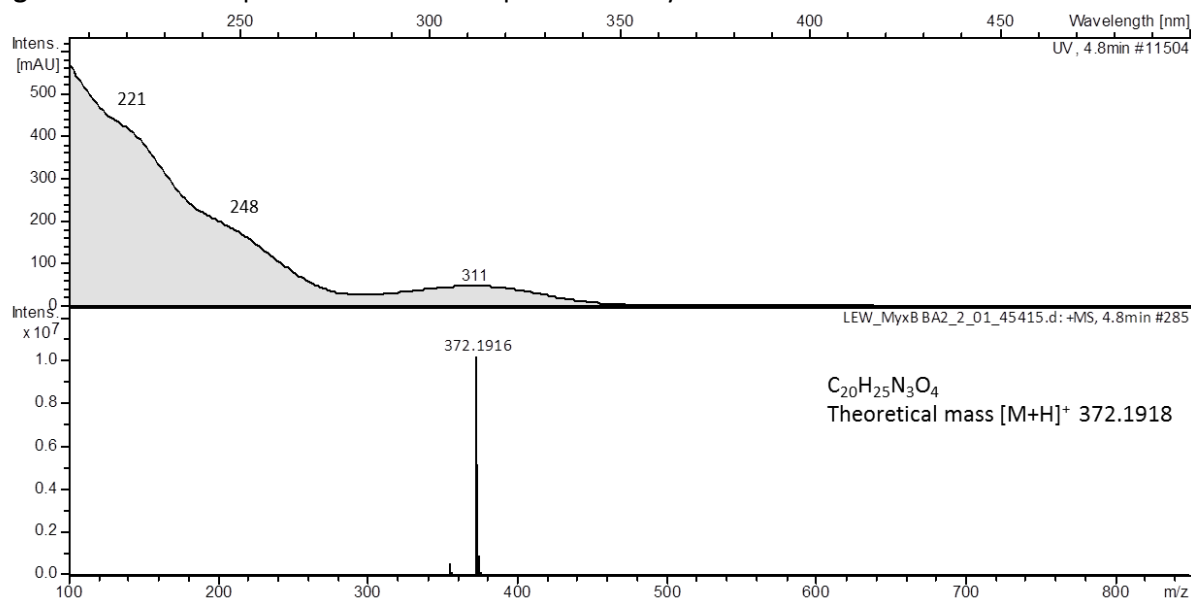
^{1}H NMR (600 MHz, methanol-d_4, 300 K) δ 7.83 (1H, d, J = 7.8 Hz, H-2'), 7.83 (1H, d, J = 7.8 Hz, H-6'), 7.53 (1H, t, J = 7.8 Hz, H-4'), 7.43 (1H, t, J = 7.8 Hz, H-3'), 7.43 (1H, t, J = 7.8 Hz, H-5'), 7.16 (1H, d, J = 8.0 Hz, H-6''), 6.92 (1H, d, J = 8.0 Hz, H-4''), 6.68 (1H, t, J = 8.0 Hz, H-5''), 4.33 (1H, ddt, J = 9.9, 7.2, 3.8 Hz, H-2), 3.40 (2H, t, J = 6.9 Hz, H-6), 3.17 (1H, dd, J = 13.0, 3.8 Hz, H-1a), 3.02 (1H, dd, J = 13.0, 9.9 Hz, H-1b), 1.73 (2H, m, H-3), 1.67 (2H, m, H-5), 1.56 (1H, m, H-4a), 1.48 (1H, m, H-4b);

^{13}C NMR (150 MHz, methanol-d_4, 300 K) δ 171.5 (C, C-7''), 171.4 (C, C-7'), 150.2 (C, C-2''), 147.4 (C, C-3''), 135.1 (C, C-1'), 133.0 (CH, C-4'), 129.6 (CH, C-3'), 129.6 (CH, C-5'), 128.5 (CH, C-2'), 128.5 (CH, C-6'), 119.6 (CH, C-4''), 119.6 (CH, C-5''), 118.6 (CH, C-6''), 116.8 (C, C-1''), 49.6 (CH, C-2), 45.1 (CH$_2$, C-1), 40.0 (CH$_2$, C-6), 32.7 (CH$_2$, C-3), 30.0 (CH$_2$, C-5), 24.3 (CH$_2$, C-4);

[α]$^{20}_D$ −8.95 (c 0.42, MeOH);

UV/VIS λ_{max} (MeOH) nm (log ε): 248 (sh) (3.89), 314 (3.35) nm;

HRMS (ESI): m/z 372.1916 (calcd for C$_{20}$H$_{26}$N$_3$O$_4$, 372.1918).

Figure S9. ^{1}H NMR spectrum (600 MHz, CD$_3$OD) of myxochelin B$_2$.
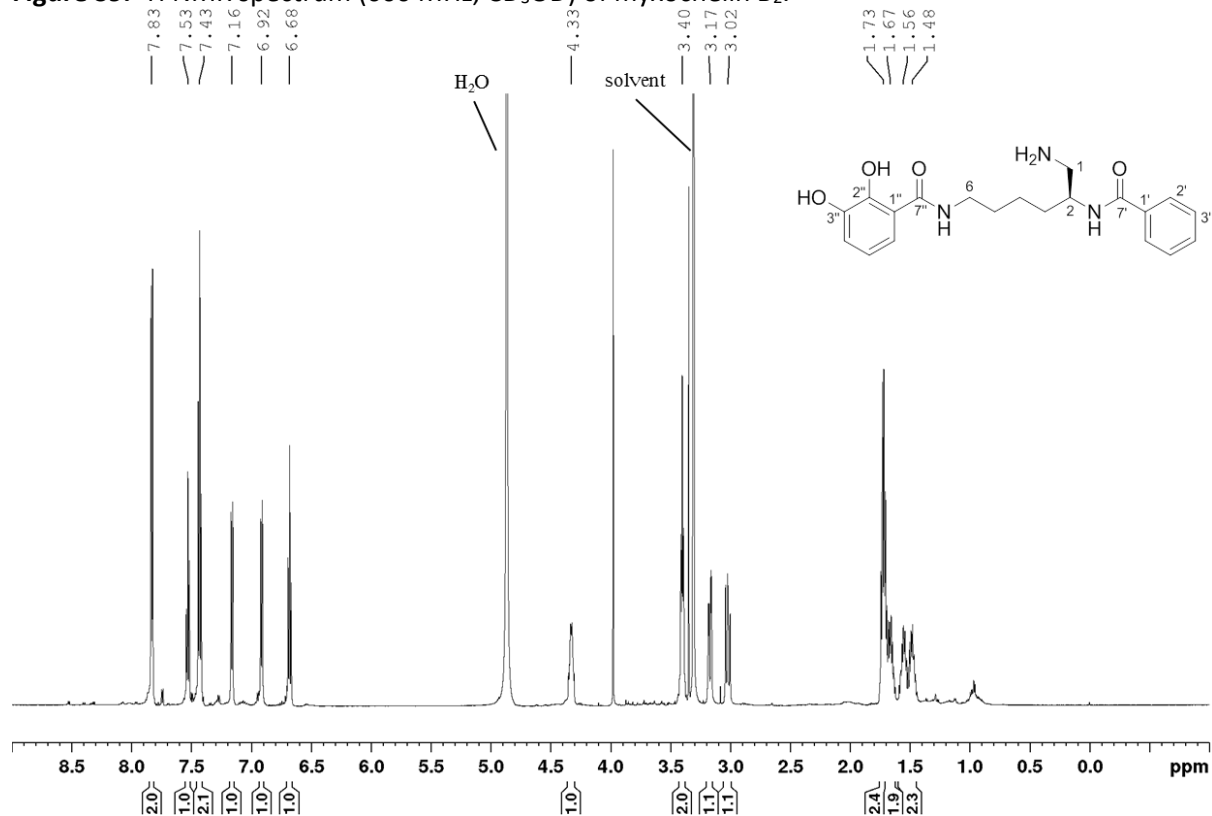
Figure S10. ^{1}H-decoupled ^{13}C NMR spectrum (150 MHz, CD$_3$OD) of myxochelin B$_2$.
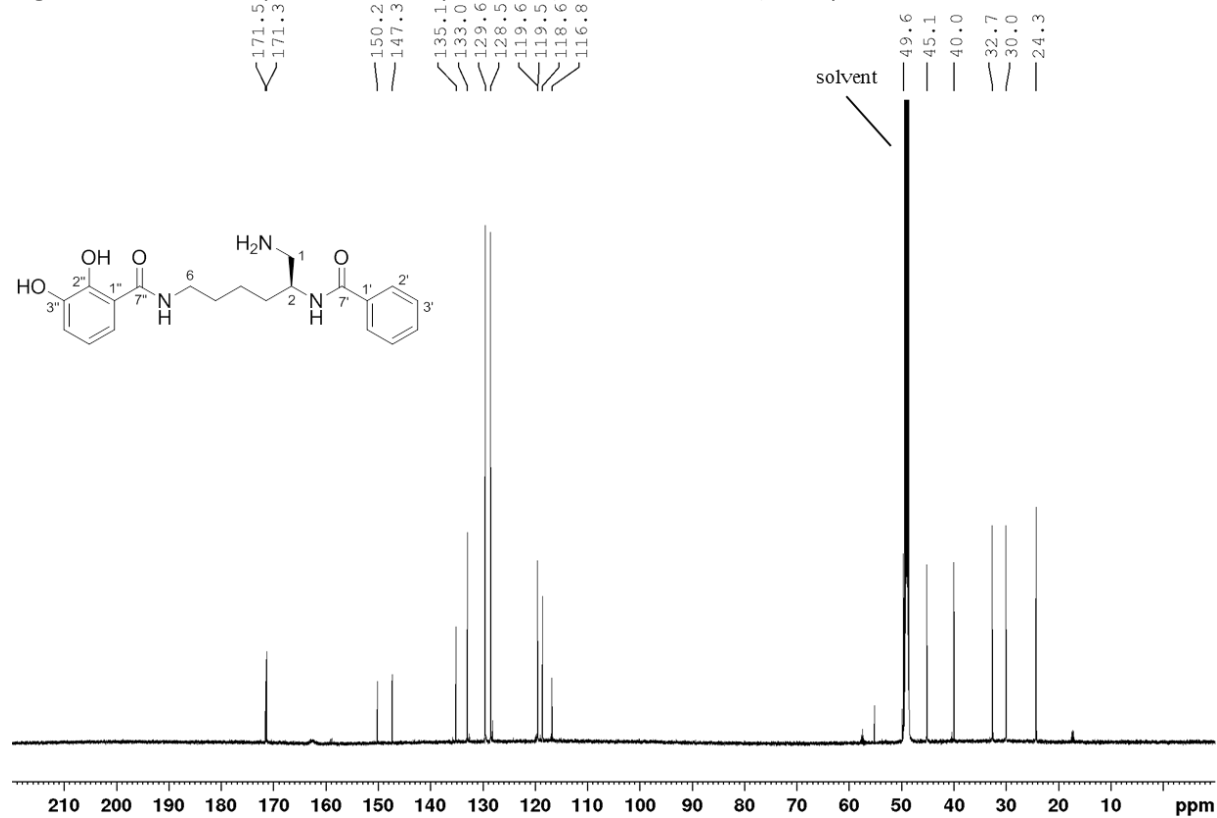
5.2.3.3 Myxochelin B$_4$

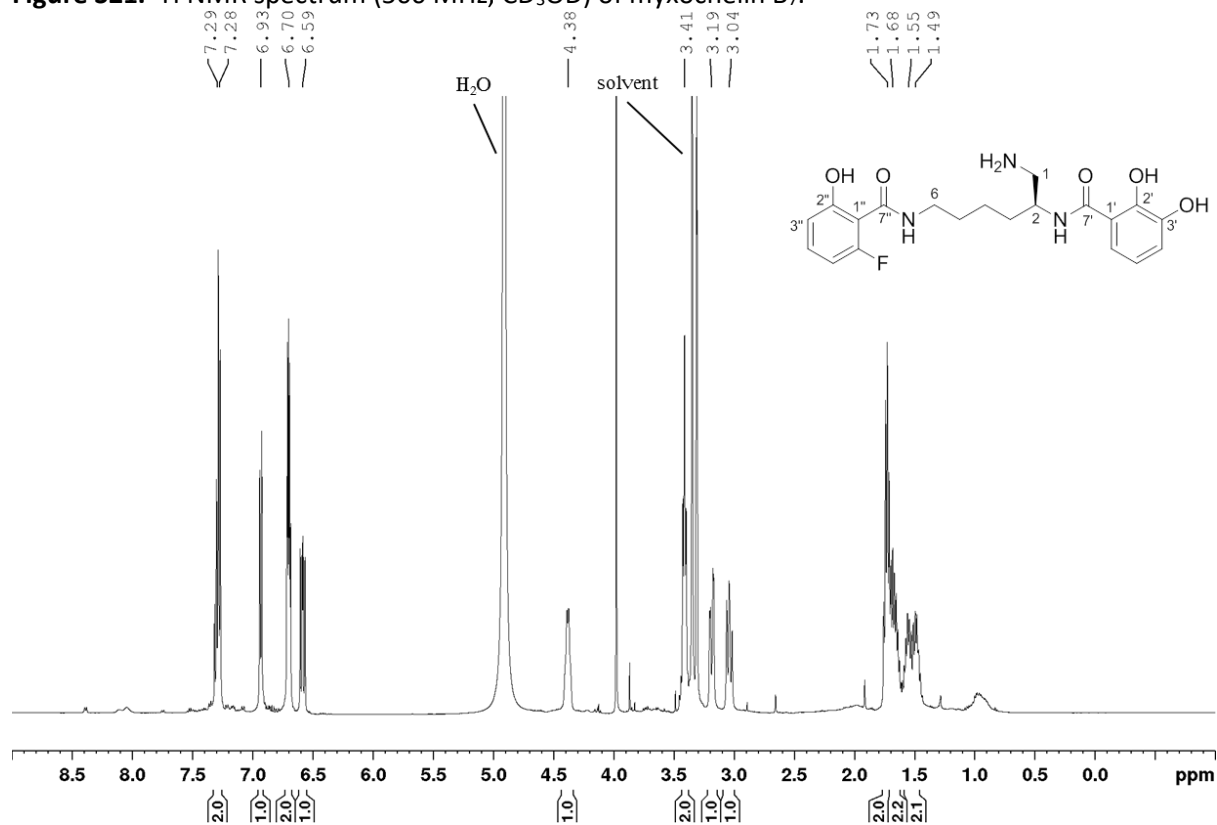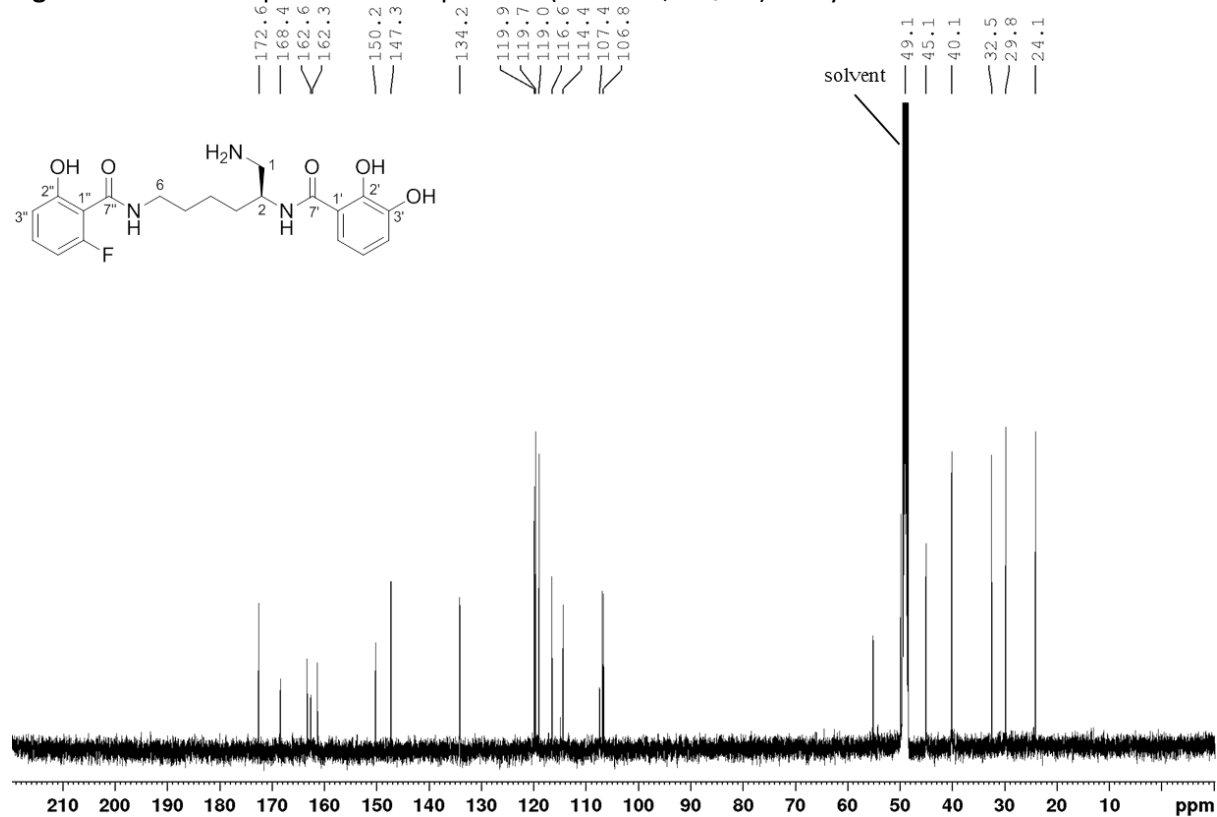**Figure S11.** HPLC-UV spectrum and ESI-MS spectrum of myxochelin B$_4$.
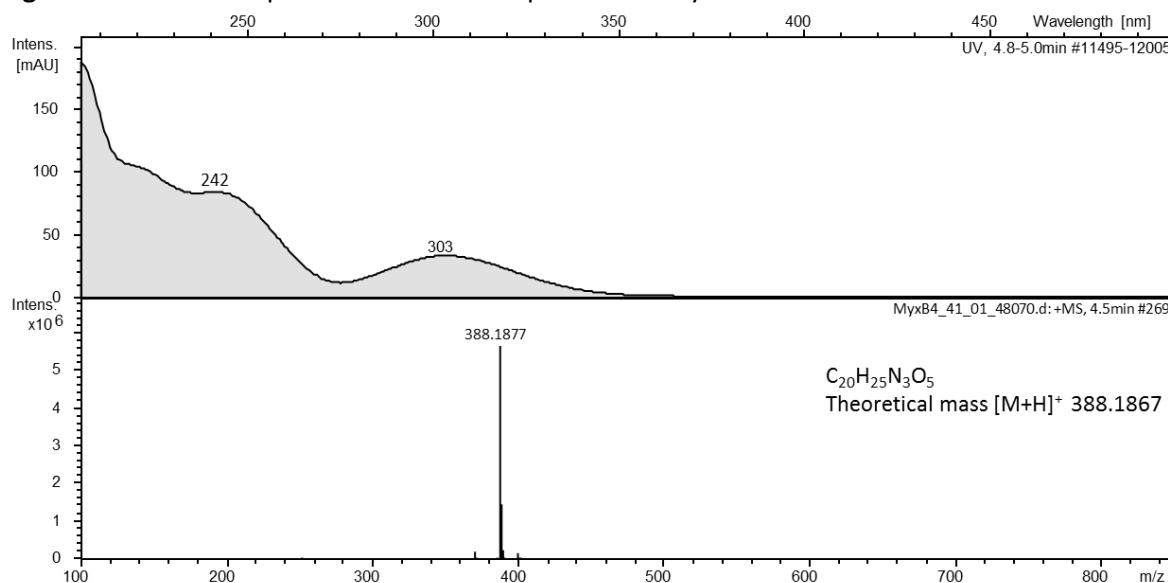
^{1}H NMR (600 MHz, methanol-d_4, 300 K) δ 7.69 (1H, dd, J = 8.0, 1.8 Hz, H-6''), 7.35 (1H, ddd, J = 8.3, 7.2, 1.8 Hz, H-4''), 7.27 (1H, dd, J = 8.1, 1.6 Hz, H-6'), 6.94 (1H, dd, J = 7.9, 1.6 Hz, H-4'), 6.87 (1H, dd, J = 8.3, 1.2 Hz, H-3''), 6.84 (1H, ddd, J = 8.0, 7.2, 1.2 Hz, H-5''), 6.70 (1H, t, J = 8.0 Hz, H-5'), 4.38 (1H, m, H-2), 3.40 (2H, m, H-6), 3.18 (1H, dd, J = 13.1, 2.5 Hz, H-1a), 3.04 (1H, dd, J = 13.0, 10.0 Hz, H-1b), 1.73 (2H, m, H-3), 1.68 (2H, m, H-5), 1.55 (1H, m, H-4a), 1.48 (1H, m, H-4b);

^{13}C NMR (150 MHz, methanol-d_4, 300 K) δ 172.5 (C, C-7'), 171.0 (C, C-7''), 161.1 (C, C-2''), 150.2 (C, C-2'), 147.3 (C, C-3'), 134.7 (CH, C-4''), 128.7 (CH, C-6''), 120.1 (CH, C-5''), 119.9 (CH, C-4'), 119.7 (CH, C-5'), 119.0 (CH, C-6'), 118.4 (CH, C-3''), 117.0 (C, C-1''), 116.6 (C, C-1'), 49.0 (CH, C-2), 45.1 (CH$_2$, C-1), 40.0 (CH$_2$, C-6), 32.5 (CH$_2$, C-3), 30.0 (CH$_2$, C-5), 24.3 (CH$_2$, C-4);

[α]^{20}$_D$ −9.31 (c 0.31, MeOH);

UV/VIS λ_{max} (MeOH) nm (log ε): 239 (sh) (3.92), 305 (3.55) nm;

HRMS (ESI): m/z 388.1877 (calcd for C$_{20}$H$_{26}$N$_3$O$_5$, 388.1867).

Figure S12. ^{1}H NMR spectrum (600 MHz, CD$_3$OD) of myxochelin B$_4$.
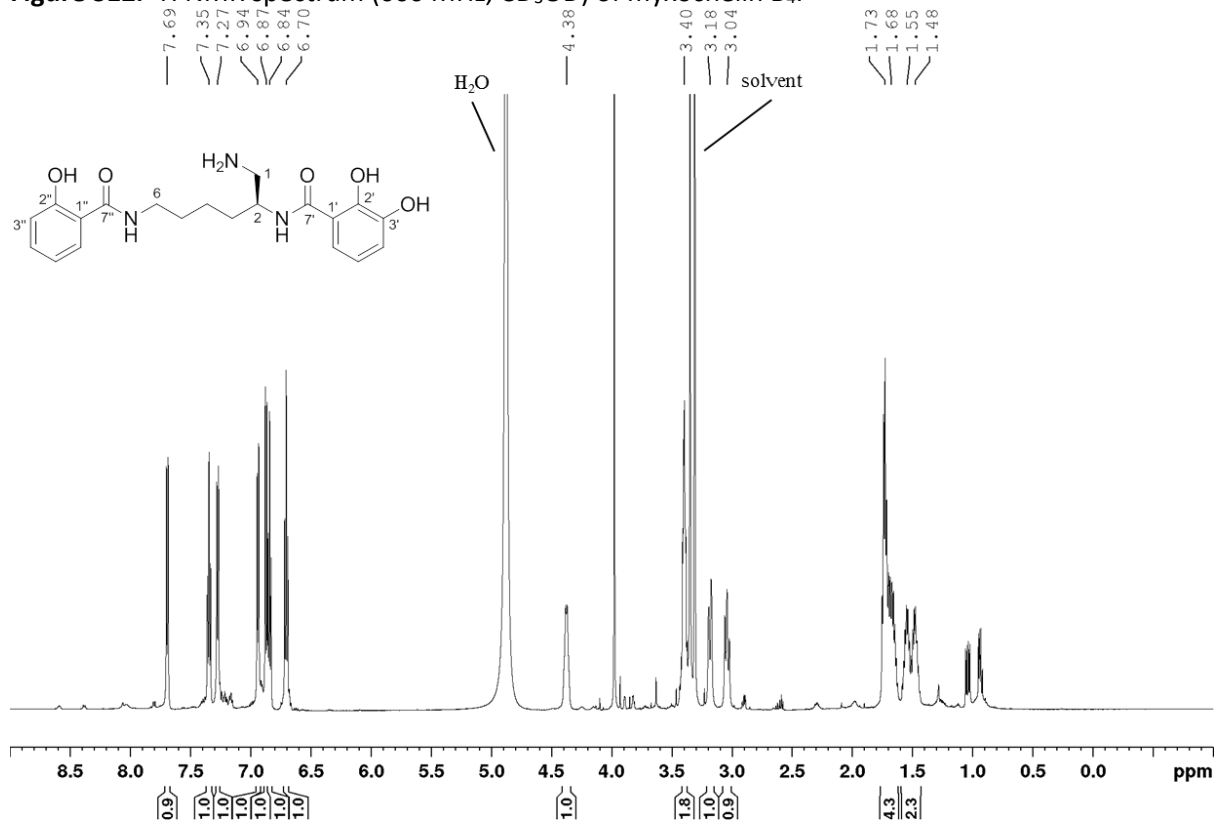
Figure S13. ^{1}H-decoupled ^{13}C NMR spectrum (150 MHz, CD$_3$OD) of myxochelin B$_4$**.**
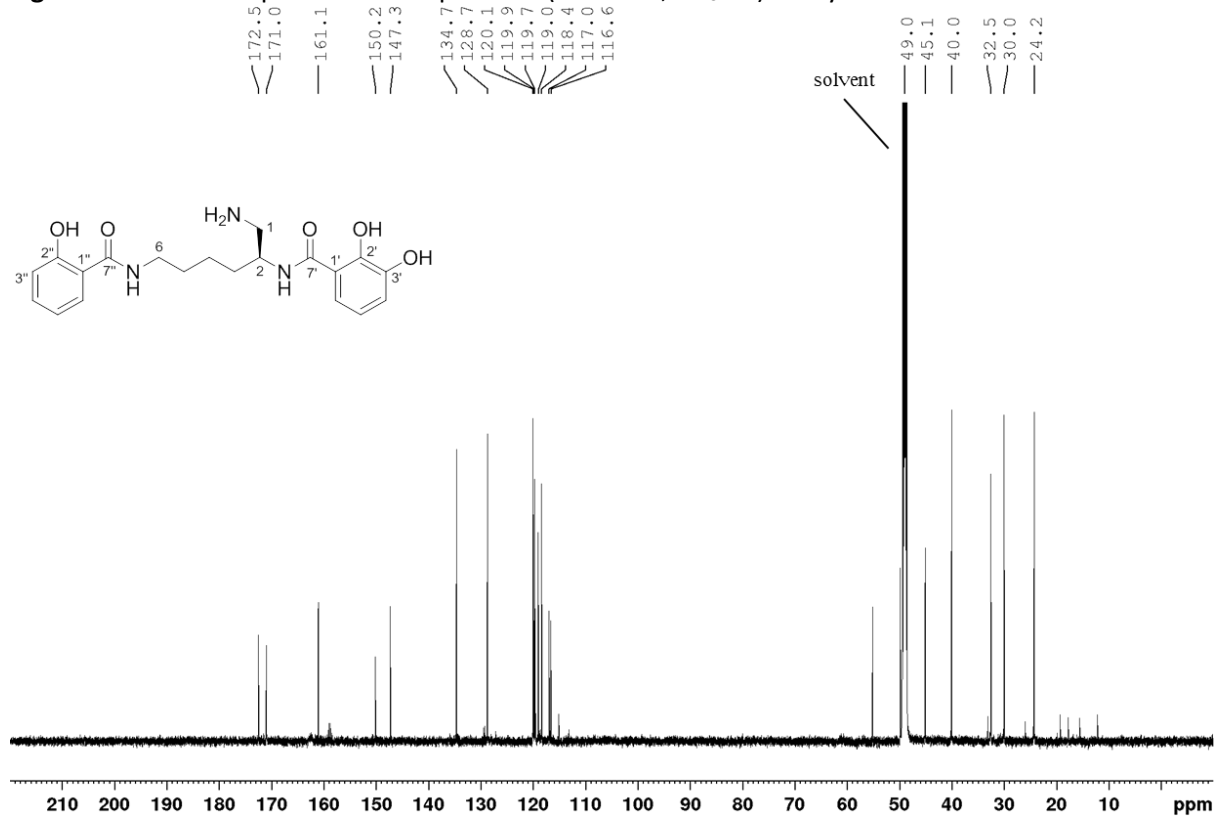
5.2.3.4 Myxochelin B₅

Figure S14. HPLC-UV spectrum and ESI-MS spectrum of myxochelin B₅.
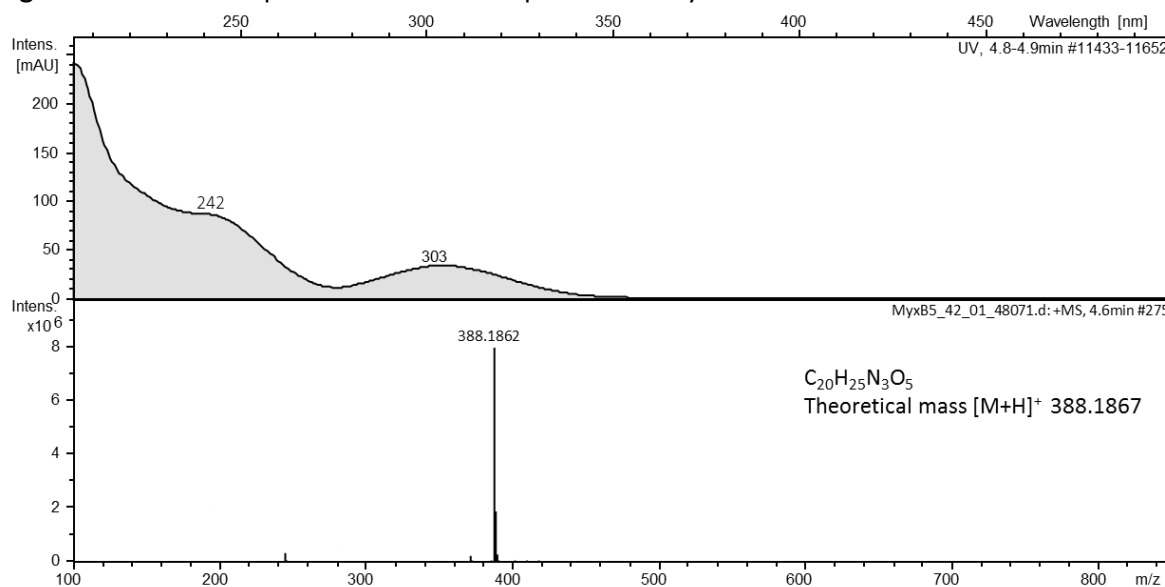
^{1}H NMR (600 MHz, methanol-d_4, 300 K) δ 7.79 (1H, dd, J = 8.0, 1.7 Hz, H-6'), 7.38 (1H, ddd, J = 8.4, 7.1, 1.7 Hz, H-4'), 7.16 (1H, dd, J = 8.1, 1.3 Hz, H-6''), 6.91 (1H, dd, J = 8.3, 1.2 Hz, H-4''), 6.90 (1H, dd, J = 8.3, 1.2 Hz, H-3'), 6.88 (1H, ddd, J = 8.0, 7.2, 1.2 Hz, H-5'), 6.68 (1H, t, J = 8.0 Hz, H-5''), 4.37 (1H, m, H-2), 3.39 (2H, J = 6.5 Hz, H-6), 3.18 (1H, dd, J = 13.1, 3.4 Hz, H-1a), 3.04 (1H, dd, J = 13.1, 10.0 Hz, H-1b), 1.74 (2H, m, H-3), 1.69 (2H, m, H-5), 1.55 (1H, m, H-4a), 1.49 (1H, m, H-4b);

^{13}C NMR (150 MHz, methanol-d_4, 300 K) δ 172.0 (C, C-7'), 171.5 (C, C-7''), 161.1 (C, C-2'), 150.1 (C, C-2''), 147.3 (C, C-3''), 135.1 (CH, C-4'), 129.2 (CH, C-6'), 120.2 (CH, C-5'), 119.6 (CH, C-4''), 119.6 (CH, C-5''), 118.6 (CH, C-6''), 118.4 (CH, C-3'), 116.9 (C, C-1'), 116.8 (C, C-1''), 49.1 (CH, C-2), 45.2 (CH₂, C-1), 40.0 (CH₂, C-6), 32.6 (CH₂, C-3), 30.0 (CH₂, C-5), 24.3 (CH₂, C-4);

[α]^{20}$_D$ −11.07 (c 0.58, MeOH);

UV/VIS λ_{max} (MeOH) nm (log ε): 240 (sh) (3.87), 305 (3.55) nm;

HRMS (ESI): m/z 388.1862 (calcd for C₂₀H₂₆N₃O₅, 388.1867)

Figure S15. ^{1}H NMR spectrum (600 MHz, CD$_3$OD) of myxochelin B$_5$.
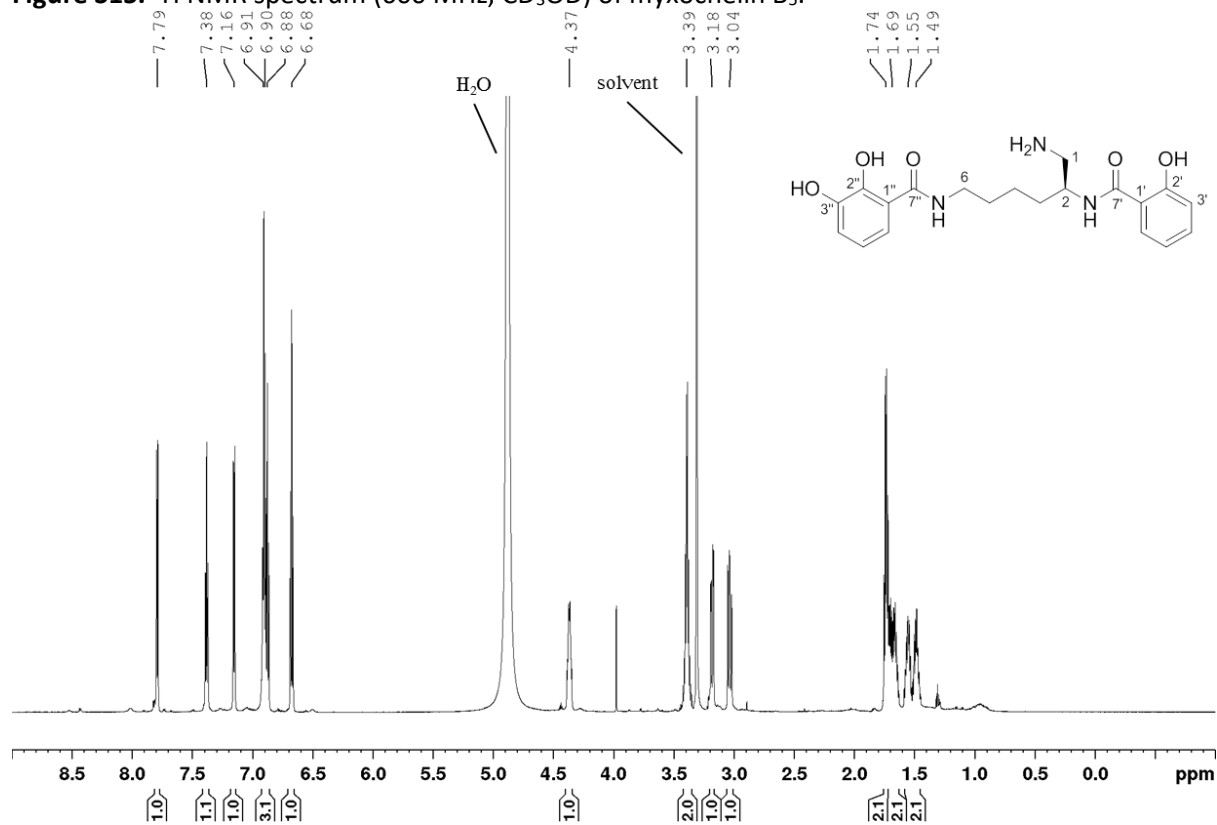
Figure S16. ^{1}H-decoupled ^{13}C NMR spectrum (150 MHz, CD$_3$OD) of myxochelin B$_5$.
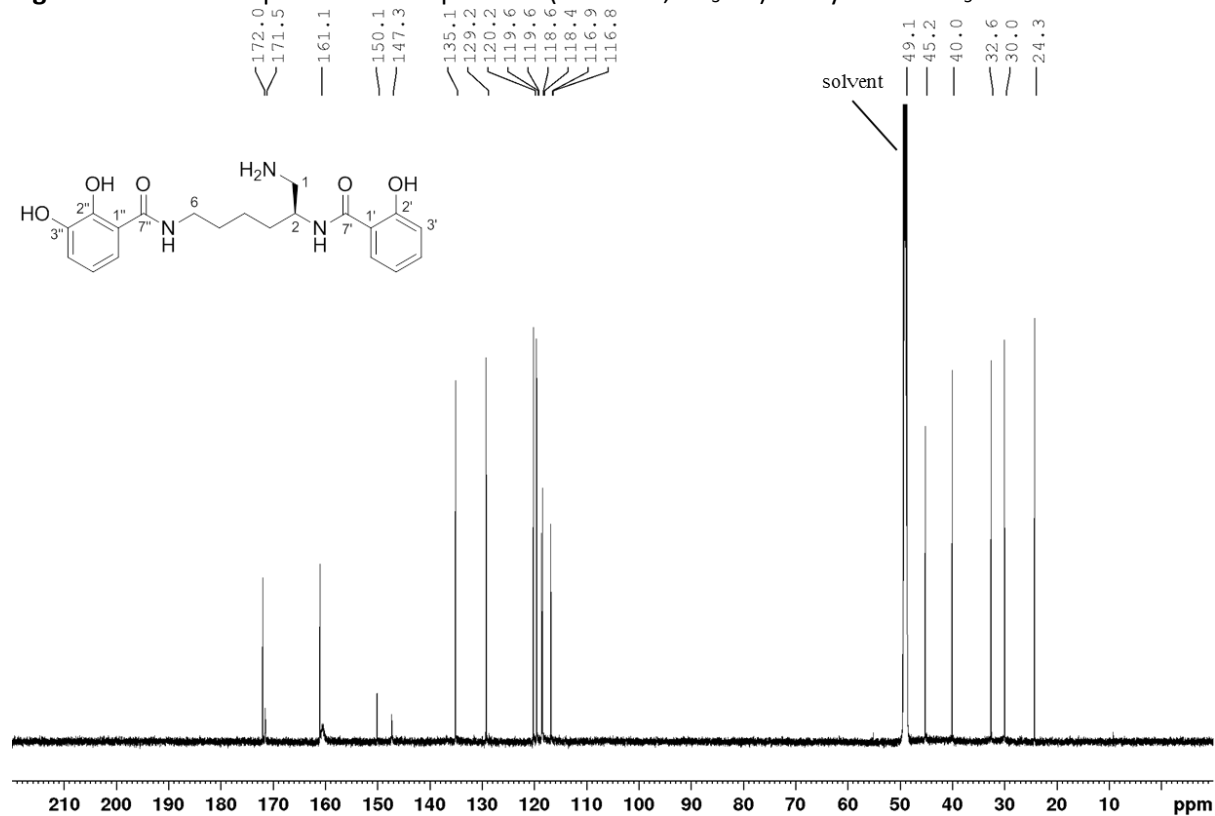
5.2.3.5 Myxochelin B$_6$

Figure S17. HPLC-UV spectrum and ESI-MS spectrum of myxochelin B$_6$.
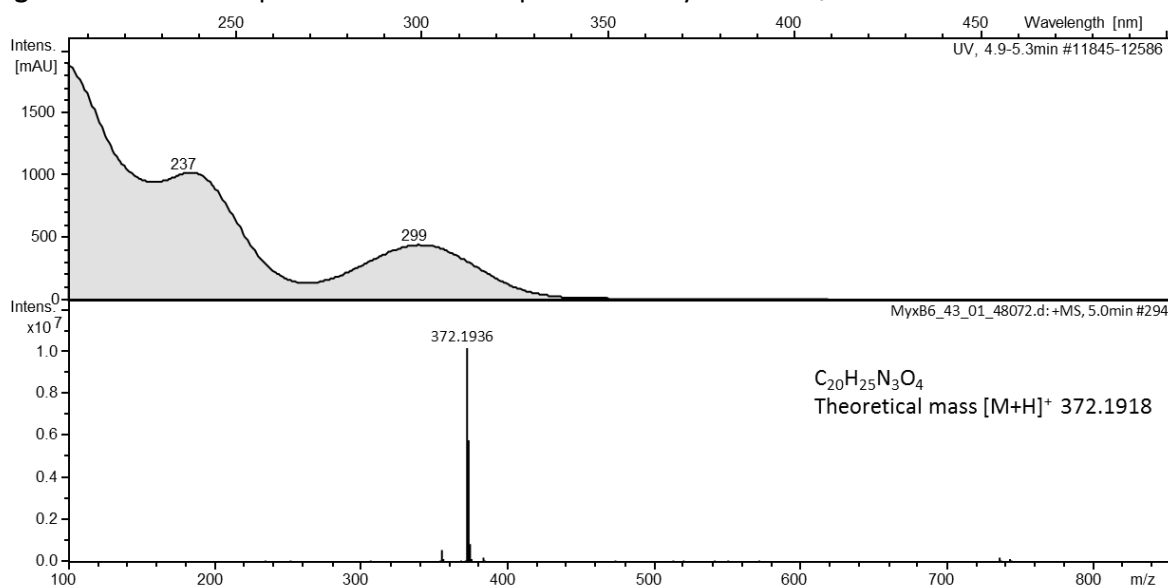
^{1}H NMR (600 MHz, methanol-d_4, 300 K) δ 7.80 (1H, dd, J = 8.0, 1.8 Hz, H-6'), 7.69 (1H, dd, J = 8.0, 1.8 Hz, H-6''), 7.38 (1H, ddd, J = 8.3, 7.2, 1.8 Hz, H-4'), 7.35 (1H, ddd, J = 8.3, 7.2, 1.8 Hz, H-4''), 6.90 (1H, dd, J = 8.3, 1.1 Hz, H-3'), 6.87 (1H, dd, J = 8.3, 1.0 Hz, H-3''), 6.87 (1H, ddd, J = 8.0, 7.2, 1.2 Hz, H-5'), 6.84 (1H, ddd, J = 8.0, 7.2, 1.2 Hz, H-5''), 4.40 (1H, m, H-2), 3.40 (2H, m, H-6), 3.18 (1H, dd, J = 13.2, 3.5 Hz, H-1a), 3.04 (1H, dd, J = 13.4, 9.8 Hz, H-1b), 1.74 (2H, m, H-3), 1.69 (2H, m, H-5), 1.55 (1H, m, H-4a), 1.49 (1H, m, H-4b);

^{13}C NMR (150 MHz, methanol-d_4, 300 K) δ 172.0 (C, C-7'), 171.0 (C, C-7''), 161.1 (C, C-2'), 161.1 (C, C-2''), 135.1 (CH, C-4'), 134.7 (CH, C-4''), 129.2 (CH, C-6'), 128.7 (CH, C-6''), 120.2 (CH, C-5'), 120.1 (CH, C-5''), 118.5 (CH, C-3'), 118.5 (CH, C-3''), 117.0 (C, C-1''), 116.8 (C, C-1'), 49.2 (CH, C-2), 45.1 (CH$_2$, C-1), 40.1 (CH$_2$, C-6), 32.6 (CH$_2$, C-3), 30.0 (CH$_2$, C-5), 24.3 (CH$_2$, C-4);

[α]^{20}$_D$ -12.62 (c 1.03, MeOH);

UV/VIS λ_{max} (MeOH) nm (log ε): 237 (3.84), 301 (3.51) nm;

HRMS (ESI): m/z 372.1936 (calcd for C$_{20}$H$_{26}$N$_3$O$_4$, 372.1918).

Figure S18. ^{1}H NMR spectrum (600 MHz, CD$_3$OD) of myxochelin B$_6$.
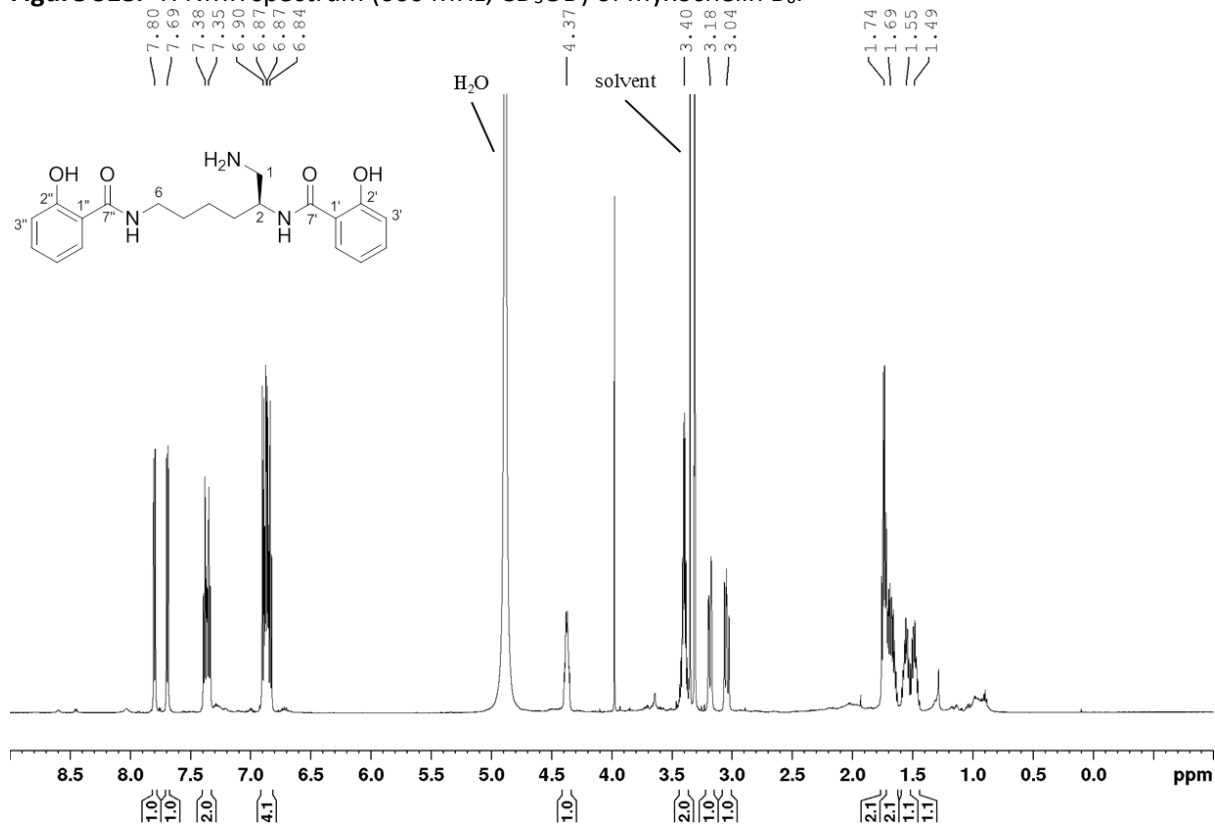
Figure S19. ^{1}H-decoupled ^{13}C NMR spectrum (150 MHz, CD$_3$OD) of myxochelin B$_6$.
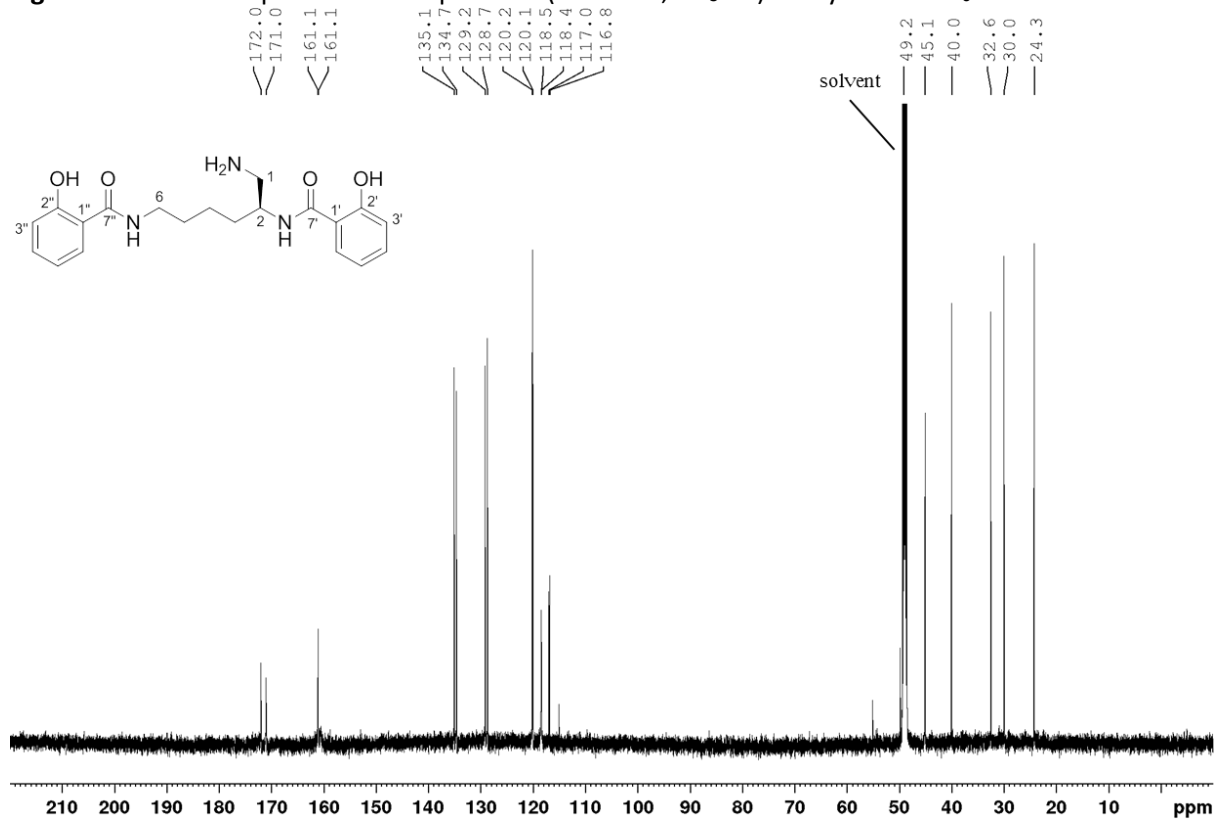
5.2.3.6 Myxochelin B$_7$

Figure S20. HPLC-UV spectrum and ESI-MS spectrum of myxochelin B$_7$.
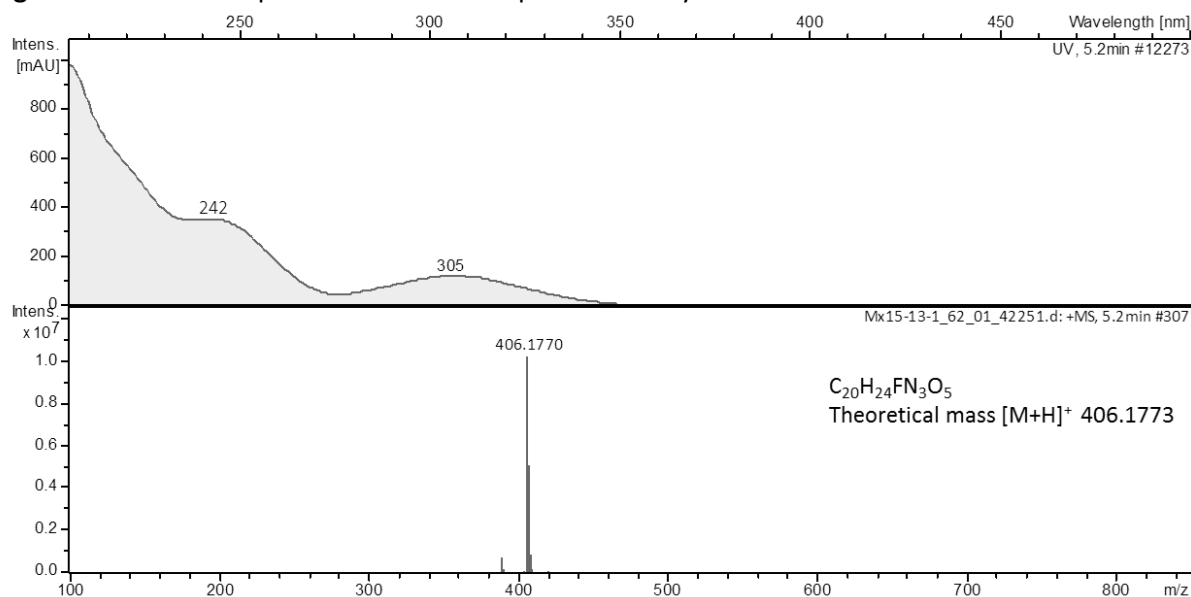
^{1}H NMR (600 MHz, methanol-d_4, 300 K) δ 7.29 (1H, dt, J = 8.4, 6.8 Hz, H-4''), 7.28 (1H, dd, J = 8.0, 1.3 Hz, H-6'), 6.93 (1H, dd, J = 8.0, 1.3 Hz, H-4'), 6.70 (1H, t, J = 8.0 Hz, H-5'), 6.70 (1H, dd, J = 8.4, 1.2 Hz, H-3''), 6.59 (1H, ddd, J = 11.5, 8.2, 1.2 Hz, H-5''), 4.38 (1H, m, H-2), 3.41 (2H, t, J = 6.6 Hz, H-6), 3.19 (1H, dd, J = 13.3, 2.9 Hz, H-1a), 3.04 (1H, dd, J = 13.3, 10.0 Hz, H-1b), 1.73 (2H, m, H-3), 1.68 (2H, m, H-5), 1.55 (1H, m, H-4a), 1.49 (1H, m, H-4b);

^{13}C NMR (150 MHz, methanol-d_4, 300 K) δ 172.6 (C, C-7'), 168.4 (C, d, J = 1.8 Hz, C-7''), 162.6 (C, d, J = 4.9 Hz, C-2''), 162.3 (C, d, J = 247.0 Hz, C-6''), 150.2 (C, C-2'), 147.3 (C, C-3'), 134.2 (CH, d, J = 12.5 Hz, C-4''), 119.9 (CH, C-4'), 119.7 (CH, C-5'), 119.0 (CH, C-6'), 116.6 (C, C-1'), 114.4 (CH, d, J = 2.8 Hz, C-3''), 107.4 (C, d, J = 14.8 Hz, C-1''), 106.8 (CH, d, J = 24.5 Hz, C-5''), 49.1 (CH, C-2), 45.1 (CH$_2$, C-1), 40.1 (CH$_2$, C-6), 32.5 (CH$_2$, C-3), 29.8 (CH$_2$, C-5), 24.1 (CH$_2$, C-4);

[α]$^{20}_D$ −15.03 (c 0.36, MeOH);

UV/VIS λ_{max} (MeOH) nm (log ε): 242 (sh) (3.96), 307 (3.53) nm;

HRMS (ESI): m/z 406.1770 (calcd for C$_{20}$H$_{25}$FN$_3$O$_5$, 406.1773).

Figure S21. ^{1}H NMR spectrum (500 MHz, CD$_3$OD) of myxochelin B$_7$.

Figure S22. ^{1}H-decoupled ^{13}C NMR spectrum (125 MHz, CD$_3$OD) of myxochelin B$_7$.

5.2.3.7 Myxochelin B$_8$

Figure S23. HPLC-UV spectrum and ESI-MS spectrum of myxochelin B$_8$.
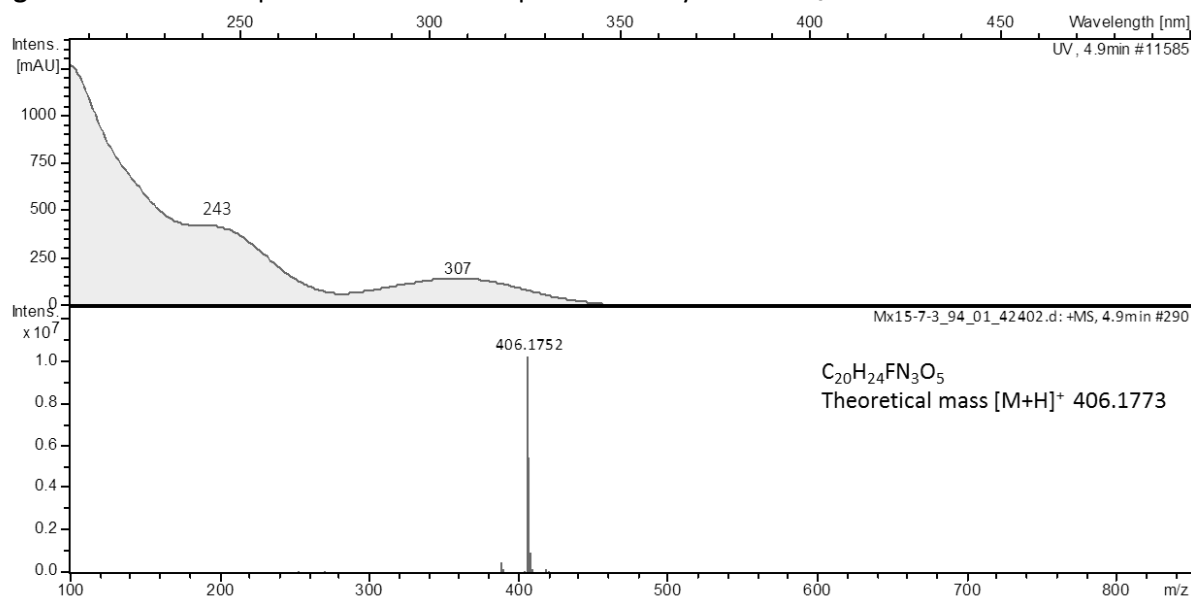
^{1}H NMR (600 MHz, methanol-d_4, 300 K) δ 7.33 (1H, dt, J = 8.4, 6.7 Hz, H-4'), 7.17 (1H, dd, J = 8.1, 1.4 Hz, H-6''), 6.91 (1H, dd, J = 7.9, 1.4 Hz, H-4''), 6.74 (1H, dd, J = 8.4, 1.2 Hz, H-3'), 6.68 (1H, t, J = 8.0 Hz, H-5''), 6.62 (1H, ddd, J = 11.5, 8.3, 1.2 Hz, H-5'), 4.40 (1H, m, H-2), 3.40 (2H, m, H-6), 3.17 (1H, dd, J = 13.1, 3.8 Hz, H-1a), 3.07 (1H, dd, J = 13.2, 9.8 Hz, H-1b), 1.72 (2H, m, H-3), 1.69 (2H, m, H-5), 1.58 (1H, m, H-4a), 1.50 (1H, m, H-4b);

^{13}C NMR (150 MHz, methanol-d_4, 300 K) δ 171.6 (C, C-7''), 169.4 (C, C-7'), 162.3 (C, d, J = 5.0 Hz, C-2'), 162.3 (C, d, J = 248.0 Hz, C-6'), 150.2 (C, C-2''), 147.3 (C, C-3''), 134.6 (CH, d, J = 12.4 Hz, C-4'), 119.5 (CH, C-4''), 119.5 (CH, C-5''), 118.6 (CH, C-6''), 116.7 (C, C-1''), 114.4 (CH, d, J = 1.9 Hz, C-3'), 107.7 (C, d, J = 14.8 Hz, C-1'), 107.0 (CH, d, J = 24.8 Hz, C-5'), 49.3 (CH, C-2), 44.8 (CH$_2$, C-1), 40.0 (CH$_2$, C-6), 32.4 (CH$_2$, C-3), 29.9 (CH$_2$, C-5), 24.1 (CH$_2$, C-4);

[α]^{20}$_D$ −10.82 (c 0.38, MeOH);

UV/VIS λ_{max} (MeOH) nm (log ε): 241 (sh) (4.02), 307 (3.59) nm;

HRMS (ESI): m/z 406.1752 (calcd for C$_{20}$H$_{25}$FN$_3$O$_5$, 406.1773).

Figure S24. ^{1}H NMR spectrum (500 MHz, CD$_3$OD) of myxochelin B$_8$.
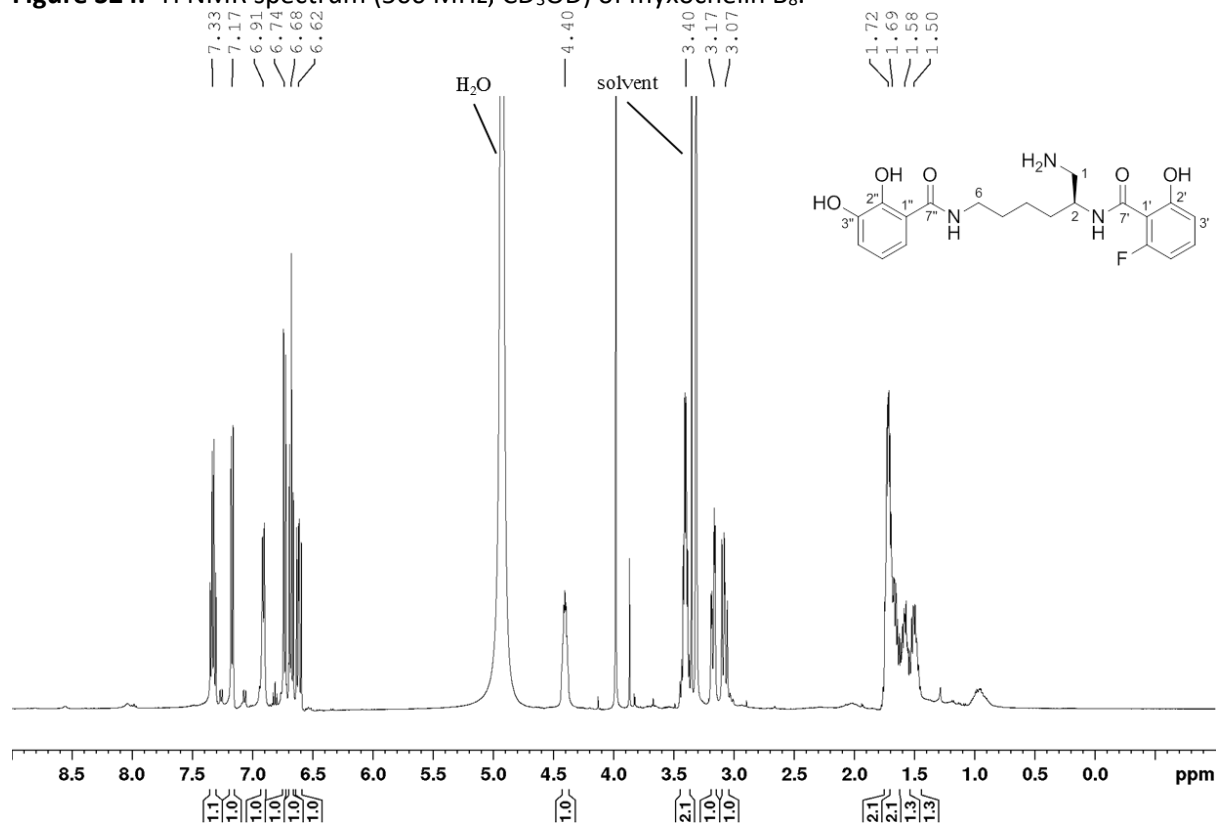
Figure S25. ^{1}H-decoupled ^{13}C NMR spectrum (125 MHz, CD$_3$OD) of myxochelin B$_8$.
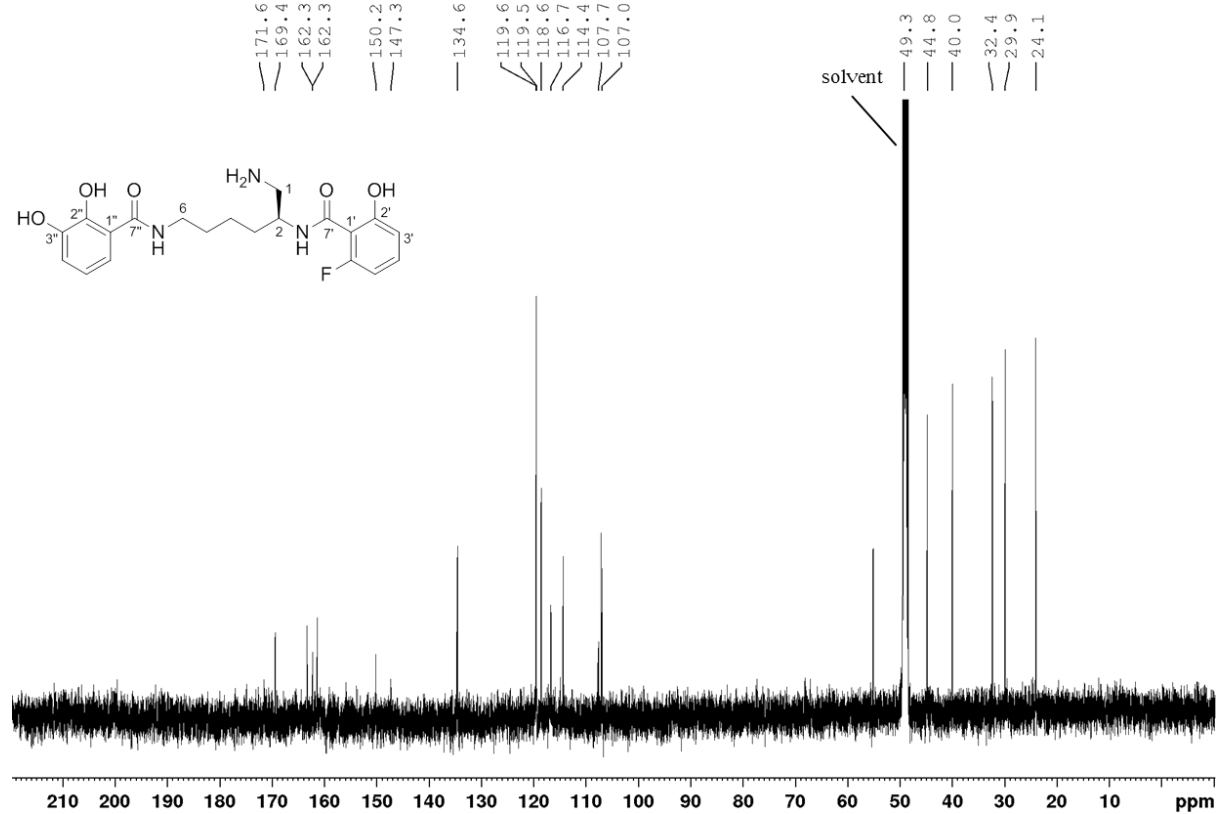
5.2.3.8 Myxochelin B$_9$

Figure S26. HPLC-UV spectrum and ESI-MS spectrum of myxochelin B$_9$.
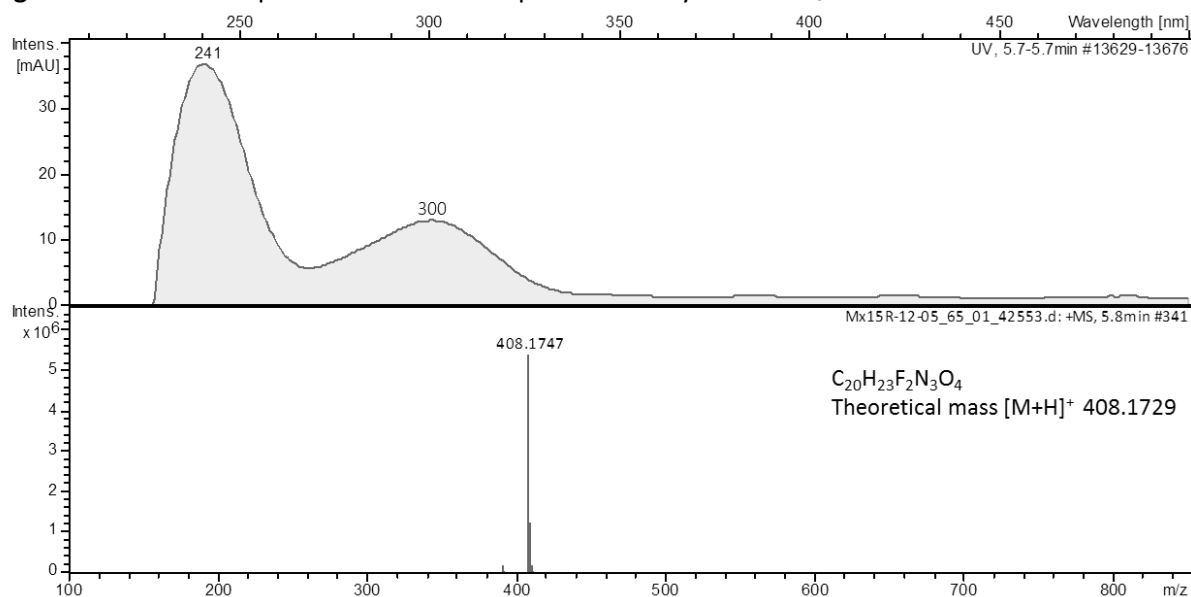
^{1}**H NMR** (600 MHz, methanol-d_4, 300 K) δ 7.34 (1H, dt, J = 8.3, 6.8 Hz, H-4'), 7.31 (1H, dt, J = 8.4, 6.7 Hz, H-4''), 6.74 (1H, dd, J = 8.4, 1.0 Hz, H-3'), 6.71 (1H, dd, J = 8.4, 1.0 Hz, H-3''), 6.63 (1H, ddd, J = 11.6, 8.2, 1.0 Hz, H-5'), 6.59 (1H, ddd, J = 11.7, 8.3, 1.0 Hz, H-5''), 4.40 (1H, m, H-2), 3.43 (2H, m, H-6), 3.17 (1H, dd, J = 12.9, 3.8 Hz, H-1a), 3.08 (1H, dd, J = 13.2, 9.8 Hz, H-1b), 1.73 (2H, m, H-3), 1.67 (2H, m, H-5), 1.60 (1H, m, H-4a), 1.52 (1H, m, H-4b);

^{13}**C NMR** (150 MHz, methanol-d_4, 300 K) δ 169.5 (C, C-7'), 168.4 (C, C-7''), 162.3 (C, d, J = 248.0 Hz, C-6'), 162.3 (C, d, J = 247.0 Hz, C-6''), 134.6 (CH, d, J = 12.3 Hz, C-4'), 134.2 (CH, d, J = 12.6 Hz, C-4''), 114.4 (CH, C-3'), 114.4 (CH, C-3''), 107.0 (C, d, J = 24.8 Hz, C-5'), 106.8 (CH, d, J = 24.7 Hz, C-5''), 49.0 (CH, C-2), 44.9 (CH$_2$, C-1), 40.1 (CH$_2$, C-6), 32.3 (CH$_2$, C-3), 29.8 (CH$_2$, C-5), 24.0 (CH$_2$, C-4);

$[\alpha]^{20}_D$ −13.56 (c 0.07, MeOH);

UV/VIS λ_{max} (MeOH) nm (log ε): 234 (sh) (3.78), 303 (3.16) nm;

HRMS (ESI): m/z 408.1747 (calcd for C$_{20}$H$_{24}$F$_2$N$_3$O$_5$, 408.1729).

Figure S27. ^{1}H NMR spectrum (700 MHz, CD$_3$OD) of myxochelin B$_9$.
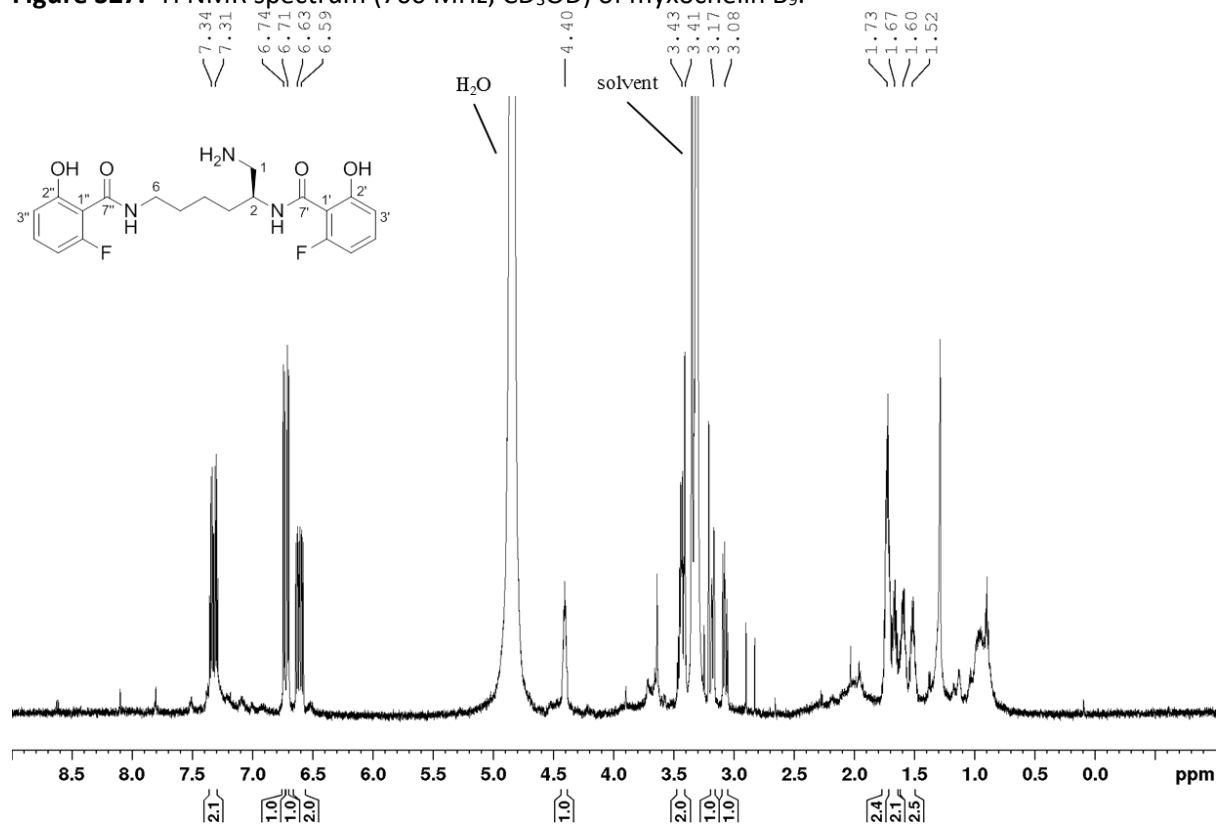
Figure S28. ^{1}H-decoupled ^{13}C NMR spectrum (175 MHz, CD$_3$OD) of myxochelin B$_9$.
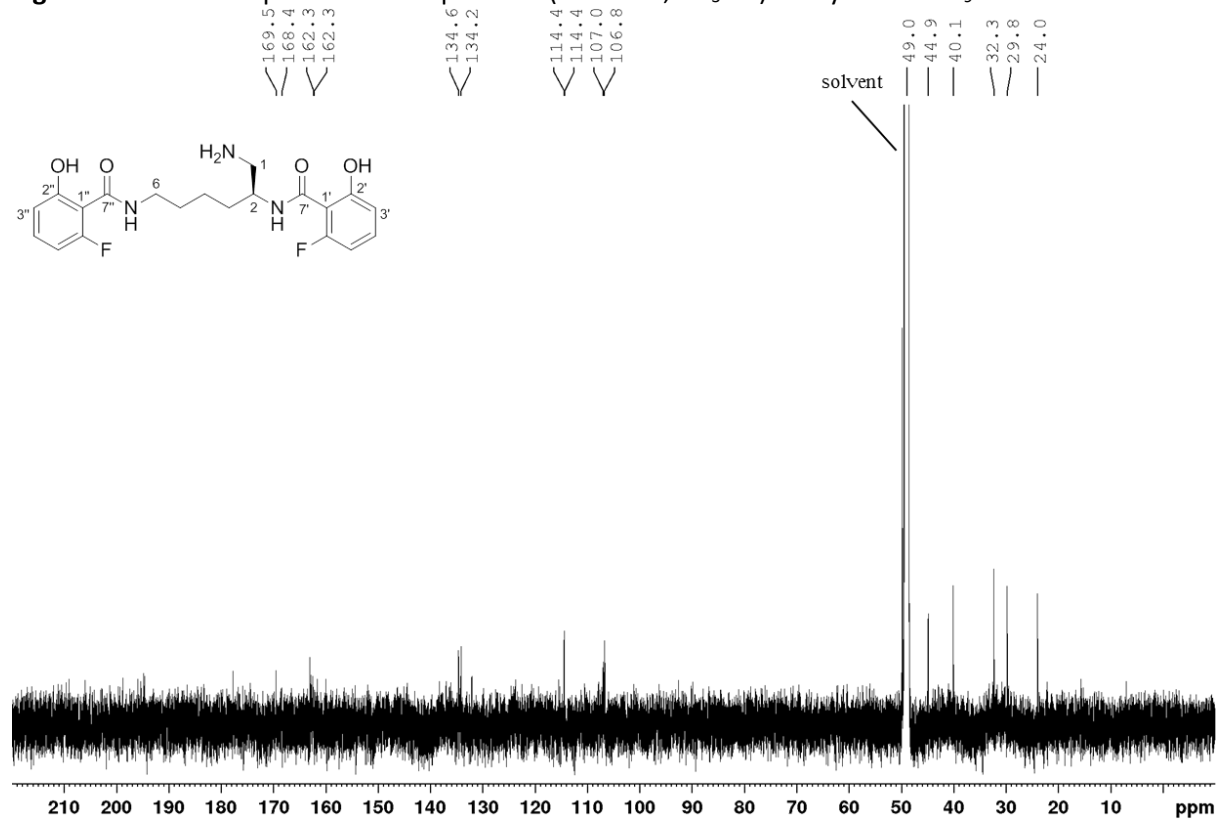
5.2.4 Pseudochelin A derivatives

5.2.4.1 Pseudochelin A$_4$

Figure S29. HPLC-UV spectrum and ESI-MS spectrum of pseudochelin A$_4$.
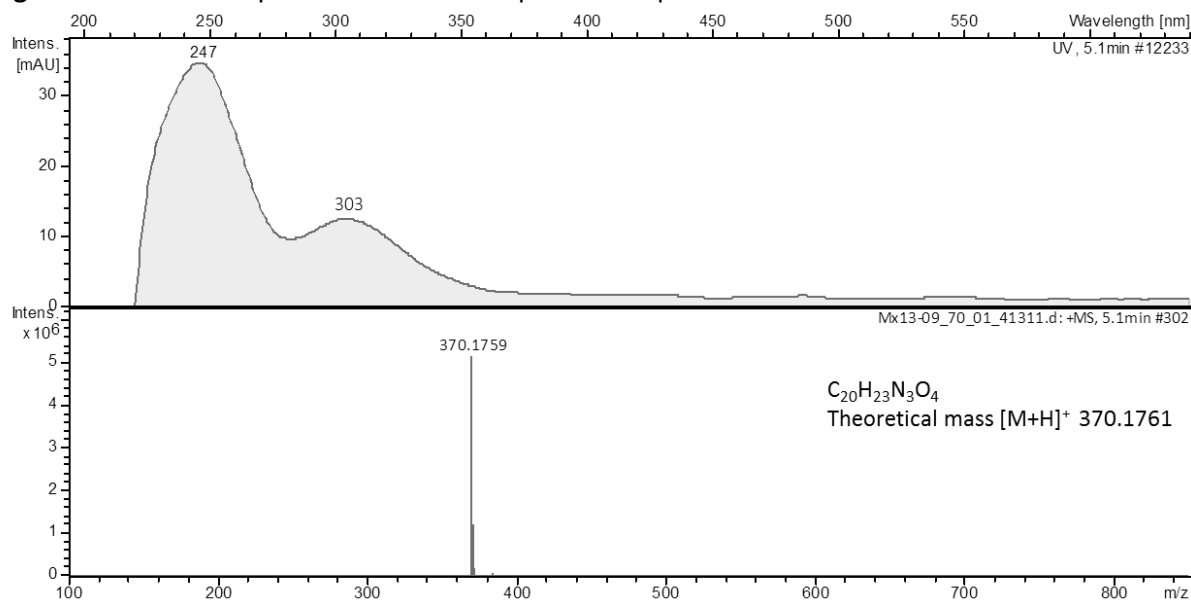
^{1}H NMR (600 MHz, methanol-d_4, 300 K) δ 7.73 (1H, d, J = 7.9 Hz, H-6''), 7.37 (1H, t, J = 7.9 Hz, H-4''), 7.16 (1H, d, J = 8.0 Hz, H-6'), 7.10 (1H, d, J = 7.9 Hz, H-4'), 6.87 (1H, m, H-5'), 6.87 (1H, m, H-3''), 6.87 (1H, m, H-5''), 4.38 (1H, m, H-2), 4.13 (1H, m, H-1a), 3.73 (1H, dd, J = 11.8, 7.7 Hz, H-1b), 3.44 (2H, t, J = 6.8 Hz, H-6), 1.88 (1H, m, H-3a), 1.79 (1H, m, H-3b), 1.72 (2H, m, H-5), 1.52 (2H, m, H-4);

^{13}C NMR (150 MHz, methanol-d_4, 300 K) δ 171.0 (C, C-7''), 164.5 (C, C-7'), 161.1 (C, C-2''), 149.0 (C, C-2'), 147.6 (C, C-3'), 134.7 (CH, C-4''), 128.8 (CH, C-6''), 121.3 (CH, C-4'), 121.3 (CH, C-5'), 120.1 (CH, C-6'), 120.1 (CH, C-5''), 118.5 (CH, C-3''), 117.0 (C, C-1''), 109.3 (C, C-1'), 58.1 (CH, C-2), 50.6 (CH$_2$, C-1), 40.0 (CH$_2$, C-6), 35.6 (CH$_2$, C-3), 30.2 (CH$_2$, C-5), 23.0 (CH$_2$, C-4);

[α]^{20}$_D$ −10.21 (c 0.20, MeOH;

UV/VIS λ$_{max}$ (MeOH) nm (log ε): 249 (sh) (n.d.), 302 (3.55) nm;

HRMS (ESI): m/z 370.1759 (calcd for C$_{20}$H$_{24}$N$_3$O$_4$, 370.1761).

Figure S30. ^{1}H NMR spectrum (600 MHz, CD$_3$OD) of pseudochelin A$_4$.
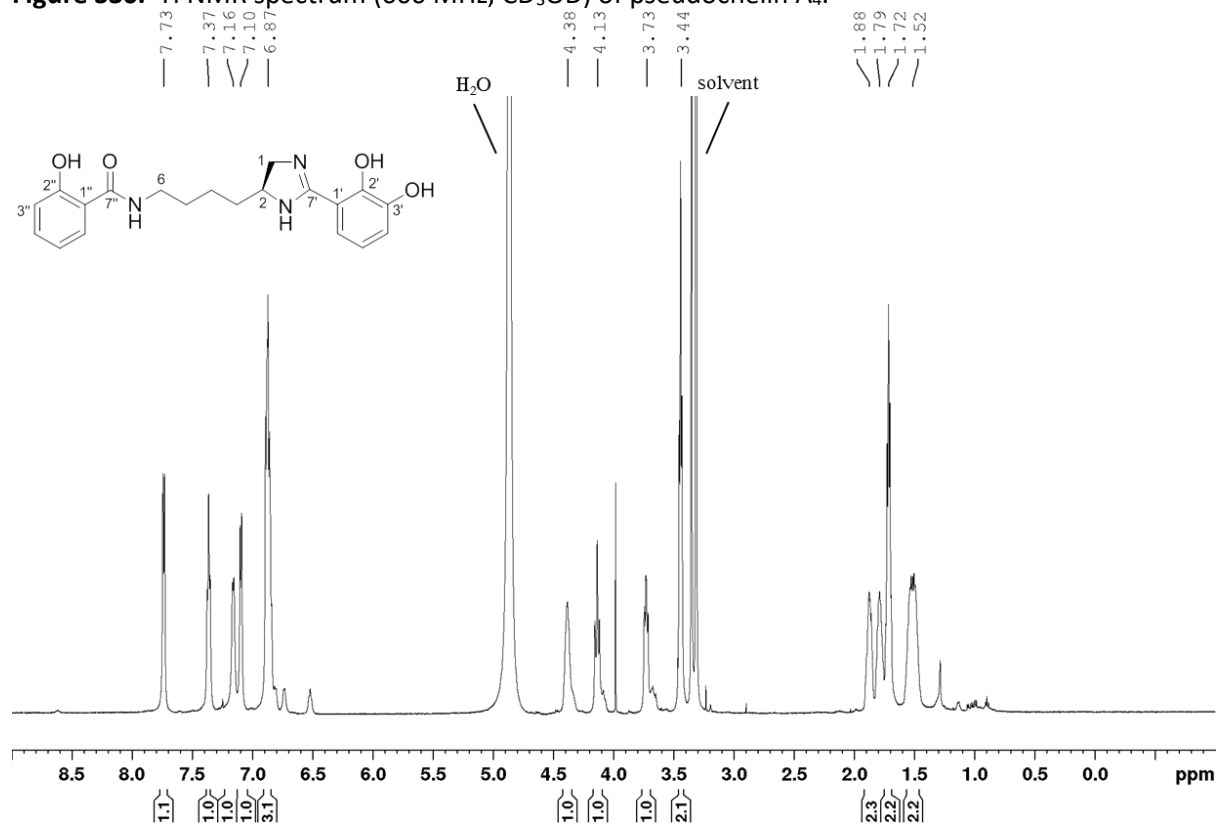
Figure S31. ^{1}H-decoupled ^{13}C NMR spectrum (150 MHz, CD$_3$OD) of pseudochelin A$_4$.
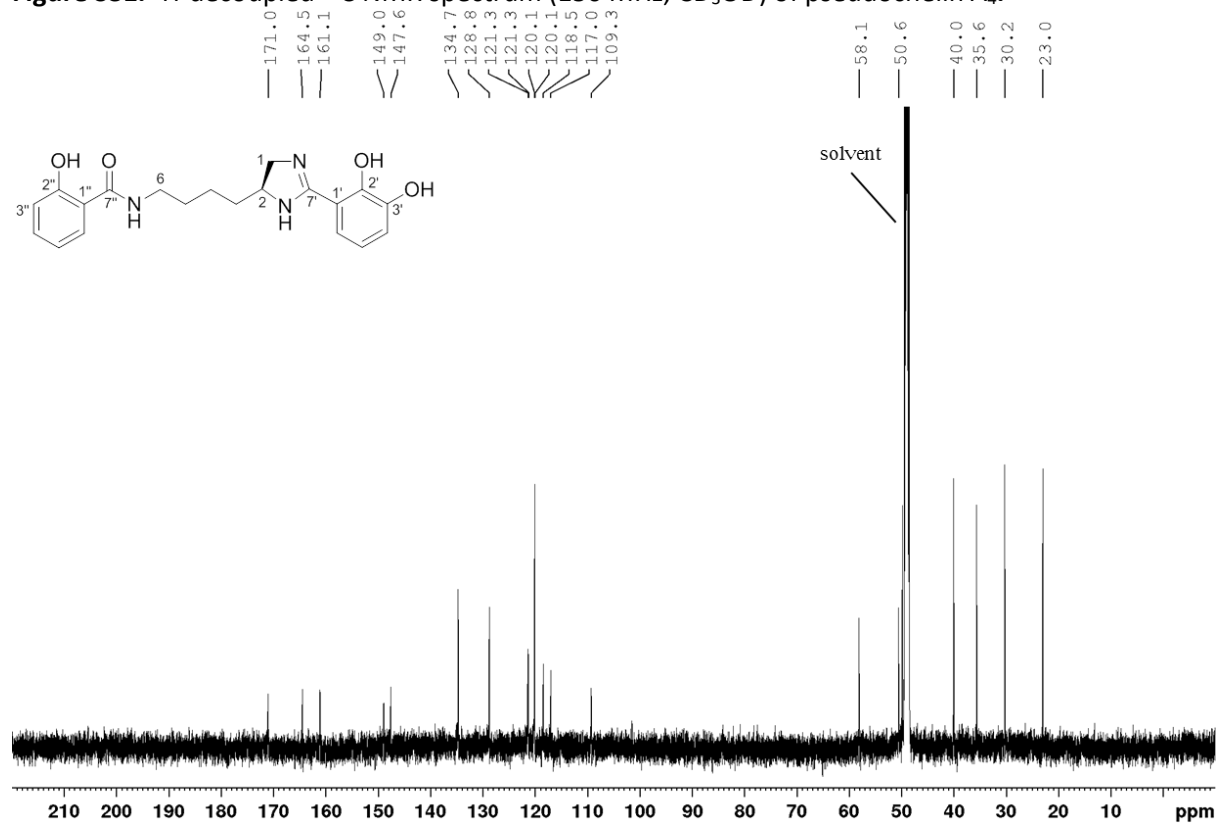
5.2.4.2 Pseudochelin A$_5$

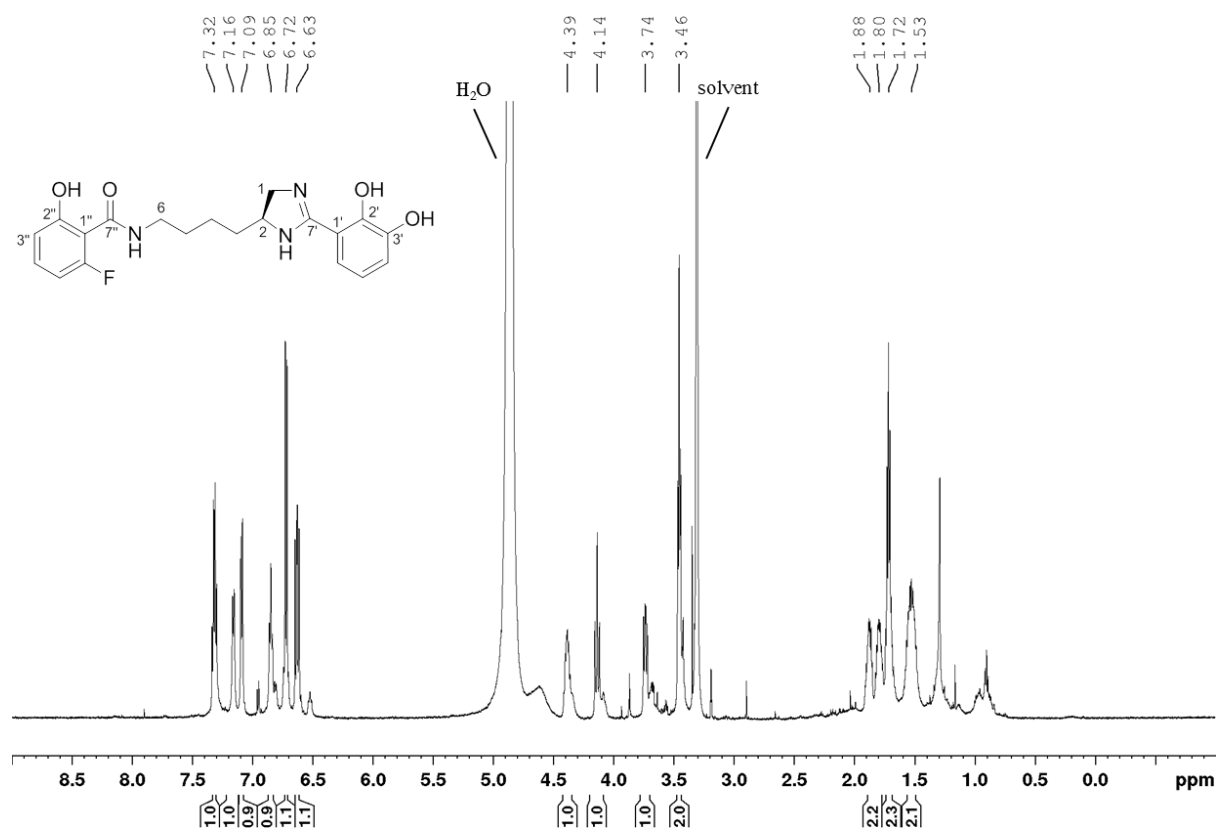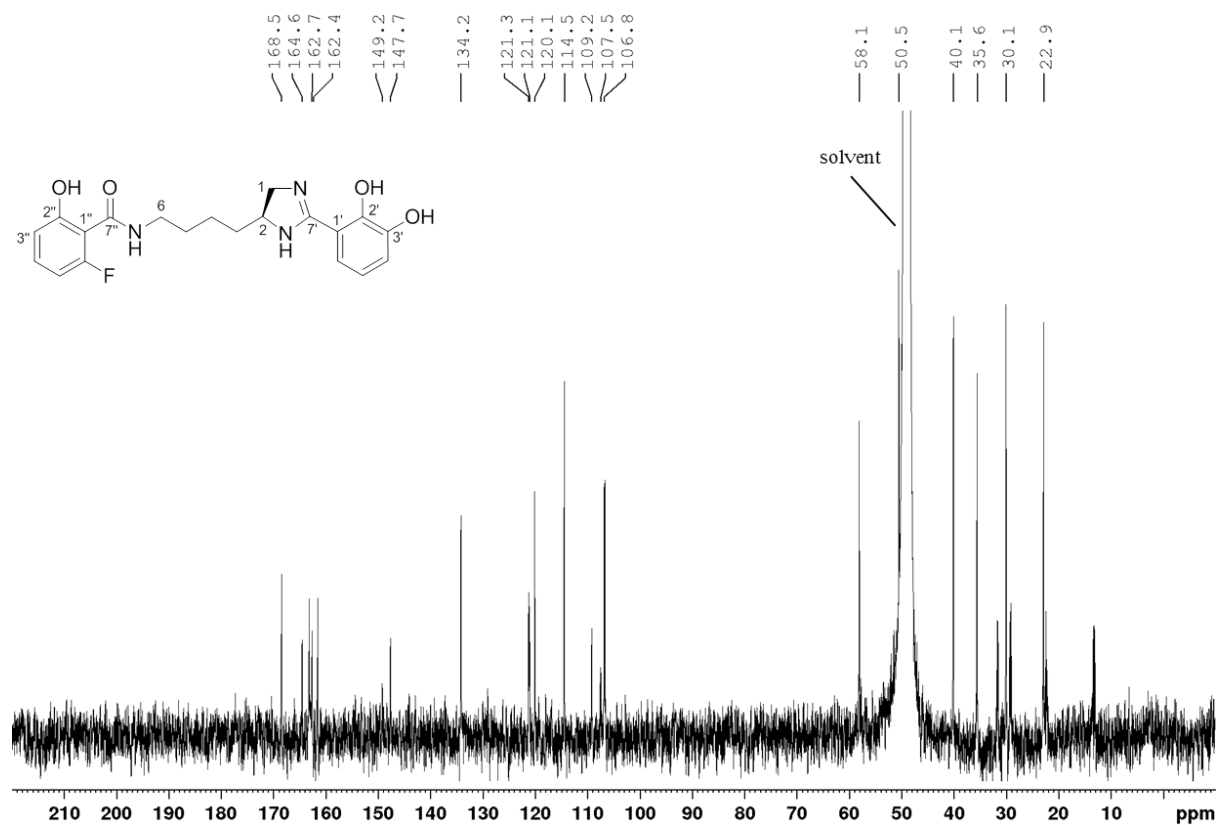**Figure S32.** HPLC-UV spectrum and ESI-MS spectrum of pseudochelin A$_5$.
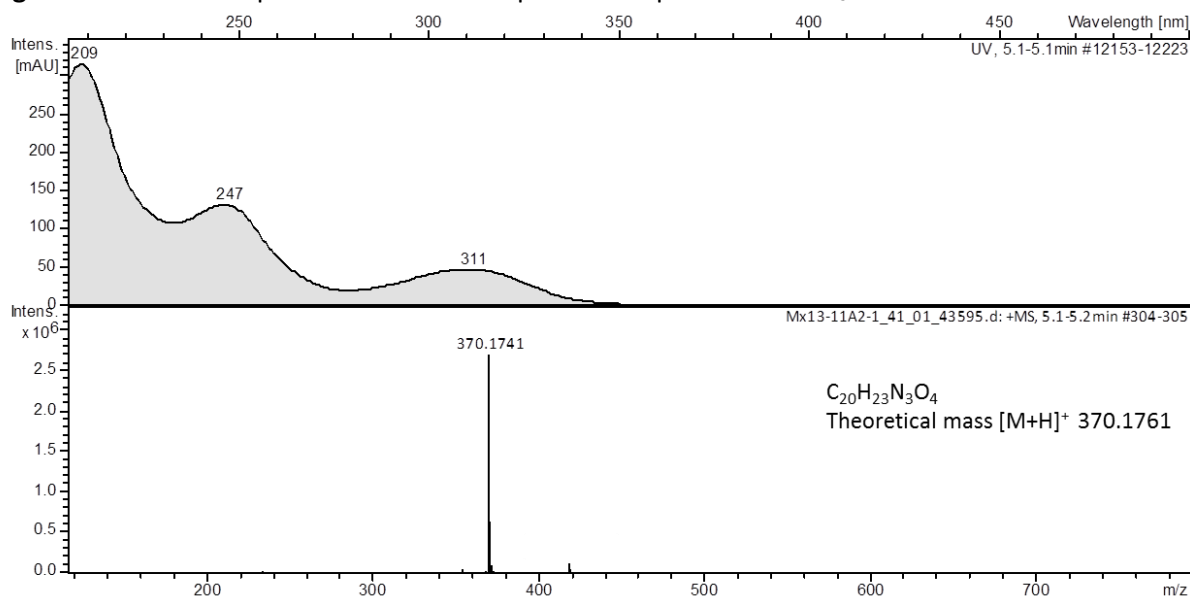
^{1}H NMR (600 MHz, methanol-d_4, 300 K) δ 7.70 (1H, dd, J = 8.0, 1.8 Hz, H-6'), 7.57 (1H, ddd, J = 8.4, 7.3, 1.8 Hz, H-4'), 7.20 (1H, dd, J = 8.1, 1.7 Hz, H-6''), 7.07 (1H, d, J = 8.4 Hz, H-3'), 7.04 (1H, dd, J = 8.0, 7.3 Hz, H-5'), 6.92 (1H, dd, J = 7.9, 1.7 Hz, H-4''), 6.71 (1H, t, J = 8.0 Hz, H-5''), 4.38 (1H, m, H-2), 4.13 (1H, t, J = 11.3 Hz, H-1a), 3.73 (1H, dd, J = 11.4, 7.6 Hz, H-1b), 3.44 (2H, t, J = 7.0 Hz, H-6), 1.88 (1H, m, H-3a), 1.80 (1H, m, H-3b), 1.72 (2H, m, H-5), 1.52 (2H, m, H-4);

^{13}C NMR (150 MHz, methanol-d_4, 300 K) δ 171.5 (C, C-7''), 164.3 (C, C-7'), 159.7 (C, C-2'), 150.2 (C, C-2''), 147.4 (C, C-3''), 137.6 (CH, C-4'), 130.7 (CH, C-6''), 121.4 (CH, C-5'), 119.6 (CH, C-4''), 119.6 (CH, C-5''), 118.6 (CH, C-6''), 118.2 (CH, C-3'), 116.8 (C, C-1''), 109.3 (C, C-1'), 58.1 (CH, C-2), 50.5 (CH$_2$, C-1), 40.0 (CH$_2$, C-6), 35.6 (CH$_2$, C-3), 30.2 (CH$_2$, C-5), 22.9 (CH$_2$, C-4);

[α]^{20}$_D$ −18.14 (c 0.09, MeOH);

UV/VIS λ$_{max}$ (MeOH) nm (log ε): 245 (4.21), 312 (3.81) nm;

HRMS (ESI): m/z 370.1741 (calcd for C$_{20}$H$_{24}$N$_3$O$_4$, 370.1761).

Figure S33. ^{1}H NMR spectrum (600 MHz, CD$_3$OD) of pseudochelin A$_5$.
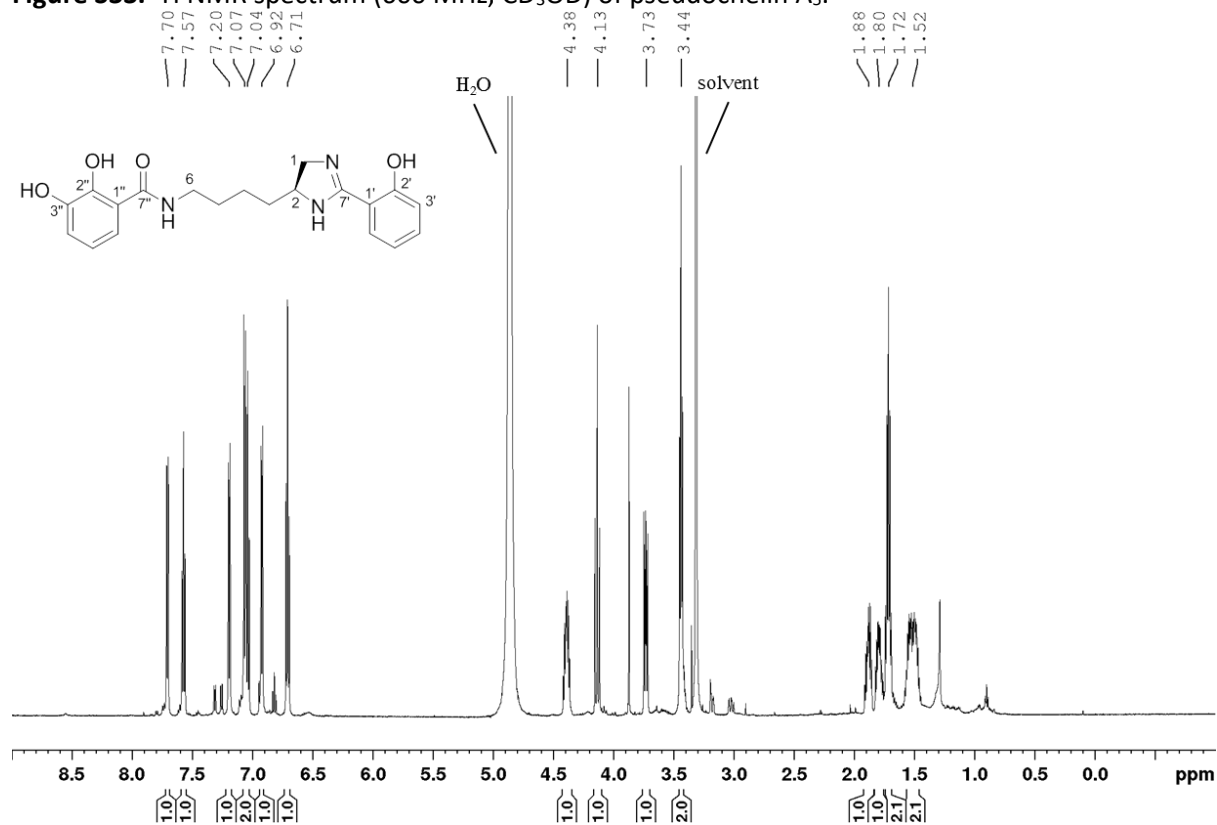
Figure S34. ^{1}H-decoupled ^{13}C NMR spectrum (150 MHz, CD$_3$OD) of pseudochelin A$_5$.
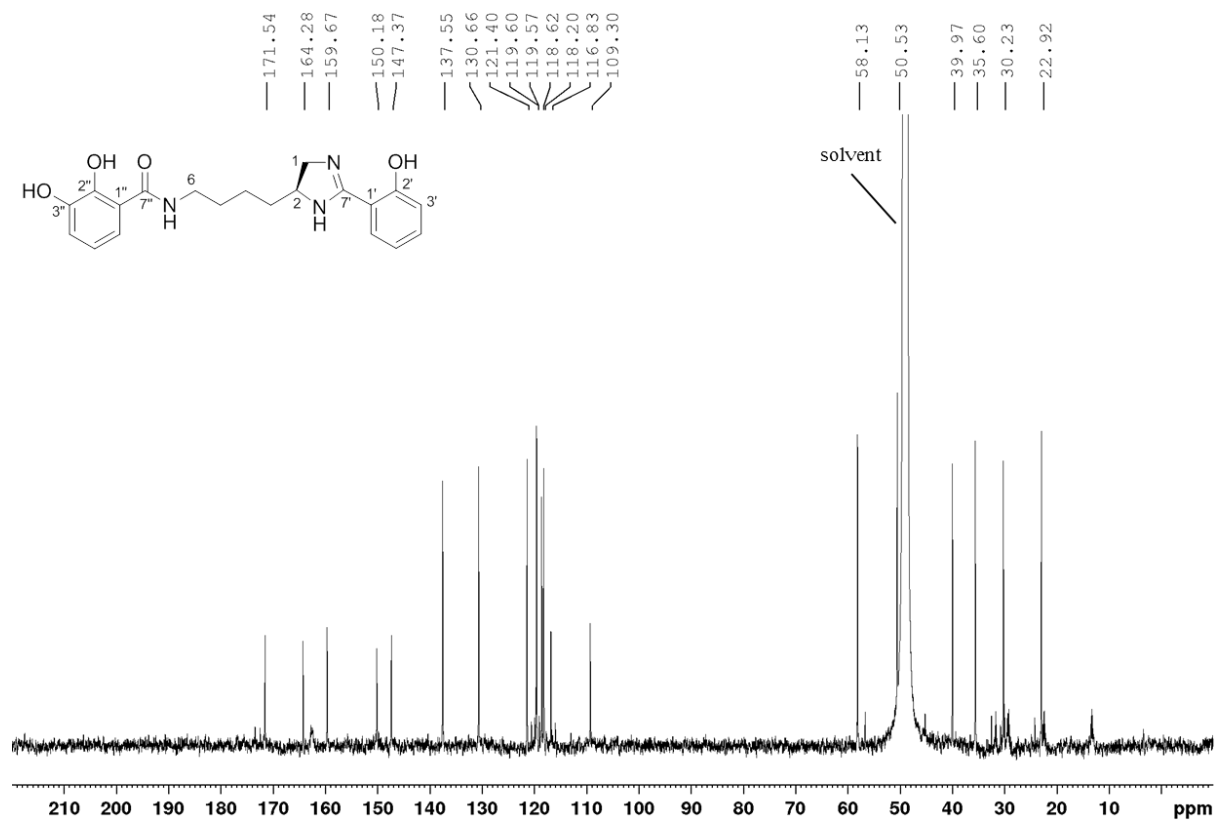
5.2.4.3 Pseudochelin A$_6$

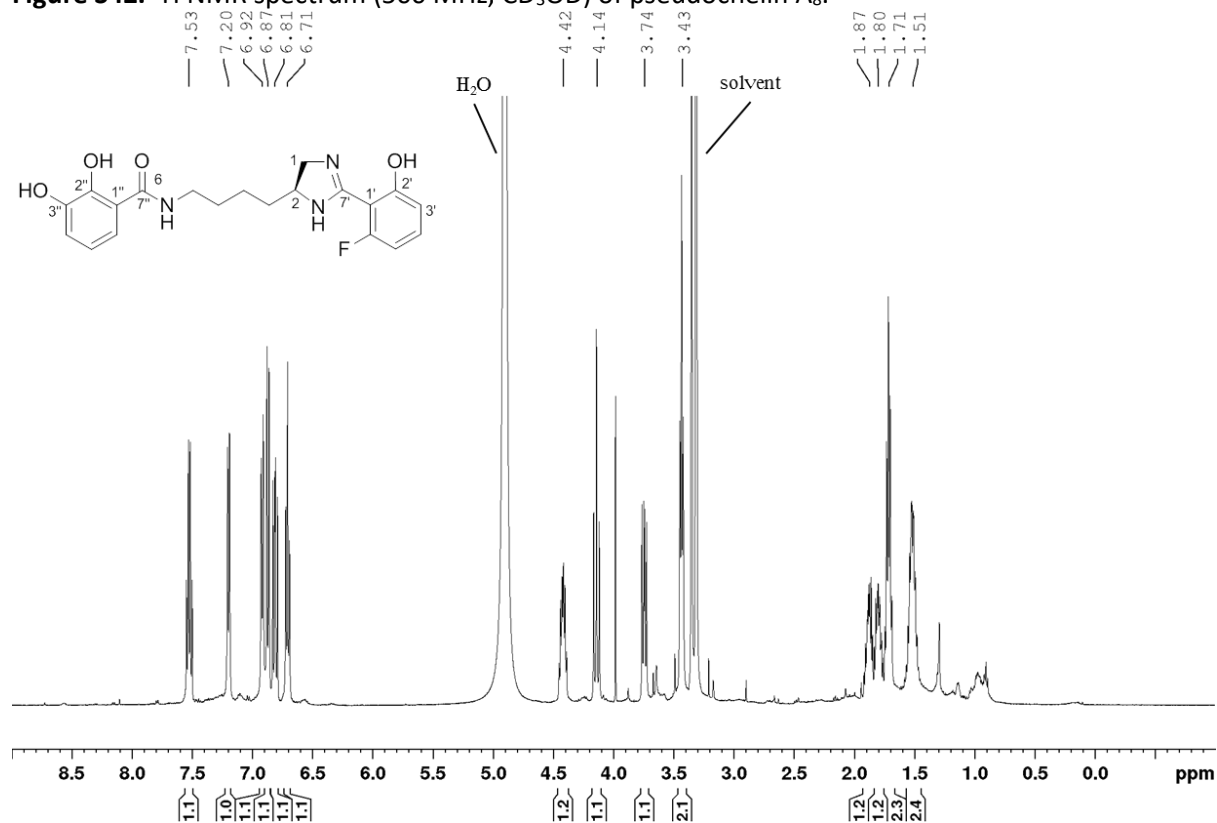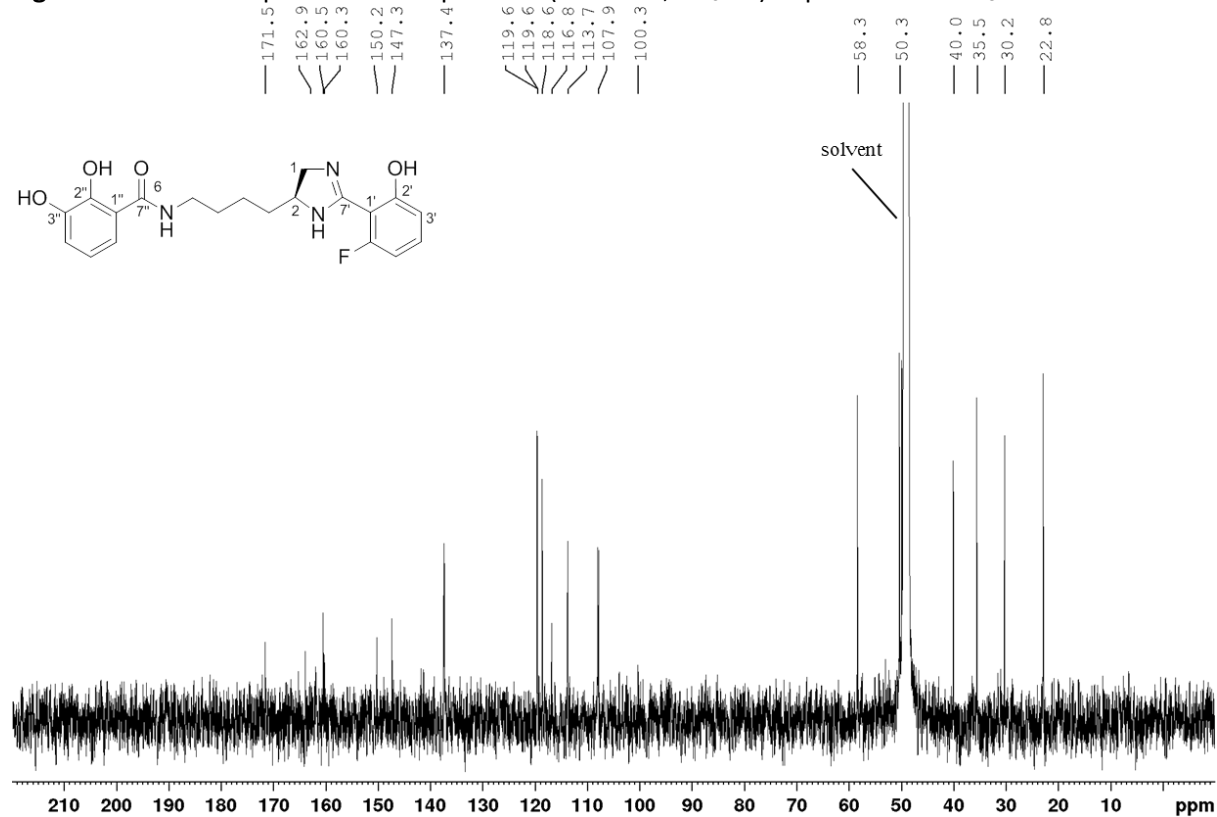**Figure S35.** HPLC-UV spectrum and ESI-MS spectrum of pseudochelin A$_6$.
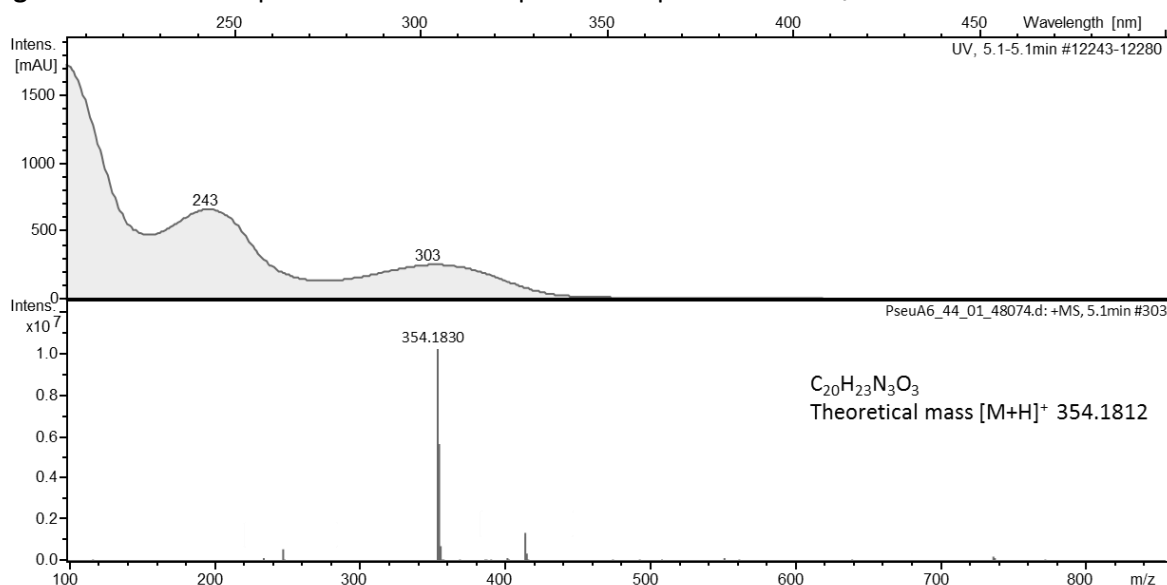
^{1}H NMR (600 MHz, methanol-d_4, 300 K) δ 7.73 (1H, dd, J = 7.9, 1.7 Hz, H-6''), 7.71 (1H, dd, J = 8.0, 1.7 Hz, H-6'), 7.57 (1H, ddd, J = 8.4, 7.3, 1.7 Hz, H-4'), 7.37 (1H, ddd, J = 8.3, 7.2, 1.7 Hz, H-4''), 7.07 (1H, dd, J = 8.4, 0.9 Hz, H-3'), 7.04 (1H, ddd, J = 7.9, 7.3, 1.0 Hz, H-5'), 6.89 (1H, dd, J = 8.2, 1.2 Hz, H-3''), 6.87 (1H, ddd, J = 7.8, 7.3, 1.2 Hz, H-5''), 4.38 (1H, m, H-2), 4.13 (1H, t, J = 11.4 Hz, H-1a), 3.73 (1H, dd, J = 11.5, 7.6 Hz, H-1b), 3.44 (2H, t, J = 7.0 Hz, H-6), 1.89 (1H, m, H-3a), 1.80 (1H, m, H-3b), 1.72 (2H, m, H-5), 1.52 (2H, m, H-4);

^{13}C NMR (150 MHz, methanol-d_4, 300 K) δ 171.0 (C, C-7''), 164.3 (C, C-7'), 161.1 (C, C-2''), 159.7 (C, C-2'), 137.5 (CH, C-4'), 134.7 (CH, C-4''), 130.7 (CH, C-6'), 128.8 (CH, C-6''), 121.4 (CH, C-5'), 120.1 (CH, C-5''), 118.5 (CH, C-3'), 118.2 (CH, C-3''), 117.0 (C, C-1''), 109.3 (C, C-1'), 58.1 (CH, C-2), 50.5 (CH$_2$, C-1), 40.0 (CH$_2$, C-6), 35.6 (CH$_2$, C-3), 30.3 (CH$_2$, C-5), 23.0 (CH$_2$, C-4);

[α]$^{20}_D$ −22.70 (c 0.35, MeOH);

UV/VIS λ_{max} (MeOH) nm (log ε): 242 (3.96), 304 (3.56) nm;

HRMS (ESI): *m/z* 354.1830 (calcd for C$_{20}$H$_{24}$N$_3$O$_3$, 354.1812).

Figure S36. ^{1}H NMR spectrum (600 MHz, CD$_3$OD) of pseudochelin A$_6$.
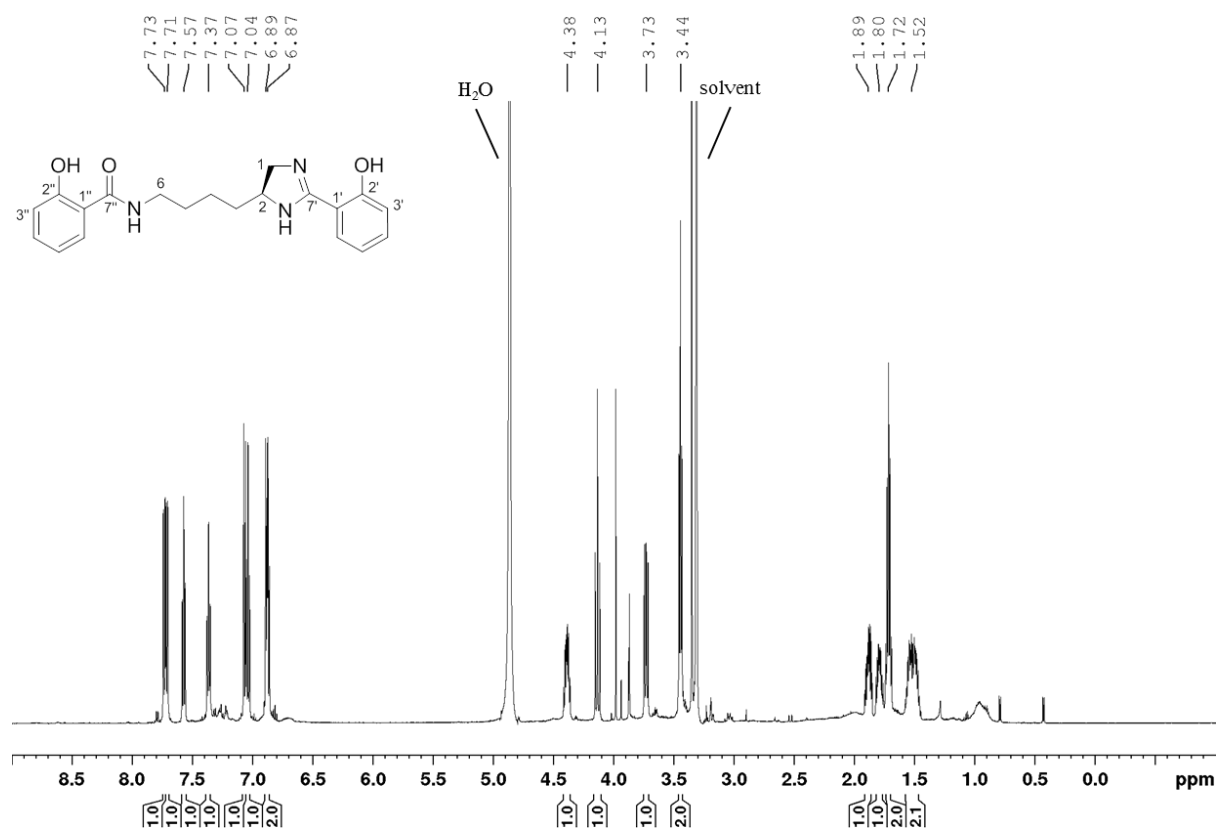
Figure S37. ^{1}H-decoupled ^{13}C NMR spectrum (150 MHz, CD$_3$OD) of pseudochelin A$_6$.
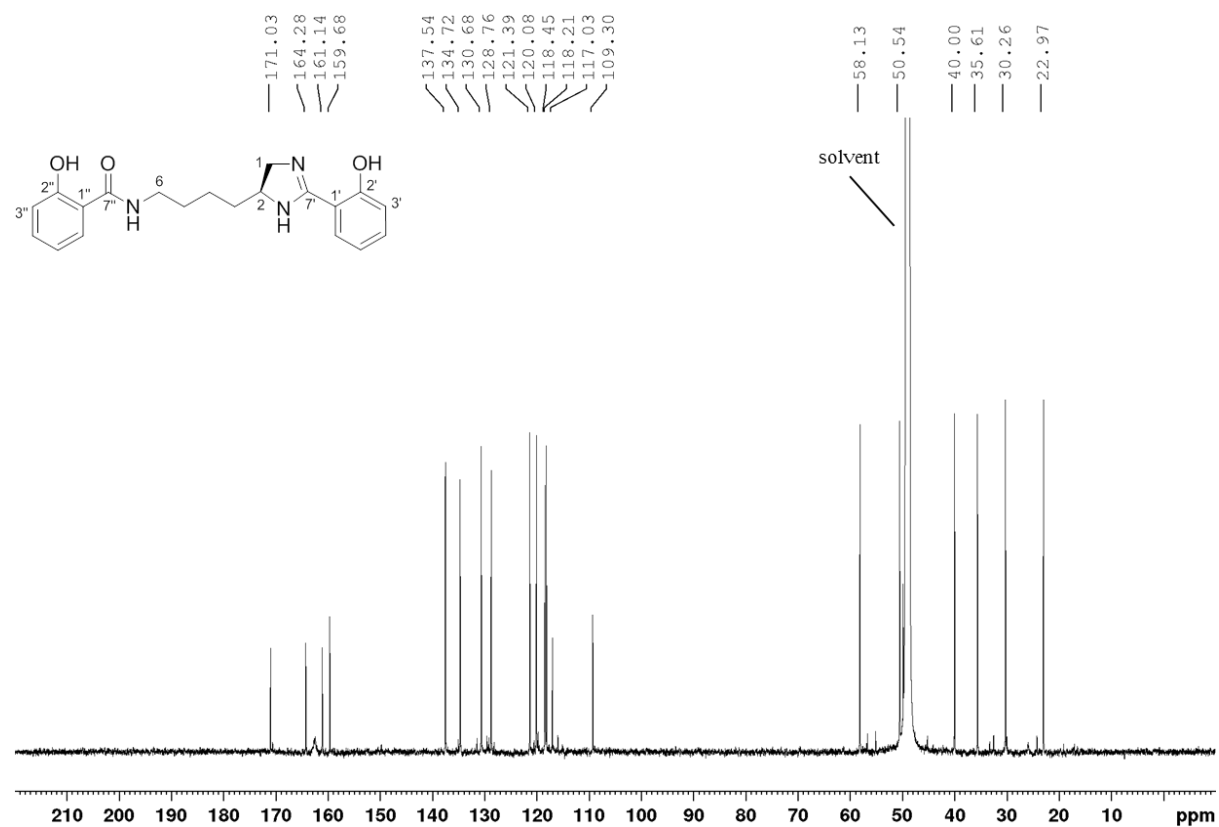
5.2.4.4 Pseudochelin A₇

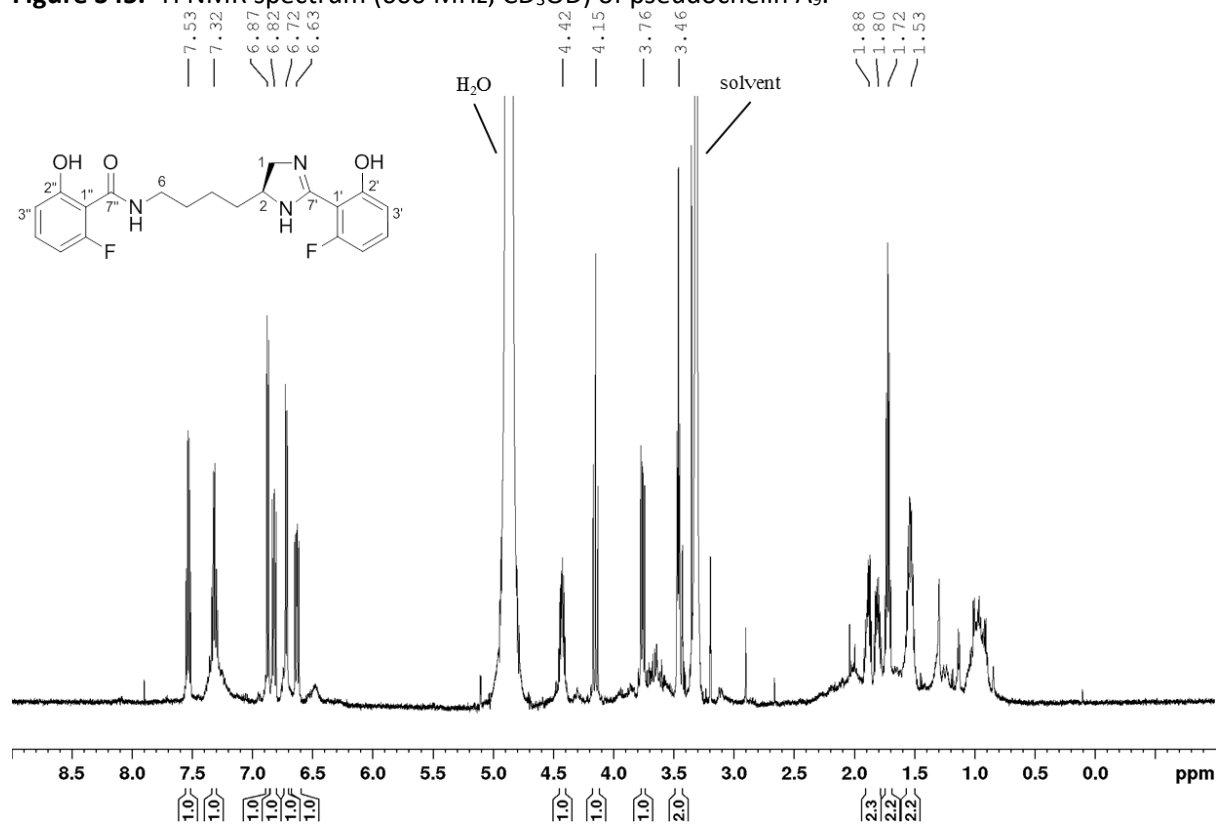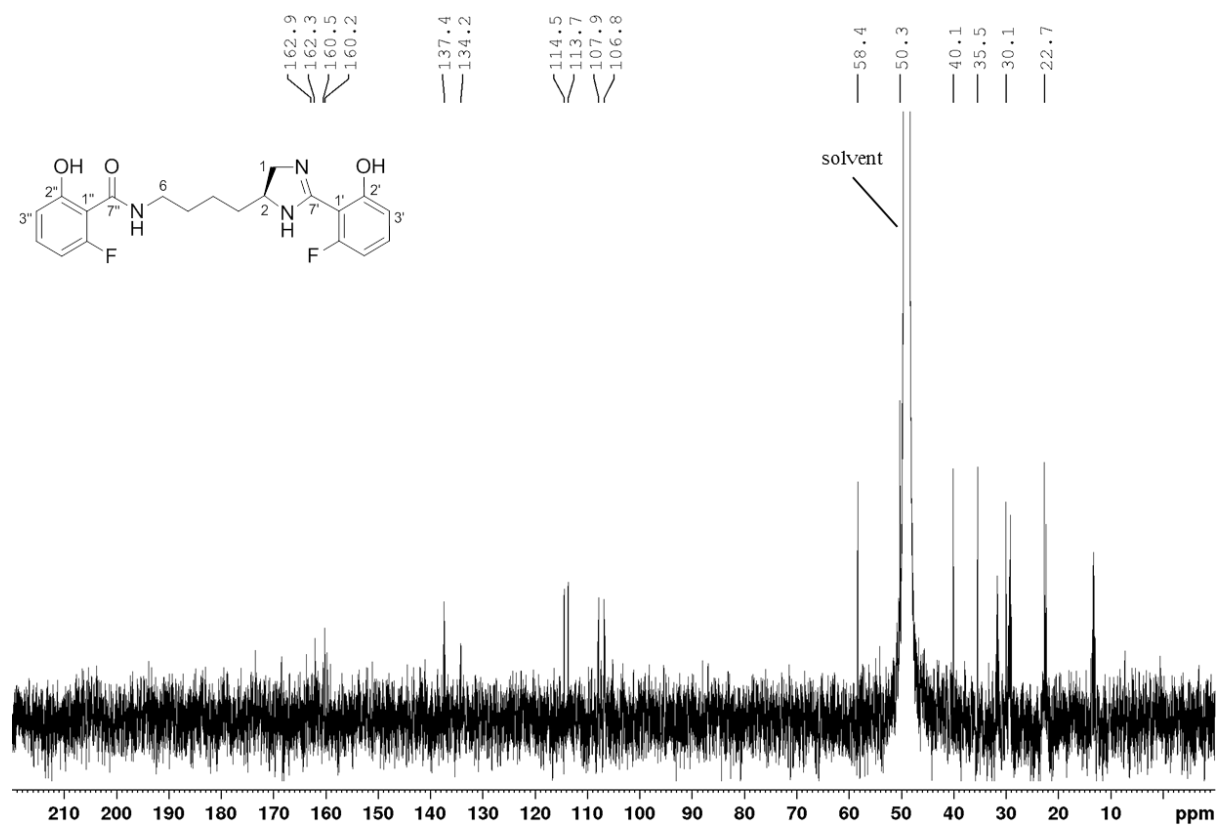**Figure S38.** HPLC-UV spectrum and ESI-MS spectrum of pseudochelin A₇.
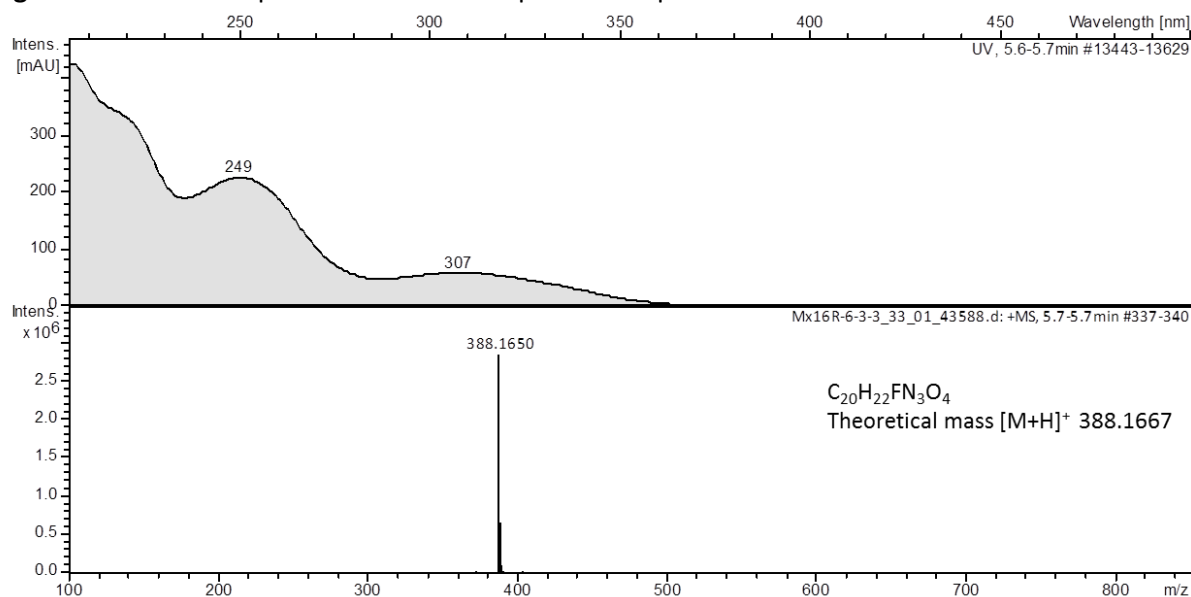
¹H NMR (600 MHz, methanol-*d₄*, 300 K) δ 7.32 (1H, dt, *J* = 8.3, 6.8 Hz, H-4''), 7.16 (1H, d, *J* = 7.8 Hz, H-6'), 7.09 (1H, d, *J* = 7.8 Hz, H-4'), 6.85 (1H, t, *J* = 7.8 Hz, H-5'), 6.72 (1H, d, *J* = 8.3, H-3''), 6.63 (1H, dd, *J* = 11.6, 8.3 Hz, H-5''), 4.39 (1H, m, H-2), 4.14 (1H, t, *J* = 11.3 Hz, H-1a), 3.74 (1H, dd, *J* = 11.3, 7.4 Hz, H-1b), 3.46 (2H, t, *J* = 6.9 Hz, H-6), 1.88 (1H, m, H-3a), 1.80 (1H, m, H-3b), 1.72 (2H, m, H-5), 1.53 (2H, m, H-4);

¹³C NMR (150 MHz, methanol-*d₄*, 300 K) δ 168.5 (C, d, *J* = 2.0 Hz, C-7''), 164.6 (C, C-7'), 162.7 (C, d, *J* = 4.7 Hz, C-2''), 162.4 (C, d, *J* = 247.0 Hz, C-6''), 149.2 (C, C-2'), 147.7 (C, C-3'), 134.2 (CH, d, *J* = 12.3 Hz, C-4''), 121.3 (CH, C-4'), 121.1 (CH, C-5'), 120.1 (CH, C-6'), 114.5 (CH, d, *J* = 2.5 Hz, C-3''), 109.2 (C, C-1'), 107.5 (C, d, *J* = 15.0 Hz, C-1''), 106.8 (CH, d, *J* = 24.3 Hz, C-5''), 58.1 (CH, C-2), 50.5 (CH₂, C-1), 40.1 (CH₂, C-6), 35.6 (CH₂, C-3), 30.1 (CH₂, C-5), 22.9 (CH₂, C-4);

[α]²⁰_D n.d.

UV/VIS λ_max (MeOH) nm (log ε): 242 (sh) (3.96), 311 (3.34) nm;

**HRMS (ESI):** *m/z* 388.1650 (calcd for C₂₀H₂₃FN₃O₄, 388.1667).

Figure S39. ^{1}H NMR spectrum (600 MHz, CD3OD) of pseudochelin A7.

Figure S40. ^{1}H-decoupled ^{13}C NMR spectrum (150 MHz, CD3OD) of pseudochelin A7.

5.2.4.5 Pseudochelin A$_8$

Figure S41. HPLC-UV spectrum and ESI-MS spectrum of pseudochelin A$_8$.
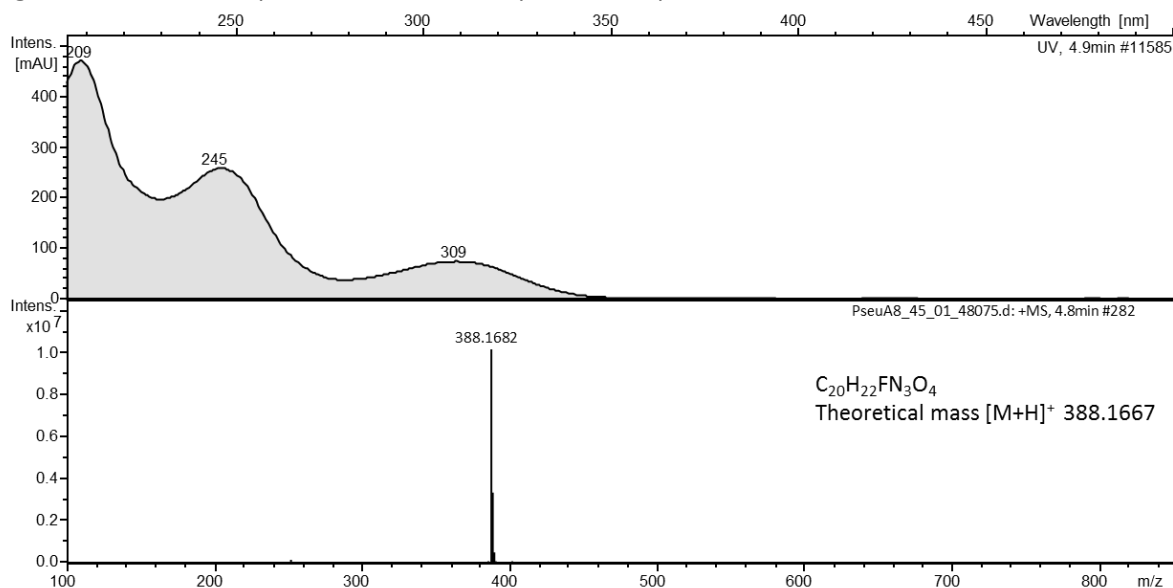
^{1}H NMR (600 MHz, methanol-d_4, 300 K) δ 7.53 (1H, dt, J = 8.5, 6.6 Hz, H-4'), 7.20 (1H, dd, J = 8.1, 1.6 Hz, H-6''), 6.92 (1H, dd, J = 7.9, 1.5 Hz, H-4''), 6.87 (1H, d, J = 8.5 Hz, H-3'), 6.81 (1H, dd, J = 11.2, 8.4, H-5'), 6.71 (1H, t, J = 8.0 Hz, H-5''), 4.42 (1H, m, H-2), 4.14 (1H, t, J = 11.5 Hz, H-1a), 3.74 (1H, dd, J = 11.5, 7.4 Hz, H-1b), 3.43 (2H, t, J = 6.9 Hz, H-6), 1.87 (1H, m, H-3a), 1.80 (1H, m, H-3b), 1.71 (2H, m, H-5), 1.51 (2H, m, H-4);

^{13}C NMR (150 MHz, methanol-d_4, 300 K) δ 171.5 (C, C-7''), 162.9 (C, d, J = 254.0 Hz, C-6'), 160.5 (C, C-7'), 160.3 (C, d, J = 5.0 Hz, C-2'), 150.2 (C, C-2''), 147.3 (C, C-3''), 137.4 (CH, d, J = 12.2 Hz, C-4'), 119.6 (CH, C-4''), 119.6 (CH, C-5''), 118.6 (CH, C-6''), 116.8 (C, C-1''), 113.7 (C, d, J = 2.9 Hz, C-3'), 107.9 (C, d, J = 22.2 Hz, C-5'), 100.3 (CH, d, J = 13.4 Hz, C-1'), 58.3 (CH, C-2), 50.3 (CH$_2$, C-1), 40.0 (CH$_2$, C-6), 35.5 (CH$_2$, C-3), 30.2 (CH$_2$, C-5), 22.8 (CH$_2$, C-4);

[α]$^{20}_D$ −23.9 (c 0.46, MeOH);

UV/VIS λ$_{max}$ (MeOH) nm (log ε): 244 (4.11), 310 (3.60) nm;

HRMS (ESI): m/z 388.1682 (calcd for C$_{20}$H$_{23}$FN$_3$O$_4$, 388.1667).

Figure S42. ^{1}H NMR spectrum (500 MHz, CD$_3$OD) of pseudochelin A$_8$.

Figure S43. ^{1}H-decoupled ^{13}C NMR spectrum (125 MHz, CD$_3$OD) of pseudochelin A$_8$.

5.2.4.6 Pseudochelin A₉

Figure S44. HPLC-UV spectrum and ESI-MS spectrum of pseudochelin A₉.
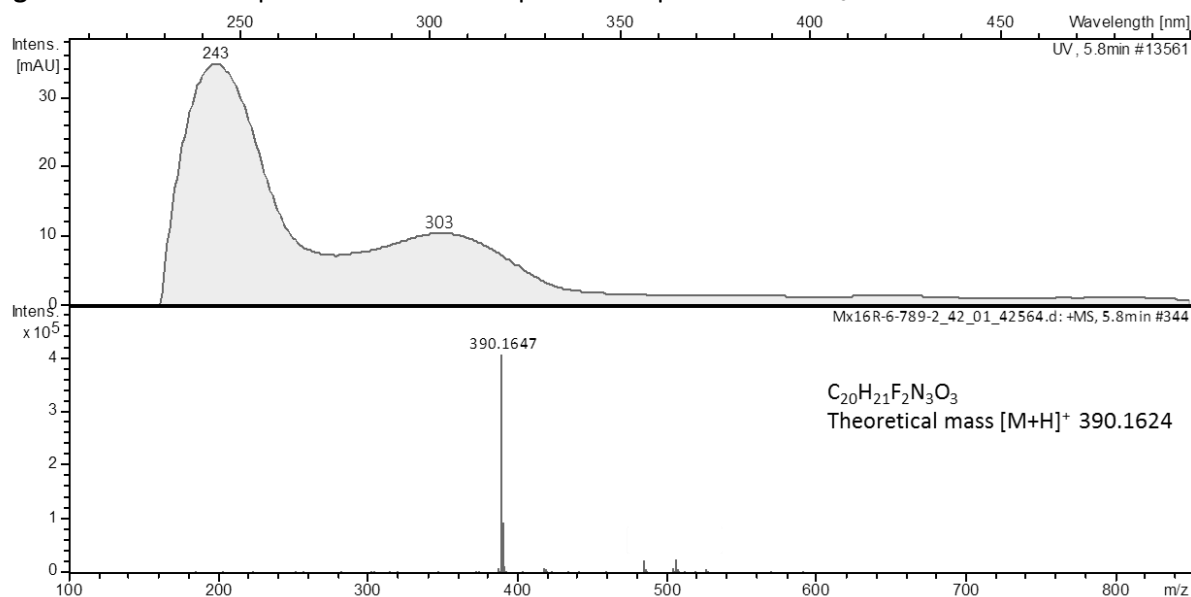
¹H NMR (600 MHz, methanol-*d₄*, 300 K) δ 7.53 (1H, dt, *J* = 8.5, 6.6 Hz, H-4'), 7.32 (1H, dt, *J* = 8.4, 6.8 Hz, H-4''), 6.87 (1H, d, *J* = 8.4 Hz, H-3'), 6.82 (1H, dd, *J* = 11.2, 8.4 Hz, H-5'), 6.72 (1H, d, *J* = 8.4 Hz, H-3''), 6.63 (1H, dd, *J* = 11.7, 8.3 Hz, H-5''), 4.42 (1H, m, H-2), 4.15 (1H, t, *J* = 11.5 Hz, H-1a), 3.76 (1H, dd, *J* = 11.6, 7.4 Hz, H-1b), 3.46 (2H, t, *J* = 6.9 Hz, H-6), 1.88 (1H, m, H-3a), 1.80 (1H, m, H-3b), 1.72 (2H, m, H-5), 1.53 (2H, m, H-4);

¹³C NMR (150 MHz, methanol-*d₄*, 300 K) δ 162.9 (C, d, *J* = 254.0 Hz, C-6'), 162.3 (C, d, *J* = 4.7 Hz, C-2''), 160.5 (C, C-7'), 160.2 (C, d, *J* = 5.0 Hz, C-2'), 137.4 (CH, d, *J* = 12.5 Hz, C-4'), 134.2 (CH, d, *J* = 13.2 Hz, C-4''), 114.5 (CH, d, *J* = 4.3 Hz, C-3''), 113.7 (CH, d, *J* = 3.4 Hz, C-3'), 107.9 (C, d, *J* = 22.1 Hz, C-5'), 106.8 (CH, d, *J* = 24.6 Hz, C-5''), 58.4 (CH, C-2), 50.3 (CH₂, C-1), 40.1 (CH₂, C-6), 35.5 (CH₂, C-3), 30.1 (CH₂, C-5), 22.7 (CH₂, C-4);

[α]²⁰_D n.d.

UV/VIS λ_max (MeOH) nm (log ε): 242 (4.33), 312 (3.83) nm;

HRMS (ESI): *m/z* 390.1647 (calcd for C20H23FN3O4, 390.1624).

I

Figure S45. ^{1}H NMR spectrum (600 MHz, CD$_3$OD) of pseudochelin A$_9$.

Figure S46. ^{1}H-decoupled ^{13}C NMR spectrum (150 MHz, CD$_3$OD) of pseudochelin A$_9$.

5.2.5 Aurachin D derivatives

Figure S47 ^{19}F NMR spectra (600 MHz, CD$_3$OD) of 8- (1a), 7- (1b) and 6-fluoroaurachin D (1c).
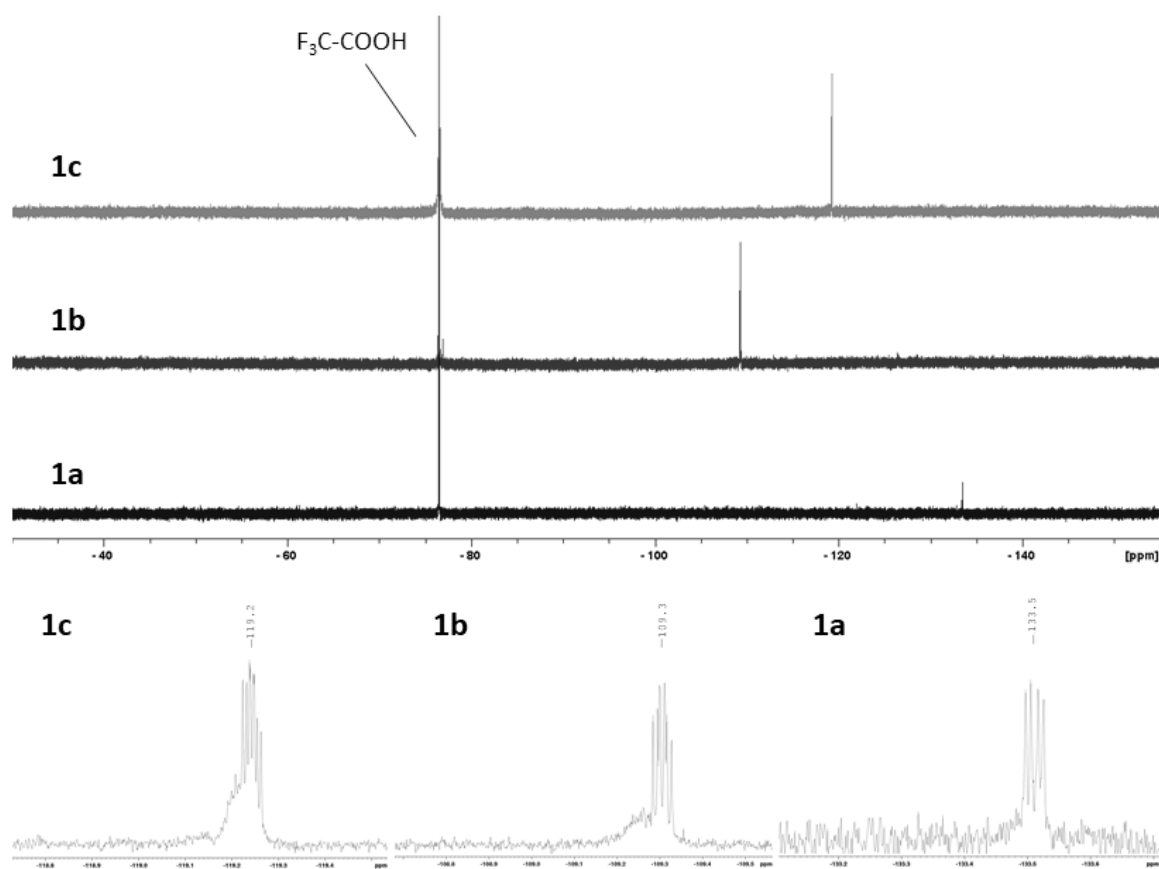
5.2.5.1 8-Fluoroaurachin D

Figure S48. HPLC-UV spectrum and ESI-MS spectrum of 8-fluoroaurachin D.
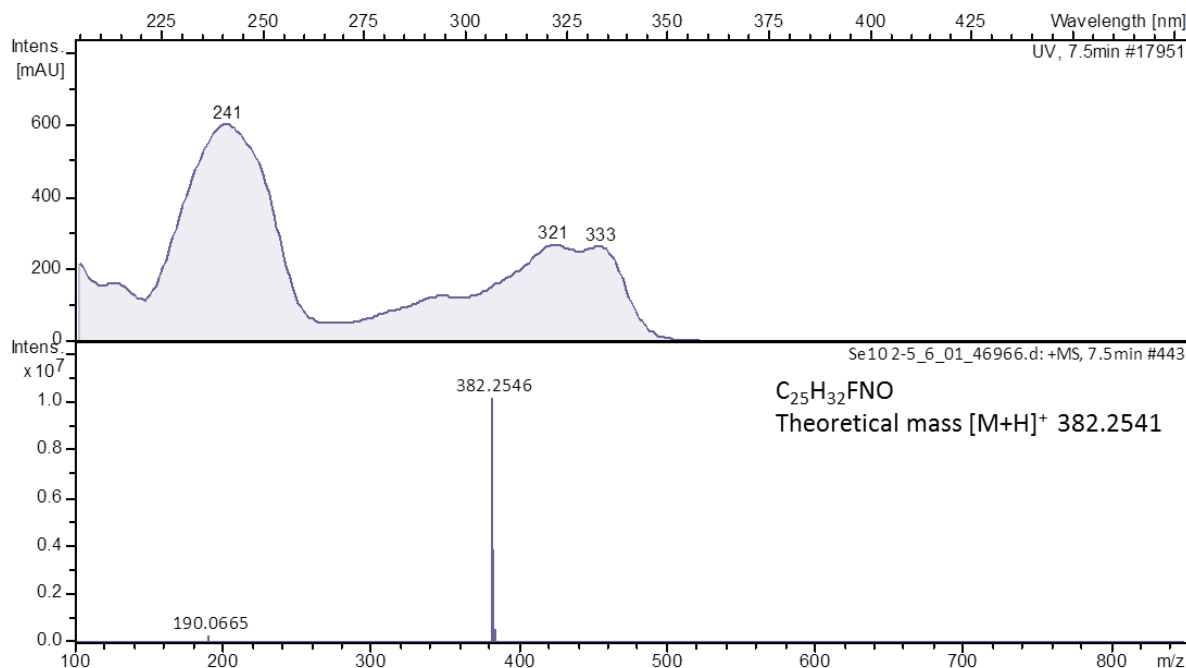
¹H NMR (600 MHz, methanol-d_4, 300 K): δ = 8.02 (dd, $J_{H,H}$ = 7.9, 1.3 Hz, 1H; CH-5), 7.43 (ddd, $J_{H,H}$ = 7.9, 1.3, $J_{H,F}$ = 11.1 Hz, 1H, CH-7), 7.30 (dt, $J_{H,H}$ = 7.9, $J_{H,F}$ = 4.9 Hz, 1H, CH-6), 5.09 (dt, $J_{H,H}$ = 6.9, 1.2 Hz, 1H, CH-2'), 5.04 (dt, $J_{H,H}$ = 6.9, 1.4 Hz, 1H, CH-6'), 4.98 (ddt, $J_{H,H}$ = 7.0, 1.5, 1.4 Hz, 1H, CH-10'), 3.40 (d, $J_{H,H}$ = 6.9 Hz, 2H, CH₂-1'), 2.51 (s, 3H, CH₃-9), 2.10 (m, 2H, CH₂-5'), 2.03 (m, 2H, CH₂-4'), 1.92 (m, 2H, CH₂-9'), 1.87 (m, 2H, CH₂-8'), 1.81 (d, $J_{H,H}$ = 1.2 Hz, 3H, CH₃-13'), 1.60 (d, $J_{H,H}$ = 1.4 Hz, 3H, CH₃-12'), 1.55 (d, $J_{H,H}$ = 1.4 Hz, 3H, CH₃-14'), 1.49 ppm (d, $J_{H,H}$ = 1.5 Hz, 3H, CH₃-15');

¹³C NMR (150 MHz, methanol-d_4, 300 K): δ = 177.8 (C-4), 153.3 (d, $J_{C,F}$ = 247.1 Hz, C-8), 150.4 (C-2), 136.1 (C-3'), 135.9 (C-7'), 132.0 (C-11'), 130.1 (C-8a), 127.1 (C-4a), 125.3 (C-6'), 125.3 (C-10'), 123.9 (d, $J_{C,F}$ = 6.9 Hz; C-6), 123.5 (C-2'), 121.7 (C-3), 122.0 (d, $J_{C,F}$ = 4.0 Hz; C-5), 116.7 (d, $J_{C,F}$ = 16.9 Hz; C-7), 40.8 (C-8'), 40.7 (C-4'), 27.8 (C-9'), 27.2 (C-5'), 25.8 (C-12'), 24.8 (C-1'), 18.0 (C-9), 17.6 (C-15'), 16.3 (C-13'), 16.2 ppm (C-14');

¹⁹F NMR (600 MHz, methanol-d_4, 300 K): δ = 133.5 ppm (dd, $J_{F,H}$ = 11.3, 4.8 Hz, 1F, CF-8);

**HRMS (ESI):** *m/z* calcd for C₂₅H₃₂FNO: 382.2541 [M+H]⁺; found: 382.2546.

Figure S49. ^{1}H NMR spectrum (600 MHz, CD₃OD) of 8-fluoroaurachin D.

Figure S50. ^{1}H-decoupled ^{13}C NMR spectrum (150 MHz, CD₃OD) of 8-fluoroaurachin D.

Figure S51. ^{1}H, ^{13}C HSQC spectrum (CD$_3$OD) of 8-fluoroaurachin D.
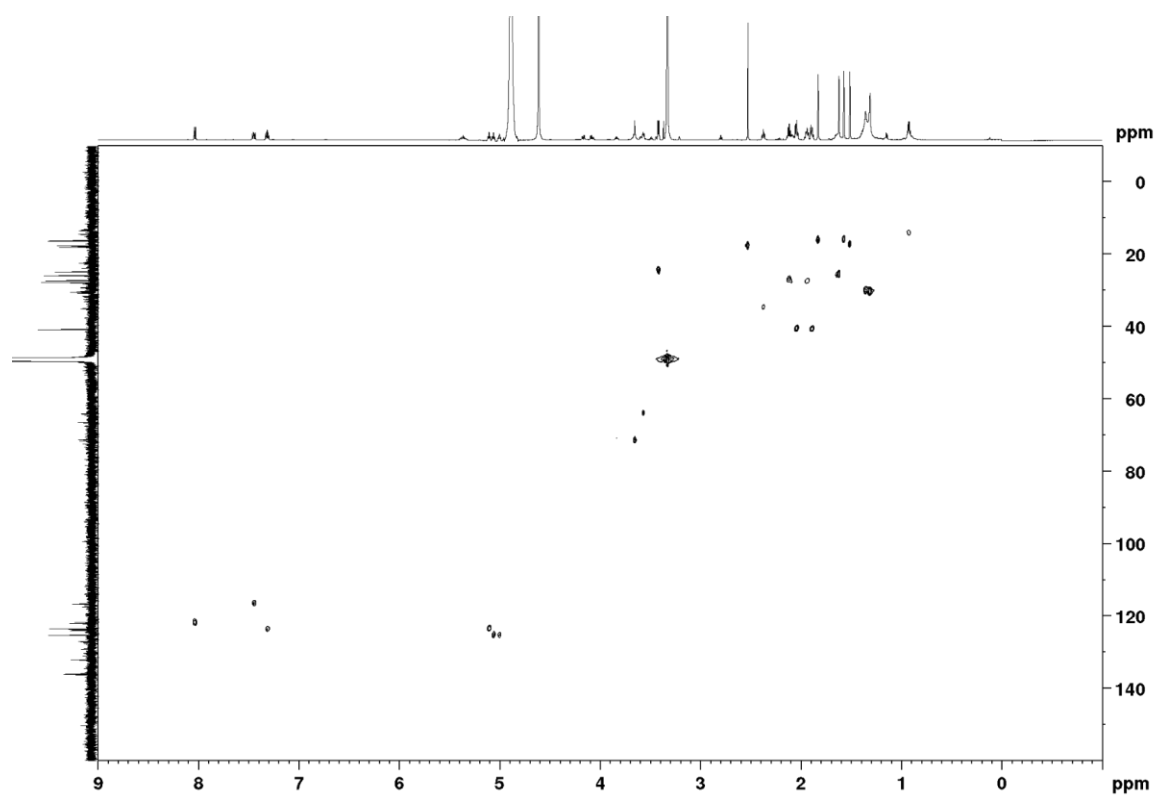
Figure S52. ^{1}H, ^{13}C HMBC spectrum (CD$_3$OD) of 8-fluoroaurachin D.
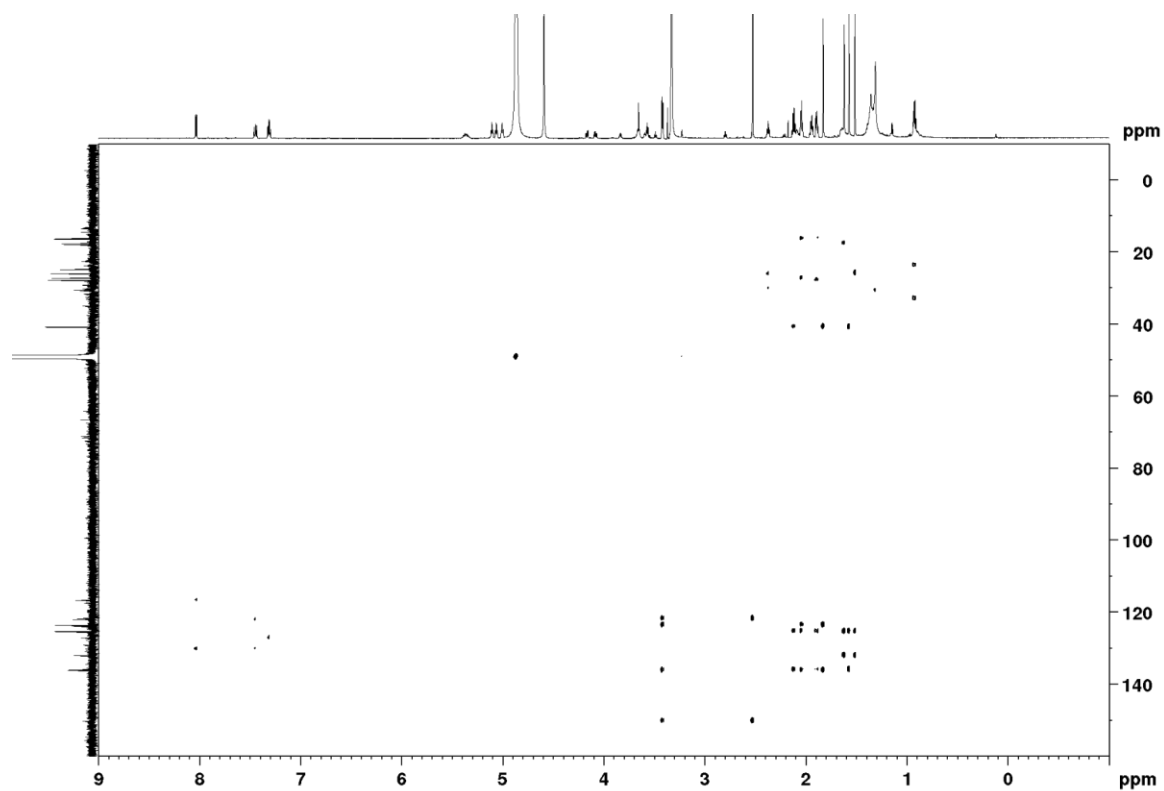
5.2.5.2 7-Fluoroaurachin D

Figure S53. HPLC-UV spectrum and ESI-MS spectrum of 7-fluoroaurachin D.
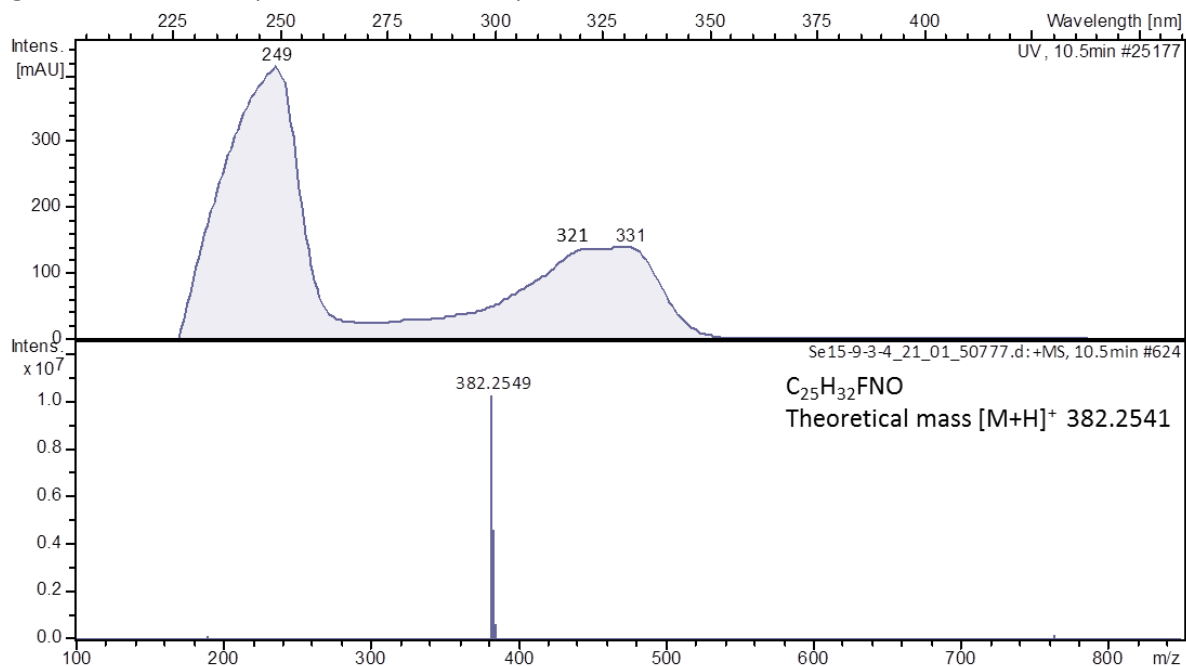
^{1}H NMR (700 MHz, methanol-d_4, 300 K): δ = 8.25 (dd, $J_{H,H}$ = 8.7, $J_{H,F}$ = 6.2 Hz, 1H; CH-5), 7.16 (dd, $J_{H,H}$ = 2.4, $J_{H,F}$ = 9.7 Hz, 1H, CH-8), 7.11 (dt, $J_{H,H}$ = 8.7, 2.4, $J_{H,F}$ = 8.7 Hz, 1H, CH-6), 5.09 (dt, $J_{H,H}$ = 7.0, 1.4 Hz, 1H, CH-2'), 5.05 (dt, $J_{H,H}$ = 7.0, 1.4 Hz, 1H, CH-6'), 4.99 (ddt, $J_{H,H}$ = 7.1, 1.5, 1.4 Hz, 1H, CH-10'), 3.38 (d, $J_{H,H}$ = 7.0 Hz, 2H, CH$_2$-1'), 2.45 (s, 3H, CH$_3$-9), 2.10 (m, 2H, CH$_2$-5'), 2.02 (m, 2H, CH$_2$-4'), 1.94 (m, 2H, CH$_2$-9'), 1.87 (m, 2H, CH$_2$-8'), 1.80 (d, $J_{H,H}$ = 1.4 Hz, 3H, CH$_3$-13'), 1.61 (d, $J_{H,H}$ = 1.4 Hz, 3H, CH$_3$-12'), 1.55 (d, $J_{H,H}$ = 1.4 Hz 3H, CH$_3$-14'), 1.51 ppm (d, $J_{H,H}$ = 1.5 Hz, 3H, CH$_3$-15');

^{13}C NMR (175 MHz, methanol-d_4, 300 K): δ = 177.9 (C-4), 165.8 (d, $J_{C,F}$ = 240.0 Hz, C-7), 150.0 (C-2), 141.4 (C-8a), 135.9 (C-7'), 135.7 (C-3'), 132.0 (C-11'), 129.5 (C-5),125.4 (C-10'), 125.2 (C-6'), 123.9 (C-2'), 121.9 (C-4a), 120.8 (C-3), 113.3 (C-6), 103.4 (C-8), 40.8 (C-4'), 40.8 (C-8'), 27.8 (C-9'), 27.2 (C-5'), 25.7 (C-12'), 24.4 (C-1'), 18.3 (C-9), 17.7 (C-15'), 16.1 (C-13'), 16.0 ppm (C-14');

^{19}F NMR (600 MHz, methanol-d_4, 300 K): δ = 109.3 ppm (ddd, $J_{F,H}$ = 9.6, 8.6, 6.2 Hz, 1F, CF-7);

**HRMS (ESI)**: *m/z* calcd for C$_{25}$H$_{32}$FNO: 382.2541 [M+H]$^+$; found: 382.2549.

**Figure S54.** ¹H NMR spectrum (700 MHz, CD₃OD) of 7-fluoroaurachin D.
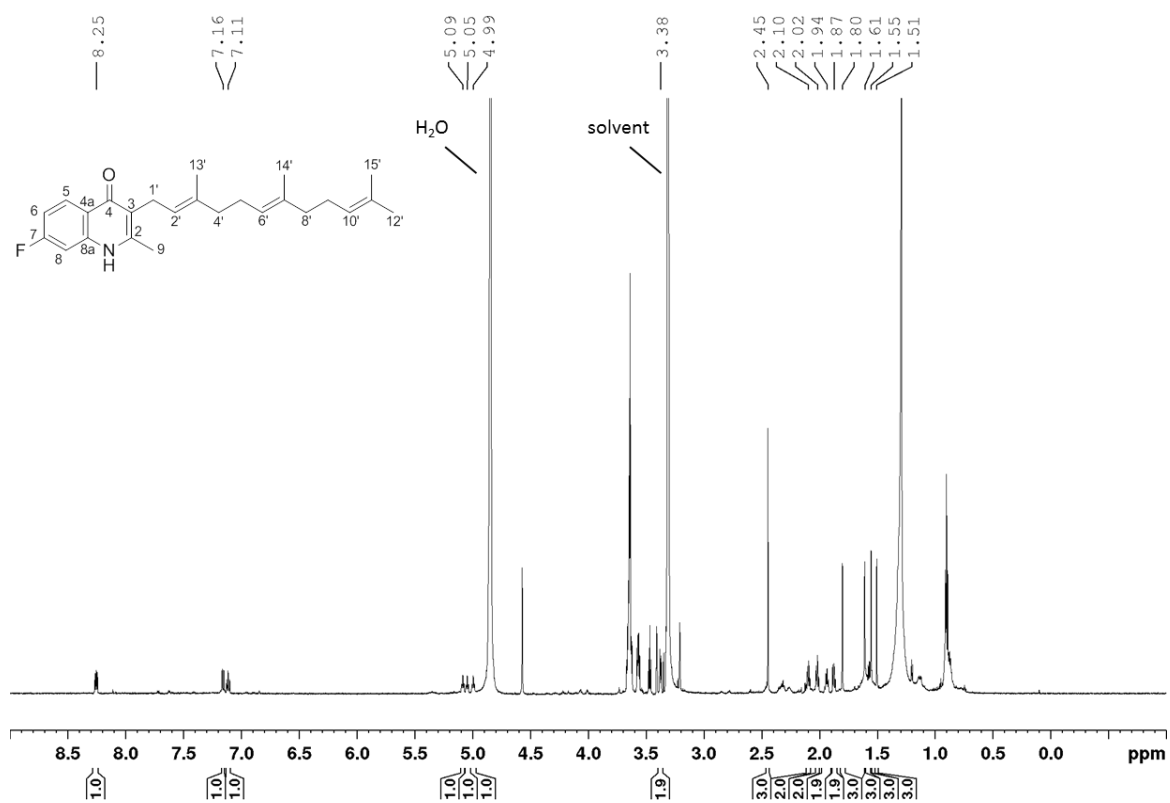
Figure S55. ¹H-decoupled ¹³C NMR spectrum (175 MHz, CD₃OD) of 7-fluoroaurachin D.
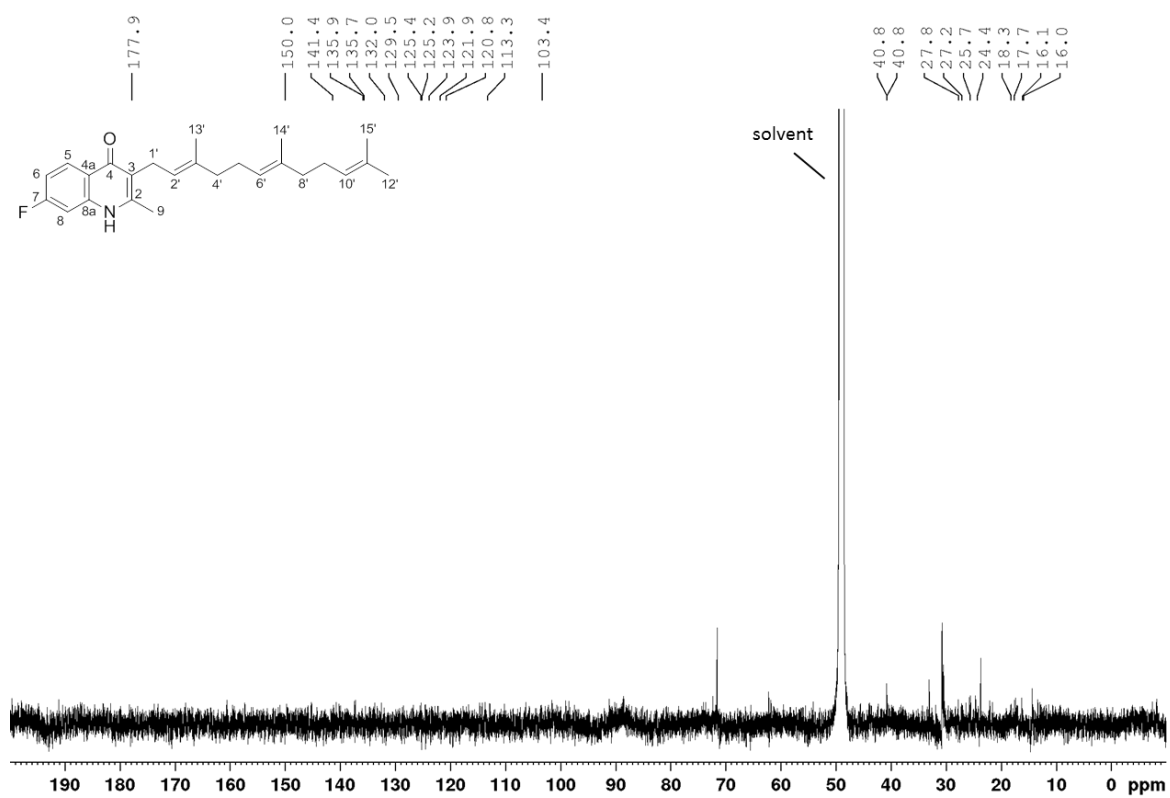
Figure S56. ^{1}H, ^{13}C HSQC spectrum (CD$_3$OD) of 7-fluoroaurachin D.
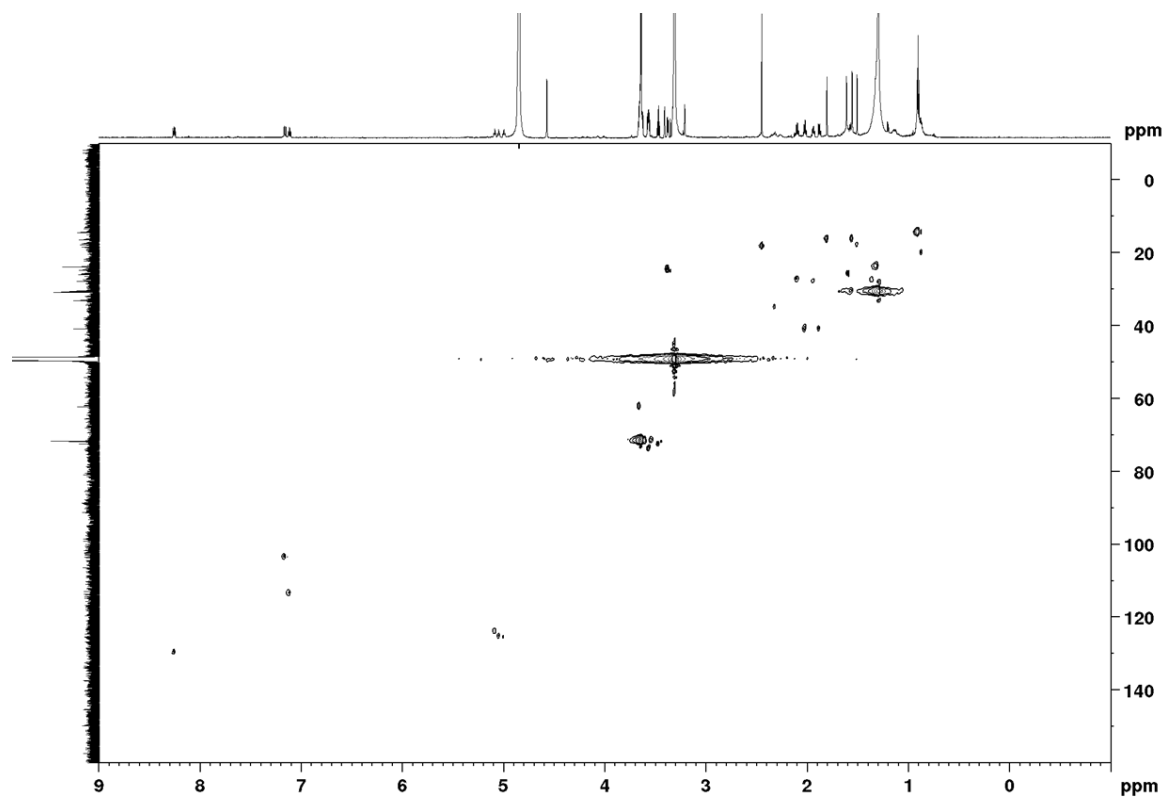
Figure S57. ^{1}H, ^{13}C HMBC spectrum (CD$_3$OD) of 7-fluoroaurachin D.
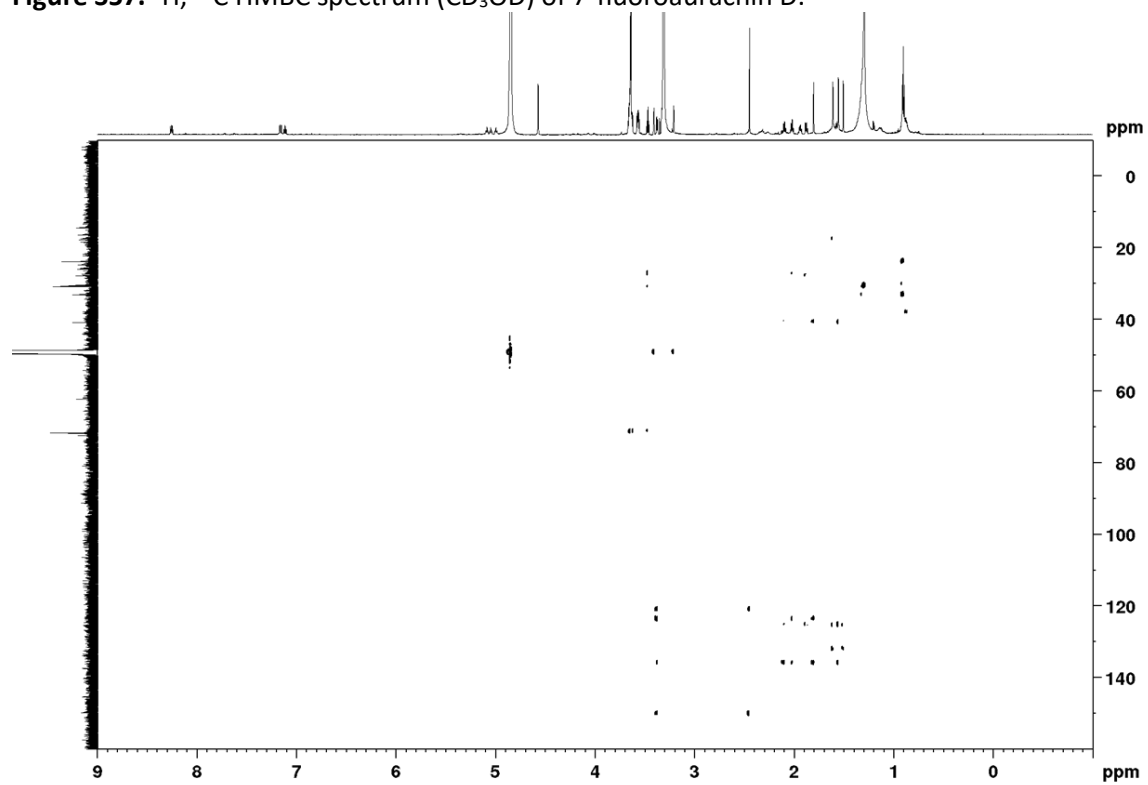
5.2.5.3 6-Fluoroaurachin D

Figure S58. HPLC-UV spectrum and ESI-MS spectrum of 6-fluoroaurachin D.
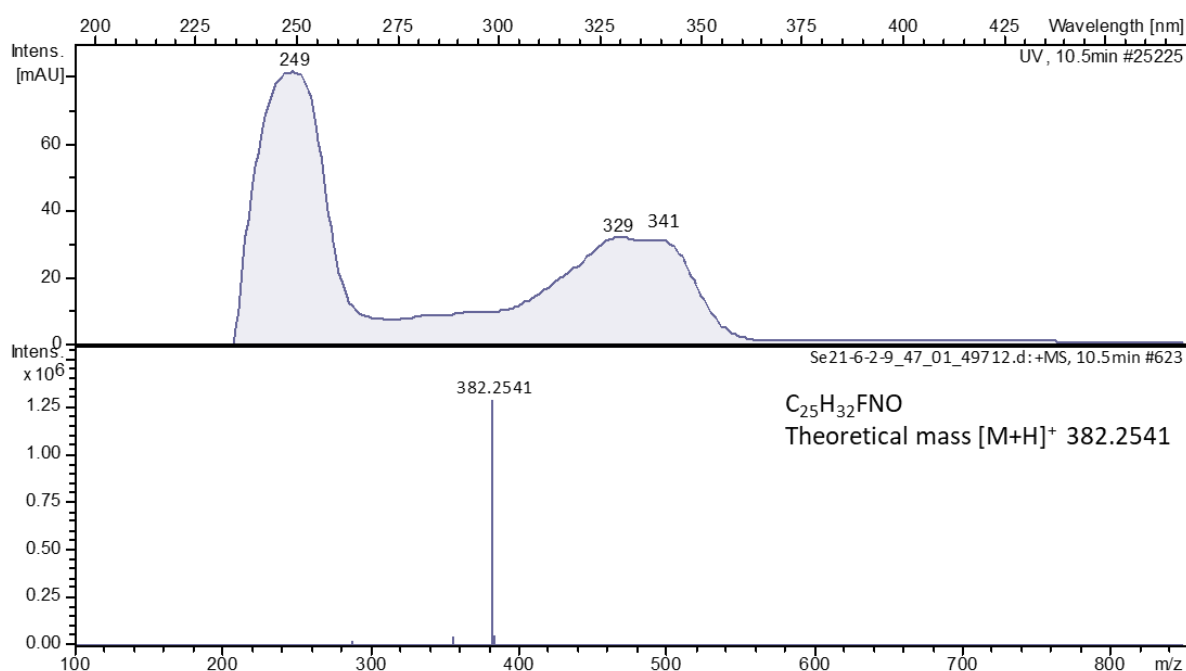
¹H NMR (600 MHz, methanol-d_4, 300 K): δ = 7.84 (dd, $J_{H,H}$ = 9.4, 2.9 Hz, 1H; CH-5), 7.56 (dd, $J_{H,H}$ = 9.1, $J_{H,F}$ = 4.5 Hz, 1H, CH-8), 7.45 (ddd, $J_{H,H}$ = 9.1, 2.9, $J_{H,F}$ = 8.1 Hz, 1H, CH-7), 5.09 (dt, $J_{H,H}$ = 6.9, 1.3 Hz, 1H, CH-2'), 5.05 (dt, $J_{H,H}$ = 6.9, 1.3 Hz, 1H, CH-6'), 4.99 (ddt, $J_{H,H}$ = 7.0, 1.5, 1.4 Hz, 1H, CH-10'), 3.40 (d, $J_{H,H}$ = 6.9 Hz, 2H, CH$_2$-1'), 2.47 (s, 3H, CH$_3$-9), 2.09 (m, 2H, CH$_2$-5'), 2.02 (m, 2H, CH$_2$-4'), 1.94 (m, 2H, CH$_2$-9'), 1.88 (m, 2H, CH$_2$-8'), 1.81 (d, $J_{H,H}$ = 1.3 Hz, 3H, CH$_3$-13'), 1.61 (d, $J_{H,H}$ = 1.4 Hz, 3H, CH$_3$-12'), 1.55 (d, $J_{H,H}$ = 1.3 Hz, 3H, CH$_3$-14'), 1.51 ppm (d, $J_{H,H}$ = 1.5 Hz, 3H, CH$_3$-15');

¹³C NMR (150 MHz, methanol-d_4, 300 K): δ = 177.7 (C-4), 160.5 (d, $J_{C,F}$ = 241.9 Hz, C-6), 150.0 (C-2), 137.2 (C-8a), 136.1 (C-3'), 135.9 (C-7'), 132.1 (C-11'), 125.4 (C-6'), 125.3 (C-10'), 126.2 (C-4a), 123.6 (C-2'), 121.6 (C-8), 121.3 (C-7), 120.8 (C-3), 110.1 (C-5), 40.8 (C-4'), 40.7 (C-8'), 27.8 (C-9'), 27.3 (C-5'), 25.8 (C-12'), 24.8 (C-1'), 18.3 (C-9), 17.6 (C-15'), 16.3 (C-13'), 16.1 ppm (C-14');

¹⁹F NMR (600 MHz, methanol-d_4, 300 K): δ = 119.2 ppm (ddd, $J_{F,H}$ = 9.4, 8.1, 4.5 Hz, 1F, CF-6);

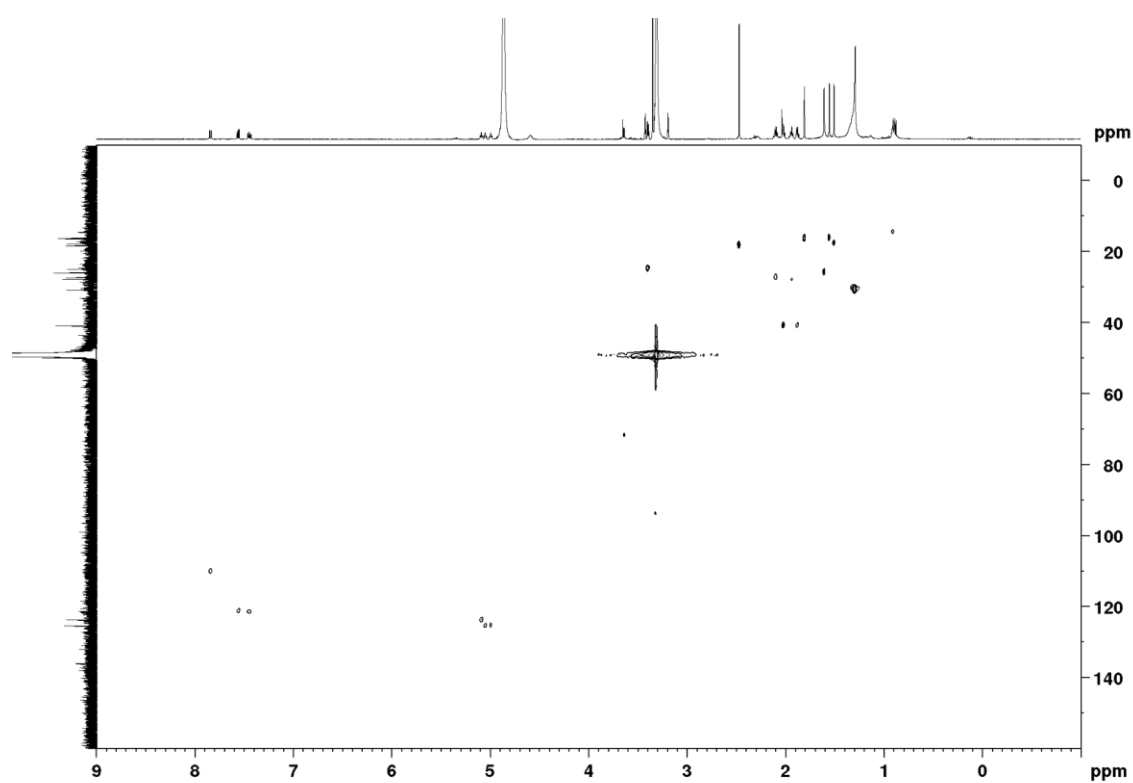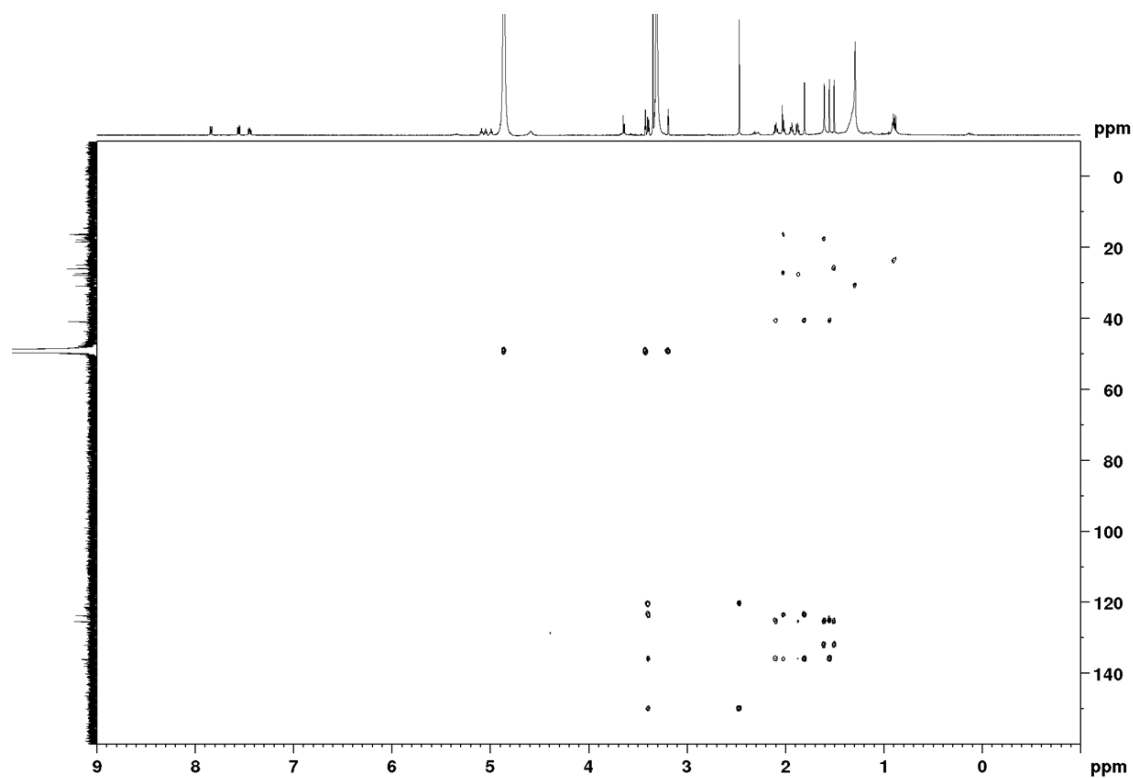**HRMS (ESI):** m/z calcd for C$_{25}$H$_{32}$FNO: 382.2541 [M+H]$^+$; found: 382.2541.
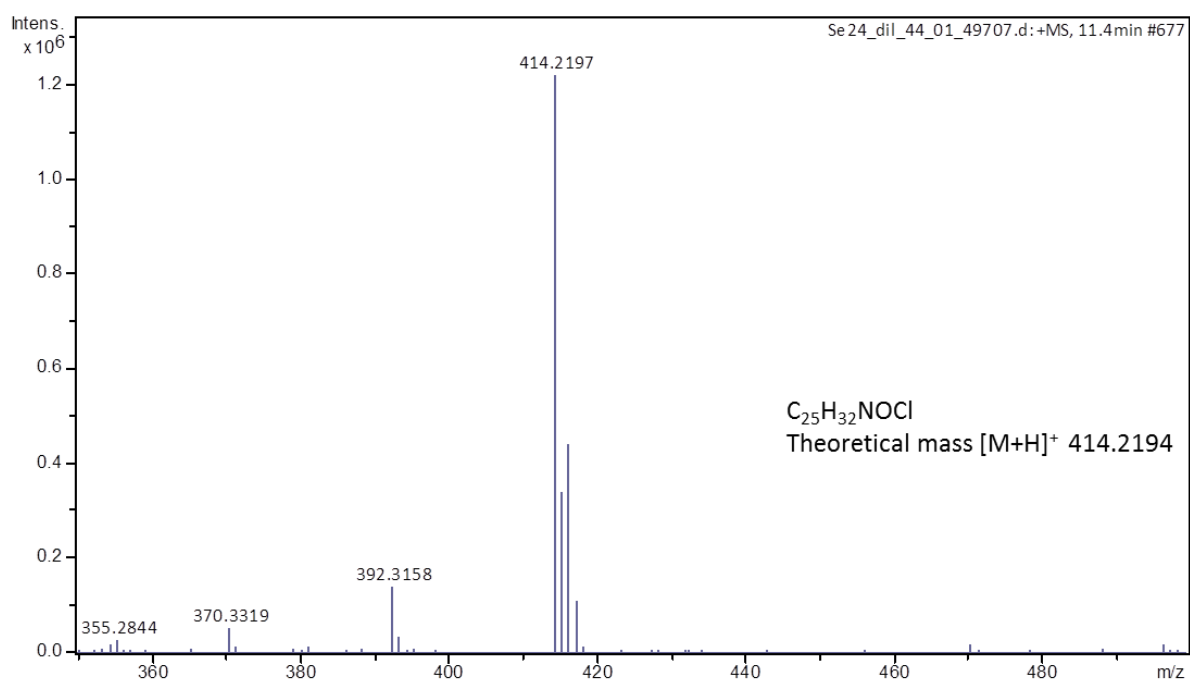
Figure S59. ¹H NMR spectrum (600 MHz, CD₃OD) of 6-fluoroaurachin D.
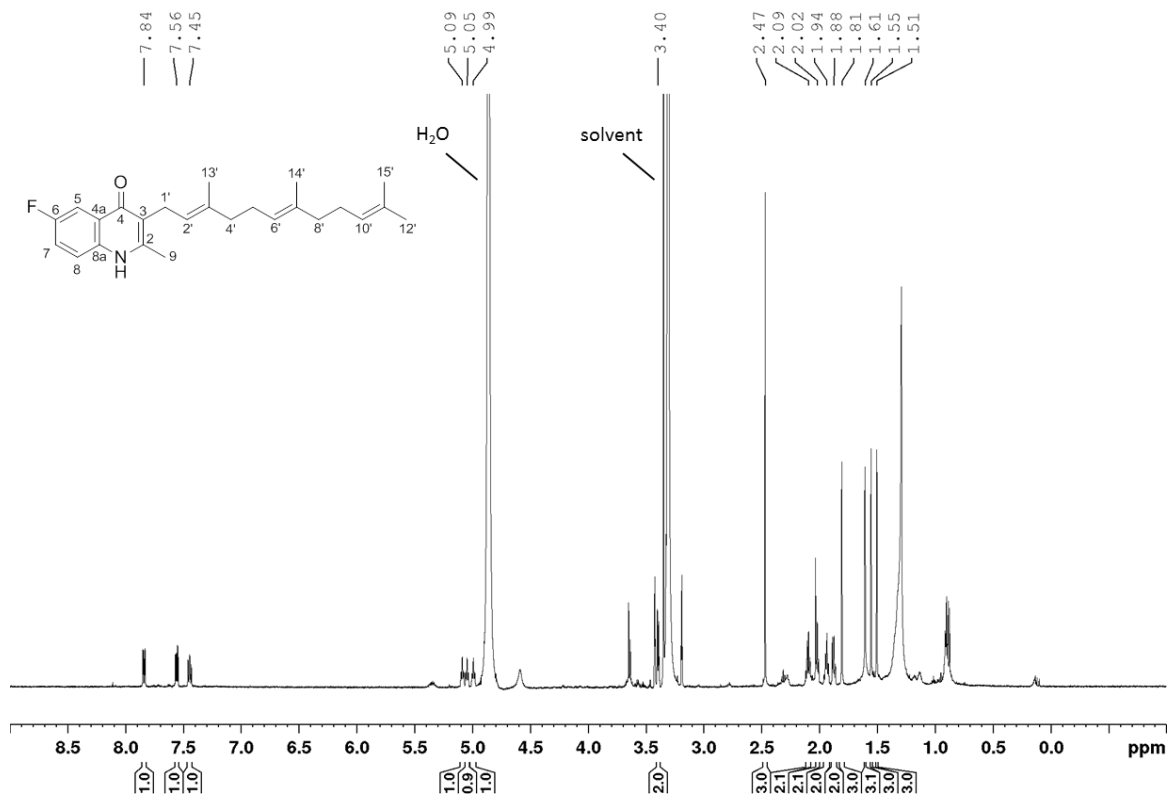
**Figure S60.** ¹H-decoupled ¹³C NMR spectrum (150 MHz, CD₃OD) of 6-fluoroaurachin D.
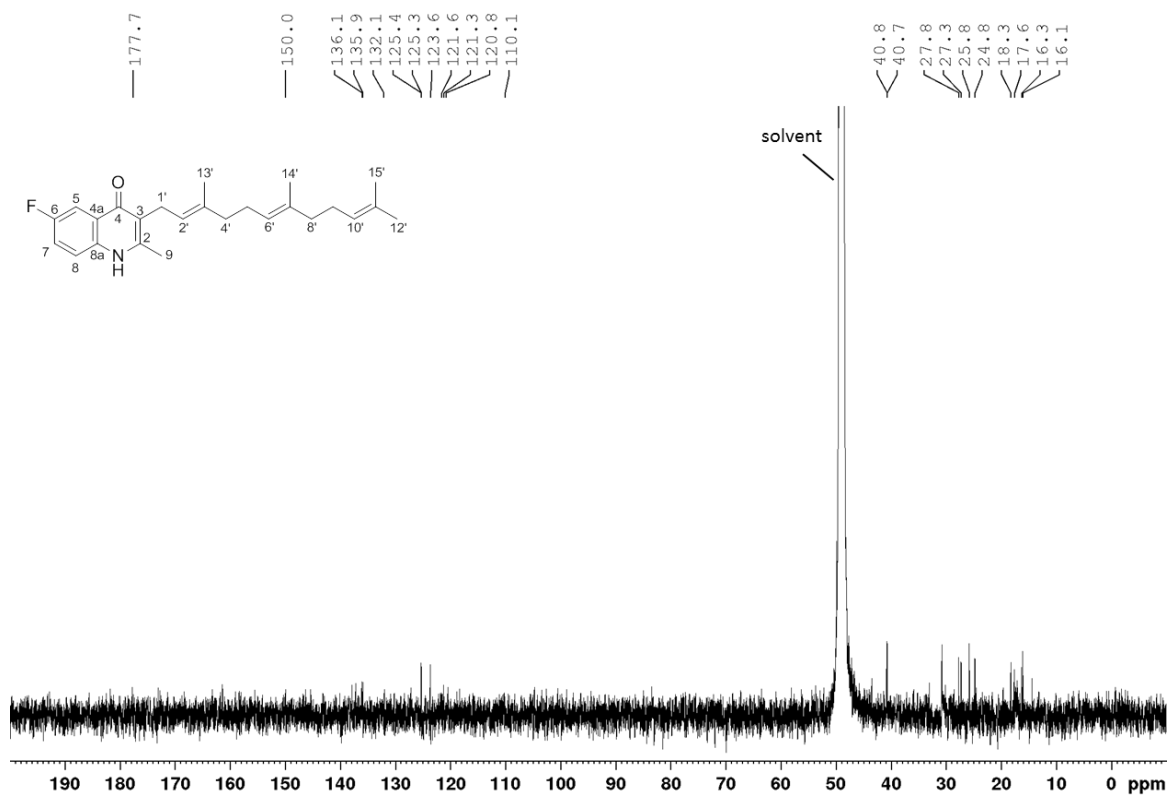
Figure S61. ^{1}H, ^{13}C HSQC spectrum (CD$_3$OD) of 6-fluoroaurachin D.

Figure S62. ^{1}H, ^{13}C HMBC spectrum (CD$_3$OD) of 6-fluoroaurachin D.

5.2.5.4 6-Chloroaurachin B/C

Figure S63. ESI-MS spectrum of 6-chloroaurachin B/C

HRMS (ESI): *m/z* calcd for $C_{25}H_{32}ClNO$: 414.2194 [M+H]$^+$; found: 414.2197.

5.2.6 5-Hexynoic micacocidin Ga³⁺

Figure S64 HPLC-UV/VIS spectrum and ESI-MS spectrum of 5-hexynoic micacocidin Ga³⁺ complex.

$C_{28}H_{35}N_3O_4S_3Ga^+$
Theoretical mass $[M+H]^+$ 642.1040
Δ + 1.4 ppm
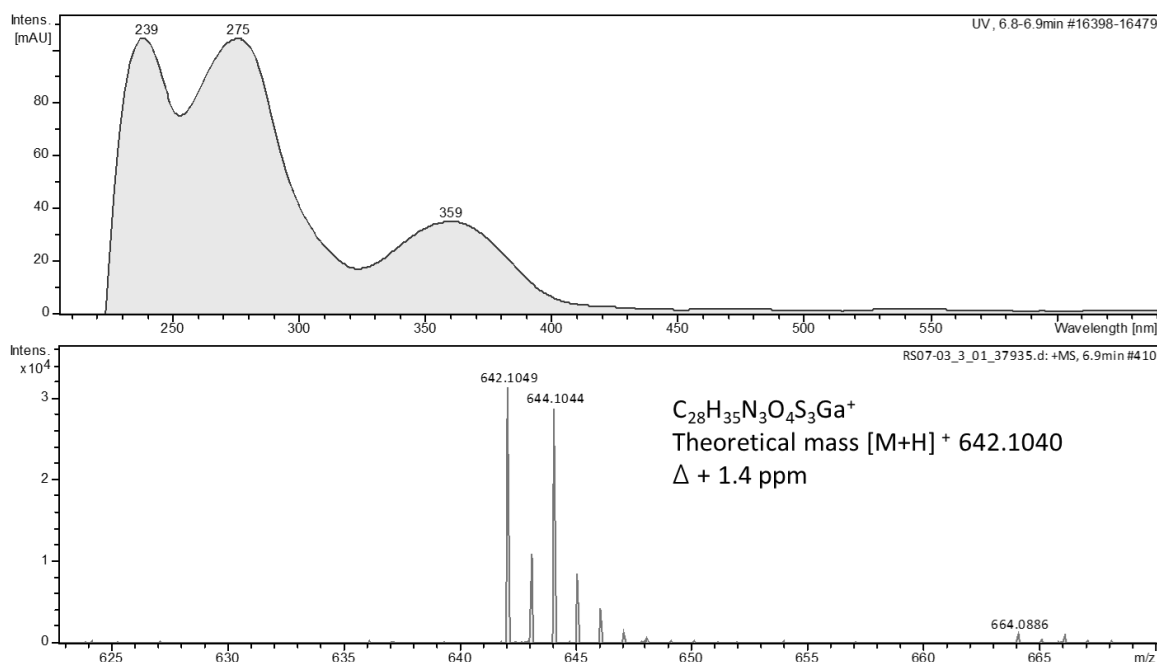
¹H NMR (600 MHz, methanol-d_4, 300 K): δ = 7.22 (dd, J = 8.4, 7.3 Hz, 1H; CH-5), 6.75 (dd, J = 8.4, 1.3 Hz, 1H, CH-6), 6.64 (dd, J = 7.4, 1.4 Hz, 1H, CH-4), 4.78 (ddd, J = 13.6, 10.6, 8.0 Hz, 1H, CH-14), 4.54 (d, J = 10.6 Hz, 1H, CH-15), 3.73 (d, J = 12.3 Hz, 1H, CH₂-24a), 3.69 (s, CH-19), 3.65 (dd, J = 10.0, 7.7 Hz, 1H, CH-17), 3.65 (dd, J = 9.2, 7.7 Hz, 1H, CH₂-16a), 3.63 (dd, J = 10.9, 8.1 Hz, 1H, CH₂-13a), 3.45 (d, J = 12.3 Hz, 1H, CH₂-24b), 3.29 (dd, J = 13.6, 11.0 Hz, 1H, CH₂-13b), 3.22 (dd, J = 11.8, 9.2 Hz, 1H, CH₂-16b), 3.19 (ddd, J = 14.3, 11.0, 5.4 Hz, 1H, CH₂-7a), 2.95 (ddd, J = 14.3, 10.9, 5.4 Hz, 1H, CH₂-7b), 2.55 (s, 3H, CH₃-18), 2.24 (m, 2H, CH₂-10), 2.23 (m, 1H, CH-28), 1.81 (m, 1H, CH₂-8a), 1.73 (m, 1H, CH₂-8b), 1.67 (s, 3H, CH₃-26), 1.63 (m, 2H, CH₂-9), 1.58 ppm (s, 3H, CH₃-21), 1.37 (s, 3H, CH₃-22);

¹³C NMR (150 MHz, methanol-d_4, 300 K): δ = 194.8 (C-23), 179.6 (C-12), 178.7 (C-27), 168.2 (C-1), 146.6 (C-3), 135.9 (C-5), 122.0 (C-6), 121.6 (C-4), 117.2 (C-2), 85.0 (C-11), 82.0 (C-15), 81.3 (C-19), 75.8 (C-17), 73.3 (C-14), 69.7 (C-28), 48.6 (C-18), 46.6 (C-20), 40.6 (C-16), 39.6 (C-24), 36.8 (C-7), 34.7 (C-13), 32.8 (C-8), 29.8 (C-9), 29.2 (C-21), 24.2 (C-26), 24.2 (C-22), 18.8 ppm (CH₂-10);

HRMS (ESI): m/z calcd for $C_{28}H_{35}N_3O_4S_3Ga^+$: 642.1040 $[M+H]^+$; found: 642.1049.
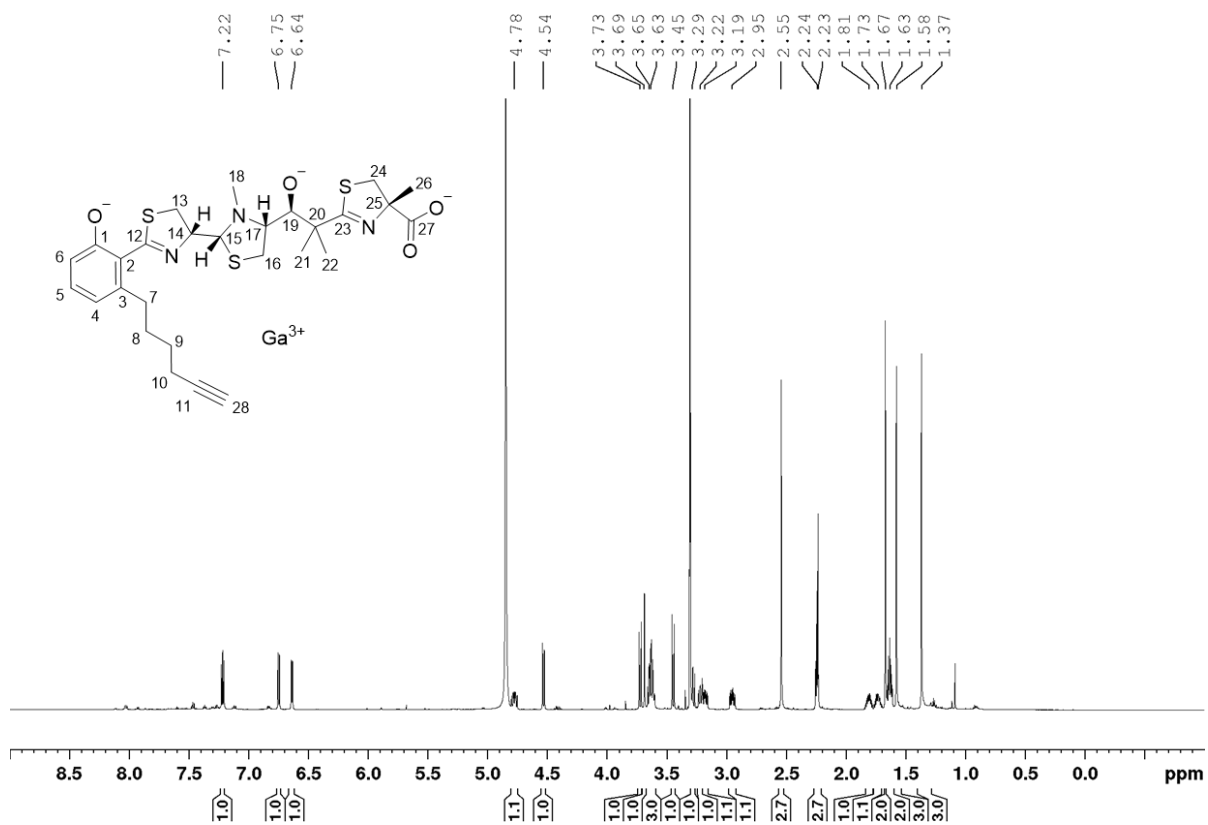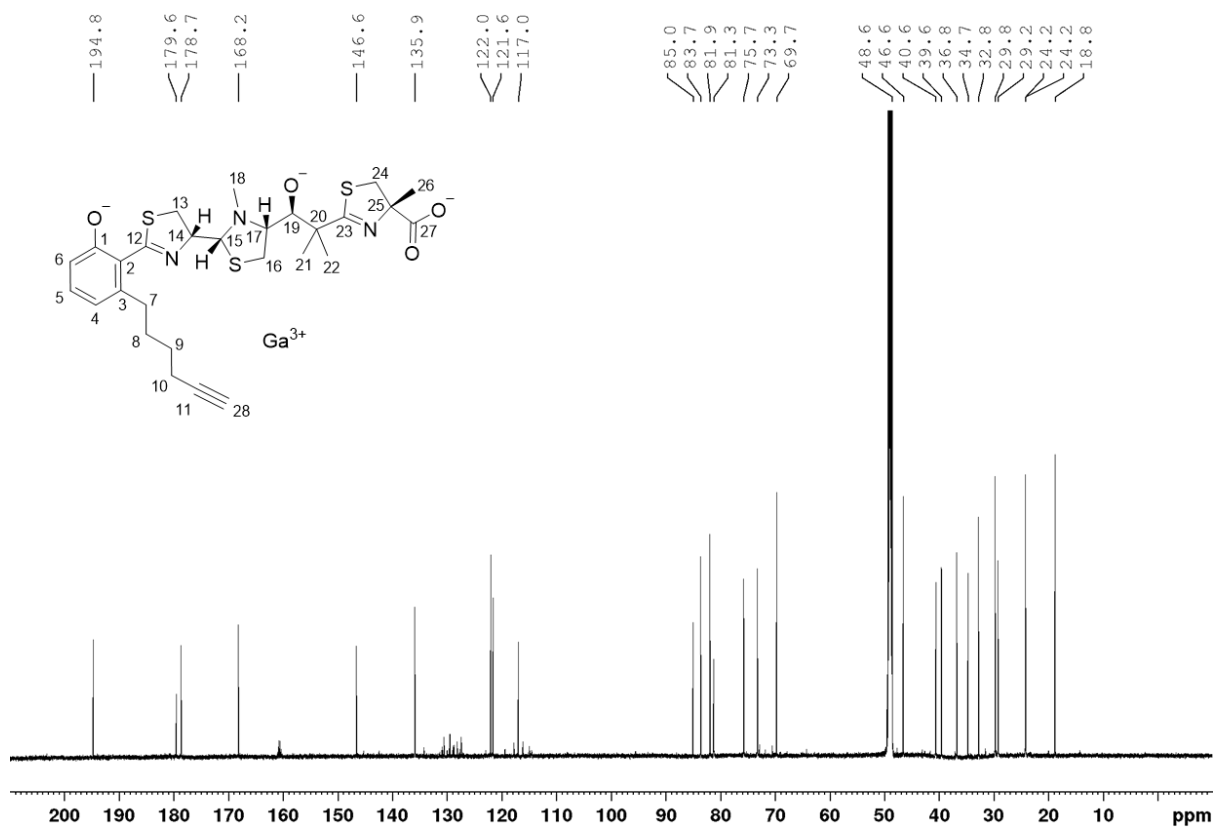
Figure S65 ^{1}H NMR spectrum (600 MHz, CD$_3$OD) of 5-hexynoic micacocidin Ga^{3+} complex.

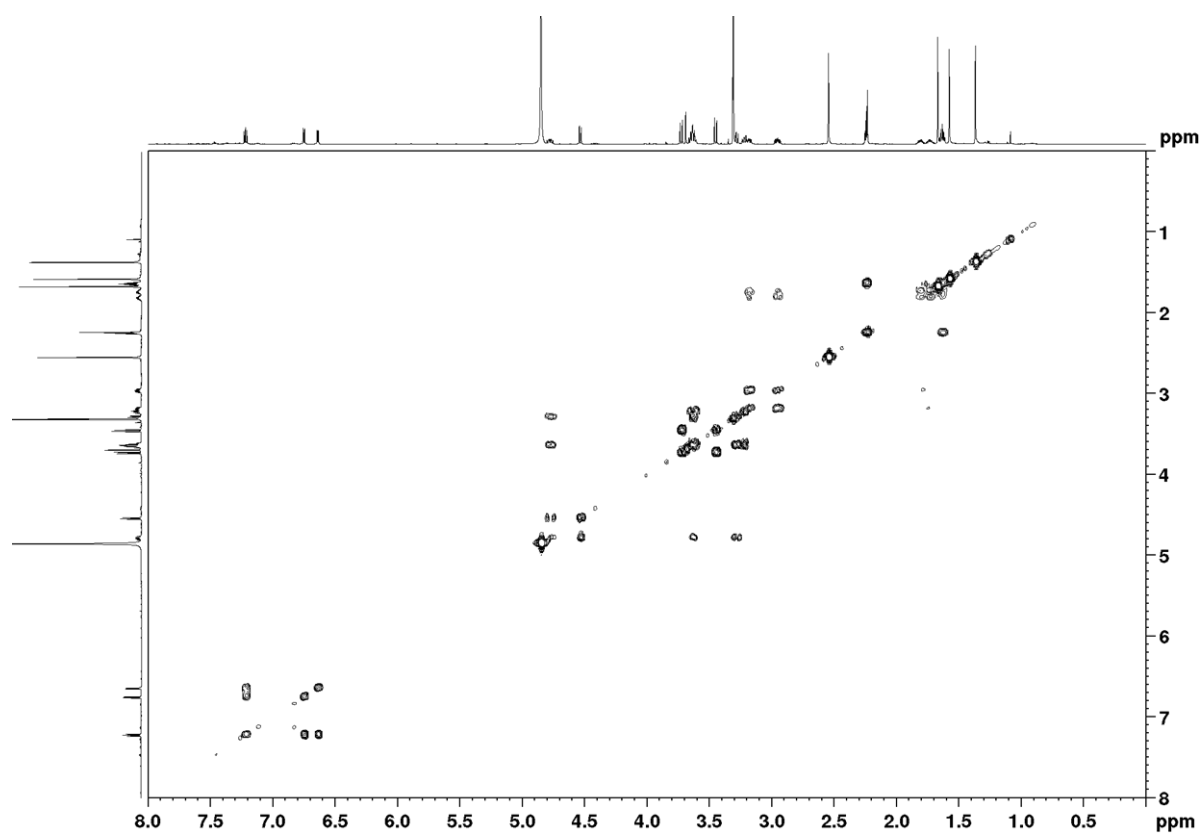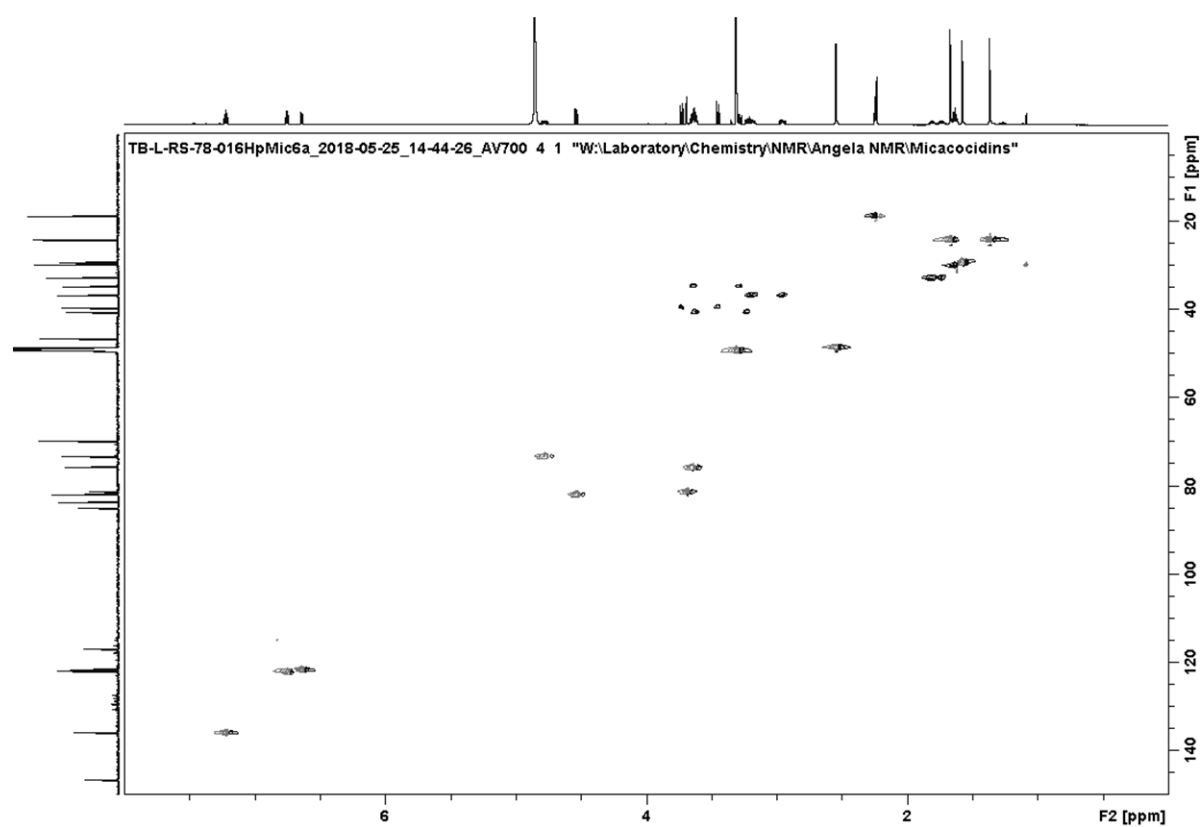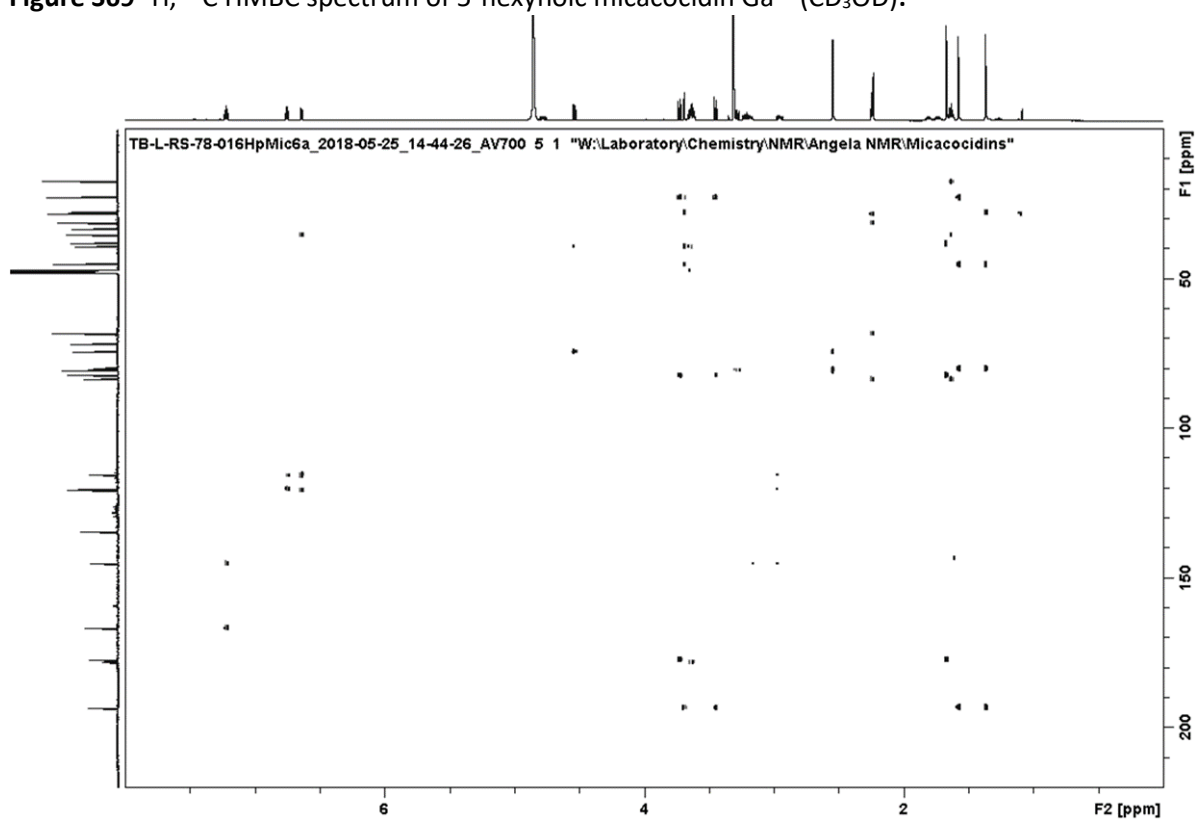**Figure S66** ^{1}H-decoupled ^{13}C NMR spectrum (150 MHz, CD$_3$OD) of 5-hexynoic micacocidin Ga^{3+} complex.

Figure S67 ^{1}H, ^{1}H COSY spectrum of 5-hexynoic micacocidin Ga^{3+} (CD$_3$OD).

Figure S68 ^{1}H, ^{13}C HSQC spectrum of 5-hexynoic micacocidin Ga^{3+} (CD$_3$OD).

Figure S69 ^{1}H, ^{13}C HMBC spectrum of 5-hexynoic micacocidin Ga^{3+} (CD$_3$OD).

6   References

(1)   Veith, I. Analysis of the Huang Ti Nei Ching Su Wên. In *The Yellow Emperor's Classic of Internal Medicine*; Nei, H. T., Wen, C. S., Eds.; University of California Press: Oakland, CA, 1975; pp 1–76. https://doi.org/10.1525/j.ctv1wxs1d.

(2)   Reißenweber, H. Japanische Medizin. In *Enzyklopädie Medizingeschichte*; Gerabek, W. E., Haage, B. D., Keil, G., Wegner, W., Eds.; De Gruyter: Berlin, Boston, 2007; pp 688–694. https://doi.org/10.1515/9783110976946.

(3)   Böck, B. Sourcing, Organizing, and Administering Medicinal Ingredients. In *The Oxford Handbook of Cuneiform Culture*; Radner, K., Robson, E., Eds.; Oxford University Press: Oxford, UK, 2011; pp 690–705. https://doi.org/10.1093/oxfordhb/9780199557301.001.0001.

(4)   Joachim, H. *Papyros Ebers.*, 2nd ed.; Walter de Gruyter & Co.: Berlin, 1973.

(5)   Franke, H.; Scholl, R.; Aigner, A. Ricin and Ricinus Communis in Pharmacology and Toxicology-from Ancient Use and "Papyrus Ebers" to Modern Perspectives and "Poisonous Plant of the Year 2018." *Naunyn. Schmiedebergs. Arch. Pharmacol.* **2019**, *392* (10), 1181–1208. https://doi.org/10.1007/s00210-019-01691-6.

(6)   Sertürner, F. W. III. Säure Im Opium. *J. der Pharm. für Ärzte und Apotheker* **1805**, *13*, 234–241.

(7)   Sertürner, F. W. Ueber Das Morphium, Eine Neue Salzfähige Grundlage, Und Die Mekonsäure, Als Hauptbestandtheile Des Opiums. *Ann. Phys.* **1817**, *55* (1), 56–89. https://doi.org/10.1002/andp.18170550104.

(8)   Friedrich, C. Von Der Pflanzlichen Droge Zum Arzneistoff. *Zeitschrift für Phyther.* **2005**, *26* (3), 106–112. https://doi.org/10.1055/s-2005-872302.

(9)   Geiger, P. L.; Hesse, L. Fortgesetzte Versuche Über Atropin. *Ann. der Pharm.* **1833**, *6* (1), 44–65.

References

(10) Lee, M. The History of *Ephedra* (Ma-Huang). *J. R. Coll. Physicians Edinb.* **2011**, *41* (1), 78–84. https://doi.org/10.4997/JRCPE.2011.116.

(11) Friedrich, C. On the History of Antirheumatic Drugs. *Pharmakon* **2016**, *4* (5), 408–415. https://doi.org/https://doi.org/10.1691/pn.20160046.

(12) Fleming, A. On the Antibacterial Action of Cultures of a *Penicillium*, with Special Reference to Teir Use in the Isolation of *B. Influenzae*. *Br. J. Exp. Pathol.* **1929**, *10* (3), 226–236.

(13) Helmstädter, A. Zufall Und Strategie – Zur Entwicklungsgeschichte Der Antibiotika Fortune and Strategy – the Development of Antibiotics. *Pharmakon* **2020**, *8* (4), 217–224. https://doi.org/10.1691/pn.20200020.

(14) Sanger, F.; Air, G. M.; Barrell, B. G.; Brown, N. L.; Coulson, A. R.; Fiddes, J. C.; Hutchison, C. A.; Slocombe, P. M.; Smith, M. Nucleotide Sequence of Bacteriophage Φx174 DNA. *Nature* **1977**, *265* (5596), 687–695. https://doi.org/10.1038/265687a0.

(15) Freeman, M. F.; Gurgui, C.; Helf, M. J.; Morinaka, B. I.; Uria, A. R.; Oldham, N. J.; Sahl, H.-G.; Matsunaga, S.; Piel, J. Metagenome Mining Reveals Polytheonamides as Posttranslationally Modified Ribosomal Peptides. *Science (80-.).* **2012**, *338* (6105), 387–390. https://doi.org/10.1126/science.1226121.

(16) Imanaka, H.; Kousaka, M.; Tamura, G.; Arima, K. Studies on Pyrrolnitrin, a New Antibiotic. 3. Structure of Pyrrolnitrin. *J. Antibiot. (Tokyo).* **1965**, *18* (5), 207–210.

(17) Gerth, K.; Steinmetz, H.; Höfle, G.; Jansen, R. Chlorotonil A, a Macrolide with a Unique *Gem*-Dichloro-1,3-Dione Functionality from *Sorangium Cellulosum*, So ce1525. *Angew. Chemie - Int. Ed.* **2008**, *47* (3), 600–602. https://doi.org/10.1002/anie.200703993.

(18) Herrmann, M.; Böhlendorf, B.; Irschik, H.; Reichenbach, H.; Höfle, G. Maracin and Maracen: New Types of Ethynyl Vinyl Ether And α-Chloro Divinyl Ether Antibiotics From *Sorangium Cellulosum* with Specific Activity Against Mycobacteria. *Angew. Chemie Int. Ed.* **1998**, *37* (9), 1253–1255. https://doi.org/10.1002/(SICI)1521-3773(19980518)37:9<1253::AID-ANIE1253>3.0.CO;2-T.

(19)   Irschik, H.; Schummer, D.; Gerth, K.; Höfle, G.; Reichenbach, H. Antibiotics from Gliding Bacteria. No.60. The Tartrolons, New Boron-Containing Antibiotics from a Myxobacterium, *Sorangium Cellulosum*. *J. Antibiot. (Tokyo).* **1995**, *48* (1), 26–30. https://doi.org/10.7164/antibiotics.48.26.

(20)   Süssmuth, R. D.; Mainz, A. Nonribosomal Peptide Synthesis-Principles and Prospects. *Angew. Chemie Int. Ed.* **2017**, *56* (14), 3770–3821. https://doi.org/10.1002/anie.201609079.

(21)   Arnison, P. G.; Bibb, M. J.; Bierbaum, G.; Bowers, A. A.; Bugni, T. S.; Bulaj, G.; Camarero, J. A.; Campopiano, D. J.; Challis, G. L.; Clardy, J.; Cotter, P. D.; Craik, D. J.; Dawson, M.; Dittmann, E.; Donadio, S.; Dorrestein, P. C.; Entian, K.-D.; Fischbach, M. A.; Garavelli, J. S.; Göransson, U.; Gruber, C. W.; Haft, D. H.; Hemscheidt, T. K.; Hertweck, C.; Hill, C.; Horswill, A. R.; Jaspars, M.; Kelly, W. L.; Klinman, J. P.; Kuipers, O. P.; Link, A. J.; Liu, W.; Marahiel, M. A.; Mitchell, D. A.; Moll, G. N.; Moore, B. S.; Müller, R.; Nair, S. K.; Nes, I. F.; Norris, G. E.; Olivera, B. M.; Onaka, H.; Patchett, M. L.; Piel, J.; Reaney, M. J. T.; Rebuffat, S.; Ross, R. P.; Sahl, H.-G.; Schmidt, E. W.; Selsted, M. E.; Severinov, K.; Shen, B.; Sivonen, K.; Smith, L.; Stein, T.; Süssmuth, R. D.; Tagg, J. R.; Tang, G.-L.; Truman, A. W.; Vederas, J. C.; Walsh, C. T.; Walton, J. D.; Wenzel, S. C.; Willey, J. M.; van der Donk, W. A. Ribosomally Synthesized and Post-Translationally Modified Peptide Natural Products: Overview and Recommendations for a Universal Nomenclature. *Nat. Prod. Rep.* **2013**, *30* (1), 108–160. https://doi.org/10.1039/C2NP20085F.

(22)   Dunbar, K. L.; Büttner, H.; Molloy, E. M.; Dell, M.; Kumpfmüller, J.; Hertweck, C. Genome Editing Reveals Novel Thiotemplated Assembly of Polythioamide Antibiotics in Anaerobic Bacteria. *Angew. Chemie Int. Ed.* **2018**, *57* (43), 14080–14084. https://doi.org/10.1002/anie.201807970.

(23)   Wenzel, S. C.; Meiser, P.; Binz, T. M.; Mahmud, T.; Müller, R. Nonribosomal Peptide Biosynthesis: Point Mutations and Module Skipping Lead to Chemical Diversity. *Angew. Chemie - Int. Ed.* **2006**, *45* (14), 2296–2301. https://doi.org/10.1002/anie.200503737.

(24)   Lee, M. D.; Dunne, T. S.; Siegel, M. M.; Chang, C. C.; Morton, G. O.; Borders, D. B. Calichemicins, a Novel Family of Antitumor Antibiotics. 1. Chemistry and Partial

Structure of Calichemicin Gamma1I. *J. Am. Chem. Soc.* **1987**, *109* (11), 3464–3466. https://doi.org/10.1021/ja00245a050.

(25)   Ueoka, R.; Bortfeld-Miller, M.; Morinaka, B. I.; Vorholt, J. A.; Piel, J. Toblerols: Cyclopropanol-Containing Polyketide Modulators of Antibiosis in Methylobacteria. *Angew. Chemie - Int. Ed.* **2018**, *57* (4), 977–981. https://doi.org/10.1002/anie.201709056.

(26)   Sheehan, J. C.; Henery-Logan, K. R. The Total Synthesis of Penicillin V. *J. Am. Chem. Soc.* **1959**, *81* (12), 3089–3094. https://doi.org/10.1021/ja01521a044.

(27)   Leimgruber, W.; Batcho, A. D.; Schenker, F. The Structure of Anthramycin. *Journal of the American Chemical Society*. American Chemical Society 1965, pp 5793–5795. https://doi.org/10.1021/ja00952a051.

(28)   Kingston, D. Recent Advances in the Chemistry of Taxol1,2. *J. Nat. Prod.* **2000**, *63* (5), 726–734. https://doi.org/10.1021/np000064n.

(29)   Harris, D. R.; McGeachin, S. G.; Mills, H. H. The Structure and Stereochemistry of Erythromycin A. *Tetrahedron Lett.* **1965**, *6* (11), 679–685. https://doi.org/10.1016/S0040-4039(00)90018-2.

(30)   Arcamone, F.; Cassinelli, G.; Fantini, G.; Grein, A.; Orezzi, P.; Pol, C.; Spalla, C. Adriamycin, 14-Hydroxydaunomycin, a New Antitumor Antibiotic from *S. Peucetius Var. Caesius*. *Biotechnol. Bioeng.* **1969**, *11* (6), 1101–1110. https://doi.org/10.1002/bit.260110607.

(31)   Helynck, G.; Dubertret, C.; Frechet, D.; Leboul, J. Isolation of RP 66453, a New Secondary Peptide Metabolite from *Streptomyces* Sp. Useful as a Lead for Neurotensin Antagonists. *J. Antibiot. (Tokyo).* **1998**, *51* (5), 512–514. https://doi.org/10.7164/antibiotics.51.512.

(32)   Barna, J. C. J.; Williams, D. H. The Structure and Mode of Action of Glycopeptide Antibiotics of the Vancomycin Group. *Annu. Rev. Microbiol.* **1984**, *38* (1), 339–357. https://doi.org/10.1146/annurev.mi.38.100184.002011.

(33) Duquesne, S.; Destoumieux-Garzón, D.; Peduzzi, J.; Rebuffat, S. Microcins, Gene-Encoded Antibacterial Peptides from Enterobacteria. *Natural Product Reports*. The Royal Society of Chemistry July 25, 2007, pp 708–734. https://doi.org/10.1039/b516237h.

(34) Bringmann, G.; Lombe, B. K.; Steinert, C.; Ioset, K. N.; Brun, R.; Turini, F.; Heubl, G.; Mudogo, V. Mbandakamines A and B, Unsymmetrically Coupled Dimeric Naphthylisoquinoline Alkaloids, from a Congolese *Ancistrocladus* Species. *Org. Lett.* **2013**, *15* (11), 2590–2593. https://doi.org/10.1021/ol4005883.

(35) Kurth, C.; Schieferdecker, S.; Athanasopoulou, K.; Seccareccia, I.; Nett, M. Variochelins, Lipopeptide Siderophores from Variovorax Boronicumulans Discovered by Genome Mining. *J. Nat. Prod.* **2016**, *79* (4), 865–872. https://doi.org/10.1021/acs.jnatprod.5b00932.

(36) Schieferdecker, S.; König, S.; Weigel, C.; Dahse, H.-M. M.; Werz, O.; Nett, M. Structure and Biosynthetic Assembly of Gulmirecins, Macrolide Antibiotics from the Predatory Bacterium *Pyxidicoccus Fallax*. *Chem. - A Eur. J.* **2014**, *20* (48), 15933–15940. https://doi.org/10.1002/chem.201404291.

(37) Newman, D. J.; Cragg, G. M. Natural Products as Sources of New Drugs over the Nearly Four Decades from 01/1981 to 09/2019. *J. Nat. Prod.* **2020**, *83* (3), 770–803. https://doi.org/10.1021/acs.jnatprod.9b01285.

(38) Cragg, G. M.; Newman, D. J. Natural Products: A Continuing Source of Novel Drug Leads. *Biochim. Biophys. Acta - Gen. Subj.* **2013**, *1830* (6), 3670–3695. https://doi.org/10.1016/j.bbagen.2013.02.008.

(39) Dewick, P. M. *Medicinal Natural Products*, 3rd ed.; John Wiley & Sons, Ltd: Chichester, UK, 2009. https://doi.org/10.1002/9780470742761.

(40) Kull, D. R.; Pfander, H. Isolation and Structure Elucidation of Carotenoid Glycosides from the Thermoacidophilic Archaea *Sulfolobus Shibatae*. *J. Nat. Prod.* **1997**, *60* (4), 371–374. https://doi.org/10.1021/np960584b.

References

(41)   Xiao, Y.; Gerth, K.; Müller, R.; Wall, D. Myxobacterium-Produced Antibiotic TA (Myxovirescin) Inhibits Type II Signal Peptidase. *Antimicrob. Agents Chemother.* **2012**, *56* (4), 2014–2021. https://doi.org/10.1128/AAC.06148-11.

(42)   Kaiser, D. Signaling in Myxobacteria. *Annu. Rev. Microbiol.* **2004**, *58* (1), 75–98. https://doi.org/10.1146/annurev.micro.58.030603.123620.

(43)   Milagres, A. M. F.; Machuca, A.; Napoleão, D. Detection of Siderophore Production from Several Fungi and Bacteria by a Modification of Chrome Azurol S (CAS) Agar Plate Assay. *J. Microbiol. Methods* **1999**, *37* (1), 1–6. https://doi.org/10.1016/S0167-7012(99)00028-7.

(44)   Timmermans, M. L.; Paudel, Y. P.; Ross, A. C. Investigating the Biosynthesis of Natural Products from Marine Proteobacteria: A Survey of Molecules and Strategies. *Marine Drugs*. MDPI AG August 1, 2017, p 235. https://doi.org/10.3390/md15080235.

(45)   Firn, R. D.; Jones, C. G. Natural Products - a Simple Model to Explain Chemical Diversity. *Nat. Prod. Rep.* **2003**, *20* (4), 382–391. https://doi.org/10.1039/b208815k.

(46)   Shen, B. A New Golden Age of Natural Products Drug Discovery. *Cell*. Cell Press December 3, 2015, pp 1297–1300. https://doi.org/10.1016/j.cell.2015.11.031.

(47)   Krug, D.; Zurek, G.; Revermann, O.; Vos, M.; Velicer, G. J.; Muller, R. Discovering the Hidden Secondary Metabolome of *Myxococcus Xanthus*: A Study of Intraspecific Diversity. *Appl. Environ. Microbiol.* **2008**, *74* (10), 3058–3068. https://doi.org/10.1128/AEM.02863-07.

(48)   Hug, J. J.; Dastbaz, J.; Adam, S.; Revermann, O.; Koehnke, J.; Krug, D.; Müller, R. Biosynthesis of Cittilins, Unusual Ribosomally Synthesized and Post-Translationally Modified Peptides from *Myxococcus Xanthus*. *ACS Chem. Biol.* **2020**, *15* (8), 2221–2231. https://doi.org/10.1021/acschembio.0c00430.

(49)   Sester, A.; Korp, J.; Nett, M. Secondary Metabolism of Predatory Bacteria. In *The Ecology of Predation at the Microscale*; Jurkevitch, E., Mitchell, R. J., Eds.; Springer International Publishing, 2020.

(50)   Weissman, K. J. The Structural Biology of Biosynthetic Megaenzymes. *Nat. Chem. Biol.* **2015**, *11* (9), 660–670. https://doi.org/10.1038/nchembio.1883.

(51)   Nett, M. Genome Mining: Concept and Strategies for Natural Product Discovery. In *Progress in the Chemistry of Organic Natural Products*; Kinghorn, A. D., Falk, H., Kobayashi, J., Eds.; Progress in the Chemistry of Organic Natural Products; Springer International Publishing: Cham, 2014; Vol. 99, pp 199–245. https://doi.org/10.1007/978-3-319-04900-7_4.

(52)   Bonner, D. P.; O'Sullivan, J.; Tanaka, S. K.; Clark, J. M.; Whitney, R. R. Lysobactin, a Novel Antibacterial Agent Produced by *Lysobacter* Sp. II. Biological Properties. *J. Antibiot. (Tokyo).* **1988**, *41* (12), 1745–1751. https://doi.org/10.7164/antibiotics.41.1745.

(53)   O'Sullivan, J.; McCullough, J. E.; Tymiak, A. A.; Kirsch, D. R.; Trejo, W. H.; Principe, P. A. . Lysobactin, a Novel Antibacterial Agent Produced by *Lysobacter* Sp. I. Taxonomy, Isolation and Partial Characterization. *J. Antibiot. (Tokyo).* **1988**, *41* (12), 1740–1744. https://doi.org/10.7164/antibiotics.41.1740.

(54)   Hou, J.; Robbel, L.; Marahiel, M. A. Identification and Characterization of the Lysobactin Biosynthetic Gene Cluster Reveals Mechanistic Insights into an Unusual Termination Module Architecture. *Chem. Biol.* **2011**, *18* (5), 655–664. https://doi.org/10.1016/j.chembiol.2011.02.012.

(55)   Balibar, C. J.; Vaillancourt, F. H.; Walsh, C. T. Generation of D Amino Acid Residues in Assembly of Arthrofactin by Dual Condensation/Epimerization Domains. *Chem. Biol.* **2005**, *12* (11), 1189–1200. https://doi.org/10.1016/j.chembiol.2005.08.010.

(56)   Hertweck, C. Decoding and Reprogramming Complex Polyketide Assembly Lines: Prospects for Synthetic Biology. *Trends Biochem. Sci.* **2015**, *40* (4), 189–199. https://doi.org/10.1016/j.tibs.2015.02.001.

(57)   Surup, F.; Viehrig, K.; Mohr, K. I.; Herrmann, J.; Jansen, R.; Müller, R. Disciformycins A and B: 12-Membered Macrolide Glycoside Antibiotics from the Myxobacterium *Pyxidicoccus Fallax* Active against Multiresistant *Staphylococci*. *Angew. Chemie - Int. Ed.* **2014**, *53* (49), 13588–13591. https://doi.org/10.1002/anie.201406973.

References

(58)   Nett, M.; Erol, Ö.; Kehraus, S.; Köck, M.; Krick, A.; Eguereva, E.; Neu, E.; König, G. M. Siphonazole, an Unusual Metabolite from *Herpetosiphon* Sp. *Angew. Chemie - Int. Ed.* **2006**, *45* (23), 3863–3867. https://doi.org/10.1002/anie.200504525.

(59)   Schieferdecker, S.; Domin, N.; Hoffmeier, C.; Bryant, D. A.; Roth, M.; Nett, M. Structure and Absolute Configuration of Auriculamide, a Natural Product from the Predatory Bacterium *Herpetosiphon Aurantiacus*. *European J. Org. Chem.* **2015**, *2015* (14), 3057–3062. https://doi.org/10.1002/ejoc.201500181.

(60)   Mir Mohseni, M.; Höver, T.; Barra, L.; Kaiser, M.; Dorrestein, P. C.; Dickschat, J. S.; Schäberle, T. F. Discovery of a Mosaic-Like Biosynthetic Assembly Line with a Decarboxylative Off-Loading Mechanism through a Combination of Genome Mining and Imaging. *Angew. Chemie - Int. Ed.* **2016**, *55* (43), 13611–13614. https://doi.org/10.1002/anie.201606655.

(61)   Braga, D.; Hoffmeister, D.; Nett, M. A Non-Canonical Peptide Synthetase Adenylates 3-Methyl-2-Oxovaleric Acid for Auriculamide Biosynthesis. *Beilstein J. Org. Chem.* **2016**, *12* (1), 2766–2770. https://doi.org/10.3762/bjoc.12.274.

(62)   Korp, J.; Winand, L.; Sester, A.; Nett, M. Engineering Pseudochelin Production in *Myxococcus Xanthus*. *Appl. Environ. Microbiol.* **2018**, *84* (22), e01789-18. https://doi.org/10.1128/AEM.01789-18.

(63)   Silakowski, B.; Kunze, B.; Nordsiek, G.; Blöcker, H.; Höfle, G.; Müller, R. The Myxochelin Iron Transport Regulon of the Myxobacterium *Stigmatella Aurantiaca* Sg A15. *Eur. J. Biochem.* **2000**, *267* (21), 6476–6485. https://doi.org/10.1046/j.1432-1327.2000.01740.x.

(64)   Gaitatzis, N.; Kunze, B.; Müller, R. In Vitro Reconstitution of the Myxochelin Biosynthetic Machinery of *Stigmatella Aurantiaca* Sg A15: Biochemical Characterization of a Reductive Release Mechanism from Nonribosomal Peptide Synthetases. *Proc. Natl. Acad. Sci. U. S. A.* **2001**, *98* (20), 11136–11141. https://doi.org/10.1073/pnas.201167098.

(65)   Schieferdecker, S.; König, S.; Koeberle, A.; Dahse, H.-M.; Werz, O.; Nett, M. Myxochelins

Target Human 5-Lipoxygenase. *J. Nat. Prod.* **2015**, *78*, 335–338. https://doi.org/10.1021/np500909b.

(66)   Sonnenschein, E. C.; Stierhof, M.; Goralczyk, S.; Vabre, F. M.; Pellissier, L.; Hanssen, K. Ø.; de la Cruz, M.; Díaz, C.; de Witte, P.; Copmans, D.; Andersen, J. H.; Hansen, E.; Kristoffersen, V.; Tormo, J. R.; Ebel, R.; Milne, B. F.; Deng, H.; Gram, L.; Jaspars, M.; Tabudravu, J. N. Pseudochelin A, a Siderophore of *Pseudoalteromonas Piscicida* S2040. *Tetrahedron* **2017**, *73* (18), 2633–2637. https://doi.org/10.1016/j.tet.2017.03.051.

(67)   Nadmid, S.; Plaza, A.; Lauro, G.; Garcia, R.; Bifulco, G.; Müller, R. Hyalachelins A–C, Unusual Siderophores Isolated from the Terrestrial Myxobacterium *Hyalangium Minutum*. *Org. Lett.* **2014**, *16* (16), 4130–4133. https://doi.org/10.1021/ol501826a.

(68)   Li, Y.; Weissman, K. J.; Müller, R.; Müller, R. Myxochelin Biosynthesis: Direct Evidence for Two- and Four-Electron Reduction of a Carrier Protein-Bound Thioester. *J. Am. Chem. Soc.* **2008**, *130* (24), 7554–7555. https://doi.org/10.1021/ja8025278.

(69)   Miyanaga, S.; Obata, T.; Onaka, H.; Fujita, T.; Saito, N.; Sakurai, H.; Saiki, I.; Furumai, T.; Igarashi, Y. Absolute Configuration and Antitumor Activity of Myxochelin A Produced by *Nonomuraea Pusilla* TP-A0861. *J. Antibiot. (Tokyo).* **2006**, *59* (11), 698–703. https://doi.org/10.1038/ja.2006.93.

(70)   Rossi, A.; Pergola, C.; Koeberle, A.; Hoffmann, M.; Dehm, F.; Bramanti, P.; Cuzzocrea, S.; Werz, O.; Sautebin, L. The 5-Lipoxygenase Inhibitor, Zileuton, Suppresses Prostaglandin Biosynthesis by Inhibition of Arachidonic Acid Release in Macrophages. *Br. J. Pharmacol.* **2010**, *161* (3), 555–570. https://doi.org/10.1111/j.1476-5381.2010.00930.x.

(71)   Korp, J.; König, S.; Schieferdecker, S.; Dahse, H.-M. M.; König, G. M.; Werz, O.; Nett, M. Harnessing Enzymatic Promiscuity in Myxochelin Biosynthesis for the Production of 5-Lipoxygenase Inhibitors. *ChemBioChem* **2015**, *16* (17), 2445–2450. https://doi.org/10.1002/cbic.201500446.

(72)   Mulwa, L.; Stadler, M. Antiviral Compounds from Myxobacteria. *Microorganisms* **2018**, *6* (3), 73. https://doi.org/10.3390/microorganisms6030073.

(73)   Kunze, B.; Höfle, G.; Reichenbach, H. The Aurachins, New Quinoline Antibiotics from Myxobacteria: Production, Physico-Chemical and Biological Properties. *J. Antibiot. (Tokyo).* **1987**, *40* (3), 258–265. https://doi.org/10.7164/antibiotics.40.258.

(74)   Höfle, G.; Irschik, H. Isolation and Biosynthesis of Aurachin P and 5-Nitroresorcinol from *Stigmatella Erecta*. *J. Nat. Prod.* **2008**, *71* (11), 1946–1948. https://doi.org/10.1021/np800325z.

(75)   Kitagawa, W.; Tamura, T. A Quinoline Antibiotic from *Rhodococcus Erythropolis* JCM 6824. *J. Antibiot. (Tokyo).* **2008**, *61* (11), 680–682. https://doi.org/10.1038/ja.2008.96.

(76)   Nachtigall, J.; Schneider, K.; Nicholson, G.; Goodfellow, M.; Zinecker, H.; Imhoff, J. F.; Süssmuth, R. D.; Fiedler, H.-P. Two New Aurachins from *Rhodococcus* Sp. Acta 2259. *J. Antibiot. (Tokyo).* **2010**, *63* (9), 567–569. https://doi.org/10.1038/ja.2010.79.

(77)   Zhang, M.; Yang, C. L.; Xiao, Y. S.; Zhang, B.; Deng, X. Z.; Yang, L.; Shi, J.; Wang, Y. S.; Li, W.; Jiao, R. H.; Tan, R. X.; Ge, H. M. Aurachin SS, a New Antibiotic from *Streptomyces* Sp. NA04227. *J. Antibiot. (Tokyo).* **2017**, *70* (7), 853–855. https://doi.org/10.1038/ja.2017.50.

(78)   Pistorius, D.; Li, Y.; Mann, S. S.; Müller, R.; Müller, R. Unprecedented Anthranilate Priming Involving Two Enzymes of the Acyl Adenylating Superfamily in Aurachin Biosynthesis. *J. Am. Chem. Soc.* **2011**, *133* (32), 12362–12365. https://doi.org/10.1021/ja203653w.

(79)   Jackson, D. R.; Tu, S. S.; Nguyen, M.; Barajas, J. F.; Schaub, A. J.; Krug, D.; Pistorius, D.; Luo, R.; Müller, R.; Tsai, S.-C. Structural Insights into Anthranilate Priming during Type II Polyketide Biosynthesis. *ACS Chem. Biol.* **2016**, *11* (1), 95–103. https://doi.org/10.1021/acschembio.5b00500.

(80)   Höfle, G.; Kunze, B. Biosynthesis of Aurachins A–L in *Stigmatella Aurantiaca*: A Feeding Study. *J. Nat. Prod.* **2008**, *71* (11), 1843–1849. https://doi.org/10.1021/np8003084.

(81)   Höfle, G.; Böhlendorf, B.; Fecker, T.; Sasse, F.; Kunze, B. Semisynthesis and Antiplasmodial Activity of the Quinoline Alkaloid Aurachin E. *J. Nat. Prod.* **2008**, *71* (11),

1967–1969. https://doi.org/10.1021/np8004612.

(82)   Stec, E.; Pistorius, D.; Müller, R.; Li, S.-M. AuaA, a Membrane-Bound Farnesyltransferase from *Stigmatella Aurantiaca*, Catalyzes the Prenylation of 2-Methyl-4-Hydroxyquinoline in the Biosynthesis of Aurachins. *ChemBioChem* **2011**, *12* (11), 1724–1730. https://doi.org/10.1002/cbic.201100188.

(83)   Pistorius, D.; Li, Y.; Sandmann, A.; Müller, R. Completing the Puzzle of Aurachin Biosynthesis in *Stigmatella Aurantiaca* Sg A15. *Mol. Biosyst.* **2011**, *7* (12), 3308–3315. https://doi.org/10.1039/c1mb05328k.

(84)   Katsuyama, Y.; Harmrolfs, K.; Pistorius, D.; Li, Y.; Müller, R. A Semipinacol Rearrangement Directed by an Enzymatic System Featuring Dual-Function FAD-Dependent Monooxygenase. *Angew. Chemie - Int. Ed.* **2012**, *51* (37), 9437–9440. https://doi.org/10.1002/anie.201204138.

(85)   Katsuyama, Y.; Li, X.-W.; Müller, R.; Nay, B. Chemically Unprecedented Biocatalytic (AuaG) Retro-[2,3]-Wittig Rearrangement: A New Insight into Aurachin B Biosynthesis. *ChemBioChem* **2014**, *15* (16), 2349–2352. https://doi.org/10.1002/cbic.201402373.

(86)   Sandmann, A.; Dickschat, J.; Jenke-Kodama, H.; Kunze, B.; Dittmann, E.; Müller, R. A Type II Polyketide Synthase from the Gram-Negative Bacterium *Stigmatella Aurantiaca* Is Involved in Aurachin Alkaloid Biosynthesis. *Angew. Chemie - Int. Ed.* **2007**, *46* (15), 2712–2716. https://doi.org/10.1002/anie.200603513.

(87)   Oettmeier, W.; Dostatni, R.; Majewski, C.; Höfle, G.; Fecker, T.; Kunze, B.; Reichenbach, H. The Aurachins, Naturally Occurring Inhibitors of Photosynthetic Electron Flow through Photosystem II and the Cytochrome B6/f-Complex. *Zeitschrift für Naturforsch. C* **1990**, *45* (5), 322–328. https://doi.org/10.1515/znc-1990-0503.

(88)   Friedrich, T.; Heek, P.; Leif, H.; Ohnishi, T.; Forche, E.; Kunze, B.; Jansen, R.; Trowitzsch-Kienast, W.; Hofle, G.; Reichenbach, H.; Weiss, H. Two Binding Sites of Inhibitors in NADH:Ubiquinone Oxidoreductase (Complex I). Relationship of One Site with the Ubiquinone-Binding Site of Bacterial Glucose:Ubiquinone Oxidoreductase. *Eur. J. Biochem.* **1994**, *219* (1–2), 691–698. https://doi.org/10.1111/j.1432-

1033.1994.tb19985.x.

(89)   Oettmeier, W.; Masson, K.; Soll, M.; Reil, E. Acridones and Quinolones as Inhibitors of Ubiquinone Functions in the Mitochondrial Respiratory Chain. *Biochem. Soc. Trans.* **1994**, *22* (1), 213–216. https://doi.org/10.1042/bst0220213.

(90)   Friedrich, T.; Ohnishi, T.; Forche, E.; Kunze, B.; Jansen, R.; Trowitzsch, W.; Höfle, G.; Reichenbach, H.; Weiss, H. Two Binding Sites for Naturally Occurring Inhibitors in Mitochondrial and Bacterial NADH: Ubiquinone Oxidoreductase (Complex I). *Biochem. Soc. Trans.* **1994**, *22* (1), 226–230. https://doi.org/10.1042/bst0220226.

(91)   Uhrig, J. F.; Jakobs, C. U.; Majewski, C.; Trebst, A. Molecular Characterization of Two Spontaneous Antimycin A Resistant Mutants of *Rhodospirillum Rubrum*. *Biochim. Biophys. Acta* **1994**, *1187*, 347–353. https://doi.org/10.1016/0005-2728(94)90008-6.

(92)   Meunier, B.; Madgwick, S. A.; Reil, E.; Oettmeier, W.; Rich, P. R. New Inhibitors of the Quinol Oxidation Sites of Bacterial Cytochromes Bo and Bd. *Biochemistry* **1995**, *34* (3), 1076–1083. https://doi.org/10.1021/bi00003a044.

(93)   Li, X.-W. W.; Herrmann, J.; Zang, Y.; Grellier, P.; Prado, S.; Müller, R.; Nay, B. Synthesis and Biological Activities of the Respirator Chain Inhibitor Aurachin D and New Ring versus Chain Analogues. *Beilstein J. Org. Chem.* **2013**, *9* (Figure 1), 1551–1558. https://doi.org/10.3762/bjoc.9.176.

(94)   Dejon, L.; Speicher, A. Synthesis of Aurachin D and Isoprenoid Analogues from the Myxobacterium *Stigmatella Aurantiaca*. *Tetrahedron Lett.* **2013**, *54* (49), 6700–6702. https://doi.org/10.1016/J.TETLET.2013.09.085.

(95)   Thaxter, R. On the Myxobacteriaceae, a New Order of Schizomycetes. *Bot. Gaz.* **1892**, *17* (12), 389–406. https://doi.org/10.1086/326866.

(96)   Dworkin, M. Research on the Myxobacteria: Past, Present, Future. In *Myxobacteria, Development and Cell Interactions*; Rosenberg, E., Ed.; Springer-Verlag: New York, NY, 1984; pp 221–243.

(97)   Singh, B. N. Myxobacteria in Soils and Composts; Their Distribution, Number and Lytic

lxxviii

Action on Bacteria. *J. Gen. Microbiol.* **1947**, *1* (1), 1–10. https://doi.org/10.1099/00221287-1-1-1.

(98) Dávila-Céspedes, A.; Hufendiek, P.; Crüsemann, M.; Schäberle, T. F.; König, G. M. Marine-Derived Myxobacteria of the Suborder Nannocystineae: An Underexplored Source of Structurally Intriguing and Biologically Active Metabolites. *Beilstein J. Org. Chem.* **2016**, *12* (1), 969–984. https://doi.org/10.3762/bjoc.12.96.

(99) Berleman, J.; Keane, R. The Predatory Life Cycle of *Myxococcus Xanthus*. *Microbiology* **2016**, *162* (1), 1–11. https://doi.org/10.1099/mic.0.000208.

(100) Rosenberg, E.; Keller, K. H.; Dworkin, M. Cell Density Dependent Growth of *Myxococcus Xanthus* on Casein. *J. Bacteriol.* **1977**, *129* (2), 770–777. https://doi.org/10.1128/jb.129.2.770-777.1977.

(101) Berleman, J. E.; Kirby, J. R. Deciphering the Hunting Strategy of a Bacterial Wolfpack. *FEMS Microbiol. Rev.* **2009**, *33* (5), 942–957. https://doi.org/10.1111/j.1574-6976.2009.00185.x.

(102) Rosenberg, E.; Varon, M. Antibiotics and Lytic Enzymes. In *Myxobacteria, Development and Cell Interactions*; Rosenberg, E., Ed.; Springer-Verlag: New York, NY, 1984; pp 109–125.

(103) Rosenberg, E.; Vaks, B.; Zuckerberg, A. Bactericidal Action of an Antibiotic Produced by *Myxococcus Xanthus*. *Antimicrob. Agents Chemother.* **1973**, *4* (5), 507–513. https://doi.org/10.1128/AAC.4.5.507.

(104) Rosenberg, E.; Fytlovitch, S.; Carmeli, S.; Kashman, Y. Chemical Properties of *Myxococcus Xanthus* Antibiotic TA. *J. Antibiot. (Tokyo).* **1982**, *35* (7), 788–793. https://doi.org/10.7164/antibiotics.35.788.

(105) Trowitzsch, W.; Wray, V.; Gerth, K.; Höfle, G. Structure of Myxovirescin {A}, a New Macrocylic Antibiotic from Gliding Bacteria. *J. Chem. Soc., Chem. Commun.* **1982**, No. 23, 1340–1342. https://doi.org/10.1039/C39820001340.

(106) Reichenbach, H.; Höfle, G. Biologically Active Secondary Metabolites from

Myxobacteria. *Biotechnol. Adv.* **1993**, *11* (2), 219–277. https://doi.org/10.1016/0734-9750(93)90042-L.

(107) Nett, M.; König, G. M. The Chemistry of Gliding Bacteria. *Nat. Prod. Rep.* **2007**, *24* (6), 1245–1261. https://doi.org/10.1039/b612668p.

(108) Herrmann, J.; Fayad, A. A.; Müller, R. Natural Products from Myxobacteria: Novel Metabolites and Bioactivities. *Nat. Prod. Rep.* **2017**, *34* (2), 135–160. https://doi.org/10.1039/C6NP00106H.

(109) Bérdy, J. Thoughts and Facts about Antibiotics: Where We Are Now and Where We Are Heading. *Journal of Antibiotics*. Nature Publishing Group April 18, 2012, pp 385–395. https://doi.org/10.1038/ja.2012.27.

(110) Weissman, K. J.; Müller, R. Myxobacterial Secondary Metabolites: Bioactivities and Modes-of-Action. *Nat. Prod. Rep.* **2010**, *27* (9), 1276. https://doi.org/10.1039/c001260m.

(111) Dickschat, J. S.; Bode, H. B.; Mahmud, T.; Müller, R.; Schulz, S. A Novel Type of Geosmin Biosynthesis in Myxobacteria. *J. Org. Chem.* **2005**, *70* (13), 5174–5182. https://doi.org/10.1021/jo050449g.

(112) Li, X.; Zee, O. P.; Shin, H. J.; Seo, Y.; Ahn, J.-W. *Soraphinol A, a New Indole Alkaloid from Sorangium Cellulosum*; 2007; Vol. 28.

(113) Sasse, F.; Leibold, T.; Kunze, B.; Höfle, G.; Reichenbach, H. Cyrmenins, New Beta-Methoxyacrylate Inhibitors of the Electron Transport. Production, Isolation, Physico-Chemical and Biological Properties. *J. Antibiot. (Tokyo).* **2003**, *56* (10), 827–831. https://doi.org/10.7164/antibiotics.56.827.

(114) Troxitzsch-Kienast W, Wray V, Gerth K, Reichenbach H, Höfle G. Antibiotika Aus Gleitenden Bakterien, XXVIII 1) Biosynthese Des Myxothiazols in *Myxococcus Fulvus* Mx F16. *Liebigs Ann. der Chemie* **1986**, *1986* (1), 93–98. https://doi.org/10.1002/jlac.198619860109.

(115) Bode, H. B.; Zeggel, B.; Silakowski, B.; Wenzel, S. C.; Reichenbach, H.; Müller, R. Steroid

lxxx

Biosynthesis in Prokaryotes: Identification of Myxobacterial Steroids and Cloning of the First Bacterial 2,3(S)-Oxidosqualene Cyclase from the Myxobacterium *Stigmatella Aurantiaca*. *Mol. Microbiol.* **2003**, *47* (2), 471–481. https://doi.org/10.1046/j.1365-2958.2003.03309.x.

(116) Bode, H. B.; Müller, R. Secondary Metabolism in Myxobacteria. In *Myxobacteria: Multicellularity and Differentiation*; Whitworth, D. E., Ed.; ASM Press: Washington, DC, 2008; pp 259–282.

(117) Bode, H. B.; Müller, R. Analysis of Myxobacterial Secondary Metabolism Goes Molecular. In *Journal of Industrial Microbiology and Biotechnology*; Springer, 2006; Vol. 33, pp 577–588. https://doi.org/10.1007/s10295-006-0082-7.

(118) Ziemert, N.; Alanjary, M.; Weber, T. The Evolution of Genome Mining in Microbes - a Review. *Natural Product Reports*. Royal Society of Chemistry August 1, 2016, pp 988–1005. https://doi.org/10.1039/c6np00025h.

(119) Schupp, T.; Toupet, C.; Cluzel, B.; Neff, S.; Hill, S.; Beck, J. J.; Ligon, J. M. A. *Sorangium Cellulosum* (Myxobacterium) Gene Cluster for the Biosynthesis of the Macrolide Antibiotic Soraphen A: Cloning, Characterization, and Homology to Polyketide Synthase Genes from Actinomycetes. *J. Bacteriol.* **1995**, *177* (13), 3673–3679. https://doi.org/10.1128/jb.177.13.3673-3679.1995.

(120) Pospiech, A.; Cluzel, B.; Bietenhader, J.; Schupp, T. A. New *Myxococcus Xanthus* Gene Cluster for the Biosynthesis of the Antibiotic Saframycin Mx1 Encoding a Peptide Synthetase. *Microbiology* **1995**, *141* (8), 1793–1803. https://doi.org/10.1099/13500872-141-8-1793.

(121) Pospiech, A.; Bietenhader, J.; Schupp, T. Two Multifunctional Peptide Synthetases and an O-Methyltransferase Are Involved in the Biosynthesis of the DNA-Binding Antibiotic and Antitumour Agent Saframycin Mx1 from *Myxococcus Xanthus*. *Microbiology* **1996**, *142* (4), 741–746. https://doi.org/10.1099/00221287-142-4-741.

(122) Ligon, J.; Hill, S.; Beck, J.; Zirkle, R.; Molnár, I.; Zawodny, J.; Money, S.; Schupp, T. Characterization of the Biosynthetic Gene Cluster for the Antifungal Polyketide

Soraphen A from *Sorangium Cellulosum* So Ce26. *Gene* **2002**, *285* (1–2), 257–267. https://doi.org/10.1016/S0378-1119(02)00396-7.

(123) Huntley, S.; Wuichet, K.; Søgaard-Andersen, L. Genome Evolution and Content in the Myxobacteria. In *Myxobacteria Genomics, Cellular and Molecular Biology*; Yang, Z., Higgs, P. I., Eds.; Caister Academic Press: Norfolk, UK, 2014; pp 31–50.

(124) Thomas, S. H.; Wagner, R. D.; Arakaki, A. K.; Skolnick, J.; Kirby, J. R.; Shimkets, L. J.; Sanford, R. A.; Löffler, F. E. The Mosaic Genome of *Anaeromyxobacter Dehalogenans* Strain 2CP-C Suggests an Aerobic Common Ancestor to the Delta-Proteobacteria. *PLoS One* **2008**, *3* (5), e2103. https://doi.org/10.1371/journal.pone.0002103.

(125) Goldman, B. S.; Nierman, W. C.; Kaiser, D.; Slater, S. C.; Durkin, A. S.; Eisen, J.; Ronning, C. M.; Barbazuk, W. B.; Blanchard, M.; Field, C.; Halling, C.; Hinkle, G.; Iartchuk, O.; Kim, H. S.; Mackenzie, C.; Madupu, R.; Miller, N.; Shvartsbeyn, A.; Sullivan, S. A.; Vaudin, M.; Wiegand, R.; Kaplan, H. B. Evolution of Sensory Complexity Recorded in a Myxobacterial Genome. *Proc. Natl. Acad. Sci. U. S. A.* **2006**, *103* (41), 15200–15205. https://doi.org/10.1073/pnas.0607335103.

(126) Korp, J.; Vela Gurovic, M. S.; Nett, M. Antibiotics from Predatory Bacteria. *Beilstein J. Org. Chem.* **2016**, *12*, 594–607. https://doi.org/10.3762/bjoc.12.58.

(127) Treuner-Lange, A.; Bruckskotten, M.; Rupp, O.; Goesmann, A.; Søgaard-Andersen, L. Draft Genome Sequence of the Fruiting Myxobacterium *Nannocystis Exedens* DSM 71. *Genome Announc.* **2017**, *5* (43). https://doi.org/10.1128/genomeA.01227-17.

(128) Garcia, R.; Gemperlein, K.; Müller, R. *Minicystis Rosea* Gen. Nov., Sp. Nov., a Polyunsaturated Fatty Acid-Rich and Steroid-Producing Soil Myxobacterium. *Int. J. Syst. Evol. Microbiol.* **2014**, *64* (Pt_11), 3733–3742. https://doi.org/10.1099/ijs.0.068270-0.

(129) Sutton, D.; Livingstone, P. G.; Furness, E.; Swain, M. T.; Whitworth, D. E. Genome-Wide Identification of Myxobacterial Predation Genes and Demonstration of Formaldehyde Secretion as a Potentially Predation-Resistant Trait of *Pseudomonas Aeruginosa*. *Front. Microbiol.* **2019**, *10*, 2650. https://doi.org/10.3389/fmicb.2019.02650.

(130) Reeves, C. D.; Murli, S.; Ashley, G. W.; Piagentini, M.; Hutchinson, C. R.; McDaniel, R. Alteration of the Substrate Specificity of a Modular Polyketide Synthase Acyltransferase Domain through Site-Specific Mutations. *Biochemistry* **2001**, *40* (51), 15464–15470. https://doi.org/10.1021/bi015864r.

(131) Stachelhaus, T.; Mootz, H. D.; Marahiel, M. A. The Specificity-Conferring Code of Adenylation Domains in Nonribosomal Peptide Synthetases. *Chem. Biol.* **1999**, *6* (8), 493–505. https://doi.org/10.1016/S1074-5521(99)80082-9.

(132) Begley, M.; Cotter, P. D.; Hill, C.; Ross, R. P. Identification of a Novel Two-Peptide Lantibiotic, Lichenicidin, Following Rational Genome Mining for LanM Proteins. *Appl. Environ. Microbiol.* **2009**, *75* (17), 5451–5460. https://doi.org/10.1128/AEM.00730-09.

(133) Wenzel, S. C.; Müller, R. Myxobacterial Natural Product Assembly Lines: Fascinating Examples of Curious Biochemistry. *Nat. Prod. Rep.* **2007**, *24* (6), 1211–1224. https://doi.org/10.1039/b706416k.

(134) Hug, J. J.; Panter, F.; Krug, D.; Müller, R. Genome Mining Reveals Uncommon Alkylpyrones as Type III PKS Products from Myxobacteria. *J. Ind. Microbiol. Biotechnol.* **2019**, *46* (3–4), 319–334. https://doi.org/10.1007/s10295-018-2105-6.

(135) Gross, F.; Luniak, N.; Perlova, O.; Gaitatzis, N.; Jenke-Kodama, H.; Gerth, K.; Gottschalk, D.; Dittmann, E.; Müller, R. Bacterial Type III Polyketide Synthases: Phylogenetic Analysis and Potential for the Production of Novel Secondary Metabolites by Heterologous Expression in *Pseudomonads*. *Arch. Microbiol.* **2006**, *185* (1), 28–38. https://doi.org/10.1007/s00203-005-0059-3.

(136) Lautru, S.; Deeth, R. J.; Bailey, L. M.; Challis, G. L. Discovery of a New Peptide Natural Product by *Streptomyces Coelicolor* Genome Mining. *Nature Chemical Biology*. Nature Publishing Group September 11, 2005, pp 265–269. https://doi.org/10.1038/nchembio731.

(137) Laureti, L.; Song, L.; Huang, S.; Corre, C.; Leblond, P.; Challis, G. L.; Aigle, B. Identification of a Bioactive 51-Membered Macrolide Complex by Activation of a Silent Polyketide Synthase in Streptomyces Ambofaciens. *Proc. Natl. Acad. Sci. U. S. A.* **2011**, *108* (15),

6258–6263. https://doi.org/10.1073/pnas.1019077108.

(138) Wang, H.; Fewer, D. P.; Holm, L.; Rouhiainen, L.; Sivonen, K. Atlas of Nonribosomal Peptide and Polyketide Biosynthetic Pathways Reveals Common Occurrence of Nonmodular Enzymes. *Proc. Natl. Acad. Sci. U. S. A.* **2014**, *111* (25), 9259–9264. https://doi.org/10.1073/pnas.1401734111.

(139) Fisch, K. M. Biosynthesis of Natural Products by Microbial Iterative Hybrid PKS-NRPS. *RSC Advances*. Royal Society of Chemistry October 28, 2013, pp 18228–18247. https://doi.org/10.1039/c3ra42661k.

(140) Udwary, D. W.; Zeigler, L.; Asolkar, R. N.; Singan, V.; Lapidus, A.; Fenical, W.; Jensen, P. R.; Moore, B. S. Genome Sequencing Reveals Complex Secondary Metabolome in the Marine Actinomycete *Salinispora Tropica*. *Proc. Natl. Acad. Sci. U. S. A.* **2007**, *104* (25), 10376–10381. https://doi.org/10.1073/pnas.0700962104.

(141) Wenzel, S. C.; Kunze, B.; Höfle, G.; Silakowski, B.; Scharfe, M.; Blöcker, H.; Müller, R. Structure and Biosynthesis of Myxochromides S1-3 in *Stigmatella Aurantiaca*: Evidence for an Iterative Bacterial Type I Polyketide Synthase and for Module Skipping in Nonribosomal Peptide Biosynthesis. *ChemBioChem* **2005**, *6* (2), 375–385. https://doi.org/10.1002/cbic.200400282.

(142) Okoth, D. A.; Hug, J. J.; Garcia, R.; Spröer, C.; Overmann, J.; Müller, R. 2-Hydroxysorangiadenosine: Structure and Biosynthesis of a Myxobacterial Sesquiterpene–Nucleoside. *Molecules* **2020**, *25* (11), 2676. https://doi.org/10.3390/molecules25112676.

(143) Pistorius, D.; Müller, R. Discovery of the Rhizopodin Biosynthetic Gene Cluster in *Stigmatella Aurantiaca* Sg A15 by Genome Mining. *ChemBioChem* **2012**, *13* (3), 416–426. https://doi.org/10.1002/cbic.201100575.

(144) Keller, L.; Plaza, A.; Dubiella, C.; Groll, M.; Kaiser, M.; Müller, R. Macyranones: Structure, Biosynthesis, and Binding Mode of an Unprecedented Epoxyketone That Targets the 20S Proteasome. *J. Am. Chem. Soc.* **2015**, *137* (25), 8121–8130. https://doi.org/10.1021/jacs.5b03833.

(145) Viehrig, K.; Surup, F.; Volz, C.; Herrmann, J.; Abou Fayad, A.; Adam, S.; Köhnke, J.; Trauner, D.; Müller, R. Structure and Biosynthesis of Crocagins: Polycyclic Posttranslationally Modified Ribosomal Peptides from *Chondromyces Crocatus*. *Angew. Chemie Int. Ed.* **2017**, *56* (26), 7407–7410. https://doi.org/10.1002/anie.201612640.

(146) Cortina, N. S.; Krug, D.; Plaza, A.; Revermann, O.; Müller, R. Myxoprincomide: A Natural Product from *Myxococcus Xanthus* Discovered by Comprehensive Analysis of the Secondary Metabolome. *Angew. Chemie - Int. Ed.* **2012**, *51* (3), 811–816. https://doi.org/10.1002/anie.201106305.

(147) Panter, F.; Krug, D.; Baumann, S.; Müller, R. Self-Resistance Guided Genome Mining Uncovers New Topoisomerase Inhibitors from Myxobacteria. *Chem. Sci.* **2018**, *9* (21), 4898–4908. https://doi.org/10.1039/c8sc01325j.

(148) Tang, X.; Li, J.; Millán-Aguiñaga, N.; Zhang, J. J.; O'Neill, E. C.; Ugalde, J. A.; Jensen, P. R.; Mantovani, S. M.; Moore, B. S. Identification of Thiotetronic Acid Antibiotic Biosynthetic Pathways by Target-Directed Genome Mining. *ACS Chem. Biol.* **2015**, *10* (12), 2841–2849. https://doi.org/10.1021/acschembio.5b00658.

(149) Diettrich, J.; Kage, H.; Nett, M. Genomics-Inspired Discovery of Massiliachelin, an Agrochelin Epimer from *Massilia* Sp. NR 4-1. *Beilstein J. Org. Chem.* **2019**, *15* (4), 1298–1303. https://doi.org/10.3762/bjoc.15.128.

(150) Kurth, C.; Kage, H.; Nett, M. Siderophores as Molecular Tools in Medical and Environmental Applications. *Org. Biomol. Chem.* **2016**, *14* (35), 8212–8227. https://doi.org/10.1039/C6OB01400C.

(151) Wolf, T.; Shelest, V.; Nath, N.; Shelest, E. CASSIS and SMIPS: Promoter-Based Prediction of Secondary Metabolite Gene Clusters in Eukaryotic Genomes. *Bioinformatics* **2016**, *32* (8), 1138–1143. https://doi.org/10.1093/bioinformatics/btv713.

(152) Bergmann, S.; Schümann, J.; Scherlach, K.; Lange, C.; Brakhage, A. A.; Hertweck, C. Genomics-Driven Discovery of PKS-NRPS Hybrid Metabolites from *Aspergillus Nidulans*. *Nat. Chem. Biol.* **2007**, *3* (4), 213–217. https://doi.org/10.1038/nchembio869.

References

(153) Blin, K.; Shaw, S.; Steinke, K.; Villebro, R.; Ziemert, N.; Lee, S. Y.; Medema, M. H.; Weber, T. AntiSMASH 5.0: Updates to the Secondary Metabolite Genome Mining Pipeline. *Nucleic Acids Res.* **2019**, *47* (W1), W81–W87. https://doi.org/10.1093/nar/gkz310.

(154) Baltz, R. H. Gifted Microbes for Genome Mining and Natural Product Discovery. *J. Ind. Microbiol. Biotechnol.* **2017**, *44* (4–5), 573–588. https://doi.org/10.1007/s10295-016-1815-x.

(155) Gregory, K.; Salvador, L. A.; Akbar, S.; Adaikpoh, B. I.; Stevens, D. C. Survey of Biosynthetic Gene Clusters from Sequenced Myxobacteria Reveals Unexplored Biosynthetic Potential. *Microorganisms* **2019**, *7* (6), 181. https://doi.org/10.3390/microorganisms7060181.

(156) Zaburannyi, N.; Bunk, B.; Maier, J.; Overmann, J. J.; Müller, R. Genome Analysis of the Fruiting Body-Forming Myxobacterium *Chondromyces Crocatus* Reveals High Potential for Natural Product Biosynthesis. *Appl. Environ. Microbiol.* **2016**, *82* (6), 1945–1957. https://doi.org/10.1128/AEM.03011-15.

(157) Lee, C.; An, D.; Lee, H.; Cho, K. Correlation between *Sorangium Cellulosum* Subgroups and Their Potential for Secondary Metabolite Production. *J. Microbiol. Biotechnol.* **2013**, *23* (3), 297–303. https://doi.org/10.4014/jmb.1210.10054.

(158) Hoffmann, T.; Krug, D.; Bozkurt, N.; Duddela, S.; Jansen, R.; Garcia, R.; Gerth, K.; Steinmetz, H.; Müller, R. Correlating Chemical Diversity with Taxonomic Distance for Discovery of Natural Products in Myxobacteria. *Nat. Commun.* **2018**, *9* (1), 803. https://doi.org/10.1038/s41467-018-03184-1.

(159) Burgard, C.; Zaburannyi, N.; Nadmid, S.; Maier, J.; Jenke-Kodama, H.; Luxenburger, E.; Bernauer, H. S.; Wenzel, S. C. Genomics-Guided Exploitation of Lipopeptide Diversity in Myxobacteria. *ACS Chem. Biol.* **2017**, *12* (3), 779–786. https://doi.org/10.1021/acschembio.6b00953.

(160) Frank, B.; Wenzel, S. C.; Bode, H. B.; Scharfe, M.; Blöcker, H.; Müller, R. From Genetic Diversity to Metabolic Unity: Studies on the Biosynthesis of Aurafurones and Aurafuron-like Structures in Myxobacteria and Streptomycetes. *J. Mol. Biol.* **2007**, *374*

(1), 24–38. https://doi.org/10.1016/j.jmb.2007.09.015.

(161) Zhang, J. J.; Tang, X.; Moore, B. S. Genetic Platforms for Heterologous Expression of Microbial Natural Products. *Nat. Prod. Rep.* **2019**, *36* (9), 1313–1332. https://doi.org/10.1039/C9NP00025A.

(162) Sester, A.; Stüer-Patowsky, K.; Hiller, W.; Kloss, F.; Lütz, S.; Nett, M. Biosynthetic Plasticity Enables Production of Fluorinated Aurachins. *ChemBioChem* **2020**, *21* (16), 2268–2273. https://doi.org/10.1002/cbic.202000166.

(163) Cannell, R. J. P. Follow-Up of Natural Product Isolation. In *Natural Products Isolation*; Sarker, S. D., Latif, Z., Gray, A. I., Eds.; Humana Press: Totowa, NJ, 2006; Vol. 20, pp 463–506. https://doi.org/10.1385/1-59259-955-9:463.

(164) Boecker, S.; Zobel, S.; Meyer, V.; Süssmuth, R. D. Rational Biosynthetic Approaches for the Production of New-to-Nature Compounds in Fungi. *Fungal Genet. Biol.* **2016**, *89*, 89–101. https://doi.org/10.1016/j.fgb.2016.02.003.

(165) Boddy, C. N.; Hotta, K.; Tse, M. L.; Watts, R. E.; Khosla, C. Precursor-Directed Biosynthesis of Epothilone in *Escherichia Coli*. *J. Am. Chem. Soc.* **2004**, *126* (24), 7436–7437. https://doi.org/10.1021/ja048108s.

(166) Goss, R. J. M.; Shankar, S.; Fayad, A. A. The Generation of "UnNatural" Products: Synthetic Biology Meets Synthetic Chemistry. *Nat. Prod. Rep.* **2012**, *29* (8), 870–889. https://doi.org/10.1039/c2np00001f.

(167) Kirschning, A.; Hahn, F. Merging Chemical Synthesis and Biosynthesis: A New Chapter in the Total Synthesis of Natural Products and Natural Product Libraries. *Angew. Chemie Int. Ed.* **2012**, *51* (17), 4012–4022. https://doi.org/10.1002/anie.201107386.

(168) Sundermann, U.; Bravo-Rodriguez, K.; Klopries, S.; Kushnir, S.; Gomez, H.; Sanchez-Garcia, E.; Schulz, F. Enzyme-Directed Mutasynthesis: A Combined Experimental and Theoretical Approach to Substrate Recognition of a Polyketide Synthase. *ACS Chem. Biol.* **2013**, *8* (2), 443–450. https://doi.org/10.1021/cb300505w.

(169) Bravo-Rodriguez, K.; Klopries, S.; Koopmans, K. R. M.; Sundermann, U.; Yahiaoui, S.;

References

Arens, J.; Kushnir, S.; Schulz, F.; Sanchez-Garcia, E. Substrate Flexibility of a Mutated Acyltransferase Domain and Implications for Polyketide Biosynthesis. *Chem. Biol.* **2015**, *22* (11), 1425–1430. https://doi.org/10.1016/j.chembiol.2015.02.008.

(170) Koryakina, I.; Kasey, C.; McArthur, J. B.; Lowell, A. N.; Chemler, J. A.; Li, S.; Hansen, D. A.; Sherman, D. H.; Williams, G. J. Inversion of Extender Unit Selectivity in the Erythromycin Polyketide Synthase by Acyltransferase Domain Engineering. *ACS Chem. Biol.* **2017**, *12* (1), 114–123. https://doi.org/10.1021/acschembio.6b00732.

(171) Kalkreuter, E.; Crowetipton, J. M.; Lowell, A. N.; Sherman, D. H.; Williams, G. J. Engineering the Substrate Specificity of a Modular Polyketide Synthase for Installation of Consecutive Non-Natural Extender Units. *J. Am. Chem. Soc.* **2019**, *141* (5), 1961–1969. https://doi.org/10.1021/jacs.8b10521.

(172) Zhou, L.; Shao, J.; Li, Q.; Van Heel, A. J.; De Vries, M. P.; Broos, J.; Kuipers, O. P. Incorporation of Tryptophan Analogues into the Lantibiotic Nisin. *Amino Acids* **2016**, *48* (5), 1309–1318. https://doi.org/10.1007/s00726-016-2186-3.

(173) Telfer, T. J.; Richardson-Sanchez, T.; Gotsbacher, M. P.; Nolan, K. P.; Tieu, W.; Codd, R. Analogues of Desferrioxamine B (DFOB) with New Properties and New Functions Generated Using Precursor-Directed Biosynthesis. *BioMetals* **2019**, *32* (3), 395–408. https://doi.org/10.1007/s10534-019-00175-7.

(174) Telfer, T. J.; Codd, R. Fluorinated Analogues of Desferrioxamine B from Precursor-Directed Biosynthesis Provide New Insight into the Capacity of DesBCD. *ACS Chem. Biol.* **2018**, *13* (9), 2456–2471. https://doi.org/10.1021/acschembio.8b00340.

(175) Clark, B. R.; O'Connor, S.; Fox, D.; Leroy, J.; Murphy, C. D. Production of Anticancer Polyenes through Precursor-Directed Biosynthesis. *Org. Biomol. Chem.* **2011**, *9* (18), 6306–6311. https://doi.org/10.1039/c1ob05667k.

(176) Chan, Y. A.; Podevels, A. M.; Kevany, B. M.; Thomas, M. G. Biosynthesis of Polyketide Synthase Extender Units. *Natural Product Reports*. The Royal Society of Chemistry December 18, 2009, pp 90–114. https://doi.org/10.1039/b801658p.

(177) Wilson, M. C.; Moore, B. S. Beyond Ethylmalonyl-CoA: The Functional Role of Crotonyl-CoA Carboxylase/Reductase Homologs in Expanding Polyketide Diversity. *Nat. Prod. Rep.* **2012**, *29* (1), 72–86. https://doi.org/10.1039/c1np00082a.

(178) Ladner, C. C.; Williams, G. J. Harnessing Natural Product Assembly Lines: Structure, Promiscuity, and Engineering. *J. Ind. Microbiol. Biotechnol.* **2016**, *43* (2–3), 371–387. https://doi.org/10.1007/s10295-015-1704-8.

(179) Morita, H.; Yamashita, M.; Shi, S. P.; Wakimoto, T.; Kondo, S.; Kato, R.; Sugio, S.; Kohno, T.; Abe, I. Synthesis of Unnatural Alkaloid Scaffolds by Exploiting Plant Polyketide Synthase. *Proc. Natl. Acad. Sci. U. S. A.* **2011**, *108* (33), 13504–13509. https://doi.org/10.1073/pnas.1107782108.

(180) Hill, A. M.; Thompson, B. L. Novel Soraphens from Precursor Directed Biosynthesis. *Chem. Commun.* **2003**, *3* (12), 1360–1361. https://doi.org/10.1039/B303543N.

(181) Harvey, C. J. B.; Puglisi, J. D.; Pande, V. S.; Cane, D. E.; Khosla, C. Precursor Directed Biosynthesis of an Orthogonally Functional Erythromycin Analogue: Selectivity in the Ribosome Macrolide Binding Pocket. *J. Am. Chem. Soc.* **2012**, *134* (29), 12259–12265. https://doi.org/10.1021/ja304682q.

(182) Rachid, S.; Krug, D.; Kunze, B.; Kochems, I.; Scharfe, M.; Zabriskie, T. M.; Blöcker, H.; Müller, R. Molecular and Biochemical Studies of Chondramide Formation-Highly Cytotoxic Natural Products from *Chondromyces Crocatus* Cm C5. *Chem. Biol.* **2006**, *13* (6), 667–681. https://doi.org/10.1016/j.chembiol.2006.06.002.

(183) Amrine, C. S. M.; Long, J. L.; Raja, H. A.; Kurina, S. J.; Burdette, J. E.; Pearce, C. J.; Oberlies, N. H. Engineering Fluorine into Verticillins (Epipolythiodioxopiperazine Alkaloids) via Precursor-Directed Biosynthesis. *J. Nat. Prod.* **2019**, *82* (11), 3104–3110. https://doi.org/10.1021/acs.jnatprod.9b00711.

(184) Xie, Y.; Cai, Q.; Ren, H.; Wang, L.; Xu, H.; Hong, B.; Wu, L.; Chen, R. NRPS Substrate Promiscuity Leads to More Potent Antitubercular Sansanmycin Analogues. *J. Nat. Prod.* **2014**, *77* (7), 1744–1748. https://doi.org/10.1021/np5001494.

References

(185) O'Connor, N. K.; Hudson, A. S.; Cobb, S. L.; O'Neil, D.; Robertson, J.; Duncan, V.; Murphy, C. D. Novel Fluorinated Lipopeptides from *Bacillus* Sp. CS93 via Precursor-Directed Biosynthesis. *Amino Acids* **2014**, *46* (12), 2745–2752. https://doi.org/10.1007/s00726-014-1830-z.

(186) Moschny, J.; Lorenzen, W.; Hilfer, A.; Eckenstaler, R.; Jahns, S.; Enke, H.; Enke, D.; Schneider, P.; Benndorf, R. A.; Niedermeyer, T. H. J. Precursor-Directed Biosynthesis and Fluorescence Labeling of Clickable Microcystins. *J. Nat. Prod.* **2020**, *83* (6), 1960–1970. https://doi.org/10.1021/acs.jnatprod.0c00251.

(187) Kries, H.; Wachtel, R.; Pabst, A.; Wanner, B.; Niquille, D.; Hilvert, D. Reprogramming Nonribosomal Peptide Synthetases for "Clickable" Amino Acids. *Angew. Chemie Int. Ed.* **2014**, *53* (38), 10105–10108. https://doi.org/10.1002/anie.201405281.

(188) Sandy, M.; Rui, Z.; Gallagher, J.; Zhang, W. Enzymatic Synthesis of Dilactone Scaffold of Antimycins. *ACS Chem. Biol.* **2012**, *7* (12), 1956–1961. https://doi.org/10.1021/cb300416w.

(189) Yan, Y.; Chen, J.; Zhang, L.; Zheng, Q.; Han, Y.; Zhang, H.; Zhang, D.; Awakawa, T.; Abe, I.; Liu, W. Multiplexing of Combinatorial Chemistry in Antimycin Biosynthesis: Expansion of Molecular Diversity and Utility. *Angew. Chemie Int. Ed.* **2013**, *52* (47), 12308–12312. https://doi.org/10.1002/anie.201305569.

(190) Kreutzer, M. F.; Kage, H.; Herrmann, J.; Pauly, J.; Hermenau, R.; Müller, R.; Hoffmeister, D.; Nett, M. Precursor-Directed Biosynthesis of Micacocidin Derivatives with Activity against *Mycoplasma Pneumoniae*. *Org. Biomol. Chem.* **2014**, *12* (1), 113–118. https://doi.org/10.1039/c3ob41839a.

(191) Kolb, H. C.; Finn, M. G.; Sharpless, K. B. Click Chemistry: Diverse Chemical Function from a Few Good Reactions. *Angew. Chemie Int. Ed.* **2001**, *40* (11), 2004–2021. https://doi.org/10.1002/1521-3773(20010601)40:11<2004::AID-ANIE2004>3.0.CO;2-5.

(192) Kolb, H. C.; Sharpless, K. B. The Growing Impact of Click Chemistry on Drug Discovery. *Drug Discov. Today* **2003**, *8* (24), 1128–1137. https://doi.org/10.1016/S1359-

xc

6446(03)02933-7.

(193) Tang, W.; Becker, M. L. "Click" Reactions: A Versatile Toolbox for the Synthesis of Peptide-Conjugates. *Chem. Soc. Rev.* **2014**, *43* (20), 7013–7039. https://doi.org/10.1039/C4CS00139G.

(194) Neumann, S.; Biewend, M.; Rana, S.; Binder, W. H. The CuAAC: Principles, Homogeneous and Heterogeneous Catalysts, and Novel Developments and Applications. *Macromol. Rapid Commun.* **2020**, *41* (1), 1900359. https://doi.org/10.1002/marc.201900359.

(195) Zhu, X.; Zhang, W. Tagging Polyketides/Non-Ribosomal Peptides with a Clickable Functionality and Applications. *Front. Chem.* **2015**, *3* (11), 5. https://doi.org/10.3389/fchem.2015.00011.

(196) Prasher, P.; Sharma, M. Tailored Therapeutics Based on 1,2,3-1H -Triazoles: A Mini Review. *Medchemcomm* **2019**, *10* (8), 1302–1328. https://doi.org/10.1039/C9MD00218A.

(197) Quader, S.; Boyd, S. E.; Jenkins, I. D.; Houston, T. A. Multisite Modification of Neomycin B: Combined Mitsunobu and Click Chemistry Approach. *J. Org. Chem.* **2007**, *72* (6), 1962–1979. https://doi.org/10.1021/jo0620967.

(198) Peterson, L. B.; Blagg, B. S. J. Click Chemistry to Probe Hsp90: Synthesis and Evaluation of a Series of Triazole-Containing Novobiocin Analogues. *Bioorg. Med. Chem. Lett.* **2010**, *20* (13), 3957–3960. https://doi.org/10.1016/j.bmcl.2010.04.140.

(199) Lin, H.; Walsh, C. T. A Chemoenzymatic Approach to Glycopeptide Antibiotics. *J. Am. Chem. Soc.* **2004**, *126* (43), 13998–14003. https://doi.org/10.1021/ja045147v.

(200) Naaz, F.; Preeti Pallavi, M. C.; Shafi, S.; Mulakayala, N.; Shahar Yar, M.; Sampath Kumar, H. M. 1,2,3-Triazole Tethered Indole-3-Glyoxamide Derivatives as Multiple Inhibitors of 5-LOX, COX-2 & Tubulin: Their Anti-Proliferative & Anti-Inflammatory Activity. *Bioorg. Chem.* **2018**, *81*, 1–20. https://doi.org/10.1016/j.bioorg.2018.07.029.

(201) Dai, Y.; Chen, X.; Zhang, X. Recent Developments in the Area of Click-Crosslinked

Nanocarriers for Drug Delivery. *Macromol. Rapid Commun.* **2019**, *40* (3), 1800541. https://doi.org/10.1002/marc.201800541.

(202) Gopinathan, J.; Noh, I. Click Chemistry-Based Injectable Hydrogels and Bioprinting Inks for Tissue Engineering Applications. *Tissue Eng. Regen. Med.* **2018**, *15* (5), 531–546. https://doi.org/10.1007/s13770-018-0152-8.

(203) Böttcher, T.; Sieber, S. A. Showdomycin as a Versatile Chemical Tool for the Detection of Pathogenesis-Associated Enzymes in Bacteria. *J. Am. Chem. Soc.* **2010**, *132* (20), 6964–6972. https://doi.org/10.1021/ja909150y.

(204) Shi, H.; Cheng, X.; Sze, S. K.; Yao, S. Q. Proteome Profiling Reveals Potential Cellular Targets of Staurosporine Using a Clickable Cell-Permeable Probe. *Chem. Commun.* **2011**, *47* (40), 11306–11308. https://doi.org/10.1039/c1cc14824a.

(205) Cassiano, C.; Margarucci, L.; Esposito, R.; Riccio, R.; Tosco, A.; Casapullo, A.; Monti, M. C. In Cell Scalaradial Interactome Profiling Using a Bio-Orthogonal Clickable Probe. *Chem. Commun.* **2014**, *50* (45), 6043–6045. https://doi.org/10.1039/c4cc00989d.

(206) Zou, Y.; Yin, J. Alkyne-Functionalized Chemical Probes for Assaying the Substrate Specificities of the Adenylation Domains in Nonribosomal Peptide Synthetases. *ChemBioChem* **2008**, *9* (17), 2804–2810. https://doi.org/10.1002/cbic.200800480.

(207) Hems, E. S.; Wagstaff, B. A.; Saalbach, G.; Field, R. A. CuAAC Click Chemistry for the Enhanced Detection of Novel Alkyne-Based Natural Product Toxins. *Chem. Commun.* **2018**, *54* (86), 12234–12237. https://doi.org/10.1039/c8cc05113e.

(208) Ross, C.; Scherlach, K.; Kloss, F.; Hertweck, C. The Molecular Basis of Conjugated Polyyne Biosynthesis in Phytopathogenic Bacteria. *Angew. Chemie Int. Ed.* **2014**, *53* (30), 7794–7798. https://doi.org/10.1002/anie.201403344.

(209) Jeon, H.; Lim, C.; Lee, J. M.; Kim, S. Chemical Assay-Guided Natural Product Isolation via Solid-Supported Chemodosimetric Fluorescent Probe. *Chem. Sci.* **2015**, *6* (5), 2806–2811. https://doi.org/10.1039/c5sc00360a.

(210) Sandmann, A.; Dickschat, J.; Jenke-Kodama, H.; Kunze, B.; Dittmann, E.; Müller, R.

Aurachin-Biosynthese Im Gram-Negativen Bakterium *Stigmatella Aurantiaca*: Beteiligung Einer Typ-II-Polyketidsynthase. *Angew. Chemie* **2007**, *119* (15), 2768–2772. https://doi.org/10.1002/ange.200603513.

(211) McKay, C. S.; Finn, M. G. Click Chemistry in Complex Mixtures: Bioorthogonal Bioconjugation. *Chemistry and Biology*. Elsevier Ltd September 18, 2014, pp 1075–1101. https://doi.org/10.1016/j.chembiol.2014.09.002.

(212) Baldeweg, F.; Kage, H.; Schieferdecker, S.; Allen, C.; Hoffmeister, D.; Nett, M. Structure of Ralsolamycin, the Interkingdom Morphogen from the Crop Plant Pathogen *Ralstonia Solanacearum*. *Org. Lett.* **2017**, acs.orglett.7b02329. https://doi.org/10.1021/acs.orglett.7b02329.

(213) Kreutzer, M. F.; Kage, H.; Gebhardt, P.; Wackler, B.; Saluz, H. P.; Hoffmeister, D.; Nett, M. Biosynthesis of a Complex Yersiniabactin-Like Natural Product via the Mic Locus in Phytopathogen *Ralstonia Solanacearum*. *Appl. Environ. Microbiol.* **2011**, *77* (17), 6117–6124. https://doi.org/10.1128/AEM.05198-11.

(214) Sester, A.; Winand, L.; Pace, S.; Hiller, W.; Werz, O.; Nett, M. Myxochelin- and Pseudochelin-Derived Lipoxygenase Inhibitors from a Genetically Engineered *Myxococcus Xanthus* Strain. *J. Nat. Prod.* **2019**, *82* (9), 2544–2549. https://doi.org/10.1021/acs.jnatprod.9b00403.

(215) Schieferdecker, S.; König, S.; Pace, S.; Werz, O.; Nett, M. Myxochelin-Inspired 5-Lipoxygenase Inhibitors: Synthesis and Biological Evaluation. *ChemMedChem* **2017**, *12* (1), 23–27. https://doi.org/10.1002/cmdc.201600536.

(216) Boucher, C. A.; Van Gijsegem, F.; Barberis, P. A.; Arlat, M.; Zischek, C. *Pseudomonas Solanacearum* Genes Controlling Both Pathogenicity on Tomato and Hypersensitivity on Tobacco Are Clustered. *J. Bacteriol.* **1987**, *169* (12), 5626–5632. https://doi.org/10.1128/jb.169.12.5626-5632.1987.

(217) Gaitatzis, N.; Kunze, B.; Müller, R. Novel Insights into Siderophore Formation in Myxobacteria. *ChemBioChem* **2005**, *6* (2), 365–374. https://doi.org/10.1002/cbic.200400206.

References

(218) Gaitatzis, N. Neuartige Modulare Megasynthasen Aus Myxobakterien: Die Stigmatellin- Und Myxochelin-Biosynthese in *Stigmatella Aurantiaca*, Dissertation, 2004.

(219) Ambrosi, H.-D.; Hartmann, V.; Pistorius, D.; Reissbrodt, R.; Trowitzsch-Kienast, W. Myxochelins B, C, D, E and F: A New Structural Principle for Powerful Siderophores Imitating Nature. *Eur. J. Org. Chem.* **1998**, 541–551.

(220) Reich, H. Hans Reich's Collection. NMR Spectroscopy. https://organicchemistrydata.org/hansreich/resources/nmr/?index=nmr_index%2F19 F_coupling (accessed Jun 8, 2021).

(221) Qian, H.; Xia, B.; He, Y.; Lu, Z.; Bie, X.; Zhao, H.; Zhang, C.; Lu, F. Expression, Purification, and Characterization of a Novel Acidic Lipoxygenase from *Myxococcus Xanthus*. *Protein Expr. Purif.* **2017**, *138*, 13–17. https://doi.org/10.1016/j.pep.2017.05.006.

(222) An, J.-U.; Song, Y.-S.; Kim, K.-R.; Ko, Y.-J.; Yoon, D.-Y.; Oh, D.-K. Biotransformation of Polyunsaturated Fatty Acids to Bioactive Hepoxilins and Trioxilins by Microbial Enzymes. *Nat. Commun.* **2018**, *9* (1), 128. https://doi.org/10.1038/s41467-017-02543-8.

(223) Goloshchapova, K.; Stehling, S.; Heydeck, D.; Blum, M.; Kuhn, H. Functional Characterization of a Novel Arachidonic Acid 12S-lipoxygenase in the Halotolerant Bacterium *Myxococcus Fulvus* Exhibiting Complex Social Living Patterns. *Microbiologyopen* **2019**, *8* (7). https://doi.org/10.1002/mbo3.775.

(224) Werz, O.; Gerstmeier, J.; Garscha, U. Novel Leukotriene Biosynthesis Inhibitors (2012-2016) as Anti-Inflammatory Agents. *Expert Opin. Ther. Pat.* **2017**, *27* (5), 607–620. https://doi.org/10.1080/13543776.2017.1276568.

(225) Gilbert, N. C.; Gerstmeier, J.; Schexnaydre, E. E.; Börner, F.; Garscha, U.; Neau, D. B.; Werz, O.; Newcomer, M. E. Structural and Mechanistic Insights into 5-Lipoxygenase Inhibition by Natural Products. *Nat. Chem. Biol.* **2020**, *16*, 783–790. https://doi.org/10.1038/s41589-020-0544-7.

(226) Kries, H. Biosynthetic Engineering of Nonribosomal Peptide Synthetases. *J. Pept. Sci.*

2016, *22* (9), 564–570. https://doi.org/10.1002/psc.2907.

(227) Schieferdecker, S.; Nett, M. A Fast and Efficient Method for the Preparation of the 5-Lipoxygenase Inhibitor Myxochelin A. *Tetrahedron Lett.* **2016**, *57* (12), 1359–1360. https://doi.org/10.1016/j.tetlet.2016.02.047.

(228) Frank, N. A.; Széles, M.; Akone, S. H.; Rasheed, S.; Hüttel, S.; Frewert, S.; Hamed, M. M.; Herrmann, J.; Schuler, S. M. M.; Hirsch, A. K. H.; Müller, R. Expanding the Myxochelin Natural Product Family by Nicotinic Acid Containing Congeners. *Preprints* **2021**, No. 2021070315. https://doi.org/10.20944/preprints202107.0315.v1.

(229) Losada, A. A.; Cano-Prieto, C.; García-Salcedo, R.; Braña, A. F.; Méndez, C.; Salas, J. A.; Olano, C. Caboxamycin Biosynthesis Pathway and Identification of Novel Benzoxazoles Produced by Cross-Talk in Streptomyces Sp. NTK 937. *Microb. Biotechnol.* **2017**, *10* (4), 873–885. https://doi.org/10.1111/1751-7915.12716.

(230) Song, H.; Rao, C.; Deng, Z.; Yu, Y.; Naismith, J. H. The Biosynthesis of the Benzoxazole in Nataxazole Proceeds via an Unstable Ester and Has Synthetic Utility. *Angew. Chemie Int. Ed.* **2020**, *59* (15), 6054–6061. https://doi.org/10.1002/anie.201915685.

(231) Winand, L.; Vollmann, D. J.; Hentschel, J.; Nett, M. Characterization of a Solvent-Tolerant Amidohydrolase Involved in Natural Product Heterocycle Formation. *Catalysts* **2021**, *11* (8), 892. https://doi.org/10.3390/catal11080892.

(232) Islam, M. N.; Hitchings, R.; Kumar, S.; Fontes, F. L.; Lott, J. S.; Kruh-Garcia, N. A.; Crick, D. C. Mechanism of Fluorinated Anthranilate-Induced Growth Inhibition in *Mycobacterium Tuberculosis*. *ACS Infect. Dis.* **2019**, *5* (1), 55–62. https://doi.org/10.1021/acsinfecdis.8b00092.

(233) Schieferdecker, S.; Exner, T. E.; Gross, H.; Roth, M.; Nett, M. New Myxothiazols from the Predatory Bacterium *Myxococcus Fulvus*. *J. Antibiot. (Tokyo).* **2014**, *67* (7), 519–525. https://doi.org/10.1038/ja.2014.31.

(234) Jones, E. W.; Berget, P. B.; Burnette III, J. M.; Anderson, C.; Asafu-Adjei, D.; Avetisian, S.; Barrie, F.; Chen, R.; Chu, B.; Conroy, S.; Conroy, S.; Dill, A.; Eimer, W.; Garrity, D.;

Greenwood, A.; Hamilton, T.; Hucko, S.; Jackson, C.; Livesey, K.; Monaco, T.; Onorato, C.; Otsuka, M.; Pai, S.; Schaeffer, G.; Shung, S.; Spath, S.; Stahlman, J.; Sweeney, B.; Wiltrout, E.; Yurovsky, D.; Zonneveld, A. The Spectrum of Trp− Mutants Isolated as 5-Fluoroanthranilate-Resistant Clones In *Saccharomyces Bayanus*, *S. Mikatae* And *S. Paradoxus*. *Yeast* **2008**, *25* (1), 41–46. https://doi.org/10.1002/yea.1552.

(235) Gou, L.; Wu, Q.; Lin, S.; Li, X.; Liang, J.; Zhou, X.; An, D.; Deng, Z.; Wang, Z. Mutasynthesis of Pyrrole Spiroketal Compound Using Calcimycin 3-Hydroxy Anthranilic Acid Biosynthetic Mutant. *Appl. Microbiol. Biotechnol.* **2013**, *97* (18), 8183–8191. https://doi.org/10.1007/s00253-013-4882-1.

(236) Wolff, H.; Bode, H. B. The Benzodiazepine-like Natural Product Tilivalline Is Produced by the Entomopathogenic Bacterium *Xenorhabdus Eapokensis*. *PLoS One* **2018**, *13* (3), e0194297. https://doi.org/10.1371/journal.pone.0194297.

(237) Yonemoto, I. T.; Li, W.; Khullar, A.; Reixach, N.; Gerratana, B. Mutasynthesis of a Potent Anticancer Sibiromycin Analogue. *ACS Chem. Biol.* **2012**, *7* (6), 973–977. https://doi.org/10.1021/cb200544u.

(238) Hermane, J.; Bułyszko, I.; Eichner, S.; Sasse, F.; Collisi, W.; Poso, A.; Schax, E.; Walter, J. G.; Scheper, T.; Kock, K.; Herrmann, C.; Aliuos, P.; Reuter, G.; Zeilinger, C.; Kirschning, A. New, Non-Quinone Fluorogeldanamycin Derivatives Strongly Inhibit Hsp90. *ChemBioChem* **2015**, *16* (2), 302–311. https://doi.org/10.1002/cbic.201402375.

(239) Agostini, F.; Sinn, L.; Petras, D.; Schipp, C. J.; Kubyshkin, V.; Berger, A. A.; Dorrestein, P. C.; Rappsilber, J.; Budisa, N.; Koksch, B. Multiomics Analysis Provides Insight into the Laboratory Evolution of Escherichia Coli toward the Metabolic Usage of Fluorinated Indoles. *ACS Cent. Sci.* **2021**, *7* (1), 81–92. https://doi.org/10.1021/acscentsci.0c00679.

(240) Zhu, X.; De Laurentis, W.; Leang, K.; Herrmann, J.; Ihlefeld, K.; van Pée, K. H.; Naismith, J. H. Structural Insights into Regioselectivity in the Enzymatic Chlorination of Tryptophan. *J. Mol. Biol.* **2009**, *391* (1), 74–85. https://doi.org/10.1016/j.jmb.2009.06.008.

(241) Gkotsi, D. S.; Ludewig, H.; Sharma, S. V.; Connolly, J. A.; Dhaliwal, J.; Wang, Y.; Unsworth,

W. P.; Taylor, R. J. K.; McLachlan, M. M. W.; Shanahan, S.; Naismith, J. H.; Goss, R. J. M. A Marine Viral Halogenase That Iodinates Diverse Substrates. *Nat. Chem.* **2019**, *11* (12), 1091–1097. https://doi.org/10.1038/s41557-019-0349-z.

(242) Bayer Vital GmbH Geschäftsbereich Pharma. *Zulassung Ciprobay® 500 Mg*; 2012.

(243) Doggett, J. S.; Nilsen, A.; Forquer, I.; Wegmann, K. W.; Jones-Brando, L.; Yolken, R. H.; Bordón, C.; Charman, S. A.; Katneni, K.; Schultz, T.; Burrows, J. N.; Hinrichs, D. J.; Meunier, B.; Carruthers, V. B.; Riscoe, M. K. Endochin-like Quinolones Are Highly Efficacious against Acute and Latent Experimental Toxoplasmosis. *Proc. Natl. Acad. Sci. U. S. A.* **2012**, *109* (39), 15936–15941. https://doi.org/10.1073/pnas.1208069109.

(244) McConnell, E. V.; Bruzual, I.; Pou, S.; Winter, R.; Dodean, R. A.; Smilkstein, M. J.; Krollenbrock, A.; Nilsen, A.; Zakharov, L. N.; Riscoe, M. K.; Doggett, J. S. Targeted Structure-Activity Analysis of Endochin-like Quinolones Reveals Potent Qi and Qo Site Inhibitors of *Toxoplasma Gondii* and *Plasmodium Falciparum* Cytochrome Bc1 and Identifies ELQ-400 as a Remarkably Effective Compound against Acute Experimental Toxoplasmosis. *ACS Infect. Dis.* **2018**, *4* (11), 1574–1584. https://doi.org/10.1021/acsinfecdis.8b00133.

(245) Szamosvári, D.; Prothiwa, M.; Dieterich, C. L.; Böttcher, T. Profiling Structural Diversity and Activity of 2-Alkyl-4(1 H)-Quinolone N-Oxides of *Pseudomonas* and *Burkholderia*. *Chem. Commun.* **2020**. https://doi.org/10.1039/D0CC02498H.

(246) Soukarieh, F.; Williams, P.; Stocks, M. J.; Cámara, M. *Pseudomonas Aeruginosa* Quorum Sensing Systems as Drug Discovery Targets: Current Position and Future Perspectives. *Journal of Medicinal Chemistry*. American Chemical Society December 13, 2018, pp 10385–10402. https://doi.org/10.1021/acs.jmedchem.8b00540.

(247) Weber, T.; Blin, K.; Duddela, S.; Krug, D.; Kim, H. U.; Bruccoleri, R.; Lee, S. Y.; Fischbach, M. A.; Müller, R.; Wohlleben, W.; Breitling, R.; Takano, E.; Medema, M. H. AntiSMASH 3.0 - a Comprehensive Resource for the Genome Mining of Biosynthetic Gene Clusters. *Nucleic Acids Res.* **2015**, *43* (W1), W237–W243. https://doi.org/10.1093/nar/gkv437.

(248) Revermann, O. Novel Secondary Metabolites from Myxobacteria and Their Biosynthetic

Machinery, Dissertation, Universität des Saarlandes, 2012.

(249) Moreno, A. J.; Fontes, M.; Murillo, F. J. IhfA Gene of the Bacterium *Myxococcus Xanthus* and Its Role in Activation of Carotenoid Genes by Blue Light. *J. Bacteriol.* **2001**, *183* (2), 557–569. https://doi.org/10.1128/JB.183.2.557-569.2001.

(250) Lorenzen, W.; Ahrendt, T.; Bozhüyük, K. A. J.; Bode, H. B. A Multifunctional Enzyme Is Involved in Bacterial Ether Lipid Biosynthesis. *Nat. Chem. Biol.* **2014**, *10* (6), 425–427. https://doi.org/10.1038/nchembio.1526.

(251) Bhat, S.; Ahrendt, T.; Dauth, C.; Bode, H. B.; Shimkets, L. J. Two Lipid Signals Guide Fruiting Body Development of *Myxococcus Xanthus*. *MBio* **2014**, *5* (1), e00939--13. https://doi.org/10.1128/mBio.00939-13.

(252) Kunze, B.; Bedorf, N.; Kohl, W.; Höfle, G.; Reichenbach, H. Myxochelin A, a New Iron-Chelating Compound from *Angiococcus Disciformis* (Myxobacterales). Production, Isolation, Physico-Chemical and Biological Properties. *J. Antibiot. (Tokyo).* **1989**, *42* (1), 14–17. https://doi.org/10.7164/antibiotics.42.14.

(253) Müller, S.; Strack, S. N.; Ryan, S. E.; Shawgo, M.; Walling, A.; Harris, S.; Chambers, C.; Boddicker, J.; Kirby, J. R. Identification of Functions Affecting Predator-Prey Interactions between *Myxococcus Xanthus* and *Bacillus Subtilis*. *J. Bacteriol.* **2016**, *198* (24), 3335–3344. https://doi.org/10.1128/JB.00575-16.

(254) Zafriri, D.; Rosenberg, E.; Mirelman, D. Mode of Action of *Myxococcus Xanthus* Antibiotic TA. *Antimicrob. Agents Chemother.* **1981**, *19* (2), 349–351. https://doi.org/10.1128/AAC.19.2.349.

(255) Xiao, Y.; Wei, X.; Ebright, R.; Wall, D. Antibiotic Production by Myxobacteria Plays a Role in Predation. *J. Bacteriol.* **2011**, *193* (18), 4626–4633. https://doi.org/10.1128/JB.05052-11.

(256) Gerth, K.; Irschik, H.; Reichenbach, H.; Trowitzsch, W. The Myxovirescins a Family of Antibiotics from *Myxococcus Virescens* (Myxobacterales). *J. Antibiot. (Tokyo).* **1982**, *35* (11), 1454–1459. https://doi.org/10.7164/antibiotics.35.1454.

(257) Trowitzsch-Kienast, W.; Gerth, K.; Wray, V.; Reichenbach, H.; Höfle, G. Myxochromid A: Ein Hochungesättigtes Lipopeptidlacton Aus *Myxococcus Virescens*. *Liebigs Ann. der Chemie* **1993**, No. 12, 1233–1237. https://doi.org/10.1002/jlac.1993199301200.

(258) Meiser, P.; Bode, H. B.; Müller, R. The Unique DKxanthene Secondary Metabolite Family from the Myxobacterium *Myxococcus Xanthus* Is Required for Developmental Sporulation. *Proc. Natl. Acad. Sci. U. S. A.* **2006**, *103* (50), 19128–19133. https://doi.org/10.1073/pnas.0606039103.

(259) Meiser, P.; Weissman, K. J.; Bode, H. B.; Krug, D.; Dickschat, J. S.; Sandmann, A.; Müller, R. DKxanthene Biosynthesis—Understanding the Basis for Diversity-Oriented Synthesis in Myxobacterial Secondary Metabolism. *Chem. Biol.* **2008**, *15* (8), 771–781. https://doi.org/10.1016/j.chembiol.2008.06.005.

(260) Gerth, K.; Jansen, R.; Reifenstahl, G.; Höfle, G.; Irschik, H.; Kunze, B.; Reichenbach, H.; Thierbach, G. The Myxalamids, New Antibiotics from *Myxococcus Xanthus* (Myxobacterales) I. Production, Physico-Chemical and Biological Properties, and Mechanism of Action. *J. Antibiot. (Tokyo).* **1983**, *36* (9), 1150–1156. https://doi.org/10.7164/antibiotics.36.1150.

(261) Jansen, R.; Reifenstahl, G.; Gerth, K.; Reichenbach, H.; Höfle, G. Antibiotika Aus Gleitenden Bakterien, XV. Myaxalamide A, B, C Und D Eine Gruppe Homologer Antibiotika Aus *Myxococcus Xanthus* Mx X12 (Myxobacterales). *Liebigs Ann. der Chemie* **1983**, *1983* (7), 1081–1095. https://doi.org/10.1002/jlac.198319830702.

(262) Bode, H. B.; Meiser, P.; Klefisch, T.; Cortina, N. S. D. J. N. S. d. J.; Krug, D.; Göhring, A.; Schwär, G.; Mahmud, T.; Elnakady, Y. A.; Müller, R. Mutasynthesis-Derived Myxalamids and Origin of the Isobutyryl-CoA Starter Unit of Myxalamid B. *ChemBioChem* **2007**, *8* (17), 2139–2144. https://doi.org/10.1002/cbic.200700401.

(263) Dickschat, J. S.; Wenzel, S. C.; Bode, H. B.; Müller, R.; Schulz, S. Biosynthesis of Volatiles by the Myxobacterium *Myxococcus Xanthus*. *ChemBioChem* **2004**, *5* (6), 778–787. https://doi.org/10.1002/cbic.200300813.

(264) Lorenzen, W.; Ring, M. W.; Schwar, G.; Bode, H. B. Isoprenoids Are Essential for Fruiting

Body Formation in *Myxococcus Xanthus*. *J. Bacteriol.* **2009**, *191* (18), 5849–5853. https://doi.org/10.1128/JB.00539-09.

(265) Zaroubi, L.; Ozugergin, I.; Mastronardi, K.; Imfeld, A.; Law, C.; Gélinas, Y.; Findlay, B. L. The Ubiquitous Terpene Geosmin Is a Warning Chemical. *bioRxiv* **2021**, 2021.03.09.434661. https://doi.org/10.1101/2021.03.09.434661.

(266) Hayashi, T.; Kitamura, Y.; Funa, N.; Ohnishi, Y.; Horinouchi, S. Fatty Acyl-AMP Ligase Involvement in the Production of Alkylresorcylic Acid by a *Myxococcus Xanthus* Type III Polyketide Synthase. *ChemBioChem* **2011**, *12* (14), 2166–2176. https://doi.org/10.1002/cbic.201100344.

(267) Kobayashi, S.; Nakai, H.; Ikenishi, Y.; Sun, W.-Y.; Ozaki, M.; Hayase, Y.; Takeda, R. Micacocidin A, B and C, Novel Antimycoplasma Agents from *Pseudomonas* Sp. II. Structure Elucidation. *J. Antibiot. (Tokyo).* **1998**, *51* (3), 328–332. https://doi.org/10.7164/antibiotics.51.328.

(268) Chaturvedi, K. S.; Hung, C. S.; Crowley, J. R.; Stapleton, A. E.; Henderson, J. P. The Siderophore Yersiniabactin Binds Copper to Protect Pathogens during Infection. *Nat. Chem. Biol.* **2012**, *8* (8), 731–736. https://doi.org/10.1038/nchembio.1020.

(269) SDBSWeb for 6-heptynoic acid http://sdbs.db.aist.go.jp/sdbs/cgi-bin/direct_frame_disp.cgi?sdbsno=2798 (accessed Feb 19, 2020).

(270) Wang, M.; Carver, J. J.; Phelan, V. V; Sanchez, L. M.; Garg, N.; Peng, Y.; Nguyen, D. D.; Watrous, J.; Kapono, C. A.; Luzzatto-Knaan, T.; Porto, C.; Bouslimani, A.; Melnik, A. V; Meehan, M. J.; Liu, W.-T.; Crüsemann, M.; Boudreau, P. D.; Esquenazi, E.; Sandoval-Calderón, M.; Kersten, R. D.; Pace, L. A.; Quinn, R. A.; Duncan, K. R.; Hsu, C.-C.; Floros, D. J.; Gavilan, R. G.; Kleigrewe, K.; Northen, T.; Dutton, R. J.; Parrot, D.; Carlson, E. E.; Aigle, B.; Michelsen, C. F.; Jelsbak, L.; Sohlenkamp, C.; Pevzner, P.; Edlund, A.; McLean, J.; Piel, J.; Murphy, B. T.; Gerwick, L.; Liaw, C.-C.; Yang, Y.-L.; Humpf, H.-U.; Maansson, M.; Keyzers, R. A.; Sims, A. C.; Johnson, A. R.; Sidebottom, A. M.; Sedio, B. E.; Klitgaard, A.; Larson, C. B.; Boya P, C. A.; Torres-Mendoza, D.; Gonzalez, D. J.; Silva, D. B.; Marques, L. M.; Demarque, D. P.; Pociute, E.; O'Neill, E. C.; Briand, E.; Helfrich, E. J. N.; Granatosky,

c

E. A.; Glukhov, E.; Ryffel, F.; Houson, H.; Mohimani, H.; Kharbush, J. J.; Zeng, Y.; Vorholt, J. A.; Kurita, K. L.; Charusanti, P.; McPhail, K. L.; Nielsen, K. F.; Vuong, L.; Elfeki, M.; Traxler, M. F.; Engene, N.; Koyama, N.; Vining, O. B.; Baric, R.; Silva, R. R.; Mascuch, S. J.; Tomasi, S.; Jenkins, S.; Macherla, V.; Hoffman, T.; Agarwal, V.; Williams, P. G.; Dai, J.; Neupane, R.; Gurr, J.; Rodríguez, A. M. C.; Lamsa, A.; Zhang, C.; Dorrestein, K.; Duggan, B. M.; Almaliti, J.; Allard, P.-M.; Phapale, P.; Nothias, L.-F.; Alexandrov, T.; Litaudon, M.; Wolfender, J.-L.; Kyle, J. E.; Metz, T. O.; Peryea, T.; Nguyen, D.-T.; VanLeer, D.; Shinn, P.; Jadhav, A.; Müller, R.; Waters, K. M.; Shi, W.; Liu, X.; Zhang, L.; Knight, R.; Jensen, P. R.; Palsson, B. Ø.; Pogliano, K.; Linington, R. G.; Gutiérrez, M.; Lopes, N. P.; Gerwick, W. H.; Moore, B. S.; Dorrestein, P. C.; Bandeira, N. Sharing and Community Curation of Mass Spectrometry Data with Global Natural Products Social Molecular Networking. *Nat. Biotechnol.* **2016**, *34* (8), 828–837. https://doi.org/10.1038/nbt.3597.

(271) Schmid, R.; Petras, D.; Nothias, L. F.; Wang, M.; Aron, A. T.; Jagels, A.; Tsugawa, H.; Rainer, J.; Garcia-Aloy, M.; Dührkop, K.; Korf, A.; Pluskal, T.; Kameník, Z.; Jarmusch, A. K.; Caraballo-Rodríguez, A. M.; Weldon, K.; Nothias-Esposito, M.; Aksenov, A. A.; Bauermeister, A.; Orio, A. A.; Grundmann, C. O.; Vargas, F.; Koester, I.; Gauglitz, J. M.; Gentry, E. C.; Hövelmann, Y.; Kalinina, S. A.; Pendergraft, M. A.; Panitchpakdi, M. W.; Tehan, R.; Le Gouellec, A.; Aleti, G.; Russo, H. M.; Arndt, B.; Hübner, F.; Hayen, H.; Zhi, H.; Raffatellu, M.; Prather, K. A.; Aluwihare, L. I.; Böcker, S.; McPhail, K. L.; Humpf, H. U.; Karst, U.; Dorrestein, P. C. Ion Identity Molecular Networking in the GNPS Environment. *bioRxiv* **2020**. https://doi.org/10.1101/2020.05.11.088948.

Abbreviations

ACN	acetonitrile
AUC	area under the curve
BGC	biosynthetic gene cluster
COSY	correlation spectroscopy
d	day / days
DHBA	dihydroxy benzoic acid
DL-PG	D/L-propargylglycine
EIC	extracted ion chromatogram
ESI	electrospray ionization
6-FAM-N_3	6-carboxyfluorescein azide
6HepA	6-heptynoic acid
HMBC	heteronuclear multiple-bond correlation
HSQC	heteronuclear single-quantum coherence
LC-MS	liquid chromatography mass spectrometry
5-LO	5-lipoxygenase
MeOH	methanol
min	minute / minutes
MS	mass spectrometry / mass spectrum
m/z	mass to charge ratio
n.d.	not detected
NRPS	non-ribosomal peptide synthetase
PDA	photon detector assembly
PKS	polyketide synthase
ppm	parts per million
RiPP	ribosomally-synthesized and post-translationally modified peptide
rpm	revolutions per minute
RT	room temperature, 20°C
wt	wild type

Index of Figures

Index of Tables

Publications

Korp, J.; Winand, L.; Sester, A.; Nett, M. Engineering Pseudochelin Production in *Myxococcus xanthus*. *Appl. Environ. Microbiol.* **2018**, 84 (22), e01789-18.

Sester, A.; Winand, L.; Pace, S.; Hiller, W.; Werz, O.; Nett, M. Myxochelin- and Pseudochelin-Derived Lipoxygenase Inhibitors from a Genetically Engineered *Myxococcus xanthus* Strain. *J. Nat. Prod.* **2019**, 82 (9), 2544–2549.

Sester, A.; Stüer-Patowsky, K.; Hiller, W.; Kloss, F.; Lütz, S.; Nett, M. Biosynthetic Plasticity Enables Production of Fluorinated Aurachins. *ChemBioChem* **2020**, 21 (16), 2268–2273.

Sester, A.; Korp, J.; Nett, M. Secondary Metabolism of Predatory Bacteria. In *The Ecology of Predation at the Microscale*; Jurkevitch, E., Mitchell, R. J., Eds.; Springer International Publishing, **2020**.

Sester, A.; Winand, L.; Nett, M. Combinatorial Biosynthesis of Lipoxygenase Inhibitors in a Genetically Engineered *Myxococcus xanthus* Strain. In *Scientific Highlights 2019*; Tiller, J. C., Ed.; Fakultät Bio- und Chemieingenieurwesen, TU Dortmund, **2020**; p 65.

Winand, L.; Sester, A.; Nett, M. Bioengineering of Anti-Inflammatory Natural Products. *ChemMedChem* **2021**, 16 (5), 767-776.

Conference Presentations

Talks

Sester A. Heterologous production of pseudochelin in *Myxococcus xanthus, VAAM Annual Conference*, Mainz, **2019**

Sester A. Generation of myxochelin-derived lipoxygenase inhibitors in a genetically modified *Myxococcus xanthus* strain, *Annual Meeting of the American Society of Pharmacognosy*, Madison, WI, USA, **2019**

Posters

Sester A.; Korp J.; Nett M.; Genomic Potential of *Pyxidicoccus fallax* HKI 727, *Annual Meeting of German Association for General and Applied Microbiology,* Freiburg, **2016**

Sester A.; Korp J.; Nett M.; Genomic Potential of *Pyxidicoccus fallax* HKI 727, *Leibniz Wirkstofftage,* Jena, **2016**

Sester A.; Korp J.; Nett M.; Genomic Potential of *Pyxidicoccus fallax* HKI 727, *VAAM Workshop "Biology of bacteria producing natural products",* Freiburg, **2016**

Sester A.; Korp J.; Winand L.; Nett M.; Engineering pseudochelin production in *Myxococcus xanthus, Emerging Trends in Natural Product Biotechnology,* Dortmund, **2018**

Sester A.; Stüer-Patowsky K.; Lütz S.; Nett M.; Precursor-directed biosynthesis towards aurachin derivatives, *VAAM Workshop "Biology of bacteria producing natural products",* Jena, **2019**